FORMATION AND FATE OF SECONDARY ORGANIC AEROSOL PRODUCED FROM NITRATE RADICAL OXIDATON OF MONOTERPENES

A Dissertation
Presented to
The Academic Faculty

by

Christopher Boyd

In Partial Fulfillment
of the Requirements for the Degree
Doctor of Philosophy in the
School of Chemical and Biomolecular Engineering

Georgia Institute of Technology
August 2016

FORMATION AND FATE OF SECONDARY ORGANIC AEROSOL PRODUCED FROM NITRATE RADICAL OXIDATON OF MONOTERPENES

Approved by:

Dr. Nga Lee (Sally) Ng, Advisor
School of Chemical and Biomolecular Engineering
Georgia Institute of Technology

Dr. Greg Huey
School of Earth and Atmospheric Sciences
Georgia Institute of Technology

Dr. Athanasios Nenes
School of Chemical and Biomolecular Engineering
Georgia Institute of Technology

Dr. Carsten Sievers
School of Chemical and Biomolecular Engineering
Georgia Institute of Technology

Dr. Rodney Weber
School of Earth and Atmospheric Sciences
Georgia Institute of Technology

Date Approved: May 31st, 2016

ACKNOWLEDGEMENTS

There is a long list of people who have contributed greatly to the completion of this dissertation. Specifically, I would like to thank my thesis advisor, Dr. Sally Ng, for her support and guidance through these last four years. She has imparted to me skills that are applicable to both my research goals and future goals, including critical thinking, effective communication, a sense of urgency in completing tasks, and personal accountability. Without this example, I would not have grown as much as I have over my time at Georgia Tech.

I would also like to thank each of my committee members for their contributions to my research. I would like to thank Dr. Athanasios Nenes for his supportive suggestions on my research at our shared group meetings. I would also like to thank Dr. Rodney Weber for his generous assistance in the construction of the chamber, his useful atmospheric chemistry, physics and instrumentation classes, and his helpful advice regarding my studies. Dr. Greg Huey has also been very supportive regarding use of and instruction for his Chemical Ionziatization Mass Spectrometer and knowledge of gas-phase chemistry. I would also like to thank Dr. Carsten Sievers, for keeping me focused on the bigger picture of the research goals.

I acknowledge my labmates not just for their contributions to my endeavors but also as supportive friends. Lu Xu and Dr. Theo Nah have provided excellent professional examples and have been quick to offer support on my presentations and papers. Javier Sanchez has always provided assistance when things just needed to get done, from equipment failure to providing good quality gas-phase data for my experiments. Wing

Tuet has also provided unbridled optimism when research was not going as planned. I would also like to thank members of the Nenes, Weber, and Huey groups for their valuable input and assistance whenever needed. In particular, I would like to thank David Tanner, whose vast knowledge of electrical and mechanical systems have contributed greatly to the construction of our chamber facility.

Finally, I would like to thank my friends and family for their continued support. I would like to thank all of my friends at Georgia Tech for sharing much laughter during our time here. I would also like to thank my parents and siblings, both by blood and by marriage, for providing me much needed love and support. I would especially like to thank my wife, Helen, who has sacrificed much these past four years to give me the best opportunity to succeed, has provided me with substantial professional development, been pleasant company in times of hardship, and is also a pretty good cook. Without their support, none of this work would have been possible.

TABLE OF CONTENTS

LIST OF TABLES

LIST OF FIGURES

SUMMARY

Atmospheric aerosol, or particulate matter, has important implications for climate, visibility and health. A large portion of atmospheric aerosol is comprised of secondary organic aerosol (SOA), which is formed by the oxidation of volatile organic compounds (VOCs) with atmospheric oxidants, including the nitrate (NO_3) radical. Reducing the impact of human pollution on aerosol formation is challenging, in large part because of the complexities in the mechanisms for the formation of organic aerosol through the oxidation of VOCs. The oxidation of biogenic volatile organic compounds (BVOCs) by NO_3 radical, formed by the reaction of O_3 with anthropogenic NO_2, provides one example of the effect of human activities on atmospheric aerosol. Due to the high aerosol mass yields of BVOC+NO_3 reactions, this pathway can contribute to a large fraction of atmospheric aerosol.

In addition to high aerosol mass yields, the BVOC+NO_3 reaction produces a large mass of particulate and gas-phase organic nitrates. Organic nitrate formation, which involves loss of atmospheric NO_x ($NO+NO_2$), can either act as a permanent sink for NO_x or a temporary reservoir for NO_x. The role of organic nitrates on the NO_x cycle is highly dependent on the types and eventual fate of organic nitrates, whether by deposition, hydrolysis to nitric acid, or release of NO_x upon photooxidation or photolysis. The effect of organic nitrates on atmospheric NO_x will impact ozone production, SOA mass and composition, and formation of atmospheric nitric acid. Nevertheless, the fate of atmospheric organic nitrates and their effect on the NO_x cycle are highly uncertain.

The goals of this work are to improve our understanding of the formation of atmospheric aerosol and organic nitrates through the BVOC+NO_3 reaction. The formation of secondary organic aerosol (SOA) from the oxidation of BVOCs via NO_3 radical is investigated in the Georgia Tech Environmental Chamber facility (GTEC). This work focuses primarily on the monoterpenes β-pinene and limonene, two globally abundant VOCs with high mass yields upon NO_3 radical oxidation. For β-pinene, aerosol yields are determined for experiments performed under both dry (RH < 2%) and humid (RH = 50% and RH = 70%) conditions. To further probe the β-pinene+NO_3 reaction, the effects of peroxy radical (RO_2) fate on aerosol formation were investigated by reacting the RO_2 radicals with either NO_3 radicals or hydroperoxy (HO_2) radicals, simulating both polluted and cleaner environments. We find that the β-pinene+NO_3 reaction leads to formation of gas-phase organic nitrate species (with molecular weights of 215 amu, 229 amu, 231 amu, and 245 amu—which are assigned molecular formulas of $C_{10}H_{17}NO_4$, $C_{10}H_{15}NO_5$, $C_{10}H_{17}NO_5$, and $C_{10}H_{15}NO_6$, respectively). Additionally, the SOA yields (defined as the mass of aerosol formed per mass of hydrocarbon reacted) in the "RO_2+NO_3 dominant" and "RO_2+HO_2 dominant" experiments and across all relative humidities are comparable. The aerosol mass yield is calculated to be 27.0-104.1% for a wide range of organic mass loadings, and approximately 45-74% of this organic aerosol is composed of organic nitrate species. It has been estimated that approximately 50% of the nighttime organic aerosol production in the southeastern United States could be due to the monoterpene oxidation by NO_3, a substantial portion of which is from the β-pinene+NO_3 reaction. This observation helps to elucidate one of the control strategies for reducing atmospheric aerosol.

While it is clear that the β-pinene+NO_3 reaction contributes to atmospheric aerosol, its impacts on organic nitrate formation and the NO_x cycle are less clear. Although humidity does not appear to affect SOA yields, there is evidence of particle-phase hydrolysis of organic nitrates, which are estimated to compose 45-74% of the organic aerosol. It is estimated that about 90 and 10% of the organic nitrates formed from the β-pinene+NO_3 reaction are primary organic nitrates and tertiary organic nitrates, respectively. While the primary organic nitrates do not appear to hydrolyze, the tertiary organic nitrates undergo hydrolysis with a lifetime of 3-4.5 hours. Organic nitrate species that do not hydrolyze are likely to either deposit and remove atmospheric NO_x or may potentially re-release NO_x into the atmosphere upon photolysis or photooxidation. The fate of these organic nitrate species must be better understood to determine their impact on the NO_x cycle.

Given the long lifetime with respect to hydrolysis of organic nitrates formed by the BVOC+NO_3 reaction, it is possible that organic nitrates formed at night will remain in the atmosphere during the night-to-day transition. The night-to-day transition is accompanied by rising surface temperatures and aerosol dilution caused by an expansion of the boundary layer. Both of these processes can potentially lead to aerosol evaporation, which must be accurately accounted for in atmospheric models in order to predict aerosol concentrations and their effect on climate, visibility, and health. We find that for the limonene+NO_3 system, very little aerosol evaporation is observed through dilution due to the non-volatile nature of SOA produced by the limonene+NO_3 reaction. To determine evaporation by heating, the enthalpy of vaporization for the limonene+NO_3 reaction is

calculated over a wide range of atmospherically relevant mass loadings. The enthalpy of vaporization is highly dependent on the aerosol mass loading and can be as high as 237 kJ mol^{-1} for loadings below 18 μg m^{-3}. We also find that there is a contrast in mass and composition between aerosol formed at 25 °C and heated to 40 °C and aerosol formed at 40 °C, indicating a resistance to aerosol evaporation. Evidence from mixtures of SOA from the limonene+NO_3 and β-pinene+NO_3 reactions suggests that high volatility species that dominate the outer edge of the aerosol hinders the evaporation of the low volatility species underneath. This resistance to evaporation can greatly affect the phase of SOA and organic nitrates form the BVOC+NO_3 system and can thus affect the organic nitrate fate.

Human activities can influence SOA formation through the BVOC+NO_3 reaction. It is clear that reductions in NO_x should therefore lead to a decrease in the contribution of SOA and organic nitrates from the BVOC+NO_3 reaction. Less certain is the fate of the organic nitrates formed from nitrate radical oxidation of BVOCs. Current evidence suggests that organic nitrates produced via nitrate radical may not be susceptible to hydrolysis, but the reaction of organic nitrates through photooxidation and photolysis are still highly uncertain. As these processes are better understood, modeling of pollutants such as O_3 and nitric acid will improve as well as the concentrations of aerosol and their impacts on climate and human health.

CHAPTER 1

INTRODUCTION

1.1 Atmospheric Organic Aerosol

Atmospheric aerosol, or particulate matter suspended in gas, has important impacts on climate, visibility, and health (Kanakidou et al., 2005). Aerosols are known to have negative health effects and has recently been characterized as a Class I carcinogen by the World Health Organization (WHO, 2014). However, there still exist many uncertainties regarding the role of atmospheric aerosol on global and regional climate. A large fraction of atmospheric aerosol is comprised of secondary organic aerosol (SOA), which is formed by the oxidation of volatile organic compounds (VOCs) with atmospheric oxidants such as the hydroxyl radical (OH), ozone (O_3), and the nitrate radical (NO_3). These oxidation processes form lower volatility products that can partition to the particle phase (Kroll and Seinfeld, 2008). Biogenic volatile organic compounds (BVOCs) such as isoprene (C_5H_8), monoterpenes ($C_{10}H_{16}$), and sesquiterpenes ($C_{15}H_{24}$), are emitted by vegetation and are believed to be the dominant contributor to global SOA formation due to their high emissions and high reactivity with major atmospheric oxidants (Kanakidou et al., 2005). Currently, there exists an apparent contradiction that ambient organic aerosol is predominantly "modern" and therefore biogenic in origin (Lewis et al., 2004; Schichtel et al., 2008; Marley et al., 2009), but it is also well-correlated with anthropogenic tracers such as carbon monoxide (Weber et al., 2007b). This apparent discrepancy can be reconciled if anthropogenic pollution influences the atmospheric oxidation of BVOCs and their aerosol formation pathways. For example, the oxidation of

BVOCs by NO_3, which is formed from the reaction of O_3 with NO_2, provides a direct link between anthropogenic pollution and the biogenic carbon in atmospheric aerosol.

The NO_3 radical is the dominant nighttime oxidant (Brown and Stutz, 2012). BVOCs react rapidly with NO_3 radicals (Atkinson and Arey, 2003a) and generally have higher SOA mass yields than the analogous photooxidation and ozonolysis reactions (e.g., (Griffin et al., 1999; Hallquist et al., 1999; Spittler et al., 2006; Ng et al., 2008b; Fry et al., 2009; Rollins et al., 2009; Fry et al., 2011; Fry et al., 2014). For example, Griffin et al. (1999) found that for β-pinene, NO_3 radical oxidation can produce as much as 4.5 and 2.4 times more aerosol than reaction with OH or O_3, respectively. The monoterpene+NO_3 reaction accounts for a substantial fraction of aerosol produced by the BVOC+NO_3 reaction due to their high global abundance (Pye et al., 2010) and high aerosol mass yields (30-100%). (Fry et al., 2014; Fry et al., 2011; Fry et al., 2009; Spittler et al., 2006; Griffin et al., 1999; Hallquist et al., 1999) As much as 15% of the global non-methane BVOC budget is comprised of monoterpenes (Guenther et al., 2012). The monoterpene+NO_3 reaction can also contribute substantially to both daytime and nighttime ambient organic aerosol since, unlike isoprene, monoterpenes are emitted both during the day and at night (Fuentes et al., 2000; Guenther et al., 2012). Previous field studies have shown that a substantial fraction of ambient organic aerosol originates from BVOC+NO_3 reactions during both daytime and nighttime (McLaren et al., 2004; Iinuma et al., 2007; Fuentes et al., 2007; Brown et al., 2009; Rastogi et al., 2011; Rollins et al., 2012; Brown et al., 2013; Rollins et al., 2013). In addition, many of these studies observed a significant increase in the amount organic aerosol and oxidation products

originating from monoterpene+NO_3 reactions at night, which suggests that monoterpene+NO_3 reactions play an important role in nighttime ambient organic aerosol formation (McLaren et al., 2004; Iinuma et al., 2007; Rastogi et al., 2011; Lee et al., 2016). The formation of SOA and particulate organic nitrates via the reaction of NO_3 with monoterpenes and their subsequent fate is the subject of this dissertation.

1.2 SOA Formation Via NO_3 Reactions

The reaction of NO_3 with unsaturated BVOCs is expected to produce a substantial amount of organic nitrate compounds, due to the direct addition of nitrate radical to the double bond (Spittler et al., 2006; Perring et al., 2009; Rollins et al., 2009; Kwan et al., 2012). Addition of the organic nitrate functionality to a molecule decreases its vapor pressure and promotes partitioning into the particle phase (Pankow and Asher, 2008). Particulate organic nitrates have been observed to form a substantial portion of atmospheric aerosol across the United States (Brown et al., 2009; Day et al., 2010; Zaveri et al., 2010; Beaver et al., 2012; Rollins et al., 2012; Fry et al., 2013; Rollins et al., 2013; Brown et al., 2013; Ayres et al., 2015; Xu et al., 2015c; Xu et al., 2015a). In the Southeastern US, particulate organic nitrates are estimated to make up to 5-10% of total organic aerosol (Xu et al., 2015a). Organic nitrate formation has a significant impact on total NO_x lifetime, especially in NO_x-limited regions where NO_x lifetime is sensitive to the formation rates of organic nitrates (Browne and Cohen, 2012).

Once formed, organic nitrates can be removed from the atmosphere through a variety of pathways—each with different implications for atmospheric nitrogen. Atmospheric NO_x can regulate O_3 concentrations, affect SOA formation, and lead to production of nitric

acid. Figure 1.1 shows a simplified diagram of the atmospheric NO_x cycle. Also shown in Figure 1.1 are the different fates of organic nitrates and how they can impact atmospheric NO_x. Deposition of gas- and particle-phase organic nitrates can effectively remove nitrogen from the atmosphere (green, Figure 1.1) while hydrolysis or photochemical reaction converts organic nitrates to other nitrogen-containing compounds (red, Figure 1.1). Photochemical conversion of organic nitrates (which includes photolysis and OH oxidation) may potentially cleave the NO_3 functional group and return NO_x to the atmosphere (Talukdar et al., 1997; Suarez-Bertoa et al., 2012; Müller et al., 2014; Nah et al., 2016). Organic nitrates can also hydrolyze to form nitric acid (Sato, 2008; Szmigielski et al., 2010; Darer et al., 2011; Hu et al., 2011; Liu et al., 2012; Bean and Hildebrandt Ruiz, 2015; Boyd et al., 2015; Rindelaub et al., 2015), which can either deposit, thus removing it from the NO_x budget, or photolyze and return NO_x to the NO_x budget. Currently, the fates of organic nitrates, and consequently how they affect the NO_x budget, are highly uncertain.

The work presented in chapters 2 and 3 of this dissertation examines the formation and fates of organic aerosol and organic nitrates formed from the β-pinene+NO_3 and limonene+NO_3 reactions, respectively. β-pinene is one of the most dominant monoterpenes in the Southeastern US (Xu et al., 2015c), while limonene is an abundant monoterpene in Northern California (Rollins et al., 2012). Previous studies have shown that limonene and β-pinene have the propensity to produce substantial organic aerosol mass upon reaction with NO_3 radicals (Fry et al., 2014; Fry et al., 2011; Fry et al., 2009; Spittler et al., 2006; Griffin et al., 1999; Hallquist et al., 1999). Nevertheless, there are no

published studies regarding SOA and organic nitrate formation under conditions that are more relevant to SE US (e.g., high RH, low particle acidity, relatively lower aerosol mass loadings). In chapter 2, we focus on aerosol and organic nitrate formation from the β-pinene+NO_3 reaction under different reaction conditions. Since surface temperatures tend to be lower at night, BVOC+NO_3 chemistry is likely to occur at high relative humidity (RH) in the ambient atmosphere. To examine the effect of humidity on aerosol formation in NO_3 reactions, aerosol yields were measured in experiments performed under both dry (RH < 2%) and humid (RH = 50% and RH = 70%) conditions. The effects of peroxy radical (RO_2) fate on aerosol formation are also studied by reacting the RO_2 radicals with either NO_3 radicals or hydroperoxy (HO_2) radicals, which mimic both polluted and cleaner environments, respectively. A fraction of the particulate organic nitrates formed from the β-pinene+NO_3 reaction undergo hydrolysis, which may convert organic nitrates to nitric acid (which subsequently evaporates from the particle). Organic nitrates that do not hydrolyze may deposit or photolyze. In chapter 3, we examine the physical changes of aerosol produced from the limonene+NO_3 reaction that typically accompany the night-to-day transition in the ambient atmosphere (i.e. aerosol dilution and heating). The night-to-day transition leads to an increase in surface temperatures and a dilution of the boundary layer. Both changes can affect the volatility and partitioning of organics and lead to the evaporation of organic aerosol. To examine the effect of temperature on the organic aerosol formed from the limonene+NO_3 reaction, the reaction was performed at an initial temperature of either 25 °C or 40 °C. The aerosol formed at these temperatures was compared to aerosol initially formed at 25 °C and heated to 40 °C. To study the effect of dilution, the chamber was diluted with air (by up to a factor of 2) in order to

induce evaporation of the organic aerosol. The evaporation of organic aerosol through either method, however, could be significantly hindered if organic aerosol exists as a viscous semi-solid. In order to probe the viscosity of products from the BVOC+NO_3 reaction, mixtures of SOA formed from the limonene+NO_3 and β-pinene+NO_3 reactions were created with different aerosol morphologies and their evaporation kinetics were determined.

In the remaining section of this chapter, an overview of the different measurement techniques and tools used in this dissertation to study SOA formation via NO_3 chemistry is presented.

1.3 Laboratory Studies of SOA Formation from NO_3 Chemistry

1.3.1 Chamber Construction/Description

All experiments are performed in the Georgia Tech Environmental Chamber facility (GTEC), which consists of two 12 m^3 flexible Teflon (FEP 2 mil) chambers suspended in a 21 ft. x 12 ft. temperature-controlled enclosure. The full operational temperature range of the facility is 4–40 ±0.5 ^oC. A schematic of the chamber facility is shown in Figure 1.2. Each of the chambers has three Teflon manifolds with multiple sampling ports. Ports allow for the introduction of clean air, gas-phase reagents, seed aerosol, and for measurements of RH, temperature, gas-phase composition, and particle-phase composition. The chambers are surrounded by blacklights (Sylvania, 24922) with output predominately in the ultraviolet region between 300 nm and 400 nm, with a maximum at 354 nm. The blacklights are supplemented by natural sunshine fluorescent lights

(Sylvania, 24477), which have wavelengths between 300 nm to 900 nm. The j_{NO2} of the chamber facility is 0.28 min^{-1} when all of the blacklights are turned on.

1.3.2 HR-ToF-AMS

Bulk particle chemical composition is measured with an Aerodyne High Resolution Time-of-Flight Aerosol Mass Spectrometer (HR-ToF-AMS). The working principles and operation of the HR-ToF-AMS are described in detail elsewhere (DeCarlo et al., 2006) and will be discussed briefly here. Aerosol is sampled through an aerodynamic lens and focuses the aerosol into a beam. The aerosol mass distribution is determined from the length of time for aerosol to be detected after passing through a rotating chopper. The aerosol is impacted onto a heated surface (600 °C) where it is flash vaporized. Once evaporated, the gas phase analytes are impacted with an electron beam and ionized before detection by a mass spectrometer. Non-refractive organics, nitrate, sulfate, ammonium, and chlorine can be measured by the HR-Tof-AMS. In the high-resolution mode, ions with the same nominal mass (e.g. NO^+ and CH_2O^+ at m/z 30) can be separated to determine the unique composition of the bulk aerosol. Elemental analysis is also performed on the data to determine the elemental composition (e.g., O:C, N:C ratios) of the bulk aerosol (Canagaratna et al., 2015) which allow for estimation of organic nitrate mass in the particle phase.

1.3.3 Q-CIMS with I- reagent

Gas-phase oxidation products and N_2O_5 are measured using a Quadrupole Chemical Ionization Mass Spectrometer (CIMS) in Chapter 2. Iodide ion (I^-) is used as the reagent ion, which has previously been shown to selectively ionize reactive nitrogen species,

peroxides, and carboxylic acids (Huey, 2007; McNeill et al., 2007; Zhao et al., 2012). Iodide ionization proceeds primarily via clustering to produce an iodide-molecule cluster which preserves the integrity of the analyte. The gas-phase species are detected as *m/z* = MW+127. Masses with specific *m/z* are selected for detection using a quadrupole mass filter. These species are then detected by an electron multiplier which amplifies incident charge through secondary electron emission to produce a measurable current that scales with gas-phase concentration. Due to unavailability of standards for the oxidation products, the instrument is not calibrated for these compounds and concentrations are not reported. Nevertheless, the CIMS data allow for the tentative identification and comparison of the abundance of specific gas-phase oxidation products formed under different experimental conditions.

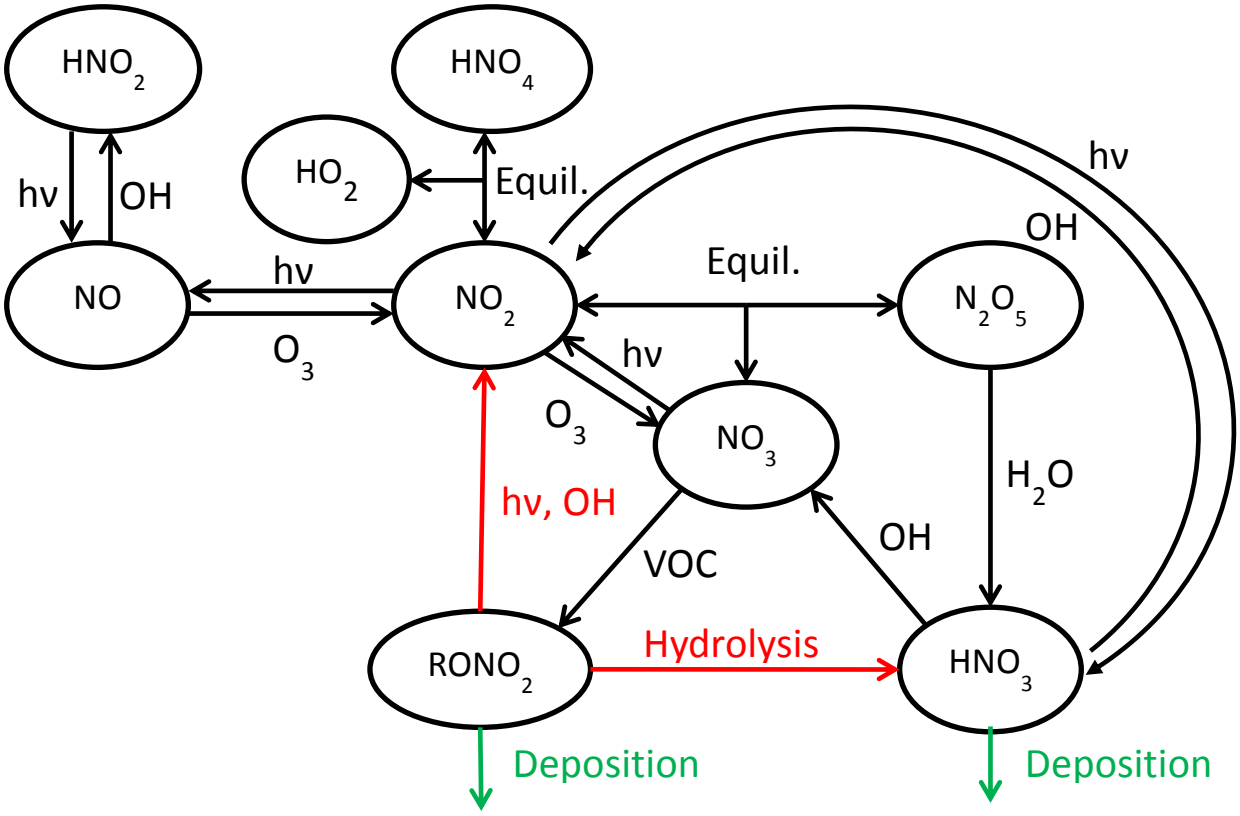

Figure 1.1: The NO_x Cycle

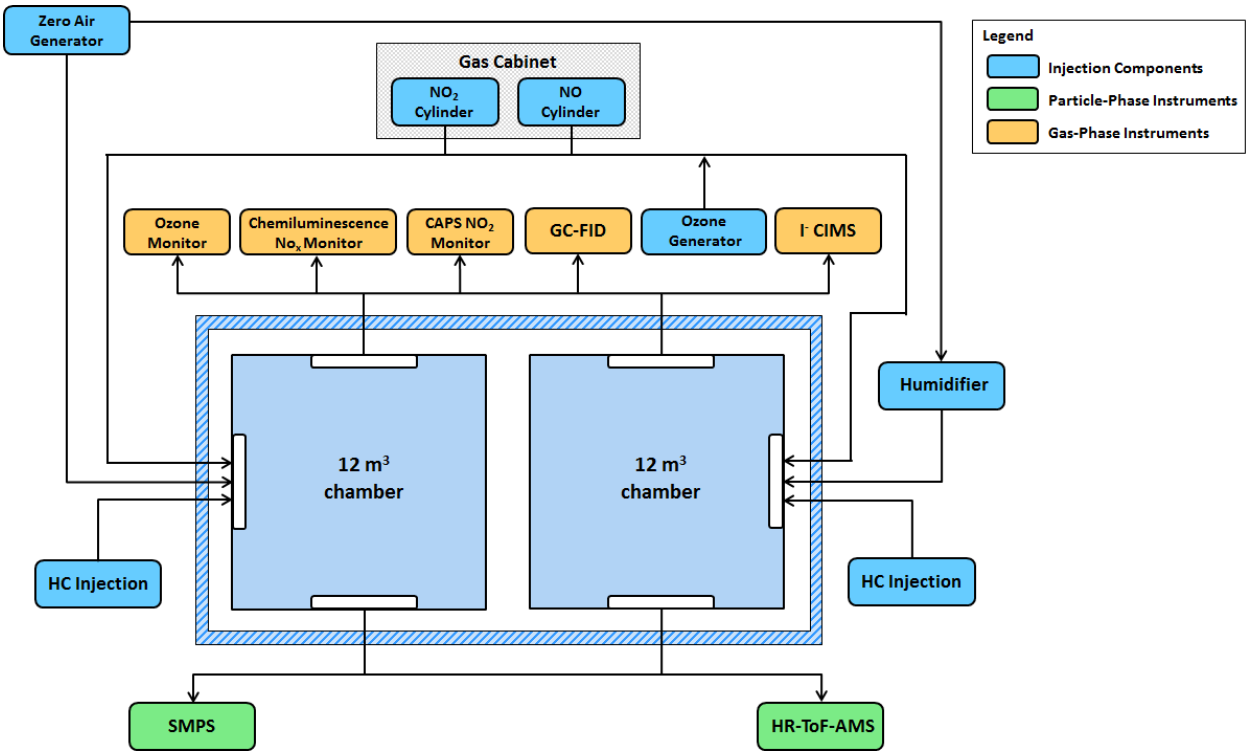

Figure 1.2: Schematic of the Georgia Tech Environmental Chamber facility (GTEC).

CHAPTER 2

SECONDARY ORGANIC AEROSOL (SOA) FORMATION FROM THE β-PINENE+NO_3 SYSTEM: EFFECT OF HUMIDITY AND PEROXY RADICAL FATE

2.1 Introduction

Owing to their high emissions and high reactivity with the major atmospheric oxidants (O_3, OH, NO_3), the oxidation of biogenic volatile organic compounds (BVOCs) emitted by vegetation, such as isoprene (C_5H_8), monoterpenes ($C_{10}H_{16}$), and sesquiterpenes ($C_{15}H_{24}$), is believed to be the dominant contributor to global secondary organic aerosol (SOA) formation (e.g., (Kanakidou et al., 2005). While this is supported by the observation that ambient organic aerosol is predominantly "modern" and therefore biogenic in origin (Lewis et al., 2004; Schichtel et al., 2008; Marley et al., 2009), there exists an apparent contradiction because ambient organic aerosol is well-correlated with anthropogenic tracers (de Gouw et al., 2005; Weber et al., 2007b). This apparent discrepancy could be reconciled if anthropogenic pollution influences the atmospheric oxidation of BVOCs and their aerosol formation pathways. The oxidation of BVOCs by nitrate radicals (NO_3), formed from the reaction of ozone with NO_2, provides a direct link between anthropogenic pollution and the abundance of biogenic carbon in atmospheric aerosol.

The text in this chapter is reproduced, in part, by: Boyd, C. M., Sanchez, J., Xu, L., Eugene, A. J., Nah, T., Tuet, W. Y., Guzman, M. I., and Ng, N. L.: Secondary organic aerosol formation from the β-pinene+NO3 system: effect of humidity and peroxy radical fate, Atmos. Chem. Phys., 15, 7497-7522, doi:10.5194/acp-15-7497-2015, 2015

Biogenic hydrocarbons react rapidly with nitrate radicals (Atkinson and Arey, 2003a) and the secondary organic aerosol (SOA) yields are generally higher than in photooxidation and ozonolysis (e.g., (Griffin et al., 1999; Hallquist et al., 1999; Spittler et al., 2006; Ng et al., 2008b; Fry et al., 2009; Rollins et al., 2009; Fry et al., 2011; Fry et al., 2014). As monoterpene emissions are not entirely light-dependent, they are emitted during the day and at night (Fuentes et al., 2000; Guenther et al., 2012) and can contribute substantially to ambient organic aerosol. Monoterpenes have also been found to make up as much as 28% of non-methane organic carbon emissions from biomass burning in both field and laboratory studies (Akagi et al., 2013; Hatch et al., 2015; Stockwell et al., 2015). Fires from biomass burning are more likely to smolder at night and are therefore more likely to emit monoterpenes, which can then react with nitrate radicals (Akagi et al., 2013). Results from previous field studies provided evidence of aerosol formation from nitrate radical oxidation of BVOCs during both daytime and nighttime (McLaren et al., 2004; Iinuma et al., 2007; Fuentes et al., 2007; Brown et al., 2009; Rastogi et al., 2011; Rollins et al., 2012; Brown et al., 2013; Rollins et al., 2013). Specifically, many of these studies found a significant increase in the amount of monoterpene organic aerosol and oxidation products at night, which could be attributed to nighttime monoterpene oxidation by nitrate radicals (McLaren et al., 2004; Iinuma et al., 2007; Rastogi et al., 2011). Results from recent flight measurements in Houston, TX also showed that organic aerosol was enhanced in the nocturnal boundary layer at levels in excess of those attributable to primary emissions, implying a source of SOA from the BVOCs+NO_3 reaction (Brown et al., 2013).

Global modeling studies showed large variations in the total SOA burden that can be attributed to the oxidation of BVOCs by nitrate radicals, ranging from ~5 to 21% (Hoyle et al., 2007; Pye et al., 2010). Specifically, Pye et al. (2010) showed that the inclusion of nitrate radical oxidation reaction doubled the total amount of terpene (monoterpenes and sesquiterpenes) aerosol, pointing to the significant contribution of this chemistry to total organic aerosol burden. In these modeling studies, all aerosol formation from the nitrate radical oxidation of terpenes was calculated based on the β-pinene+NO_3 SOA yields obtained in Griffin et al. (1999). A recent modeling study by Russell and Allen (2005) determined that as much as 20% of all nighttime SOA is from the reaction of β-pinene+NO_3. Due to the significance of nitrate radical oxidation pathway in SOA formation, it is important that the SOA yields for BVOCs+NO_3, and especially that of β-pinene+NO_3, are well-constrained from fundamental laboratory studies and accurately represented in models.

The majority of the previous laboratory studies of the BVOCs+NO_3 chemistry was performed under dry conditions (Berndt and Boge, 1997a, b; Wängberg et al., 1997; Griffin et al., 1999; Hallquist et al., 1999; Bonn and Moorgat, 2002; Spittler et al., 2006; Ng et al., 2008b; Rollins et al., 2009; Fry et al., 2009; Perraud et al., 2010; Fry et al., 2011; Kwan et al., 2012; Jaoui et al., 2013; Fry et al., 2014). The effect of relative humidity on SOA formation, however, could potentially be important for nighttime (where NO_3 radicals dominate) and early morning chemistry as the ambient RH is typically higher at these times. Several recent studies have investigated the effect of water on SOA formation from the nitrate radical oxidation pathway but the results are

inconclusive. For instance, Spittler et al. (2006) found that the SOA yield is lower at 20% RH compared to dry conditions, suggesting that water vapor may alter the gas-phase oxidation mechanism and/or partitioning into the particle phase, thus shifting the equilibrium partitioning of organic compounds. However, other studies showed that the presence of water vapor did not affect particle size distributions and SOA formation (Bonn and Moorgat, 2002; Fry et al., 2009). Thus, the role of water in SOA formation from nitrate radical oxidation of BVOCs is still unclear.

Another important parameter in SOA formation from BVOCs+NO_3 is the fate of peroxy radicals, which directly determines the oxidation products, SOA yields, and aerosol chemical and physical properties (Kroll and Seinfeld, 2008; Orlando and Tyndall, 2012; Ziemann and Atkinson, 2012). Previous studies regarding the effects of peroxy radical fates on SOA formation from BVOCs typically focused on photooxidation and ozonolysis systems (e.g., (Presto et al., 2005; Kroll et al., 2006; Ng et al., 2007b; Eddingsaas et al., 2012; Xu et al., 2014) and isoprene+NO_3 chemistry (Ng et al., 2008b; Kwan et al., 2012; Nguyen et al., 2014). To our knowledge, the effects of differing peroxy radical branching on SOA formation from nitrate radical oxidation of monoterpenes have not been investigated. The relative importance of different peroxy radical reaction channels concerning BVOCs+NO_3 chemistry in the atmosphere is not well established (Brown and Stutz, 2012). While earlier studies by Kirchner and Stockwell (1996) suggested that RO_2+NO_3 is more important in the nighttime atmosphere, a recent study by Mao et al. (2012) showed that the HO_2 mixing ratios are

often on the order of 10 ppt at night. It is therefore possible that RO_2+HO_2 pathway could be an important pathway in nighttime oxidation of BVOCs.

Nitrate radical chemistry is expected to produce a substantial amount of organic nitrate compounds, owing to direct addition of nitrate radical via reaction with a double bond. Organic nitrates have been observed to form a substantial portion of atmospheric aerosol in field studies (Brown et al., 2009; Day et al., 2010; Zaveri et al., 2010; Beaver et al., 2012; Rollins et al., 2012; Fry et al., 2013; Rollins et al., 2013; Brown et al., 2013; Xu et al., 2015a). Organic nitrate formation has a significant impact on total NO_x lifetime, especially in NO_x-limited regions where NO_x lifetime is sensitive to the formation rates of organic nitrates (Browne and Cohen, 2012). Ambient organic nitrates can be formed through photooxidation of VOCs in the presence of NO_x (Chen et al., 1998; Arey et al., 2001; Yu et al., 2008) and through nitrate radical addition (Spittler et al., 2006; Perring et al., 2009; Rollins et al., 2009; Kwan et al., 2012). One removal mechanism for atmospheric organic nitrates is hydrolysis in the particle phase (e.g., (Sato, 2008; Szmigielski et al., 2010; Darer et al., 2011; Hu et al., 2011; Liu et al., 2012; Rindelaub et al., 2015). Modeling studies have assumed that the majority (75%) of the organic nitrates formed in the day are composed of tertiary nitrates based on results from the photooxidation of α-pinene and β-pinene in the presence of NO_x (Browne et al., 2013). However, the organic nitrates formed from photooxidation and nitrate radical oxidation could have different chemical structures (primary, secondary, and tertiary) and need to be investigated to better constrain the fates of organic nitrates (e.g., hydrolysis lifetime) in the atmosphere over their entire life cycle (both day and night).

The goal of this study is to determine the aerosol yields and characterize the mechanisms and chemical composition of SOA formation from the β-pinene+NO_3 system. Laboratory chamber experiments are performed in the dark under dry and humid conditions. To investigate the effects of peroxy radical fates on SOA yields and chemical composition, the experiments are designed to probe the "RO_2+NO_3" vs. "RO_2+HO_2" reaction pathways. Aerosol yields are obtained over a wide range of initial β-pinene mixing ratios. Based on the measured gas-phase and particle-phase oxidation products, mechanisms for SOA formation from β-pinene+NO_3 are proposed. Results from this study are used to evaluate the contributions of nitrate radical oxidation of monoterpenes to ambient organic aerosol measured in the southeastern United States (US), including the Southern Oxidant and Aerosol Study (SOAS) and the Southeastern Center for Air Pollution and Epidemiology (SCAPE) study.

2.2 Experimental

2.2.1 Laboratory Chamber Experiments

All experiments are performed in the Georgia Tech Environmental Chamber facility (GTEC), which consists of two 12 m^3 flexible Teflon (FEP 2 mil) chambers suspended in a 21 ft. x 12 ft. temperature-controlled enclosure. The full operational temperature range of the facility is 4–40 ±0.5 ^oC. A schematic of the chamber facility is shown in Figure 1.2. Each of the chambers has three Teflon manifolds with multiple sampling ports. Ports allow for the introduction of clean air, gas-phase reagents, seed aerosol, and for measurements of RH, temperature, gas-phase composition, and particle-phase composition. The chambers are surrounded by blacklights (Sylvania, 24922) with output

predominately in the ultraviolet region between 300 nm and 400 nm, with a maximum at 354 nm. The blacklights are supplemented by natural sunshine fluorescent lights (Sylvania, 24477), which have wavelengths between 300 nm to 900 nm. The j_{NO2} of the chamber facility is 0.28 min^{-1} when all of the blacklights are turned on.

Experimental conditions are summarized in Table 2.1. Prior to each experiment, the chambers are cleaned by flowing pure air (generated from AADCO, 747-14) for at least 24 hours at a rate of 40 LPM, or equivalent to 0.2 chamber volumes per hour. This ensures that the ozone, NO, and NO_2 concentrations are less than 1 ppb and the particle concentration is lower than 10 cm^{-3}. Experiments are performed in the dark under either dry (RH < 2%) or humid (RH = 50%, 70%) conditions. The air is humidified by passing pure air through bubblers prior to introduction into the chamber. The temperature and humidity inside each Teflon chamber are measured using a hygrothermometer (Vaisala, HMP110). Seed aerosol is generated by atomizing an ammonium sulfate solution (8 mM) or an ammonium sulfate/sulfuric acid mixture ($[(NH_4)_2SO_4]$:$[H_2SO_4]$ = 3:5, molar ratio) into the chamber. The seed number and mass concentrations prior to typical experiments are approximately 2.0×10^4 cm^{-3} and 30 μg m^{-3}. The pH of the $(NH_4)_2SO_4$ seed and $(NH_4)_2SO_4$+H_2SO_4 seed at RH = 50% is about 4.6 and 2.4, respectively, based on calculations from prior studies (Gao et al., 2004). Nucleation experiments are performed under both dry and humid (RH = 50%, 70%) conditions to determine organic aerosol density and characterize vapor wall loss effects on SOA yields. All experiments are performed at 298 K.

Experiments are designed to probe the effects of peroxy radical chemistry (RO_2+HO_2 vs. RO_2+NO_3) on SOA formation from the reaction of β-pinene with nitrate radicals. The procedure for chemical injection depends on the desired fate of the peroxy radicals in the experiments. To enhance the branching ratio of RO_2+HO_2 in the chamber experiments, formaldehyde is first added to the chamber (Nguyen et al., 2014). Formalin solution (Sigma-Aldrich, 37% HCHO) is injected into a glass bulb and clean air is passed over the solution until it evaporates. After this, seed aerosol, NO_2 (Matheson, 500 ppm), and ozone (generated by passing zero air through a UV radiation cell, Jelight 610, 80ppm) are injected into the chamber. NO_2 and O_3 concentrations are chosen ($[NO_2]$:$[O_3]$ ≈ 4:3) to ensure that 99% of the β-pinene reacts with nitrate radicals instead of ozone. The NO_2 and O_3 react to form nitrate radicals and subsequently N_2O_5 through the following reactions:

$$NO_2 + O_3 \rightarrow NO_3 + O_2 \quad \text{(A1)}$$

$$NO_3 + NO_2 \leftrightarrow N_2O_5 \quad \text{(A2)}$$

Formaldehyde then reacts with nitrate radicals to form HO_2 radicals via the following reaction:

$$HCHO + NO_3 + O_2 \rightarrow HNO_3 + CO + HO_2 \quad \text{(A3)}$$

Enough formaldehyde (3-22 ppm) is added to the chamber to ensure that the RO_2+HO_2 radical branching ratio is an order of magnitude higher than the RO_2+RO_2 and RO_2+NO_3

pathways (Supplement). The chamber content is allowed to mix for ~30 minutes, after which a desired amount of β-pinene is injected into a glass bulb, where it is introduced into the chamber by passing clean air through the glass bulb. Introduction of β-pinene into the chamber marks the beginning of the experiment. We refer to this set of experiments as "RO_2+HO_2 dominant" experiments.

For "RO_2+NO_3 dominant" experiments, seed aerosol is first introduced into the chamber, followed by β-pinene injection. After allowing ~30 minutes for the β-pinene concentration to stabilize, N_2O_5 is injected into the chamber. To generate N_2O_5, a mixture of NO_2 and O_3 is pre-reacted in a flow tube (flow rate = 0.5 LPM NO_2 + 0.8 LPM O_3, residence time = 71 sec) before entering the chamber. The N_2O_5 concentration is estimated by modeling the reaction of NO_2 and O_3 in the flow tube. For this set of experiments, the introduction of N_2O_5 marks the beginning of the experiment. We aim for an initial N_2O_5:β-pinene ratio of ~6:1. It is noted that the ozone concentration in the chamber is sufficiently low that at least 99% of β-pinene reacts with nitrate radicals. N_2O_5 continuously dissociates to form NO_2 and nitrate radicals during the experiment to reestablish equilibrium as the nitrate radicals react with β-pinene. The high initial N_2O_5 and nitrate radical concentrations relative to β-pinene favor the RO_2+NO_3 pathway.

For all experiments except "RO_2+HO_2 dominant" experiments conducted under humid conditions (RH = 50%, 70%), a Gas Chromatograph-Flame Ionization Detector (GC-FID, Agilent 7890A) measures a β-pinene concentration of zero (below detection limit) within the first scan (scan time = 11.7 min) after the experiment begins. This suggests that β-

pinene is completely consumed within 11.7 minutes of N_2O_5 injection for the "RO_2+NO_3 dominant" experiments and that β-pinene is fully reacted away before being detected by the GC-FID in the "RO_2+HO_2 dominant" experiments under dry conditions. The concentration of β-pinene is calculated from the mass of the hydrocarbon injected and the volume of the chamber. The chamber volume is determined to be approximately 12 m^3 by injecting a known volume of NO_2 standard (Matheson, 500 ppm) into the chamber and measuring the resulting NO_2 concentration inside the chamber.

Ozone and NO_x concentrations are monitored with an O_3 Analyzer (Teledyne T400) and an ultrasensitive chemiluminescence NO_x monitor (Teledyne 200EU), respectively. Total aerosol volume and size distributions are measured with a Scanning Mobility Particle Sizer (SMPS, TSI). The SMPS consists of a differential mobility analyzer (DMA) (TSI 3040) and Condensation Particle Counter (CPC) (TSI 3775). Bulk particle chemical composition is measured with an Aerodyne High Resolution Time-of-Flight Aerosol Mass Spectrometer (HR-ToF-AMS). The working principle and operation of the HR-ToF-AMS are described in detail elsewhere (DeCarlo et al., 2006). The HR-ToF-AMS provides quantitative measurements of organics, nitrate, sulfate, ammonium, and chloride. Elemental analysis is performed on the data to determine elemental composition (e.g., O:C, N:C ratios) of the bulk aerosol (Canagaratna et al., 2015).

A suite of gas-phase oxidation products and N_2O_5 are measured using a Quadrupole Chemical Ionization Mass Spectrometer (CIMS) with I^- as the reagent ion, which has high selectivity towards reactive nitrogen species, peroxides, and carboxylic

acids (Huey, 2007; McNeill et al., 2007; Zhao et al., 2012). The CIMS uses methyl iodide to produce I^- ions that ionize gas-phase products through association (Slusher et al., 2004; Zheng et al., 2011). It has been shown that I^- addition to gas-phase molecules provides a molecule-iodide adduct that preserves the original species of the compounds being sampled. The gas-phase species are detected as *m/z* = MW+127. Masses with specific *m/z* are selected for detection using a quadrupole mass filter. These species are then detected by an electron multiplier which amplifies incident charge through secondary electron emission to produce a measurable current that scales with gas-phase concentration. Due to unavailability of standards for the oxidation products, the instrument is not calibrated for these compounds and concentrations are not reported. However, the CIMS data allow for identification and comparison of the abundance of specific gas-phase oxidation products formed in different experimental conditions.

2.2.2 Analysis of Particle-Phase Products

Aerosol samples are collected on Teflon filters (Pall Corp. R2PL047, 1-μm pore size and 47-mm diameter) during the SOA experiments (Experiments 9, 10, 22, 23, 32, 33 in Table 2.1) and for a series of blank/control experiments. These blank experiments are 1) clean chamber (no aerosol) at RH < 2%, 2) clean chamber (no aerosol) at RH = 50%, 3) clean chamber at RH =50% with only N_2O_5 injected, and 4) clean chamber at RH < 2% with only β-pinene injected. All filters collected during the chamber experiments and controls are stored at a temperature below −20°C before sample extraction and preparation for chromatographic analysis.

Each filter is extracted twice by sonication (Branson 3510) for 15 min in 2.50 mL acetonitrile (Fisher Optima, LC-MS grade). After combining both aliquots, each extracted sample is blown dry under a gentle stream of nitrogen (Scott-Gross, UHP), reconstituted with 1000 μL acetonitrile, and transferred to a chromatographic vial. Samples are analyzed with an Accela (Thermo Fisher Scientific) ultra-high-performance liquid chromatographer (UHPLC) equipped with a 1250 quaternary delivery pump, a photodiode array detector (PDA) with a 5-cm LightPipe flow cell, and a mass spectrometry (MS) detector (Thermo MSQ Plus). Samples are injected (50 μL) with an Accela autosampler into the reversed-phase chromatographic column (Hypersil gold C18, 50 × 2.1 mm, 1.9 μm particle size, Thermo Scientific). Excalibur software is used to control the UHPLC-PDA-MS system. Chromatographic separation at a constant flow rate of 800 μL min^{-1} from 0 to 1 min is isocratic with 90% (A) 0.10 mM formic acid (Fisher Optima, LC-MS grade) in ultrapure water (18.2 MΩ cm Purelab Flex, Veolia) and 10% (B) 0.10 mM formic acid in acetonitrile. Gradient elution from 1 to 8 min reaches a 10:90 ratio of solvents A:B and remain isocratic from 8 to 10 min. Selected chromatograms utilize 0.4-1.0 mM acetic acid (Acros, glacial ACS, 100.0% by assay) instead of 0.1 mM formic acid in the mobile phase. After the PDA registered the UV–visible spectra from 190 to 700 nm, the flow is interfaced with an electrospray ionization (ESI) probe (1.9 kV needle voltage, 350°C probe temperature, and 70 psi N_2 nebulizing gas) to the MS detector set to detect negative ions in the range of *m/z* 50 to 650 amu. Selected samples are analyzed under variable cone voltage (10-100 V) to register the fragmentation pattern of the peaks and gain structural information of the products. The extraction method

shows an efficient 98.8% recovery, when 98.6 μg of 4-nitrophenol (Acros, 98.0%) are spiked onto a blank filter.

2.3 Results

Gas-phase oxidation and aerosol growth is observed to be a rapid process in the β-pinene+NO_3 reaction. Peak aerosol growth is typically observed within 10-15 minutes for all reaction conditions except in humid (RH= 50%, 70%) "RO_2+HO_2 dominant" experiments, where aerosol reaches peak growth in about 30 minutes. Figure A.1 shows a typical mass spectrum for the CIMS data. Specifically, the major gas-phase products are detected at *m/z* 342, 356, 358, and 372 (which correspond to MW = 215 amu, 229 amu, 231 amu, 245 amu, respectively). These compounds likely correspond to organic nitrate species with molecular assignments of $C_{10}H_{17}NO_4$, $C_{10}H_{15}NO_5$, $C_{10}H_{17}NO_5$, and $C_{10}H_{15}NO_6$, respectively. Figure 2.2 shows the time series of these species and the aerosol growth over the course of a typical "RO_2+HO_2 dominant" experiment in dry conditions. The products at *m/z* 356 and 358 (MW = 229 amu and 231 amu) decrease over the course of the experiment. While this can be attributed to vapor phase wall loss, it is also possible that these gas-phase compounds undergo further reaction. This is further supported by the increase in the species at *m/z* 372 (MW = 245 amu). The proposed gas-phase oxidation mechanism and formation of compounds at *m/z* 372 from compounds at *m/z* 356 will be discussed further in Section 2.4.1.

Although all the above gas-phase species are observed under all reaction conditions, *m/z* 358 (MW = 231 amu) is significantly higher in the "RO_2+HO_2 dominant" experiments than in the "RO_2+NO_3 dominant" experiments (Figure A.2), which is indicative of

differences in the gas-phase chemistry depending on the RO_2 fate. Under both "RO_2+HO_2 dominant" and "RO_2+NO_3 dominant" conditions, experiments conducted under dry conditions have significantly higher N_2O_5 concentrations than humid conditions (by at least a factor of 2) as measured by CIMS. This is likely due to N_2O_5 uptake (loss) on the wet chamber surfaces and/or seed aerosol. The relative abundance of N_2O_5 under different experimental conditions is important in terms of β-pinene reaction rate and aging of aerosol, which are discussed in Sections 2.4.2.2 and 2.4.4, respectively.

All SOA growth data are corrected for particle wall loss by applying size-dependent wall loss coefficients determined from wall loss experiments at GTEC following the methodology described in Keywood et al. (2004). The size-dependent particle wall loss rates calculated for both chambers at GTEC are shown in Figure A.3. Figures 2.2 and 2.3 show the SOA yields for "RO_2+NO_3 dominant" and "RO_2+HO_2 dominant" experiments over a wide range of aerosol mass loadings (ΔM_o = 5.1-216.1 μg m^{-3}). The SOA yields lie in the range of 27.0-104.1% over the conditions studied. Aerosol mass yield (Y) is defined as the aerosol mass concentration produced (ΔM_o) divided by the mass concentration of hydrocarbon reacted (ΔHC), $Y = \Delta M_o/\Delta HC$ (Odum et al., 1996; Bowman et al., 1997; Odum et al., 1997b; Odum et al., 1997a). For all experiments, aerosol mass concentration is obtained from the SMPS aerosol volume concentration (averaged over 30 min at peak growth) and the calculated aerosol density. The aerosol density is calculated from the SMPS volume distribution and the HR-ToF-AMS mass distribution in the nucleation experiments (Bahreini et al., 2005). The densities of the organic aerosol generated in nucleation experiments under dry and humid (RH = 50%, 70%) conditions

are determined to be 1.41 g cm^{-3} and 1.45 g cm^{-3} for the "RO_2+NO_3 dominant" experiments and 1.54 g cm^{-3} and 1.61 g cm^{-3} for the "RO_2+HO_2 dominant" experiments.

It can be seen from Figure 2.2 that the aerosol yields in the "RO_2+NO_3 dominant" experiments under dry vs. humid conditions in the presence of $(NH_4)_2SO_4$ seed are similar. The presence of the more acidic $(NH_4)_2SO_4$+H_2SO_4 seed does not appear to enhance SOA production in the "RO_2+NO_3 dominant" experiments (Figure A.4). Therefore, we fit the Odum two-product model (Odum et al., 1996; Odum et al., 1997a) to all of our experimental data shown in Figure 2.2 to obtain a single yield curve. The SOA yield parameters are given in Table 2.2. Shown in Figure 2.3 are the aerosol yields from "RO_2+HO_2 dominant" experiments under dry vs. humid (RH = 70%) conditions. The SOA yield curve (solid red line) for the "RO_2+NO_3 dominant" experiments is also shown for comparison.

For comparison, SOA yields from previous β-pinene+NO_3 laboratory chamber studies (Griffin et al., 1999; Fry et al., 2009) are also shown in Figure 2.2. Without adding HCHO as an additional HO_2 source, it is likely that the experiments in Griffin et al. (1999) and Fry et al. (2009) are more similar to our "RO_2+NO_3 dominant" experiments. Specifically, Fry et al. (2009) noted that the β-pinene+NO_3 reaction likely does not produce significant concentrations of HO_2 radicals and therefore have a low HO_2/RO_2 ratio. As Griffin et al. (1999) assumed an aerosol density of 1.0 g cm^{-3}, the experimental data from Griffin et al. (1999) shown in Figure 2.2 has been multiplied by the density calculated in our study for "RO_2+NO_3 dominant" experiments under dry conditions (i.e.,

1.41 g cm^{-3}). The data shown in Figure 2.2 from Fry et al. (2009) have also incorporated a particle density of 1.6 g cm^{-3} calculated in their study. In addition to correcting for density, the yield curve partitioning coefficient, K, from Griffin et al. (1999) has been adjusted from 306K to 298K using an enthalpy of vaporization of 42 kJ mol^{-1} for comparison to results from our study (Chung and Seinfeld, 2002). It is noted that the SOA yields obtained in the current study are higher than those in Griffin et al. (1999) and Fry et al. (2009), particularly at lower aerosol mass loadings that are more relevant to ambient environments. These results are discussed in more detail in Section 2.4.2.

Bulk aerosol composition from the experiments is characterized by the HR-ToF-AMS. A typical high-resolution mass spectrum for aerosol formed under dry conditions where the RO_2+NO_3 pathway is dominant (Experiment 5 in Table 2.1) is shown in Figure 2.4. A key feature of the mass spectrum is the high intensity of the nitrate ions at NO^+ and NO_2^+, which make up about 11% of the combined organics and nitrate signals. The majority (> 90%) of the nitrogen atoms is detected at these two ions with the remaining nitrogen-containing ions detected at higher masses as $C_xH_yO_zN$. The mass spectra for the aerosol generated in the "RO_2+HO_2 dominant" and "RO_2+NO_3 dominant" experiments are similar. One notable difference between the "RO_2+HO_2 dominant" and "RO_2+NO_3 dominant" experiments is the NO^+:NO_2^+ ratio for the organic nitrates (R-ON), which ranges from 4.8-10.2 in all experiments. While the NO^+:NO_2^+ ratio averages 6.5 for "RO_2+NO_3 dominant" experiments, it averages 8.6 for "RO_2+HO_2 dominant" experiments. Since the values of R-ON may depend on the instrument, we normalize the R-ON to the NO^+:NO_2^+ of ammonium nitrate (R-AN), which is expected to be a better

metric (Farmer et al., 2010). In our study, multiple measurements of R-AN are obtained from the ionization efficiency (IE) calibrations and the average value is about 1.8 (range of 1.2-2.7). Applying the nearest R-AN measured to each experiment, we calculate the average R-ON:R-AN ratio to be 3.2 for "RO_2+NO_3 dominant" experiments and 4.8 for "RO_2+HO_2 dominant" experiments.

For both types of experiments, there is a negligible difference in the mass spectrum of the aerosol produced in dry or high humidity (RH = 50%, 70%) conditions. In Figure 2.4, nitrate and organic ions are each assigned a different color to indicate an individual AMS HR ion family. There are a few notable ions in the aerosol mass spectrum. The signals at *m/z* 67 ($C_5H_7^+$) and *m/z* 91 ($C_7H_7^+$), while not significant in the high resolution mass spectra of several biogenic SOA systems (Ng et al., 2008b; Chhabra et al., 2010), are relatively large for β-pinene+NO_3 SOA. These ions also make up a larger fraction of the HR-ToF-AMS signal for SOA formed from the ozonolysis of β-caryophyllene (Chen et al., 2015) when compared to other biogenic SOA. Therefore, *m/z* 67 ($C_5H_7^+$) and *m/z* 91 ($C_7H_7^+$) could potentially serve as useful indicators for SOA formed from monoterpene/sesquiterpene oxidation in ambient aerosol mass spectra. However, more studies of SOA formed from the oxidation of biogenic VOCs are necessary to apportion ambient OA based on these fragments.

Figure 2.5 shows the time evolution of the major organic families relative to sulfate measured by the HR-ToF-AMS for a typical dry "RO_2+NO_3 dominant" experiment (Experiment 5 in Table 2.1). Sulfate is used to normalize the decay of the organic

families because it is non-volatile and any decrease in sulfate is reflective of particle wall loss and changes in aerosol collection efficiency (CE) in the HR-ToF-AMS (Henry and Donahue, 2012). Any change of each organic family relative to sulfate is therefore interpreted as a change in organic mass unrelated to particle wall loss or CE. Non-oxidized fragments (CH family in green) decrease more rapidly relative to sulfate than the more oxidized fragments (CHO1 family in purple, CHOgt1 "fragments with greater than 1 oxygen atom" family in pink). The change in mass for each organic family is determined over a 2.5 hour period following peak aerosol growth (at t ~ 15 min) in each "RO_2+NO_3 dominant" experiment (dry and humid). We find that the CHOgt1 family increases by 4% in dry experiments and remains relatively constant in humid experiments. This is consistent with a larger extent of aerosol aging in the dry experiments and is further discussed in Section 2.4.4.

Figure 2.6 shows the time evolution of HR-ToF-AMS nitrate-to-organics ratio in the "RO_2+NO_3 dominant" experiments at RH = 50% normalized by that in the corresponding dry experiments with the same initial hydrocarbon concentration. For simplicity, we refer to this ratio as $(\text{Nitrate:Org})_{\text{norm}}$. Normalizing the nitrate-to-organics ratio obtained from the humid experiments to the dry experiments allow for determining the extent of possible organic nitrate hydrolysis under humid conditions. Since only the relative change in the $(\text{Nitrate:Org})_{\text{norm}}$ ratio is important for comparison purposes, the maximum $(\text{Nitrate:Org})_{\text{norm}}$ measurement for each experiment is set to be unity. Nitrate mass is defined here as the sum of the mass of the NO^+ and NO_2^+ ions. This does not account for the $C_xH_yO_zN$ fragments, but these fragments only account for less than 10% (by mass) of

the nitrate functional groups detected by HR-ToF-AMS. As the experiment progresses, the $(Nitrate:Org)_{norm}$ ratio decreases and stabilizes at a value of about 0.9, indicating that there is no further decrease in the mass of nitrate relative to the mass of organics beyond this point. From our particle wall loss experiments, we establish that the particles are lost to the chamber wall with comparable rates under dry and humid conditions, suggesting that the observed decrease in the $(Nitrate:Org)_{norm}$ ratio is not a result of differing particle wall loss in dry and humid experiments. Instead, the decrease under humid conditions is attributed to hydrolysis of organic nitrate compounds in the particle phase. This is further discussed in Section 2.4.3.2.

2.4 Discussion

2.4.1 Proposed Mechanisms

Figure 2.7 shows the proposed scheme for the generation of species observed by CIMS and UHPLC-PDA-MS analyses from the oxidation of β-pinene with nitrate radicals. The oxidation process starts with Reaction (R1) for the sterically preferred addition of nitrate radical to the primary carbon (C_1) in the double bond of β-pinene (Wayne et al., 1991). The tertiary alkyl radical formed on C_2 can undergo 1) addition of O_2 to form a peroxy radical via Reaction (R2) (Atkinson and Arey, 2003b), 2) a 1,5-CH_3 shift indicated by Reaction (R3) (Miller, 2003) and, 3) rearrangement via Reaction (R4) (Stolle et al., 2009; Schröder et al., 2010). Reaction (R4) is thought to be a favorable pathway because it relieves the ring strain from the cyclobutane while generating a tertiary alkyl radical with a new reactive double bond. In the presence of oxygen, O_2 combines with the alkyl radical to make a peroxy radical, which is then converted to an alkoxy radical via Reaction (R5) (denoted as R^5O here) (Atkinson and Arey, 2003b; Vereecken and Peeters,

2012). Reactions which can be accomplished by any of the radicals present (RO_2, HO_2, NO_3, etc.) are symbolized by reaction with generic radical $\mathbf{L}^{\bullet}$, while hydrogen abstractions are symbolized by reaction with generic radical $\mathbf{Q}^{\bullet}$ (e.g., NO_3, RO_2, etc.). R^5O can undergo intramolecular addition to the less substituted C_7 of the newly formed double bond via Reaction (R6), generating a cyclic ether alkyl radical (Vereecken and Peeters, 2004; Vereecken and Peeters, 2012). Alternatively, R^5O can undergo hydrogen abstraction from another species via Reaction (R7) to form a hydroxynitrate of MW = 215 amu (R^7OH), a gas-phase species detected by CIMS. The cyclic ether alkyl radical generated by Reaction (R6) combines with O_2 to make peroxy radical **U** by Reaction (R8). The fate of radical **U** is to produce a cyclic ether hydroxynitrate with MW = 231 amu via Reaction (R9) (Russell, 1957; Atkinson and Arey, 2003b). A compound with the same molecular weight as this species is detected by CIMS.

The alkyl radical formed in Reaction (R1) can also undergo a 1,5-CH_3 shift as indicated by Reaction (R3), which forms a tertiary alkyl radical that then combines with O_2 by Reaction (R10). Reaction (R10) produces a hydroxynitrate ($R^{10}OH$) with MW = 215 amu, an isomer that could also correspond to the species observed by CIMS. Further functionalization of $R^{10}OH$ continues after hydrogen abstraction by Reaction (R11), which bond strength calculations predict occur preferentially at the C_3 position (Vereecken and Peeters, 2012). The resulting secondary alkyl radical from Reaction (R11) reacts with O_2 to form peroxy radical **S** via Reaction (R12). The reaction $\mathbf{S} + \mathbf{L}^{\bullet}$ forms either a hydroxycarbonyl nitrate with MW = 229 amu by Reaction (R13), or a

dihydroxynitrate with MW = 231 amu by Reaction (R14) (Russell, 1957; Atkinson and Arey, 2003b). Both are gas-phase species detected by CIMS.

The peroxy radical formed in Reaction (R2) can be converted to a hydroperoxide with MW = 231 amu (observed in CIMS) by reaction with an HO_2 radical (R15). Since Reaction (R15) is only associated with the RO_2+HO_2 channel, the signal corresponding to the species with MW = 231 amu is expected be higher in the "RO_2+HO_2 dominant" experiments. Figure A.2 shows the CIMS signal at m/z = 358 (MW = 231 amu) normalized to Br_2 sensitivity for each type of experiment ("RO_2+NO_3 dominant" and "RO_2+HO_2 dominant", dry and humid conditions). The higher signal in the "RO_2+HO_2 dominant" experiments supports the formation of more ROOH species in the gas phase under this reaction condition.

The peroxy radical formed from Reaction (R2) can also be converted into an alkoxy radical, $R^{16}O$, via Reaction (R16). Hydrogen abstraction by the alkoxy radical $R^{16}O$ can form a third hydroxynitrate isomer with MW = 215 amu by Reaction (R17). Alternatively, $R^{16}O$ can undergo a 1,5-H shift from a $-CH_3$ group by Reaction (R18) to form an alkyl radical at one of the terminal carbons (Carter et al., 1976; Eberhard et al., 1995; Atkinson, 1997a; Dibble, 2001). The alkyl radical then reacts with O_2 to form a peroxy radical and subsequently forms an aldehyde with MW = 229 amu by the overall Reaction (R19) (Russell, 1957; Atkinson and Arey, 2003b). The aldehydic hydrogen is especially susceptible to undergoing hydrogen abstraction (Miller, 1999), followed by O_2 addition to form a peroxy acid radical, and final conversion to a carboxylic acid (Russell,

1957; Atkinson and Arey, 2003b). $R^{20}COOH$ with MW = 245 amu is produced by Reaction (R20), a species registered as an anion by UHPLC-MS at *m/z* 244 (MW = 245 amu) (Figure A.5). CIMS data also support the pathways via Reaction (R20) (Figure 2.1). The Br_2-normalized CIMS signal for species at *m/z* 356 (MW = 229 amu) decreases with a subsequent increase in species at *m/z* 372 (MW = 245 amu) in the gas phase over the course of the experiment. Due to the lower vapor pressure of carboxylic acid species compared to carbonyl species (Pankow and Asher, 2008), the majority of carboxylic acid formed from this channel is expected to partition into the particle phase. In addition to Reaction (R20), $R^{20}COOH$ can also be formed through a more direct route by addition of O_2 to the alkyl radical product and then subsequent reaction of the peroxy radical with HO_2 via the sequence of Reactions (R18) + (R21) + (R22) (Ziemann and Atkinson, 2012).

The hydroxynitrate formed by Reaction (R17) can also undergo hydrogen abstraction at the C_3 position, as indicated by Reaction (R23). (Vereecken and Peeters, 2012). Reaction (R24) shows how O_2 addition to the resulting secondary alkyl radical gives peroxy radical **T**, which can either react with $\mathbf{L}^{\bullet}$ to form a dihydroxynitrate with MW = 231 amu via Reaction (R25) or form a hydroxycarbonyl nitrate with MW = 229 amu via Reaction (R26) (Russell, 1957; Atkinson and Arey, 2003b). In the absence of hydrogen atoms in the C_3 position, hydrogen abstraction occurs from C_4 of the hydroxycarbonyl nitrate species via Reaction (R27) (Vereecken and Peeters, 2012), which then forms a peroxy radical **V** by Reaction (R28) (Atkinson and Arey, 2003b). Reaction (R29), $\mathbf{V} + \mathbf{L}^{\bullet}$, yields a dihydroxycarbonyl nitrate with MW = 245 amu (Russell, 1957; Atkinson and Arey,

2003b). This dihydroxycarbonyl nitrate is not expected to be the species appearing in the UHPLC-MS chromatogram (Figure A.5) at *m/z* 244 (MW = 245 amu) because it lacks a –COOH group and likely has a higher vapor pressure than the carboxylic acid species with MW = 245 amu. Instead, it is likely that the dihydroxycarbonyl nitrate is the species observed by CIMS at *m/z* 372 (MW = 245 amu). A third possible isomer (not shown in Figure 2.7) with MW = 245 amu and containing a non-carboxylic C=O group, could be similarly formed from the product of Reaction (R13). Likewise, other isomers to those generated after Reaction (R26) can be formed from each possible structure with MW = 229 amu, providing a wide array of precursors to form heavier MW products. The confirmation that several isomers with MW = 245 amu are present in the filter extracts is revealed from the extracted ion chromatogram, EIC, which shows closely eluting peaks at *m/z* 244 (MW = 245 amu) when substituting formic acid for acetic acid (Li et al., 2011) as the modifier in the mobile phase (Figure A.5).

2.4.2 Aerosol Yields

2.4.2.1 SOA Yields Over a Wide Range of Organic Mass Loadings

The SOA yields obtained from this study are shown in Figure 2.2 and Figure 2.3 In recent years, it has been suggested that the loss of organic vapors to the chamber wall could affect SOA yields (Matsunaga and Ziemann, 2010; Loza et al., 2010; Yeh and Ziemann, 2014; Zhang et al., 2014; Zhang et al., 2015b). Specifically, Zhang et al. (2014) demonstrated that vapor wall loss could lead to an underestimation of SOA yields by as much as a factor of 4. To evaluate the potential effect of organic vapor wall loss on SOA yields in our study, experiments without seed are carried out at different conditions (dry

and humid (RH = 50, 70%); "RO_2+NO_3 dominant" and "RO_2+HO_2 dominant" conditions). The yields from the nucleation experiments are reported in Figure A.9 along with the yield curve obtained from seeded experiments. The similar yields for nucleation/seeded "RO_2+NO_3 dominant" experiments (dry and humid) in our study suggest that vapor wall loss has a negligible effect on aerosol yields in these experiments. It is likely that rapid reaction of β-pinene with nitrate radicals in this study mitigate the effect of organic vapor wall loss on SOA yields. Based on the rapid SOA growth (peak growth typically achieved within 10-15 minutes) for these experiments, it is estimated that the effective reaction rate of β-pinene in our experiments is an order of magnitude higher than the rates reported in Zhang et al. (2014). Although the aerosol mass yields for the "RO_2+HO_2 dominant" nucleation experiments are lower than the corresponding seeded experiments, further increase in the seed concentration does not have a significant effect on yield. Zhang et al. (2014) determined that if vapor phase wall loss is significant in chamber experiments, the addition of more seed particles will lead to an increase in SOA yield. Therefore, it is likely vapor phase wall loss is also negligible in our seeded "RO_2+HO_2 dominant" experiments. It is unclear at this time why nucleation experiments have lower SOA yield only for the "RO_2+HO_2 dominant" experiments. One possibility is that the chamber-wall uptake of ROOH species (which is likely higher in "RO_2+HO_2 dominant" experiments as measured by CIMS (Figure 2.1)) is more rapid than other gas-phase species.

A comparison of aerosol yields obtained for the oxidation of β-pinene with nitrate radicals is also shown in Figure 2.2. Griffin et al. (1999) performed the first

comprehensive study of SOA formation from nitrate radical oxidation of BVOCs. The aerosol yield curve reported for β-pinene+NO_3 by Griffin et al. (1999) is shown next to our yield curve in Figure 2.2. The yield curve in Griffin et al. (1999) was generated from chamber experiments with ΔM_o > 45 μg m^{-3} (range of ΔM_o = 45–660 μg m^{-3}) and extrapolated down to lower loadings. The yield curve generated in the current study, however, includes measurements at mass loadings < 10 μg m^{-3} and does not require any extrapolation beyond the bounds of the data to include lower, atmospherically relevant aerosol loadings. As shown in Figure 2.1., while the SOA yields from this study are consistent with Griffin et al. (1999) for ΔM_o > 45 μg m^{-3}, the yields from this study are as much as a factor of 4 higher than those reported by Griffin et al. (1999) at lower mass loadings.

Instances where the measured yields at low mass loading do not match those extrapolated from higher loadings have been observed for α-pinene ozonolysis (Presto and Donahue, 2006). We attribute this result to limitations of the two-product model, which bins all compounds into only two semi-volatile products of differing vapor pressures, to cover the entire spectrum of volatilities for all chemical products. At higher mass loadings, semi-volatile and volatile compounds can condense onto the particle phase and can potentially make up the majority of the aerosol. When a two-product yield curve is fit to high mass loadings only, the parameters are likely to be biased by the semi-volatile and high volatility products. Therefore, a yield curve fit using data from only high mass loadings will not account for the low-volatility products, which might be the minority products at high organic mass loadings. The two-product fit using high mass loadings therefore

cannot be used to predict yields at low mass loadings, where the SOA is mostly comprised of low-volatility products. Since the yield curve generated as part of this study spans a wide range of organic mass loadings, the fitting parameters account for both the low-volatility products and the higher volatility products.

Fitting yield data to the volatility basis set described in Donahue et al. (2006) illustrates how higher volatility bins (products) are favored at higher aerosol mass loadings. The fit coefficients for the volatility basis set are shown in Table 2.3 for the aerosol yields of β-pinene+NO_3 from this study and that of Griffin et al. (1999). It is noted that the data from Griffin et al. (1999) have been adjusted to a temperature of 298 K and density of 1.41 g cm^{-3} for comparison to results from our study. As seen in Table 2.3, the stoichiometric coefficients for the fit of Griffin et al. (1999) are weighted towards higher volatility products while the coefficients fit to the data collected in this study are distributed among lower and higher volatility products.

Fry et al. (2009) conducted a pair of β-pinene+NO_3 chamber experiments under dry and humid (RH = 60%) conditions. Their results are also shown in Figure 2.2. The yields from Fry et al. (2009) are about 20% lower than the current study. A more recent study by Fry et al. (2014) reported aerosol mass yields in the range of 33-44% for the β-pinene+NO_3 system at an organic mass loading of 10 μg m^{-3} in a continuous flow chamber under dry conditions. This is approximately 10-30% lower than the yield reported at a similar mass loading in this study. While various experimental conditions can contribute to the difference in aerosol mass yields, we note that the aerosol formation

rate in both Fry et al. (2009) and Fry et al. (2014) is slower than this study, which is likely caused by lower oxidant concentrations in Fry et al. (2009) and Fry et al. (2014) compared to this study. Slower reaction times could allow more time for the gas-phase species to partition onto the chamber walls and reduce the amount that partitions onto aerosol (Ng et al., 2007a; Zhang et al., 2014). Thus, organic vapor wall loss might play a role in the lower yields observed in Fry et al. (2009) and Fry et al. (2014). There is a substantial difference between our β-pinene+NO_3 SOA yield and that from Hallquist et al. (1999), which reported an aerosol mass yield of 10% for a mass loading of 4 μg m^{-3}. A possible explanation for this is that the mass of β-pinene reacted was not directly measured in Hallquist et al. (1999), instead, it was assumed that the concentration of β-pinene reacted was equivalent to the concentration of N_2O_5 reacted. If there were other loss processes for N_2O_5 in the experiments conducted by Hallquist et al. (1999), the yield reported in their study could be substantially lower than the actual aerosol yield.

2.4.2.2 Effects of RH and Acidity on SOA Yields

For the "RO_2+NO_3 dominant" experiments, the yields between experiments conducted at dry conditions with ammonium sulfate seed are similar to experiments conducted under high humidity (RH = 50% and RH = 70%) (Figure 2.2). Our results indicate that the relative humidity does not have appreciable effects on the aerosol mass yield. These results are consistent with previous humidity effects studies on photooxidation (Nguyen et al., 2011) and nitrate radical chemistry (Bonn and Moorgat, 2002; Fry et al., 2009). However, these results are inconsistent to the study performed by Spittler et al. (2006), where lower SOA yields were obtained for the α-pinene+NO_3 system under humid

conditions (RH = 20%)**.** Spittler et al. (2006) proposed that either the presence of water vapor altered the gas-phase chemistry or that the aerosol water on seed particles prevented gas-phase partitioning. These do not seem to be the case in our study. Similar gas-phase oxidation products are detected by CIMS under both dry and humid conditions and the organics size distribution measured by HR-ToF-AMS overlaps that of the seed aerosol, indicating that the oxidation products are condensing onto the seed particles.

The presence of aerosol water can potentially affect SOA formation through hydrolysis of organic nitrates. It has been observed in previous studies that organic nitrates in aqueous filter extract can undergo hydrolysis to form alcohols and nitric acid (Sato, 2008). The change from nitrate to hydroxyl functional groups could affect gas-particle partitioning and aerosol yields if the organic nitrates and alcohols have different vapor pressures. However, previous studies have shown that hydroxyl groups lower the vapor pressure of an organic compound to the same extent as organic nitrate groups (Pankow and Asher, 2008). In this study, hydrolysis does not appear to be a major reaction pathway for β-pinene+NO_3 SOA under humid conditions. As shown in Section 2.4.4, only < 10% of OA undergoes hydrolysis. Thus, even if there is a difference in the vapor pressures between organic nitrates and their hydrolysis products, it is unlikely that this would affect aerosol yields in our case.

Aerosol water can also enhance SOA yields by providing a medium for water-soluble species (e.g., glyoxal) to dissolve into the particulate aqueous phase (Ervens et al., 2011). Nitrate radical addition is predicted to add predominantly to a double bond instead of

cleaving carbon to carbon bonds (Wayne et al., 1991) and hence fragmentation to small carbon compounds is unlikely. As shown in Figure 2.7, the proposed mechanism does not involve carbon cleaving reactions which could result in small, water-soluble compounds. This is further supported by the similarities in SOA yields between dry and humid conditions. If these carbon cleaving reactions dominate and form small, water-soluble species, the yields should be much higher for the humid conditions than the dry conditions.

We find that aerosol acidity has a negligible effect on the SOA yield for the β-pinene+NO_3 system (Figure A.4). This is opposite to some previous studies where increases in aerosol yields have been found under acidic conditions for other SOA systems (using the same seeds as in our study), such as ozonolysis of α-pinene and photooxidation of isoprene (e.g., (Gao et al., 2004; Surratt et al., 2007). Acid-catalyzed particle-phase reaction such as oligomerization has been proposed for such "acid effects". Although aerosol produced by the β-pinene+NO_3 reaction can potentially undergo oligomerization as well, it appears that the aerosol products are of low enough volatility that further particle-phase reactions (if any) do not enhance SOA yields. This indicates that the "acid effect" is likely different for different SOA systems, which would depend on the parent hydrocarbon, oxidant (ozone, OH, nitrate radicals), and other reaction conditions. In general, the SOA yields for nitrate radical oxidation of BVOCs are higher than corresponding yields in ozonolysis or OH radical oxidation (e.g., Griffin et al., 1999), suggesting that no further particle-phase reaction is needed to make the oxidation products more non-volatile and the "acid effect" could be limited.

2.4.2.3 Effects of RO_2+NO_3 vs. RO_2+HO_2 Chemistry on SOA Yields

Previous studies have shown that the fate of peroxy radicals can have a substantial effect on SOA formation (Kroll and Seinfeld, 2008; Ziemann and Atkinson, 2012). For instance, it has been shown in laboratory chamber studies that the aerosol yields can differ by a factor of 2 depending on the RO_2 fate for the isoprene+NO_3 system (Ng et al., 2008b). Although studies have proposed that RO_2+NO_3 is the major nighttime RO_2 fate in the ambient environments (Kirchner and Stockwell, 1996), results from recent field studies suggested that HO_2 radicals are abundant at night (Mao et al., 2012). The high HO_2 radical concentration could result in the RO_2+HO_2 reaction becoming the dominant RO_2 radical fate in the nighttime atmosphere. In our study, the experimental protocols are designed to promote the "RO_2+NO_3" or "RO_2+HO_2" reaction channel. These two scenarios would be representative of nitrate radical oxidation in environments with varying levels of NO_x. To our knowledge, this is the first study in which the fate of peroxy radicals is considered in SOA formation from nitrate radical oxidation of monoterpenes. A simple kinetic model based on MCMv3.2 (Saunders et al., 2003a) is developed to simulate the gas-phase chemistry for the β-pinene+NO_3 reaction. The simulation results suggest that in both "RO_2+NO_3 dominant" and "RO_2+HO_2 dominant" experiments, the cross-reactions of RO_2 radicals are not a significant reaction pathway (Figure A.10). Figure 2.3 shows that the SOA yields from the "RO_2+HO_2 dominant" experiments are similar to the "RO_2+NO_3 dominant" experiments. The similar yields under these different reaction conditions could arise from a comparable suite of reaction products between the two reaction pathways. The reaction of RO_2+NO_3 produces an RO radical (Figure 2.7, Reaction R16) which can undergo decomposition or isomerization

(Orlando and Tyndall, 2012; Ziemann and Atkinson, 2012). Typically, it is expected that the RO_2+HO_2 reaction will lead to the formation of peroxides (Orlando and Tyndall, 2012; Ziemann and Atkinson, 2012). However, a recent study by Hasson et al. (2012) showed that for highly substituted peroxy radicals, the RO_2+HO_2 reaction favors the formation of RO radicals. Additionally, several previous studies showed that as carbon chain length increases (C2-C4), the RO_2+HO_2 reaction becomes less likely to form the ROOH product and more likely to form the RO product (Jenkin et al., 2007; Dillon and Crowley, 2008; Hasson et al., 2012). In the case of β-pinene+NO_3, RO_2 radicals are expected to form on the tertiary carbon as the nitrate radicals tend to attack the least substituted carbon of a double bond, leading to the formation of tertiary peroxy radicals (Wayne et al., 1991) (Figure 2.7). Given β-pinene is a C10 compound and forms a highly substituted peroxy radical, we hypothesize that the RO_2+HO_2 reaction pathway in our study forms RO radicals as suggested by Hasson et al. (2012), leading to a similar peroxy radical fate as in the "RO_2+NO_3 dominant" experiments. We note that the RO_2+HO_2 reaction still leads to formation of ROOH as measured by CIMS (Figure A.2). Thus it appears that the RO_2+HO_2 channel does not exclusively produce RO radicals in our case. Nevertheless, based on the similar SOA yields in the " RO_2+NO_3 dominant" and "RO_2+HO_2 dominant" experiments, we propose that either the RO radical is the dominant product of the RO_2+HO_2 reaction pathway, or that ROOH has a similar volatility to the products formed from the RO radicals in the "RO_2+NO_3 dominant" experiments.

SOA is collected on filters for several experiments and analyzed using UHPLC in order to characterize the particle composition. Figure 2.8 shows the ratios of the total areas

under the UV-visible chromatograms for "RO_2+HO_2 dominant" and "RO_2+NO_3 dominant" experiments, under both humid and dry conditions. Chromatograms collected at 205, 235, and 270 nm are integrated to get the total area at each wavelength and the standard deviation from two measurements. Total areas are normalized by the estimated organic mass loading on the corresponding filters. The wavelengths chosen represent a good proxy for certain functional groups that absorb in these regions. More specifically, λ = 235 nm corresponds to a region of strong absorption by ROOR and ROOH (Farmer et al., 1943; Turrà et al., 2010; Ouchi et al., 2013), while λ = 270 nm is a compromise wavelength that represents both carbonyl and alkyl nitrate functional groups (Xu et al., 1993; Pavia et al., 2008). Finally, λ = 205 nm is chosen as the normalization wavelength because practically all organic matter present in the sample absorbs in this UV region. Figure 2.8 shows the ratio of total areas at 235 nm and 270 nm relative to the value at 205 nm, which provides a qualitative comparison of the samples. By comparing the amounts (areas) of the 235 and 270 nm absorbing species, the effect of humidity on each branching pathway (RO_2+HO_2 or RO_2+NO_3) can be assessed. How much -ONO_2, -C=O, ROOR and ROOH is produced under each humidity level determines the relative reactivity between the humid vs. dry conditions of each branching pathway. The relative reactivity for both reaction channels is similar within one standard deviation for all humidity conditions studied, indicating that each condition may have a similar product distribution. A comparison between the RO_2 + HO_2 and RO_2 + NO_3 pathways cannot be made in this manner because NO_3 concentrations are different. The seemingly smaller areas for species produced in the HO_2 panel could simply be due to a larger amount of non-nitrated organic matter being produced that absorbs at the normalization wavelength.

However, one slight difference is the enhancement in the production of $C_{10}H_{15}NO_6$ (*m/z* 244, an RCOOH species) in the "RO_2+HO_2 dominant" experiments, which increases by 2 and 7 times under dry and humid conditions, respectively, relative to the "RO_2+NO_3 dominant" experiments. This observation indicates that in the presence of additional HO_2, the oxidation is directed toward the synthesis of $C_{10}H_{15}NO_6$ (*m/z* 244) more efficiently. This can be explained by an enhancement of the reaction sequence R21 + R22 in Figure 2.7, which is enhanced at high HO_2 radical concentrations.

2.4.3 Particulate Organic Nitrate Formation and Hydrolysis

2.4.3.1 Organic Nitrate Formation

The mass spectrum in Figure 2.4 indicates the presence of a large fraction (11%) of nitrate in the aerosol formed from the β-pinene+NO_3 reaction. Approximately 90% of the N atoms in the spectrum are found on the NO^+ and NO_2^+ fragments. Most of the nitrate signal is assumed to be from organic species (i.e., organic nitrates) as N_2O_5 uptake to the particles is negligible and the NO^+:NO_2^+ ratio is high. In humid experiments, the heterogeneous hydrolysis of N_2O_5 could lead to the formation of inorganic nitrates (e.g., HNO_3). To evaluate the contribution of inorganic nitrates to the total NO^+ and NO_2^+ ions measured by the HR-ToF-AMS, we perform two characterization experiments (RH = 50%) in which only N_2O_5 (the maximum amount of N_2O_5 used in our aerosol experiments) and seed aerosol ($(NH_4)_2SO_4$ seed or $(NH_4)_2SO_4$+H_2SO_4 seed) are injected into the chambers. In both cases, using a relative ionization efficiency (RIE) of 1.1 for nitrate results in a nitrate growth of less than 0.1 μg m^{-3} detected by the HR-ToF-AMS (Rollins et al., 2009). The uptake of N_2O_5 is even less likely in the SOA yield

experiments. It has been shown that when comparing to inorganic seed only, the presence of organic matter decreased N_2O_5 uptake by 80% (Gaston et al., 2014). Therefore, the contribution of inorganic nitrates to the total nitrate signals measured by the HR-ToF-AMS in our experiments is negligible.

It has been shown previously that the NO^+:NO_2^+ ratio in the HR-ToF-AMS mass spectrum can be used to infer the presence of particle-phase organic nitrates (Farmer et al., 2010). Specifically, Farmer et al. (2010) suggested that the NO^+:NO_2^+ ratio is much higher for organic nitrates (ratio = 5-15) than inorganic nitrates (ratio ~2.7) and therefore, aerosol with a high NO^+:NO_2^+ ratio likely also has a high concentration of organic nitrates. Figure 2.4 shows that approximately only two-thirds of the signal at *m/z* 30 is from NO^+, while the remaining signal is from organic CH_2O^+ fragment. At peak aerosol growth under dry and humid conditions, we determine from the high-resolution AMS data that the average R-ON value for β-pinene+NO_3 aerosol is 6.5 in "RO_2+NO_3 dominant" experiments and an average of 8.6 in "RO_2+HO_2 dominant" experiments. Previous studies (Fry et al., 2009; Bruns et al., 2010) on the β-pinene+NO_3 reaction suggested that the R-ON for β-pinene+NO_3 SOA is on the order of 10:1, higher that the values determined in this study. One possible explanation for the difference in R-ON between this study and previous literature is instrument bias. Different instruments may have different R-ON values. One way to circumvent this bias is to compare the R-ON:R-AN ratio. The average R-ON:R-AN for all experiments is 3.9, which is in agreement with values calculated by Fry et al. (2009) and Bruns et al. (2010) (range 3.7-4.2).Another explanation for this difference is the close proximity of the CH_2O^+ ion to the NO^+ ion in

the aerosol mass spectrum, which may result in a small bias in the calculated R-ON. Specifically, if we were to include the contribution of the organic CH_2O^+ and $CH_2O_2^+$ fragments at *m/z* 30 and *m/z* 46 (in addition to contribution from NO^+ and NO_2^+) respectively, the corresponding NO^+:NO_2^+ ratios would be higher, i.e., 9:1 for "RO_2+NO_3 dominant" experiments and 11:1 for "RO_2+HO_2 dominant" experiments. Therefore, when using the NO^+:NO_2^+ ratio to estimate organic nitrate contribution in ambient OA, it is imperative that one excludes the organic contribution (if any) at *m/z* 30 when calculating the ratio.

One possible way to estimate the molar fraction of organic nitrates in the aerosol from the HR-ToF-AMS data is to use the N:C ratio of the aerosol formed in the experiments. Since β-pinene is a monoterpene, we assume its oxidation products have approximately 10 carbon atoms. This is a reasonable assumption based on the gas-phase oxidation products detected by CIMS (Figure 2.7). The dominant reaction pathway of nitrate radicals is addition via attack of the double bond, adding one nitrate group to the primary carbon and forming a peroxy radical. With one nitrate group and 10 carbons from the β-pinene precursor, the organic nitrate products are expected to have an N:C ratio of about 1:10. If 100% of the SOA formed is composed of organic nitrates, the HR-ToF-AMS data should have an N:C ratio of 0.1. The average N:C ratio for all experiments measured by the HR-ToF-AMS is approximately 0.074 for SOA formed from β-pinene+NO_3 at peak growth. Thus, as an upper bound, it is approximated that the molar fraction of organic nitrates in the aerosol is 74%. Even if there is fragmentation, the organic nitrate fraction in the aerosol would remain fairly high. For instance, if the organic nitrate species only has 9

carbons, the upper-bound molar organic nitrate fraction is approximately 67%. If we assume the organic nitrate and non-organic nitrate species have the same molecular weight, the molar organic nitrate fraction in the aerosol is equal to the fraction of aerosol mass composed of organic nitrates. In addition to N:C, the HR-ToF-AMS Nitrate:Org mass ratio can also be used to estimate the particle organic nitrate fraction. The average Nitrate:Org mass ratio measured by the HR-ToF-AMS for all experiments is about 0.16. We assume the organic nitrate compound has an average molecular weight between 200 and 300 amu based on the predicted products (Figure 2.7), where 62 amu is attributed to the nitrate group while the remaining mass is from the organic mass. Using both the Nitrate:Org mass ratio and the assumed range of molecular weights for the organic nitrate species, the fraction of aerosol mass composed of organic nitrates is estimated to be 45-68%. We estimate that the fraction of aerosol mass composed of organic nitrates is 60%, based on the average value of the extremes of the two estimates. This is comparable to the fraction of aerosol mass composed of organic nitrates estimated by Fry et al. (2014) (56%) but higher than that reported by Fry et al. (2009) (30-40%). The different experimental conditions in our study vs. those in Fry et al. (2009) may have contributed to the difference in the fraction of aerosol mass composed of organic nitrates. For example, the ratio of NO_2 to O_3 used to make NO_3 radicals in Fry et al. (2009) is lower than this study, which may have led to differing branching ratios of β-pinene+NO_3 vs. β-pinene+O_3.

2.4.3.2 Hydrolysis and Organic Nitrate Fate

As shown in Figure 2.6, for experiments with the same initial hydrocarbon concentration, the AMS nitrate-to-organics ratio of the humid experiments normalized by the dry experiments stabilize at a ratio of about 0.9. The nitrate radical addition at the double bond of β-pinene can lead to the formation of either primary or tertiary nitrates. Previous studies of organic nitrate hydrolysis in bulk solutions showed that while saturated primary nitrates hydrolyze on the order of months, tertiary nitrates hydrolyze on the order of hours (Darer et al., 2011). Primary organic nitrates with double bonds can hydrolyze on the order of minutes (Jacobs et al., 2014), but oxidation products from the β-pinene+NO_3 reaction are likely saturated compounds due to the lone double bond of β-pinene (Figure 2.7). Therefore, the point at which nitrate mass stops decreasing is interpreted as when all tertiary nitrates have hydrolyzed. As the oxidation products typically contain only one nitrate group (Figure 2.7), we infer that, within experimental error, approximately 90% of the organic nitrates formed from the β-pinene+NO_3 reaction are primary nitrates. These results are consistent with findings that nitrate radical is more likely to attack the less substituted carbon, which, in the case for β-pinene, is the terminal carbon (Wayne et al., 1991). Since the nitrate addition is the first reaction step, any subsequent differences in peroxy radical fate (e.g., RO_2+NO_3 vs. RO_2+HO_2) will not affect the relative amount of primary vs. tertiary nitrates in our systems.

Based on the decay rate of $(Nitrate:Org)_{norm}$, the hydrolysis lifetime of the tertiary nitrates formed in the reaction of β-pinene with nitrate radicals is calculated to be approximately 3-4.5 hr. This is on the same order of magnitude as the hydrolysis lifetime (6 hr) of the

proposed tertiary organic nitrates formed from photooxidation of trimethyl benzene in the presence of NO_x (Liu et al., 2012). Results from our study therefore do not suggest that nitrate radical chemistry produces organic nitrates with different hydrolysis rates than what is previously known for primary or tertiary organic nitrates. Instead, this study proposes that the fraction of tertiary organic nitrates produced from nitrate radical chemistry is much lower than SOA produced from photooxidation in the presence of NO_x. While we directly demonstrate this to be true in the case of the β-pinene+NO_3 system, this can also be applied to commonly emitted terpenes, including those with internal double bonds. From the list of terpenes in Guenther et al. (2012), all unsaturated terpenes have at least one double bond with a secondary or primary carbon. For example, α-pinene contains an internal double bond connecting a tertiary carbon to a secondary carbon. The nitrate radical is more likely to attack the less substituted carbon (i.e. the secondary carbon) and form a secondary organic nitrate. As primary/secondary and tertiary organic nitrates have drastically different hydrolysis rates, it is imperative that their relative contribution be accurately represented in models when determining the fate of ambient organic nitrates. A recent study by Browne et al. (2013) modeled the hydrolysis of organic nitrates in a forested region by assuming that 75% of atmospheric organic nitrates formed in the day are composed of tertiary organic nitrates, based on the average fraction of tertiary organic nitrates from the photooxidation of α-pinene and β-pinene in the presence of NO_x. This has implications on not only the organic nitrate fate, but also on the formation of nitric acid, a byproduct of organic nitrate hydrolysis (Sato, 2008). With this, Browne et al. (2013) predicted that hydrolysis of organic nitrates produced in the day time could account for as much as a third to half of all nitric acid

production. However, when considering organic nitrates formed both in the day and at night, the fraction of tertiary organic nitrates in ambient organic nitrates is likely lower than that used by Browne et al. (2013). This is especially true in areas where nitrate radical oxidation is the dominant source of organic nitrates (e.g., NO_x > 75 ppt in forested regions as noted in Browne et al. (2014)). It is recommended that future modeling studies of organic nitrates fates should consider organic nitrates formed both in the day and at night in order to take into account the large contribution of primary organic nitrates (which do not hydrolyze appreciably) formed from nitrate radical oxidation of monoterpenes.

Previous studies suggested that hydrolysis of organic nitrates can be an acid-catalyzed process in both solution (Szmigielski et al., 2010) and directly in the particle phase (Rindelaub et al., 2015). However, it has been found that primary and secondary organic nitrates are stable unless the aerosol is very acidic (pH < 0) (Darer et al., 2011; Hu et al., 2011). We calculate the corresponding change in $(\text{Nitrate:Org})_{\text{norm}}$ ratio for the experiments where $(NH_4)_2SO_4$+H_2SO_4 seed is used (data not shown in Figure 2.6). We find that for these experiments, the $(\text{Nitrate:Org})_{\text{norm}}$ ratio also becomes constant at around 0.9, similar to that of the $(NH_4)_2SO_4$ seed experiments. However, the experiments using $(NH_4)_2SO_4$+H_2SO_4 seed have a more rapid rate of decrease in the $(\text{Nitrate:Org})_{\text{norm}}$ ratio. This suggests that while hydrolysis of tertiary nitrates is accelerated under more acidic conditions, primary organic nitrates do not hydrolyze at an observable rate for the pH conditions employed in this study. As the majority of the particulate organic nitrates formed in our experiments are primary nitrates, we infer that particle acidity may not

have a significant impact on the hydrolysis of organic nitrates formed in the BVOCs+NO_3 reaction, except in the cases where the double bond on the BVOCs connects two tertiary carbons, such as terpinolene.

2.4.4 Aerosol Aging in the Dark

While the aging of SOA has been extensively investigated in multiple photooxidation studies and shown to affect aerosol mass (e.g., (Donahue et al., 2012; Henry and Donahue, 2012), little is known regarding aerosol aging by nitrate radicals (Qi et al., 2012). A number of theoretical (Kerdouci et al., 2010, 2014; Rayez et al., 2014) and experimental studies (Atkinson, 1991; Wayne et al., 1991) suggested that hydrogen abstraction by nitrate radicals occurs, especially for hydrogen atoms attached to aldehyde groups. As shown in Figure 2.7, the β-pinene+NO_3 reaction can lead to the formation of compounds with carbonyl groups, allowing for potential nighttime aging of SOA by nitrate radicals. We focus our aerosol aging discussion on the "RO_2+NO_3 dominant" experiments, where the oxidant (nitrate radicals) concentrations are higher.

As aerosol ages, first-generation products either functionalize, which decreases volatility, or fragment, which can lead to an overall increase in volatility (Kroll et al., 2009). If fragmentation is the dominant pathway, a decrease in organic mass is expected as products become more volatile and re-partition back to the gas phase. We use the AMS Org:Sulfate ratio as a proxy to examine the effect of aerosol aging on organics mass in our experiments. As wall loss of particles will lead to a decrease in organic loading, normalizing the organic loadings by sulfate allows us to examine the net change in the

organics mass over the course of the experiments. The use of Org:sulfate is a good proxy for aerosol aging when the organics only condense onto existing ammonium sulfate particles. A study by (Loza et al., 2012) has demonstrated that in the case of rapid condensation of organic species, the time scale of condensation is less than the time scale of diffusion to existing seed particle. When in this "diffusion-limited growth" regime, the organic mass partially nucleates to form new particles. Since the nucleated particles are smaller than those particles in which ammonium sulfate acted as a seed for condensation, organics contained in these nucleated particles will be lost to the chamber walls more rapidly than the existing seed particles (Figure A.3). This could lead to an overall decrease in the Org:sulfate ratio. In our study, the Org:Sulfate ratio decreases after SOA reaches peak growth (Figure 2.5). It is possible that this decrease is caused by wall loss of organic particles formed in the diffusion-limited growth regime. It is also possible that fragmentation of aerosol components is the dominant aging pathway, resulting in a decrease in the Org:Sulfate ratio. . Regardless, there is still evidence of increased functionalization over the course of the experiments. Rapid loss of organics due to particle wall loss or fragmentation of SOA would cause all AMS organic families to either decrease or remain constant relative to sulfate. However, Figure 2.5 shows that the highly-oxidized fragments (CHOgt1, fragments with greater than 1 oxygen atom) increase slightly relative to sulfate while the non-oxidized fragments (CH) are lost at nearly twice the rate as the slightly oxidized fragments (CHO1). Since non-oxidized fragments are lost more quickly than less-oxidized fragments, it is possible that further particle-phase reactions are leading to the formation of highly oxidized compounds.

For the β-pinene+NO_3 reaction, carboxylic acids can be formed from the abstraction of hydrogen from aldehydes and subsequent oxidation (Figure 2.7). The observed ions at *m/z* 356 and *m/z* 372 in CIMS likely correspond to a hydroxy carbonyl nitrate and carboxylic acid, respectively. As shown in Figure 2.1, *m/z* 356 decreases over the course of the experiment while *m/z* 372 increases. The possible conversion of aldehydes to carboxylic acids is also noticeable in the aerosol chemical composition. The *m/z* 44 (CO_2^+) fragment in the HR-ToF-AMS data likely arise from thermal-decomposition of carboxylic acids (Duplissy et al., 2011) and is commonly used to infer the extent of aerosol aging (Ng et al., 2011). Although the f_{44} (fraction of CO_2^+ ion to total organics) in the typical mass spectrum of β-pinene+NO_3 SOA is low (< 3%), there is a noticeable and continued increase in f_{44} after peak aerosol growth (Figure 2.5). Specifically, during the 2.5 hours following peak growth, f_{44} increases by as much as 30% under dry conditions. Under humid conditions, the increase in f_{44} is only 6%. These correspond to a 17% and 6% increase in O:C ratio (calculated by including contributions from nitrate fragments) of the aerosol under dry (O:C ranging from 0.46 to 0.54 for all experiments) and humid conditions (O:C ranging from 0.47 to 0.50), respectively. The lower degree of aging in humid experiments is consistent with the observation that the CIMS N_2O_5 signals, while not quantified, are clearly lower (by at least a factor of 2) in the humid "RO_2+NO_3 dominant" experiments when compared to dry experiments. This is likely due to the uptake of N_2O_5 to wet chamber and/or aerosol surfaces (Thornton et al., 2003).

It is unlikely that the observed decrease in organic species relative to sulfate and the decrease in gas phase species are due to differences in vapor phase wall loss. Matsunaga

and Ziemann (2010) determined that highly-oxidized gaseous organic compounds are lost to the chamber walls faster than compounds that have a lower degree of oxidation. Additionally, the gas-wall partitioning coefficient for a specific compound has also been shown to increase with decreasing vapor pressure (Yeh and Ziemann, 2014), with highly oxidized species typically having lower vapor pressures than less oxidized species (Pankow and Asher, 2008). If vapor-phase wall loss is the driving factor for the decrease of organics in this study, it would be expected that oxidized compounds would be lost to the walls more rapidly. Subsequently, these highly oxidized compounds would re-partition back to the gas phase in order to re-establish particle-gas equilibrium. The decrease in organics shown in Figure 2.5, however, indicates more rapid losses of non-oxidized fragments compared to oxidized fragments. The less oxidized species measured by CIMS (lower molecular weight) as shown in Figure 2.1 also decrease more rapidly than the more oxidized species. Therefore, the change in chemical composition and decrease in vapor phase species is more likely attributable to aerosol aging than to vapor-wall partitioning.

2.5 Relevance to Ambient Measurements

Results from this study provide the fundamental information to evaluate the extent to which nitrate radical oxidation of monoterpenes contributes to ambient organic aerosol. This reaction provides a direct mechanism for linking anthropogenic and biogenic emissions, and is likely substantial in the southeastern United States, where both types of emissions are high. A recent field campaign, the Southeastern Oxidant and Aerosol Study (SOAS), took place in Centreville, Alabama from June 1st – July 15th, 2013 to investigate the effects of anthropogenic pollution in a region with large natural emissions. Based on

positive matrix factorization (PMF) analysis of the HR-ToF-AMS data obtained in SOAS, Xu et al. (2015c) identified an OA subtype termed as less-oxidized oxygenated organic aerosol (LO-OOA), which accounted for 32% of the total OA at Centreville. LO-OOA peaks at night and is well-correlated with particle-phase organic nitrates. These suggest that LO-OOA is produced predominantly from nighttime monoterpene+NO_3 chemistry, especially from β-pinene+NO_3 as β-pinene has a high nighttime concentration (Xu et al., 2015c). Results from the current laboratory chamber study provide the relevant fundamental data for estimating the amount of aerosol produced from monoterpene+NO_3 in SOAS. The campaign-average loading of non-refractory PM_1 in SOAS is about 8 μg m^{-3} and it has been determined that the aerosol is highly acidic (pH = 0.94±0.59) and contains a large amount of particulate water (5.09±3.76 μg m^{-3}) (Cerully et al., 2014; Guo et al., 2014). At night, the RH can reach up to 90% during the SOAS measuring period (Guo et al., 2014). The current chamber study is designed to probe SOA formation from nitrate radical oxidation under atmospherically relevant loadings, under high humidity, and in the presence of seed aerosol of different acidity. The fates of peroxy radicals at night are highly uncertain, which mainly arises from the lack of constraints on the reaction rates of the peroxy radicals with other species, such as RO_2+NO_3 (Brown and Stutz, 2012). In our study, the experiments are conducted under both "RO_2+NO_3 dominant" and "RO_2+HO_2 dominant" regimes to explore the effects of peroxy radial fates on SOA formation. Using a SOA yield of 50% (for a mass loading of 8 μg m^{-3} obtained from the yield curve) in the presence of acidic seed at RH = 70% obtained from "RO_2+HO_2 dominant" experiments, Xu et al. (2015c) estimated that about 50% of

nighttime OA production could be due to the reaction of monoterpenes with nitrate radicals, a large fraction of which may be the β-pinene+NO_3 reaction, in SOAS.

It is noted that the LO-OOA factor is also resolved at both rural and urban sites around the greater Atlanta area in all seasons, where HR-ToF-AMS measurements were conducted as part of the Southeastern Center for Air Pollution and Epidemiology study (SCAPE) (Verma et al., 2014; Xu et al., 2015a; Xu et al., 2015c). It is found that LO-OOA made up 18-36% of the total OA in rural and urban areas, suggesting that a fairly large fraction of total OA in the southeastern United States could arise from nitrate radical oxidation of monoterpenes.

Figure 2.9 shows a comparison of the aerosol mass spectrum from a typical β-pinene+NO_3 experiment from this study and the LO-OOA factor obtained from SOAS data. As LO-OOA could have other sources in addition to monoterpene+NO_3, the two spectra are not in perfect agreement but they do show similar features above *m/z* 60. Most noticeable of these are *m/z* 67 ($C_5H_7^+$) and *m/z* 91 ($C_7H_7^+$) with a ratio of these two ions ($C_5H_7^+$: $C_7H_7^+$) of about 2.9 (ranging from 2.5-3.6 in other experiments). The mass spectra for the other SOA-forming systems predicted to be of importance at SOAS, namely, α-pinene ozonolysis (Chhabra et al., 2010), isoprene photooxidation (Chhabra et al., 2010), and nitrate radical initiated isoprene chemistry (Ng et al., 2008b), do not show significant intensities at either of these two ions. Therefore, it is likely that high signals at $C_5H_7^+$ and $C_7H_7^+$ in ambient aerosol mass spectrum could be indicative of the presence of β-pinene+NO_3 reaction products. We note that the average NO^+:NO_2^+ ratio for aerosol

measured at SOAS is 7.1, consistent with the high NO^+:NO_2^+ ratio from the SOA formed from nitrate radical oxidation of β-pinene in this study.

The gas-phase oxidation products detected by the CIMS in this study can also be used to help interpret ambient data to evaluate the possible contribution of β-pinene+NO_3 reaction. For instance, a significant amount of gas-phase organic nitrate species with MW of 215 amu and 231 amu have been observed during the BEARPEX campaign in Fall 2009 (Beaver et al., 2012). As these species exhibited a nighttime peak, Beaver et al. (2012) suggested that they could arise from nighttime oxidation of α-pinene or β-pinene by nitrate radicals. The proposed mechanism for β-pinene+NO_3 (Figure 2.7) show multiple reaction pathways to form species with MW = 215 amu and MW = 231 amu. Therefore, the oxidation of β-pinene by nitrate radicals represents one possible pathway for the formation of the species detected by Beaver et al. (2012). As the β-pinene+NO_3 reaction has shown to be important at SOAS (Xu et al., 2015c), it is expected that the gas-phase compounds observed in this chamber study could help explain some of the species detected by the multiple CIMS deployed during the SOAS study.

2.6 Atmospheric Implications

Although photooxidation is expected to be the major oxidation pathway for atmospheric VOCs, nitrate radical oxidation can account for as much as 20% of global BVOCs oxidation and is predicted to lead to an aerosol mass increase by as much as 45% when compared to the modeled case where this chemistry is excluded (Pye et al., 2010). Due to high SOA yields, evaluating the mass of aerosol produced by nitrate radical initiated chemistry is essential to estimate the total organic aerosol burden, both on regional and

global scales. Currently, the aerosol yields from nitrate radical oxidation of monoterpenes in most models are assumed to be the same as those determined from β-pinene+NO_3 reactions in Griffin et al. (1999) (Pye et al., 2010). In this study, we systematically investigate SOA formation from the nitrate radical oxidation of β-pinene under various reaction conditions (dry, humid, differing radical fate) and a wide range of initial hydrocarbon concentrations that are atmospherically relevant. We determine that the SOA yields from the β-pinene+NO_3 systems are consistent with Griffin et al. (1999) for mass loadings > 45 μg m^{-3}, but as much as a factor of 4 higher than those reported in Griffin et al. (1999) for lower mass loadings. The lower SOA yields reported in Griffin et al. (1999) could arise from uncertainties in extrapolating data from higher mass loadings to lower mass loadings in that study, as well from slower reaction rates and vapor wall loss effects (Zhang et al., 2014). While it is likely that the SOA yields from the nitrate radical oxidation of various monoterpenes are different (Fry et al., 2014), updating SOA formation from β-pinene+NO_3 with the new yield parameters in future modeling studies would lead to a more accurate prediction of the amount of aerosol formed from this reaction pathway.

Currently, the fate of peroxy radicals (RO_2+HO_2 vs RO_2+NO_3, etc.) in the nighttime atmosphere is still highly uncertain (Brown and Stutz, 2012), though recent studies showed that the HO_2 mixing ratio is often on the order of 10 ppt (Mao et al., 2012). Thus, RO_2+HO_2 could be the dominant nighttime fate of peroxy radicals. In this study, we examine the effect of RO_2 fate on aerosol yields for the β-pinene+NO_3 system. Although more ROOH species are produced through the RO_2+HO_2 channel, the SOA yields in the

"RO_2+NO_3 dominant" and "RO_2+HO_2 dominant" experiments are comparable. This indicates that for this system, the overall product chemical composition and volatility distribution may not be very different for the different peroxy radical fates. This is in contrast to results from nitrate radical oxidation of smaller biogenic species, such as isoprene, which have large differences in SOA yields depending on the RO_2 fate (Ng et al., 2008b). This suggests that the fates of peroxy radicals in nitrate radical experiments for larger BVOCs (such as monoterpenes and sesquiterpenes) may not be as important as it is for small compounds (such as isoprene) and in photooxidation and ozonolysis experiments (e.g., (Presto et al., 2005; Kroll et al., 2006; Ng et al., 2007b; Eddingsaas et al., 2012; Xu et al., 2014). This warrants further studies.

The results from this study provide the first insight for the specific organic nitrate branching ratio on the β-pinene+NO_3 system. We determine that about 90 and 10% of the organic nitrates formed from the β-pinene+NO_3 reaction are primary organic nitrates and tertiary organic nitrates, respectively. As primary and tertiary organic nitrates hydrolyze at drastically different rates, the relative contribution of primary vs. tertiary organic nitrates determined in this work would allow for improved constraints regarding the fates of organic nitrates in the atmosphere. Specifically, we find that the primary organic nitrates do not appear to hydrolyze and the tertiary organic nitrates undergo hydrolysis with a lifetime of 3-4.5 hours. Updating the branching ratio (primary vs. tertiary) with organic nitrates formed by the NO_3-initiated oxidation of BVOCs will improve model predictions of hydrolysis of organic nitrates. Hydrolysis of organic nitrates has the potential to create a long term sink for atmospheric nitrogen in the form of nitric acid.

Organic nitrates that do not hydrolyze, however, can potentially be photolyzed or oxidized by OH radicals to release NO_x back into the atmosphere (Suarez-Bertoa et al., 2012) or lost by dry or wet deposition.

Results from this chamber study are used to evaluate the contributions from the nitrate radical oxidation of BVOCs to ambient OA in the southeastern United States, where this chemistry is expected to be substantial owing to high natural and anthropogenic emissions in the area. Factor analysis of HR-ToF-AMS data from SOAS and SCAPE field measurements identified an OA subtype (LO-OOA) at these sites which is highly correlated with organic nitrates (Xu et al., 2015a; Xu et al., 2015c). The β-pinene+NO_3 SOA yields obtained under reaction conditions relevant to these field studies are directly utilized to estimate the amount of ambient OA formed from this reaction pathway (Xu et al., 2015c). Specifically, it is estimated that 50% of nighttime OA production occurs through reaction of monoterpenes with nitrate radicals in SOAS (Xu et al., 2015c). Results from this study and Xu et al. (2015c) illustrate the substantial insights one can gain into aerosol formation chemistry and ambient aerosol source apportionment through coordinated fundamental laboratory studies and field measurement studies. Further, multiple gas-phase organic nitrate species are identified in this chamber study, which could be used to help interpret ambient gas-phase composition data obtained from the large suite of gas-phase measurements in SOAS. Owing to difficulties in measuring complex atmospheric processes, laboratory studies are critical in generating fundamental data to understand and predict SOA formation regionally and globally. In this regard, it is imperative not to view laboratory studies as isolated efforts, but instead to make them

essential and integrated parts of research activities in the wider atmospheric chemistry community (e.g., field campaigns).

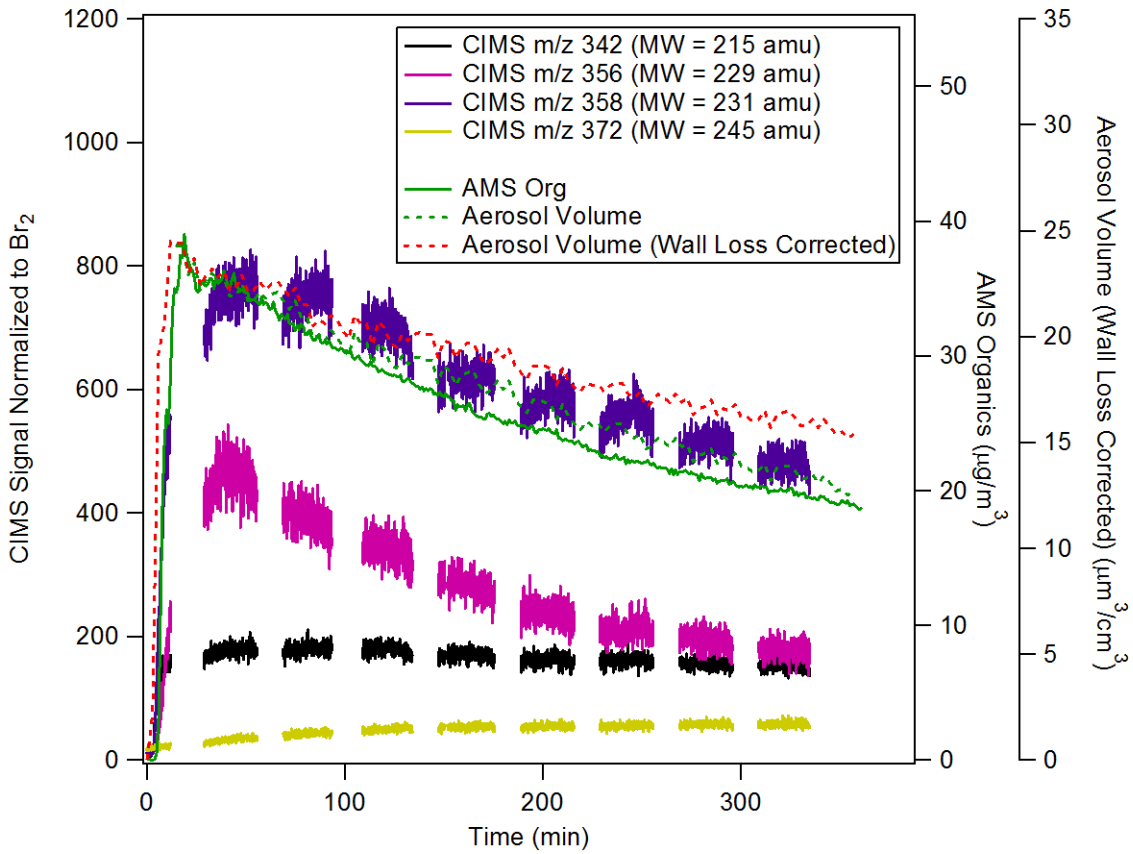

Figure 2.1: Time series of the gas-phase organic nitrate species measured by the CIMS and the corresponding aerosol formation measured by HR-ToF-AMS (organics mass) and SMPS (aerosol volume) (Experiment 30 in Table 2.1). The gas-phase species at *m/z* 356 decreases over the course of the experiment while the species at *m/z* 372 increases steadily

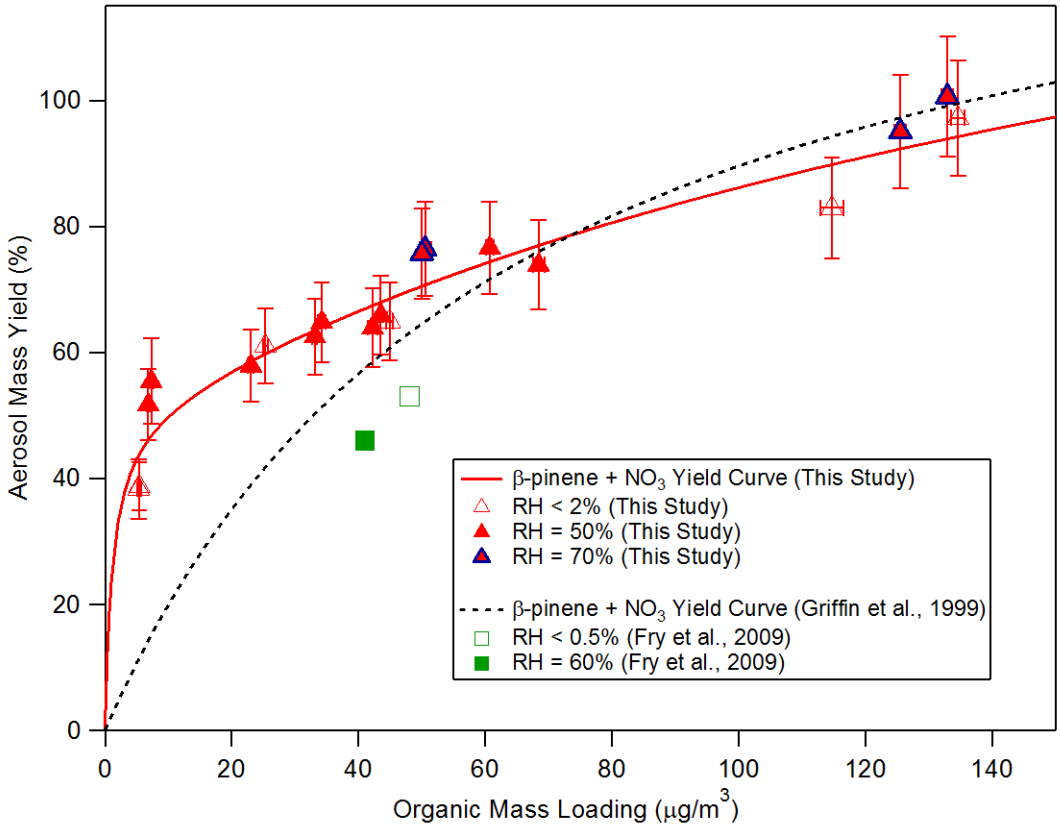

Figure 2.2: Aerosol mass yield as a function of organic mass loading for the β-pinene+NO_3 reaction under "RO_2+NO_3 dominant" conditions. The aerosol mass yields obtained in this study are compared to those measured in previous chamber studies by Griffin et al. (1999) and Fry et al. (2009). The aerosol mass yields obtained in this study are fitted using the two-product model proposed previously by Odum et al. (1996). The yield parameters obtained in this study and those from Griffin et al. (1999) are shown in Table 2.2. In order to better compare the aerosol mass yields obtained in this study to that by Griffin et al. (1999), measurements by Griffin et al. (1999) are adjusted to a temperature of 298K and density of 1.41 g cm^{-3}. The x-axis error bars represent one standard deviation of volume measured by SMPS at peak growth. The y-axis error bars represent uncertainty in yield calculated by an 8% uncertainty in chamber volume, 5% uncertainty in hydrocarbon injection, and one standard deviation of the aerosol volume measured by SMPS at peak growth.

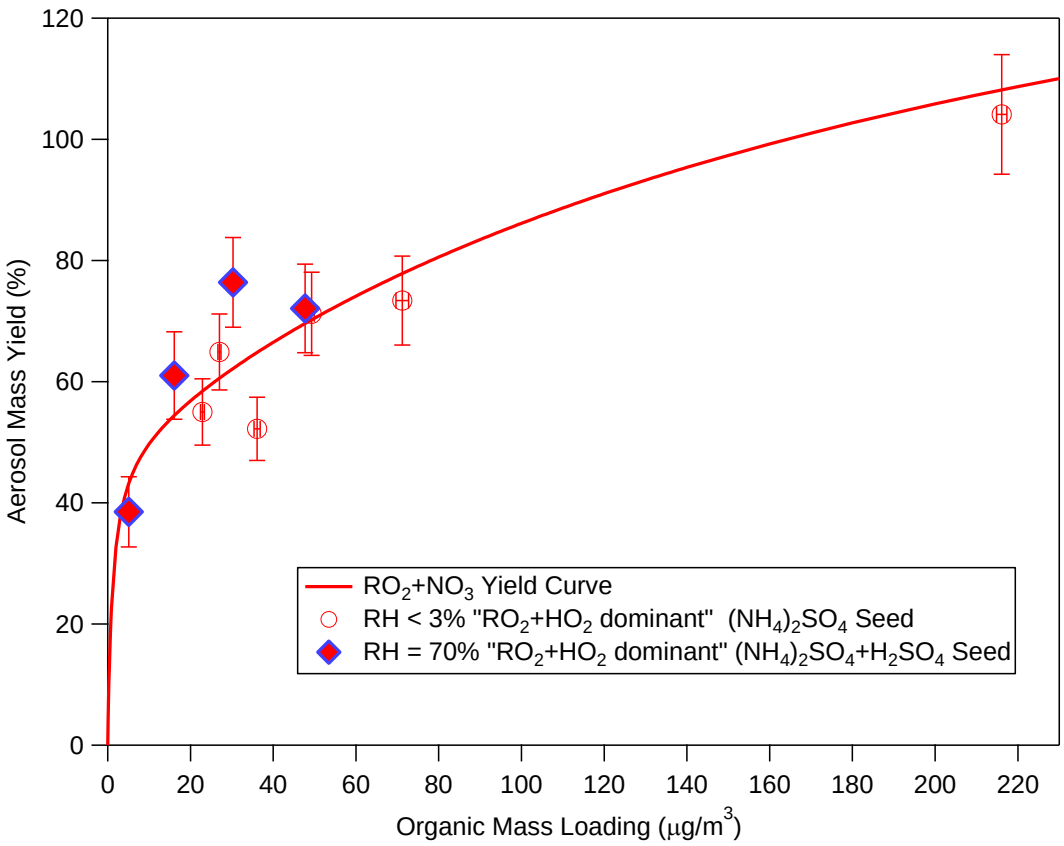

Figure 2.3: Aerosol mass yield as a function of organic mass loading for the β-pinene+NO_3 reaction under "RO_2+HO_2 dominant" conditions. These aerosol mass yields are compared to the yield curve (solid line) for the NO_3+β-pinene reaction under "RO_2+NO_3 dominant" conditions. The x-axis error bars represent one standard deviation of volume measured by SMPS at peak growth. The y-axis error bars represent uncertainty in yield calculated by an 8% uncertainty in chamber volume, 5% uncertainty in hydrocarbon injection, and one standard deviation of the aerosol volume measured by SMPS at peak growth.

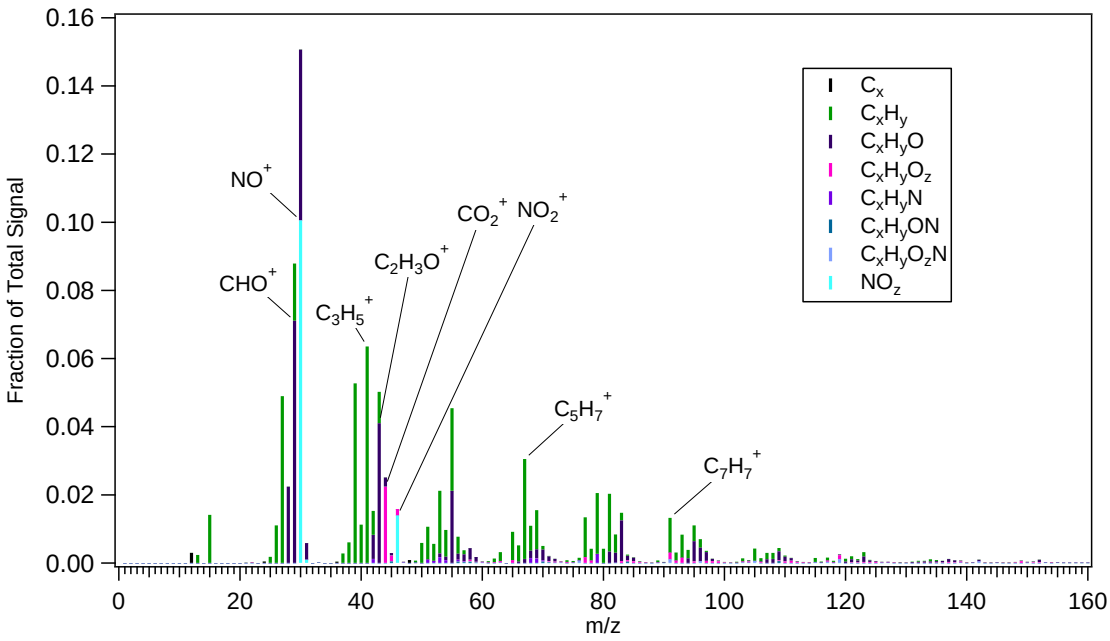

Figure 2.4: High-resolution aerosol mass spectrum of the SOA formed from the β-pinene+NO_3 reaction under dry, ammonium sulfate seed, and "RO_2+NO_3 dominant" conditions (Experiment 5 in Table 2.1). The mass spectrum is colored by the ion type to indicate the contribution of each ion type to the mass spectrum. Only ions up to *m/z* 160 are shown as the signals beyond *m/z* 160 are minimal. Ions that contribute significantly to the total signal are also labeled.

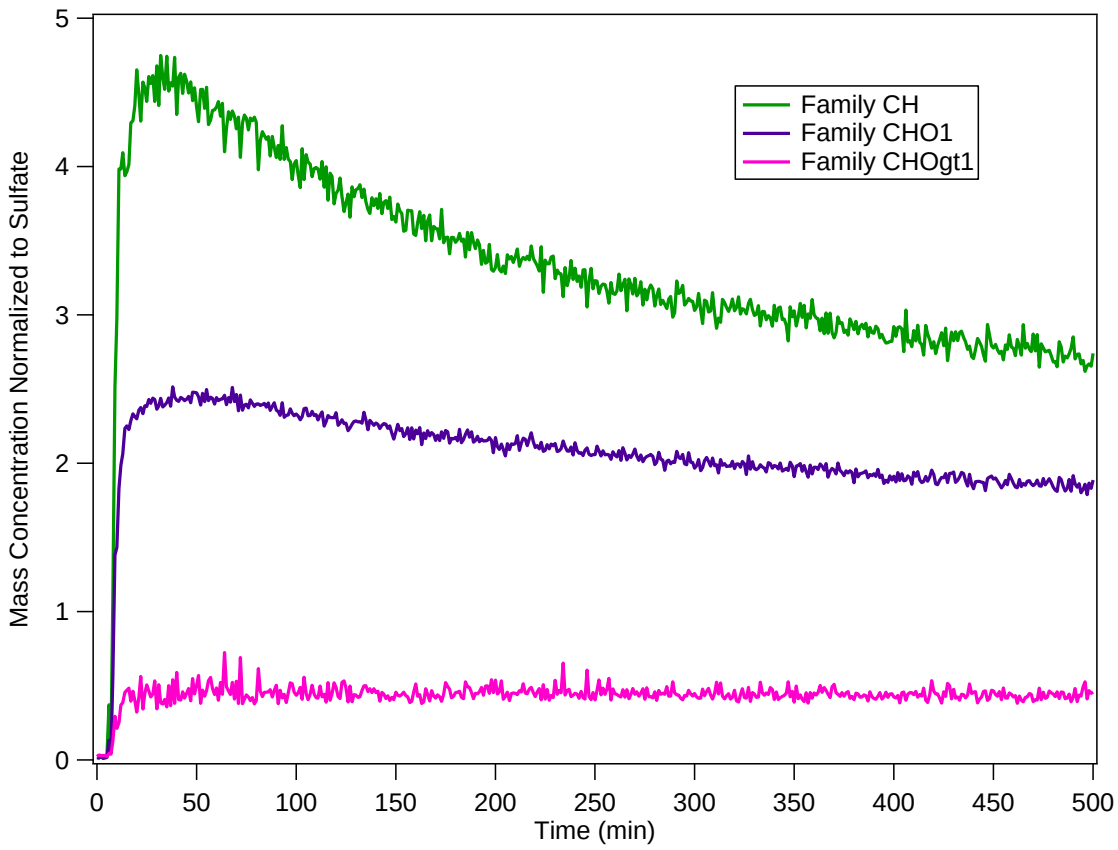

Figure 2.5: Time series of mass concentrations of the major organic families (normalized to the sulfate mass concentration) as measured by the HR-ToF-AMS at RH < 2% under "RO_2+NO_3 dominant" conditions (Experiment 5 in Table 2.1). The least oxidized organic species (i.e. Family CH) decreases rapidly at the start of the experiment and has the largest decrease among the three major organic families.

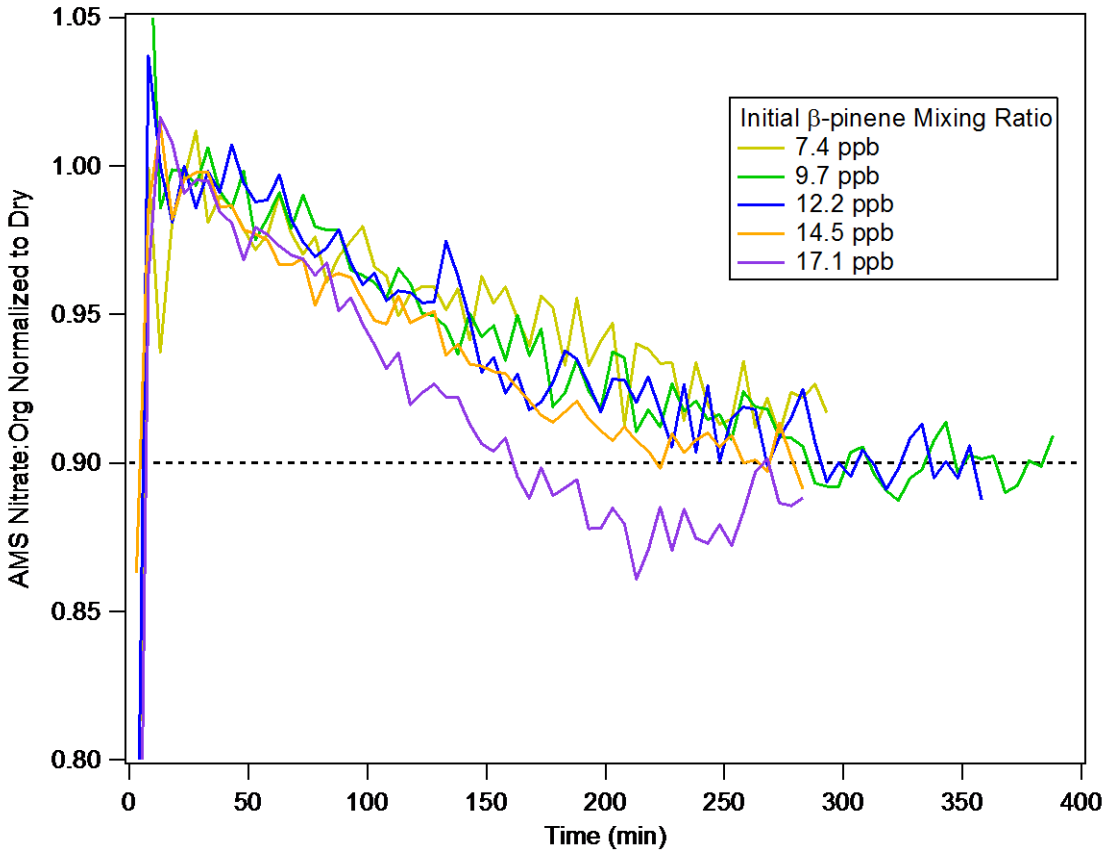

Figure 2.6: The AMS Nitrate:Org ratio of humid (RH = 50%) experiments normalized to the corresponding dry experiments with same initial β-pinene mixing ratio, five-minute averaged, for "RO_2+NO_3 dominant" experiments. This ratio is referred to as $(Nitrate:Org)_{norm}$ in the main text. For comparison purposes, all data are normalized to the highest $(Nitrate:Org)_{norm}$ ratio.

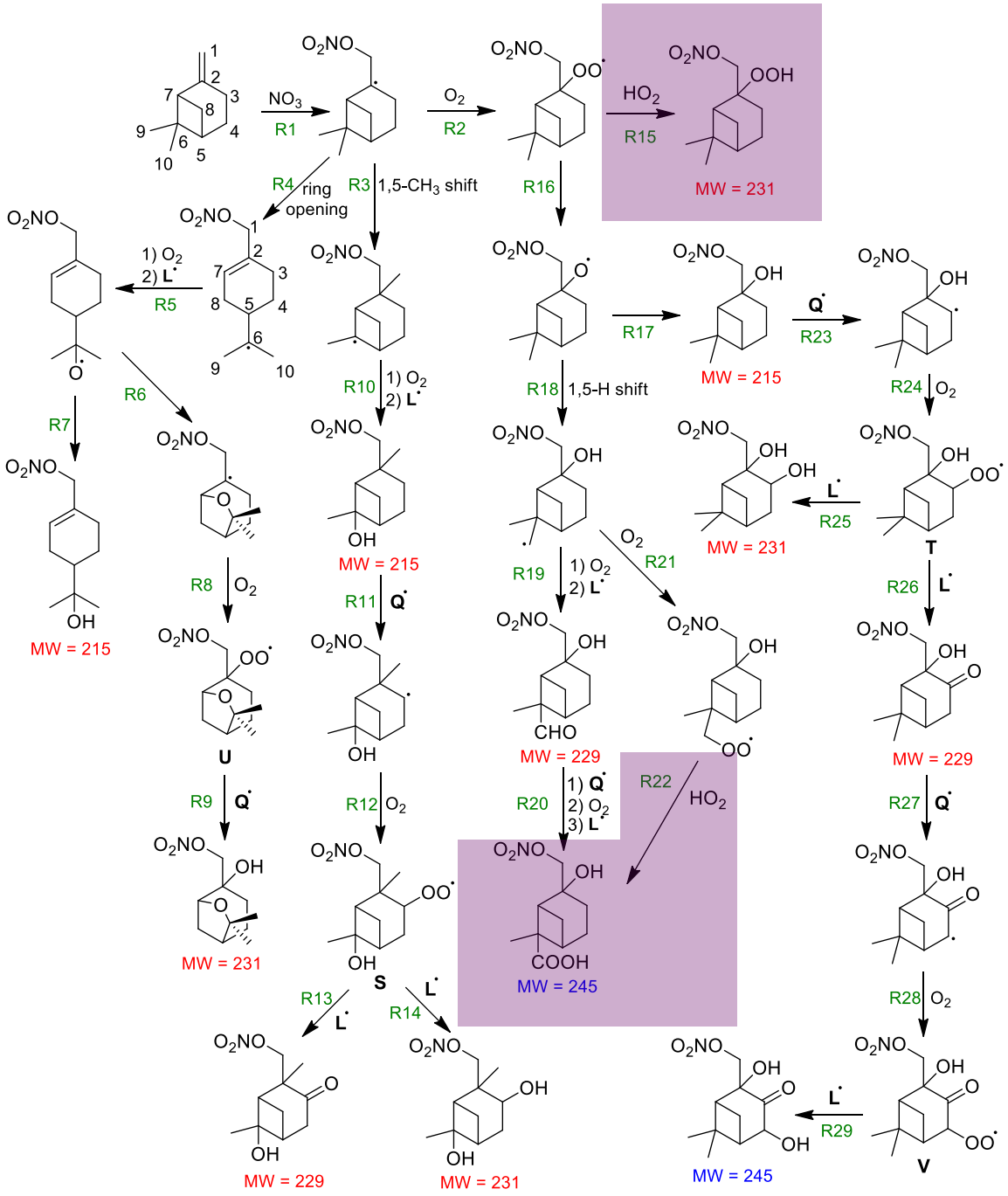

Figure 2.7: Generation of gas-phase species with molecular weights (MW) of 215, 229, and 231 amu detected by CIMS (red font), aerosol species with MW = 245 amu in filters analyzed by UHPLC-MS (blue font). Reaction numbers are given in green font and reaction with generic radical $\mathbf{Q}^{\cdot}$ (e.g., NO_3, RO_2, etc.) is used to symbolize any species abstracting hydrogen atoms. Reactions which can be accomplished by any of the radicals present (RO_2, HO_2, NO_3 etc.) are symbolized by reaction with generic radical $\mathbf{L}^{\cdot}$. Reactions enhanced in the RO_2+HO_2 dominant pathway are highlighted in purple.

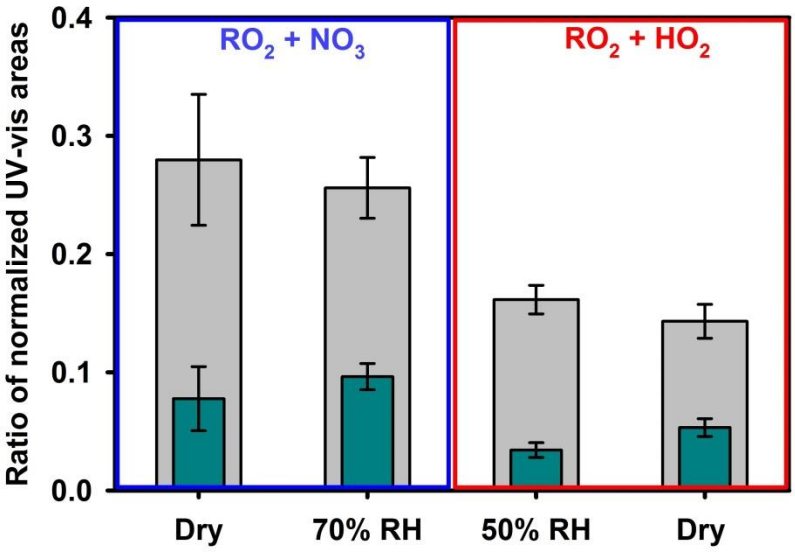

Figure 2.8: Ratio of the total areas integrated under UV-visible chromatograms collected at 235 nm (gray bars, ROOR and ROOH) and 270 nm (teal bars, -C=O and -ONO_2) relative to 205 nm for experiments dominated by (left-hand side panel) RO_2+NO_3 reaction and (right-hand side panel) RO_2+HO_2 reaction under both humid and dry conditions.

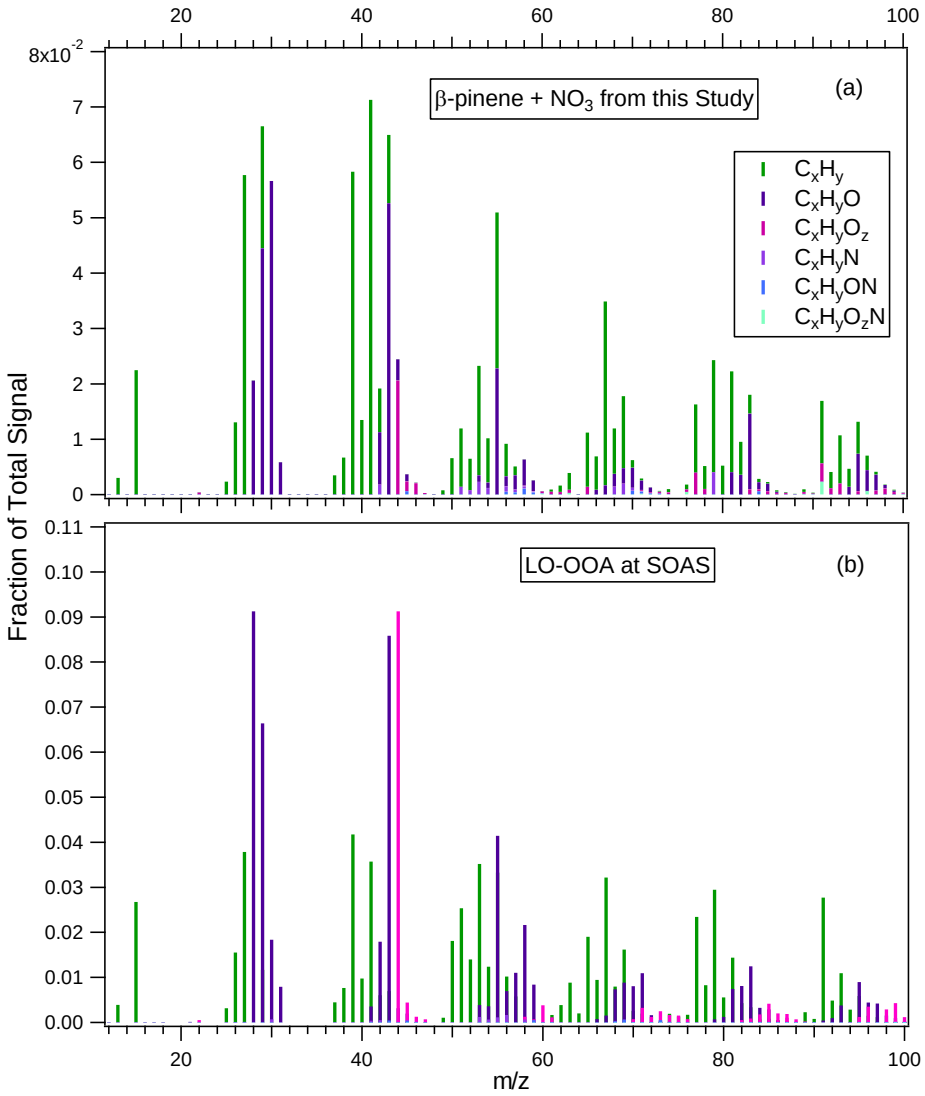

Figure 2.9: A comparison of mass spectra obtained from this work and the LO-OOA factor identified from PMF analysis of the HR-ToF-AMS data from the SOAS field campaign. (a) Mass spectrum of the SOA formed from the β-pinene+NO_3 reaction at RH = 70 % under "RO_2+HO_2 dominant" conditions and $(NH_4)_2SO_4$+H_2SO_4 seed (Experiment 34 in Table 2.1). (b) Mass spectrum for the LO-OOA factor identified from PMF analysis of the SOAS HR-ToF-AMS data (Xu et al., 2015c). The mass spectra are colored by the ion type to indicate their contribution to the mass spectra. Ions $C_5H_7^+$ (*m/z* 67) and $C_7H_7^+$ (*m/z* 91) are distinctive for the β-pinene mass spectrum (Section 2.5). To facilitate comparison, *m/z* > 50 have been multiplied by a factor of 3 in the LO-OOA spectrum.

Table 2.1: Experimental conditions and aerosol mass yields for all experiments

Experiment	RH (%)	Condition	Seed	ΔHC[c] (ppb)	ΔHC[c] ($\mu g\ m^{-3}$)	ΔM_o[d] ($\mu g\ m^{-3}$)	Mass Yield (%)
1	< 2	RO_2+NO_3	AS[a]	2.5±0.2	13.8±1.3	5.3±0.41	38.3±5.5
2	< 2	RO_2+NO_3	AS	2.5±0.2	13.8±1.3	5.4±0.15	38.7±4.0
3	< 2	RO_2+NO_3	AS	7.4±0.7	41.5±3.9	25.3±0.54	61.0±6.0
4	< 2	RO_2+NO_3	AS	9.9±0.9	55.4±5.2	--[e]	--
5	< 2	RO_2+NO_3	AS	12.4±1.2	69.2±6.5	--	--
6	< 2	RO_2+NO_3	AS	12.4±1.2	69.2±6.5	44.9±0.73	64.9±6.3
7	< 2	RO_2+NO_3	AS	14.9±1.4	83.0±7.8	--	--
8	< 2	RO_2+NO_3	AS	17.4±1.6	96.9±9.1	--	--
9	< 2	RO_2+NO_3	AS	24.8±2.4	138.4±13.1	134.6±1.51	97.2±9.3
10	< 2	RO_2+NO_3	AS	24.8±2.4	138.4±13.1	114.7±2.51	82.9±8.2
11	51	RO_2+NO_3	AS	2.4±0.2	13.2±1.2	7.3±0.57	55.4±8.2
12	50	RO_2+NO_3	AS	2.4±0.2	13.2±1.2	6.8±0.36	51.7±6.3
13	49	RO_2+NO_3	AS	7.1±0.7	39.6±3.7	23.0±0.65	57.9±6.0
14	49	RO_2+NO_3	AS	9.5±0.9	52.8±5.0	34.2±0.89	64.8±6.6
15	51	RO_2+NO_3	AS	9.5±0.9	52.8±5.0	33.1±0.56	62.5±6.1
16	50	RO_2+NO_3	AS	11.9±1.1	66.1±6.2	43.5±0.60	65.9±6.4
17	50	RO_2+NO_3	AS	11.9±1.1	66.1±6.2	42.2±0.98	63.9±6.4
18	51	RO_2+NO_3	AS	14.2±1.3	79.3±7.5	60.7±0.83	76.6±7.4
19	51	RO_2+NO_3	AS	16.6±1.6	92.5±8.7	68.4±1.26	73.9±7.2
20	71	RO_2+NO_3	AS	11.9±1.1	66.1±6.2	50.5±1.32	76.4±7.8
21	70	RO_2+NO_3	AS	11.9±1.1	66.1±6.2	50.0±0.44	75.7±7.2
22	72	RO_2+NO_3	AS	23.7±2.2	132.1±12.5	125.5±1.35	95.0±9.0
23	68	RO_2+NO_3	AS	23.7±2.2	132.1±12.5	132.9±1.33	100.6±9.5
24	51	RO_2+NO_3	AS+SA[b]	7.1±0.7	39.6±3.7	25.5±0.69	64.4±6.6
25	50	RO_2+NO_3	AS+SA	11.9±1.1	66.1±6.2	46.4±1.10	70.4±6.8
26	51	RO_2+NO_3	AS+SA	16.6±1.6	92.5±8.7	74.4±1.23	80.5±7.7
27	< 3	RO_2+HO_2	AS	7.4±0.7	41.5±3.9	27.0 ±0.54	64.9±6.4
28	< 3	RO_2+HO_2	AS	7.4±0.7	41.5±3.9	22.9±0.71	55.0±5.8
29	< 3	RO_2+HO_2	AS	12.4±1.2	69.2±6.5	49.3±0.97	71.2±7.1
30	< 3	RO_2+HO_2	AS	12.4±1.2	69.2±6.5	36.1±1.17	52.2±5.6
31	< 2	RO_2+HO_2	AS	17.4±1.6	96.9±9.1	71.2±2.32	73.4±7.8
32	< 3	RO_2+HO_2	AS	37.3±3.5	207.6±19.6	216.1±1.96	104.1±9.9
33	49	RO_2+HO_2	AS	35.6±3.4	198.2±18.7	147.8±1.42	74.6±7.1
34	69	RO_2+HO_2	AS+SA	2.4±0.2	13.2±1.2	5.1±0.59	38.5±8.1
35	69	RO_2+HO_2	AS+SA	4.7±0.4	26.4±2.5	16.1±1.14	61.0±9.0
36	66	RO_2+HO_2	AS+SA	7.1±0.7	39.6±3.7	30.3±0.71	76.4±7.8
37	66	RO_2+HO_2	AS+SA	11.9±1.1	66.1±6.2	47.7±1.77	72.1±8.1
38	< 1	RO_2+NO_3	None	12.4±1.2	69.2±6.5	42.3±0.46	61.1±5.8

Table 2.1 Continued

39	50	RO_2+NO_3	None	11.9±1.1	66.1±6.2	44.3±0.34	67.0±6.4
40	<2	RO_2+HO_2	None	12.4±1.2	69.2±6.5	18.7±0.51	27.0±2.8
41	66	RO_2+HO_2	None	11.9±1.1	66.1±6.2	28.5±0.60	43.1±4.2
42	50	RO_2+HO_2	None	11.9±1.1	66.1±6.2	18.4±0.34	27.8±2.7
43	<2	RO_2+HO_2	AS*	12.4±1.2	69.2±6.5	33.6±0.79	48.5±4.9
44	68	RO_2+HO_2	AS+SA*	11.9±1.1	66.1±6.2	46.6±0.86	70.6±7.0
45	66	RO_2+HO_2	AS+SA*	11.9±1.1	66.1±6.2	44.5±0.87	67.3±6.7

*Experiments with seed concentrations greater than the typical seed concentrations for investigating vapor wall loss effects

[a]$(NH_4)_2SO_4$ Seed

[b]$(NH_4)_2SO_4+H_2SO_4$ Seed

[c]Uncertainties in hydrocarbon concentration are calculated from an 8% uncertainty in chamber volume and 5% uncertainty in hydrocarbon mass

[d]Uncertainties in aerosol mass loading are calculated from one standard deviation of aerosol volume as measured by the SMPS

[e]"--" denotes experiments where there is no SMPS data

Table 2.2: Fit parameters for two-product model proposed by Odum et al. (1996)

	α_1	K_1	α_2	K_2
β-pinene+NO_3 (this study)	1.187	0.004546	0.496	0.880
Griffin et al. (1999)	1.464	0.0158		

Table 2.3: Coefficients for the Volatility Basis Set Proposed by Donahue et al. (2006)

	Saturation Vapor Pressure, C* (μg m^{-3})			
	0.1	1	10	100
β-pinene+NO_3 (this study)	0.373	0.033	0.000	0.941
Griffin et al. (1999)	0.000	0.000	0.301	1.204

CHAPTER 3

EFFECT OF TEMPERATUE, HUMIDITY, AND DILUTION ON SECONDARY ORGANIC AEROSOL (SOA) FORMED FORM NO_3 OXIDATION OF MONOTERPENES: A CASE STUDY FOR AEROSOL MIXING AND EVAPORATION DURING NIGHT-TO-DAY TRANSITION

3.1 Introduction

The nitrate radical (NO_3) oxidation of biogenic volatile organic compounds (BVOC) is an important contributor to the secondary organic aerosol (SOA) burden due to its high reactivity (Atkinson and Arey, 2003a) and large SOA mass yields (Griffin et al., 1999; Hallquist et al., 1999; Spittler et al., 2006; Ng et al., 2008b; Rollins et al., 2009; Fry et al., 2009; Fry et al., 2011; Kwan et al., 2012; Jaoui et al., 2013; Fry et al., 2014; Boyd et al., 2015). The reaction of BVOC with NO_3 radical, which is formed by the reaction of NO_2 with O_3, provides a direct link between observations that organic aerosol is well correlated with anthropogenic pollutants (Weber et al., 2007a) but contain carbon that is mostly biogenic in origin (Lewis et al., 2004; Marley et al., 2009). Modeling studies estimate that 5-21% of global SOA is produced by NO_3 chemistry (Hoyle et al., 2007; Pye et al., 2010). Monoterpene+NO_3 chemistry is especially important at night because NO_3 is the dominant nocturnal oxidant and monoterpenes are typically emitted during the day and at night (Fuentes et al., 2000; Guenther et al., 2012). Limonene and β-pinene are two of the most important monoterpenes due to their high global abundance (Pye et al.,

The text in this chapter is reproduced, in part, by: Boyd, C. M., Nah, T., Xu, L., Ng, N. L.: Effect of Temperature, Humidity, and Dilution on Secondary Organic Aerosol (SOA) formed from NO_3 Oxidation of Monoterpenes: A Case Study for Aerosol Mixing and Evaporation during Night-to-Day Transition, Environ. Sci. Technol, 2016 (Submitted)

2010) and aerosol mass yields (30-100%) (Griffin et al., 1999; Hallquist et al., 1999; Spittler et al., 2006; Fry et al., 2009; Fry et al., 2011; Fry et al., 2014; Boyd et al., 2015). In the southeastern United States, recent studies show that NO_3 oxidation of monoterpenes can produce a substantial fraction of organic aerosol (Ayres et al., 2015; Boyd et al., 2015; Xu et al., 2015c; Xu et al., 2015b). Based on coordinated laboratory and field studies, Xu et al. (2015c) shows that this reaction contributes to 50% of total nighttime OA production in the southeastern US, a large fraction of which is from β-pinene+NO_3 chemistry.

Aerosol lifetimes in the atmosphere typically range between 1 to 2 weeks, half of which is at night and the remaining half in the day. Thus, it is important to study the changes in the physicochemical properties of SOA formed by BVOC+NO_3 reactions during the transition from night to day. Since BVOC+NO_3 reactions produce large amounts of SOA and organic nitrates, these changes could have impacts on the NO_x cycle and total aerosol loading. Nah et al. (2016) shows that the SOA and organic nitrates formed from the nighttime monoterpene+NO_3 reaction can serve as a NO_x sink or reservoir upon photochemical oxidation, depending on the precursor hydrocarbons. During the day, in addition to photochemical oxidation, surface temperature and boundary layer height also increase, which lead to dilution of gas- and particle-phase organics. Aerosol evaporation is expected to occur as a result of dilution (Pankow, 1994) and increasing temperatures. Understanding evaporation of nighttime SOA upon daybreak is important to accurately predict the dynamics of aerosol loading and properties over its lifetime.

Aerosol evaporation can be predicted by either the Odum two-product model (Odum et al., 1996) or the volatility basis set (Donahue et al., 2006; Grieshop et al., 2007). Previous studies have shown that bulk aerosol volatility is highly dependent on temperature (Offenberg et al., 2006; Saathoff et al., 2009; Svendby et al., 2008; Warren et al., 2009; Qi et al., 2010). The temperature-dependent SOA mass yield can be approximated using the SOA mass yield at a reference temperature and the Clausius-Clapeyron equation (Chung and Seinfeld, 2002) if the bulk enthalpy of vaporization for the SOA is known. Although previous studies have shown that enthalpy of vaporization increases with decreasing saturation concentration (C^*) (Epstein et al., 2009; Saathoff et al., 2009; Grieshop et al., 2009; Saha and Grieshop, 2016), a single value is often assumed for a single SOA system (Chung and Seinfeld, 2002; Offenberg et al., 2006; Svendby et al., 2008) or used to estimate aerosol loadings in global models. (Tsigaridis et al., 2014). Furthermore, many chamber and thermodenuder studies (Offenberg et al., 2006; Warren et al., 2009) that evaluate the enthalpy of vaporization typically use mass loadings that are higher than what is considered to be atmospherically relevant (~10 μg m^{-3}) (Xu et al., 2015c). As a result these studies may underestimate the enthalpies of vaporization and evaporation of ambient aerosol may be underpredicted when these values are used in atmospheric models. To accurately predict aerosol loadings, both the thermodynamics and kinetics of aerosol evaporation must be understood. Typically, aerosol is assumed to be liquid-like, with no kinetic resistance and evaporation governed solely by thermodynamics (i.e., determined by the Clausius-Clapeyron equation). However, a number of recent studies showed that SOA formed in some reactions exists as a viscous semi-solid (Cappa and Wilson, 2011; Vaden et al., 2011; Abramson et al.,

2013; Renbaum-Wolff et al., 2013), which may significantly slow the evaporation of organic aerosol.

In this study, we investigate the effect of temperature on SOA formed from the NO_3 oxidation of limonene and evaluate the enthalpy of vaporization for the limonene+NO_3 system. Furthermore, we study the effect of isothermal dilution and increasing temperatures on the evaporation of aerosol formed from NO_3 chemistry. The evaporation of aerosol mixtures produced from limonene+NO_3 and β-pinene+NO_3 is also investigated as a function of relative humidity and aerosol morphology. This study provides fundamental data for understanding the changes in physical properties for organic aerosol formed by BVOC+NO_3 reactions.

3.2 Experimental

All experiments are performed in the Georgia Tech Environmental Chamber Facility, which consists of two 12 m^3 Teflon chambers (Boyd et al., 2015). Experimental conditions are shown in Table 3.1. Reactions are conducted at either 25 ^oC or at 40 ^oC under dry conditions. The limonene+NO_3 reaction is also performed under humid conditions (RH ~ 50%) (Experiments 13 and 14) to examine the effects of humidity on aerosol yield. In all experiments, formaldehyde is introduced to the chamber to enhance the RO_2+HO_2 reaction pathway (Nguyen et al., 2014; Boyd et al., 2015). The injection of formaldehyde, inorganic seed, hydrocarbons, and N_2O_5 are detailed in Boyd et al. (2015) and are briefly summarized in Appendix B. The introduction of N_2O_5 into the chamber marks the beginning of the experiment. About 3-5 hours after peak SOA growth, the SOA in the chamber is either isothermally diluted or heated. In isothermal dilution

experiments, dry zero air is reintroduced into the chamber at a rate of 40 L min^{-1}. This dilutes the particle- and gas-phase products by approximately a factor of two. In aerosol heating experiments, the chamber temperature is increased from 25 to 40 °C with a typical temperature profile shown in Figure B.1.

To examine the extent of mixing between aerosol from two different BVOC+NO_3 reactions, we perform two types of experiments to mix SOA from the limonene+NO_3 reaction (hereafter referred to as 'limonene SOA') and SOA from the β-pinene+NO_3 reaction (hereafter referred to as 'β-pinene SOA'). In the first type of experiment (Experiments 15, 16, and 17), subsequently referred to as 'Limonene Core' experiments, limonene is first introduced into the chamber and oxidized by NO_3. Approximately 3 hours after peak aerosol growth, β-pinene is then introduced into the chamber followed by a second injection of N_2O_5. Aerosol is either heated immediately after (Experiment 15) or an hour after (Experiments 16 and 17) β-pinene SOA growth. In the second set of experiments (Experiment 18 and Experiment 19), subsequently referred as the 'Mixed' experiments, limonene and β-pinene are oxidized simultaneously in order to achieve as homogenous an aerosol mixture as possible. Aerosol is heated 3 hours after peak SOA growth.

O_3 and NO_x concentrations are measured using an O_3 analyzer (Teledyne T400) and a chemiluminescence NO_x monitor (Teledyne 200EU), respectively. Hydrocarbon concentrations are measured using Gas Chromatography-Flame Ionization Detector (GC-FID) (Agilent 7890A). Aerosol number and volume distributions are measured with a

Scanning Mobility Particle Sizer (SMPS, TSI) consisting of a differential mobility analyzer (DMA) (TSI 3040) and Condensation Particle Counter (CPC) (TSI 3775). Bulk aerosol composition is measured using an Aerodyne High Resolution Time-of-Flight Aerosol Mass Spectrometer (HR-ToF-AMS) (DeCarlo et al., 2006). The HR-ToF-AMS NO family ions are included in the calculation of the N:C ratio but are excluded in the calculation of the O:C ratio.

3.3 Results and Discussion

3.3.1 Aerosol Yields and Composition for limonene+NO_3

Figures 3.1a and 3.1b show the typical high resolution aerosol mass spectra for the limonene+NO_3 and β-pinene+NO_3 systems, respectively. The mass spectrum for the β-pinene+NO_3 system (Figure 3.1b) is similar to that reported in Boyd et al. (2015). The average NO^+/ NO_2^+ ratios for limonene SOA and β-pinene SOA are both 6.3. This ratio is on the lower end of reported NO^+/ NO_2^+ ratios in Boyd et al. (2015) and is much higher than typical values for inorganic nitrates (Farmer et al., 2010). Therefore, the nitrate species in the aerosol phase are likely organic nitrates. The average N:C ratio of limonene SOA in all seeded experiments is ~0.104. This corresponds to an organic nitrate yield of about 104% if we assume each organic nitrate has one nitrate group and ten carbon atoms (Boyd et al., 2015). For limonene+NO_3, the organic nitrate yield is more than 100% because limonene has two double bonds that can react with NO_3 via radical addition. The N:C ratio of SOA formed from the β-pinene+NO_3 reaction is about 0.076, in good agreement with the N:C ratio of 0.074 reported in Boyd et al. (2015) Using the approach described in Boyd et al. (2015), the rate of organic nitrate hydrolysis can be inferred from

the change in the AMS NO_3:Org ratio (Figure B.2). Similar to the β-pinene+NO_3 system, particulate organic nitrates produced by the limonene+NO_3 system appear to undergo slow hydrolysis and are likely primary/secondary organic nitrates (SI) (Darer et al., 2011; Hu et al., 2011).

The aerosol mass yields (defined as the mass of aerosol produced divided by the mass of hydrocarbon reacted) (Odum et al., 1996) at 25 and 40 °C under dry conditions for the limonene+NO_3 system are shown in Figure 3.2 (calculation shown in Appendix B). The aerosol mass yield at 25 °C for the limonene+NO_3 reaction is approximately constant at 174%, which is higher than aerosol mass yields measured in other BVOC+NO_3 systems (Griffin et al., 1999; Hallquist et al., 1999; Spittler et al., 2006; Ng et al., 2008b; Fry et al., 2009; Fry et al., 2014; Boyd et al., 2015). A constant SOA mass yield suggests that the volatility of the aerosol-forming products of the limonene+NO_3 reaction are low enough to be completely in the particle-phase under the conditions studied. Aerosol mass yields for the limonene+NO_3 reaction under humid conditions (RH = 50%) are shown in Figure B.3. In contrast to the β-pinene+NO_3 reaction (Boyd et al., 2015), aerosol mass yields are enhanced at higher humidity for the limonene+NO_3 reaction. This suggests that water may have different effects on different BVOC+NO_3 reactions and warrants further study. Aerosol mass yields for nucleation experiments are also shown in Figure B.3 for both dry and humid conditions. The aerosol mass yields are comparable to seeded experiments. Since seed aerosol does not enhance the aerosol mass yield and limonene oxidation by NO_3 is rapid, it is likely that the SOA formation from limonene+NO_3 reaction is not significantly affected by vapor phase wall loss (Boyd et al., 2015).

Aerosol mass yields at 25 °C for previous limonene+NO_3 studies (Hallquist et al., 1999; Fry et al., 2011; Fry et al., 2014) range from 20-40 % (also shown in Figure 3.2). Spittler et al. (2006) show that the aerosol mass yield for the limonene+NO_3 can range from 21-40%, depending on the use of either inorganic ammonium sulfate seed or organic seed produced by ozonolysis of limonene. The differences between the previously reported yields and this study are likely due to the difference in reaction conditions between this study and previous work. For example, while the experiments in this study are designed to oxidize both double bonds of limonene with NO_3 (with the use of excess NO_3, and absence of ozone), the limonene in previous work may have unreacted double bonds (Hallquist et al., 1999; Spittler et al., 2006; Fry et al., 2014) or have one or both double bonds oxidized by ozone (Fry et al., 2011). Although SOA yields reported in previous studies may be relevant for BVOC-rich environments where only one of limonene's two double bonds reacts (Rollins et al., 2012), these yields may underpredict SOA formed from the limonene+NO_3 reaction in regions where NO_x and NO_3 concentrations are high enough to oxidize both of limonene's double bonds.

Unlike the SOA yields at 25 °C, SOA yields at 40 °C are not constant. The aerosol mass yields at 40 °C can be fitted using a variant of the Odum two-product model (Odum et al., 1996). Fitting the traditional two-product model requires a high equilibrium partitioning coefficient for one of the two products and suggests the presence of non-volatile products. By assuming one of the volatility bins (with coefficient α_1) is non-volatile, the data at 40 °C are fitted using Eq. (3.1):

$$Y = \alpha_1 + \frac{M_o \alpha_2 K_2}{1 + M_o K_2} \quad (3.1)$$

Fitting Eq. (3.1) to the experimental data results in the following yield parameters: [α_1, α_2, K_2]= [0.673, 1.11, 0.0139]. The coefficient for α_1 is larger than the second term on the right side of Eq. (3.1) within the two-product model for mass loadings below 110 μg m^{-3}, indicating that the majority of SOA at 40 °C is non-volatile under the conditions studied. The abundance of low-volatility products has important implications for the evaporation of SOA and will be discussed further in the next section.

3.3.2 Isothermal Dilution

Figures 3.3a and 3.3b show the SMPS Volume:AMS SO_4 ratio and the AMS Org:SO_4 ratio for all aerosol dilution experiments, respectively. Time zero is defined as the time when the diluting air is introduced into the chamber. We use these two ratios as bounding parameters for aerosol evaporation. The SMPS volume has contribution from inorganic seeds and thus the SMPS Volume:AMS SO_4 ratio is less sensitive to evaporation as would be if only organics were considered. However, the AMS Org:SO_4 ratio can be affected by diffusion-limited growth (Loza et al., 2012), where nucleated organic-only particles are smaller than sulfate-containing particles and are lost to the walls faster. The AMS Org:SO_4 therefore could decease even if there is no evaporation present. Therefore, both of these are likely bounding parameters for the organic evaporation. Normalizing the SMPS volume and AMS Org by AMS SO_4 accounts for the decrease in aerosol concentration that is caused by an increase of chamber volume associated with isothermal dilution. While the decrease in the SMPS volume and AMS Org is due to both dilution and evaporation of organic aerosol, AMS SO_4 is expected to decrease solely due to

dilution because it is non-volatile below 40 °C (Xu et al., 2016). Therefore, any organic evaporation induced by isothermal dilution will result in a decrease in the SMPS Volume:AMS SO_4 and the AMS Org:SO_4.

The SMPS Volume:AMS SO_4 ratio is approximately constant during isothermal dilution, suggesting that the aerosol does not evaporate appreciably, as a lower bound. The AMS Org:SO_4 ratio does decrease slightly during the early stages of dilution, likely due to faster loss of nucleated pure organic particles to chamber walls. Nevertheless, both the SMPS Volume:AMS SO_4 ratio and the AMS Org:SO_4 ratio show an insignificant decrease over the time of dilution, which suggests that a negligible portion of the limonene SOA is evaporating. These results are somewhat unsurprising since the majority of the limonene SOA is composed of low-volatility products and the mass loading of aerosol is not expected to affect the gas-particle partitioning substantially. These observations suggest that the evaporation of limonene SOA from dilution is thermodynamically unfavorable under the conditions studied here. Therefore, the primary driving force for aerosol evaporation during the night-to-day transition is likely due to heating.

3.3.3 Aerosol Heating and Enthalpy of Vaporization

Figure 3.2 shows that aerosol mass yields for the limonene+NO_3 system depend strongly on temperature, by as much as a factor of two. As the difference in aerosol yield (between the two temperatures) is not constant across the entire range of organic mass loadings, a

single enthalpy of vaporization could not be applied to one yield curve to obtain the other yield curve.

We propose a method for determining the enthalpy of vaporization as a function of mass loading for a given SOA system based on yield curves obtained for two different temperatures and the Clausius-Claperyon equation (Chung and Seinfeld, 2002). The mathematical details of this analysis are in Appendix B with results shown in Figure 3.4. The enthalpy of vaporization likely decreases with mass loading due a larger fraction of products with low C^* (which correlates with high enthalpy of vaporization for a wide arrange of organic compounds) (Epstein et al., 2009) at low mass loadings. These results highlight the importance of determining the enthalpy of vaporization. Currently, most atmospheric models use enthalpies that range from 18-156 kJ mol^{-1} with over 80% of them using a value of less 60 kJ mol^{-1} (Tsigaridis et al., 2014). This is lower than the enthalpies of vaporization calculated for SOA produced by the limonene+NO_3 reaction in this study (117-237 kJ mol^{-1}). If the enthalpies of vaporization of SOA produced by other systems are similarly underpredicted, this may have a significant effect on the aerosol mass calculated in atmospheric models.

When heated from 25 °C to 40 °C, the SOA formed from the limonene+NO_3 evaporates less than expected based on the difference in yield at 25 °C and 40 °C. To quantify this difference, we define the 'Heating Ratio' and 'Formation Ratio'. The 'Heating Ratio' is determined to be the mass of OA remaining after heating the aerosol formed at 25 °C to 40 °C divided by the mass of OA formed at 25 °C. This is calculated by dividing the

AMS Org:SO_4 (15-minute averaged) after the chamber has achieved a temperature of 38 °C by the AMS Org:SO_4 prior to heating. The 'Formation Ratio' is determined to be the mass of aerosol formed at 40 °C divided by the mass of aerosol formed at 25 °C. There is a large difference between the 'Heating Ratio' and 'Formation Ratio' (Figure B.4), which suggests that there is a resistance to aerosol evaporation. These ratios are calculated for experiments over a range of mass loadings and we find that the 'Heating Ratio' for limonene SOA is fairly independent of mass loading (Figure B.5). There are several possibilities for this observation: 1) oligomerization following condensation may produce low volatility particle-phase compounds (Saleh et al., 2013; Kolesar et al., 2015; Robinson et al., 2015), 2) the products produced at 25 °C and 40 °C have large differences in chemical composition, or 3) the aerosol has a kinetic limitation and does not evaporate on the time scales of hours, which is longer than the predicted time scales of minutes in other SOA systems (Riipinen et al., 2010; Saleh et al., 2013) or for pure components (Riipinen et al., 2010; Zhang et al., 2015a). If oligomerization occurs after condensation, the 'Heating Ratio' and the 'Formation Ratio' should be different for all cases, but this difference is not present at high mass loadings. It is also unlikely that the products of the limonene+NO_3 reaction formed at 25 °C and 40 °C have substantial chemical differences (Appendix B). We examine the possibility that the limonene SOA is semi-solid, with the outer layers of aerosol hindering the evaporation of inner layers. We demonstrate this possibility further in Section 3.3.4 using SOA produced by two reaction systems (limonene and β-pinene).

3.3.4 Limitations to Aerosol Evaporation

It is challenging to quantify the degree of homogeneity within an aerosol particle formed from a single VOC oxidation system (i.e., either pure β-pinene SOA or pure limonene SOA). It has been demonstrated in previous studies that evaporation of organic aerosol may be hindered if it is coated with organic aerosol from a different precursor (Loza et al., 2013). In this study, experiments to mix SOA are performed to examine the interactions between SOA formed from the limonene+NO_3 and β-pinene+NO_3 reactions. We heat up the mixed SOA produced from two different methods, which are described in Section 3.2 as the "Limonene Core" and "Mixed" experiments.

We use the differences in the mass spectra of limonene SOA and β-pinene SOA (Figure 3.1) to quantify the extent of evaporation for each SOA type upon heating. Limonene SOA is characterized by an abundance of the $C_2H_3O^+$ ion (*m/z* 43), whereas the β-pinene SOA spectrum has notably high $C_5H_7^+$ (*m/z* 67) and high $C_7H_7^+$ (*m/z* 91). The mass spectrum of total OA, [MS], is assumed to be a linear combination of limonene SOA, [Lim], and β-pinene SOA, [Bpin] spectra, as represented by Eq. (3.2).

$$[MS] = a \cdot [Lim] + b \cdot [Bpin] \quad (3.2)$$

The coefficients of this linear combination, a and b, (summed to 1) represent the mass fractions of limonene SOA and β-pinene SOA in the total aerosol, respectively. From these mass fractions and the AMS Org:SO_4 ratio, the limonene SOA:SO_4 and β-pinene SOA:SO_4 ratios over the course of the experiments can be determined. By normalizing to SO_4, we can account for changes in AMS collection efficiency and particle wall loss. Since heating is slow right after increasing the temperature set point (Figure B.1), the

evaporation of aerosol is not considered until the chamber temperature has reached 26 °C to avoid noise in measurements. The SOA:SO_4 ratios are normalized by the average SOA:SO_4 ratio during the first five minutes to facilitate comparison between experiments. The change in SOA:SO_4 can therefore be used as a proxy for SOA evaporation for each precursor. The results of this analysis are shown in Figure 3.5, which shows the fractions of limonene SOA (3.5a) and β-pinene SOA (3.5b) remaining are different depending on how the initial SOA is formed (i.e., "Limonene Core" vs. "Mixed" experiments).

Less limonene SOA and more β-pinene SOA evaporate in the 'Limonene Core' experiments than in the 'Mixed' experiments as shown in Figure 3.5. If evaporation were governed solely by thermodynamics, the 'Limonene Core' and 'Mixed' experiments should have no difference in aerosol evaporation. Possible reasons for our observation include: 1) the products from the β-pinene+NO_3 reaction nucleate into particles smaller than the limonene SOA in the 'Limonene Core' experiment and are thus lost to the chamber wall more rapidly, and 2) the β-pinene SOA forms a shell and hinders the evaporation of the limonene SOA core in the 'Limonene Core' experiment. Possibility 1) can be eliminated because the particle concentration does not increase appreciably (<7%) upon formation of β-pinene SOA for any of the 'Limonene Core' experiments (Figure B.7). Therefore, it is likely there is a limitation to mixing in either or both of the 'Limonene Core' and 'Mixed' experiments.

A limitation to mixing could be the result of either high aerosol viscosity or because the products of one aerosol system are immiscible with the other system. Although mixing of aerosol has been observed between two different SOA systems, this has been limited to SOA formed from photooxidation or ozonolysis (Hildebrandt et al., 2011; Loza et al., 2013; Robinson et al., 2013). If mixing of organics from two different sources is thermodynamically favorable, the aerosol mass yield of one SOA system should be enhanced in the presence of other SOA (Hildebrandt et al., 2011; Song et al., 2011; Ye et al., 2016). Figure B.8 shows an increase in aerosol mass yield for the β-pinene+NO_3 system when limonene SOA is present. This suggests that products from the β-pinene+NO_3 reaction products adsorb to limonene SOA and have the potential to form a mixture and may partially mix. Mixing is further evidenced by more evaporation of β-pinene SOA in the 'Immediate Heating' experiment compared to the 'Delayed Heating' experiment, which suggests that the β-pinene SOA partially mixes with the limonene SOA core in the span of an hour. Given a coating of β-pinene SOA of about 40 nm and a maximum time of diffusion of an hour, the lower bound of diffusivity of SOA is estimated to be about $2.5 \cdot 10^{-19}$ m^2 s^{-1}. This is well within the characteristic diffusivities of semi-solids (10^{-14}-10^{-24} m^2 s^{-1}) (Shiraiwa et al., 2011). Therefore, the observed kinetic limitation in the 'Limonene Core' experiments may be the result of aerosol being highly viscous, thus having a core-shell structure where a highly viscous shell rich in β-pinene SOA hinders the evaporation of limonene SOA underneath. The effect of morphology on aerosol evaporation is different from recent results by Robinson et al. (2015) which finds no dependence on whether squalane is introduced before or after SOA formed from ozonolysis of α-pinene. However, this may be the result of squalane having different

interactions with α-pinene SOA than the interactions between SOA produced by two BVOC+NO_3 reactions.

Studies have shown that higher relative humidity may decrease viscosity and enhance mixing of aerosol particles (Renbaum-Wolff et al., 2013; Zhou et al., 2013; Song et al., 2015; Wilson et al., 2015). To determine if the presence of water can alter aerosol mixing and evaporation for the BVOC+NO_3 system, the 'Mixed' and 'Delayed Heating' experiments are also performed under humid conditions (RH =70%). Figure 3.5 shows that humidity has a negligible effect on the evaporation of limonene SOA and β-pinene SOA in the 'Mixed' experiments, and the evaporation of limonene SOA in the 'Limonene Core-Delayed Heating' experiments. This suggests that diffusion of limonene and β-pinene SOA does not increase and aerosol viscosity does not decrease with increasing humidity. Previous studies have shown that aerosol from different precursors exhibit differences in the relationship between particle bounce (metric for viscosity) and relative humidity (Saukko et al., 2012). The aerosol produced by the limonene+NO_3 reaction may therefore still be viscous at the RH used in this study. We note that unlike limonene SOA, the evaporation of β-pinene SOA appears to be enhanced in the 'Limonene Core-Delayed Heating' experiments, though the reason for this is unclear (Figure 3.5 and Figure B.9). Nevertheless, these results suggest that the amount of aerosol water present in these experiments has a limited effect on aerosol evaporation for the BVOC+NO_3 reaction.

The potential of kinetic limitations to evaporation observed in the 'Limonene Core' and 'Mixed' experiments have important implications on the evaporation of SOA formed

from the oxidation of a single VOC precursor (Section 3.3.3). Our observations suggest that the outer layer of aerosol preferentially evaporates over the inner layers. This can be applied to the case of the limonene+NO_3 reaction, as discussed in section 3.3.3, where the 'Heating Ratio' is larger than the 'Formation Ratio'. Low-volatility products will likely condense first while little organic mass is present. As organic mass increases, the higher volatility products can then begin to condense (Pankow, 1994) and form a shell over the lower-volatility products. These lower-volatility products have thermodynamic potential to evaporate at higher temperatures, but the higher-volatility shell hinders their evaporation upon heating. This effect is strongest at low mass loadings, when the reaction products at the aerosol core are more likely to partition between the gas- and particle-phases. At high mass loadings, these products are likely fully within the particle phase and therefore have no thermodynamic driving force for evaporation. For the limonene+NO_3 system, we calculate an enthalpy of evaporation for each bin within the basis set with C* = [0.1,1,10,100] using data from Figure 3.2 and either the 'Heating Ratio' or the 'Formation Ratio' (Appendix B). The enthalpy of the most volatile bin is most similar for the two ratios, which suggests that the most volatile, and hence outermost, bin controls aerosol evaporation (Appendix B).

3.4 Atmospheric Implications

Our study shows that NO_3 oxidation of both double bonds of limonene (applicable in regions with high NO_x emissions) results in substantially higher SOA yields than previously reported (Hallquist et al., 1999; Spittler et al., 2006; Fry et al., 2011; Fry et al., 2014). Implementation of these yields in future modeling studies will lead to more accurate prediction of SOA formation from BVOC+NO_3. In addition to being an

efficient SOA-forming system, the limonene+NO_3 reaction is a large source of particle-phase organic nitrates, with an organic nitrate yield of ~104%. Although organic nitrates have the potential to hydrolyze (Sato, 2008; Szmigielski et al., 2010; Darer et al., 2011; Hu et al., 2011; Liu et al., 2012; Bean and Hildebrandt Ruiz, 2015; Rindelaub et al., 2015), a recent study by Boyd et al. (2015) suggested that organic nitrates formed from β-pinene+NO_3 reactions largely comprise of primary/secondary nitrates and do not hydrolyze efficiently. We demonstrate that this is also the case for particulate organic nitrates formed from the limonene+NO_3 system.

In order to fully account for the dynamics and transport of aerosol and its physiochemical properties in models, it is imperative to evaluate the evaporation of nighttime aerosol induced by dilution or heating. Owing to the near constant SOA yields of the limonene+NO_3 system at 25 ^{o}C, little aerosol evaporation is observed through dilution in this study. Therefore, SOA produced by the limonene+NO_3 reaction will not undergo evaporation via dilution in the morning as boundary layer height increases. It is noted that this might not be the same for aerosol produced by other BVOC+NO_3 systems where there is a strong dependence of aerosol mass yield on organic mass loading (Hallquist et al., 1999; Griffin et al., 1999; Ng et al., 2008b; Boyd et al., 2015). To determine the effect of temperature on aerosol mass loading, the enthalpy of vaporization for the limonene+NO_3 reaction is calculated over a wide range of mass loadings and can be as high as 237 kJ mol^{-1} for loadings below 18 μg m^{-3}. This is significantly higher than the 42-70 kJ mol^{-1} typically used in atmospheric models (Tsigaridis et al., 2014). A larger enthalpy of vaporization will result in a larger temperature dependence of aerosol mass

loadings in models. This study also emphasizes the need to consider that the enthalpy of vaporization for a particular aerosol system is not constant and may increase with decreasing aerosol mass loading (Epstein et al., 2009). Currently, the dependence of enthalpy of vaporization on C* is only implemented in a few models (Barsanti et al., 2013), but as more experimental data become available, more rigorous parameterizations of enthalpy of vaporization in models could be feasible.

Our study presents a contrast in mass loading between aerosol formed at 25 °C and heated to 40 °C versus aerosol formed at 40 °C, in experiments with mass loadings below 50 μg m^{-3}. These results suggest that there is some resistance to aerosol evaporation. For SOA formed from the oxidation of either limonene or β-pinene, it is possible that this resistance to evaporation is due to the high-volatility species that dominate the outer edge of the aerosol hindering evaporation of organic species present in the center of the particle. For SOA formed from the oxidation of two BVOC (limonene and β-pinene), the shell rich in β-pinene SOA appears to prevent evaporation of the limonene SOA in the 'Limonene Core' experiments. If this limitation to evaporation is due to a highly viscous aerosol, it is possible that ambient aerosol has a morphology similar to the 'Limonene Core' experiments during the night-to-day transition, where products formed from BVOC+NO_3 reactions may coat aerosol formed from the previous day and hinder their evaporation when temperature increases in the morning. More work is needed to determine how organics produced at night interact with organics formed in the previous day.

Field studies support equilibrium partitioning of ambient organic aerosol thus equilibrium may occur on time scales similar to atmospheric processes (Rollins et al., 2013) in some regions. However, we find that aerosol evaporation may still be kinetically limited even when the 'Limonene Core' experiments are conducted at high relative humidity (RH = 70%), suggesting SOA produced by BVOC+NO_3 reactions is viscous at high humidity. This may be due to low liquid water content caused by potentially low hygroscopicity of SOA formed from the monoterpene+NO_3 reaction, which warrants future laboratory studies. Xu et al. showed that monoterpene+NO_3 can contribute ~50% of less oxidized oxygenated organic aerosol (LO-OOA) in the southeastern US (Xu et al., 2015c), which has the lowest hygroscopicity compared to more oxidized oxygenated organic aerosol (MO-OOA) and OA derived from isoprene (Cerully et al., 2015). The interactions between OA produced from different sources and oxidation mechanisms are uncertain and may influence the liquid water content, phase, viscosity, and evaporation of ambient aerosol. This warrants further studies and highlights the importance of understanding interactions of different sources and oxidation mechanisms of ambient aerosol when applying laboratory results to ambient data.

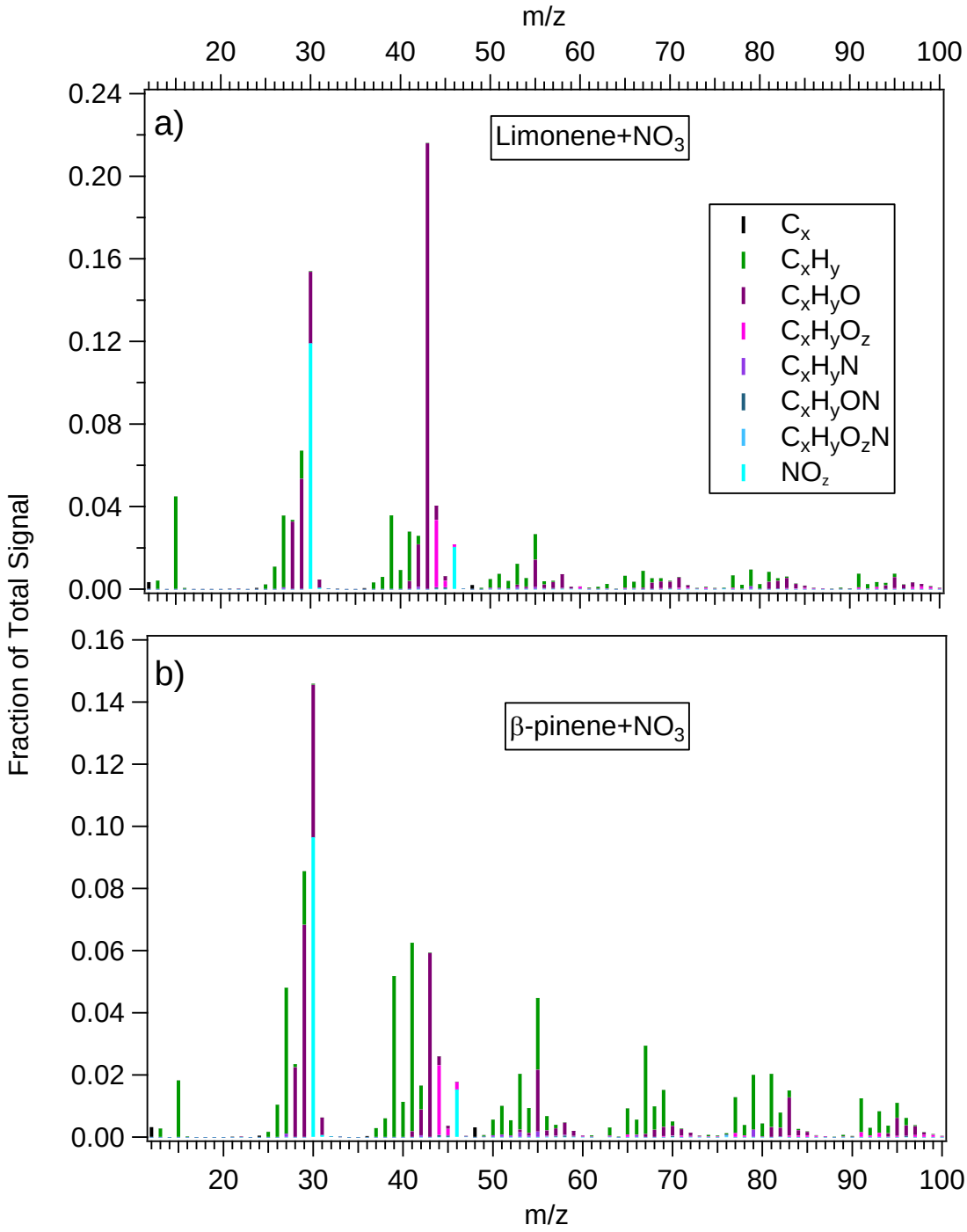

Figure 3.1: Typical high-resolution mass spectra of SOA formed by the reactions of limonene+NO_3 (a, Experiment 2) and β-pinene+NO_3 (b, Experiment 20). Each spectrum is colored to show the relative contribution of each ion type. Only $m/z \leq 100$ are shown because the contribution of ions at $m/z > 100$ is negligible.

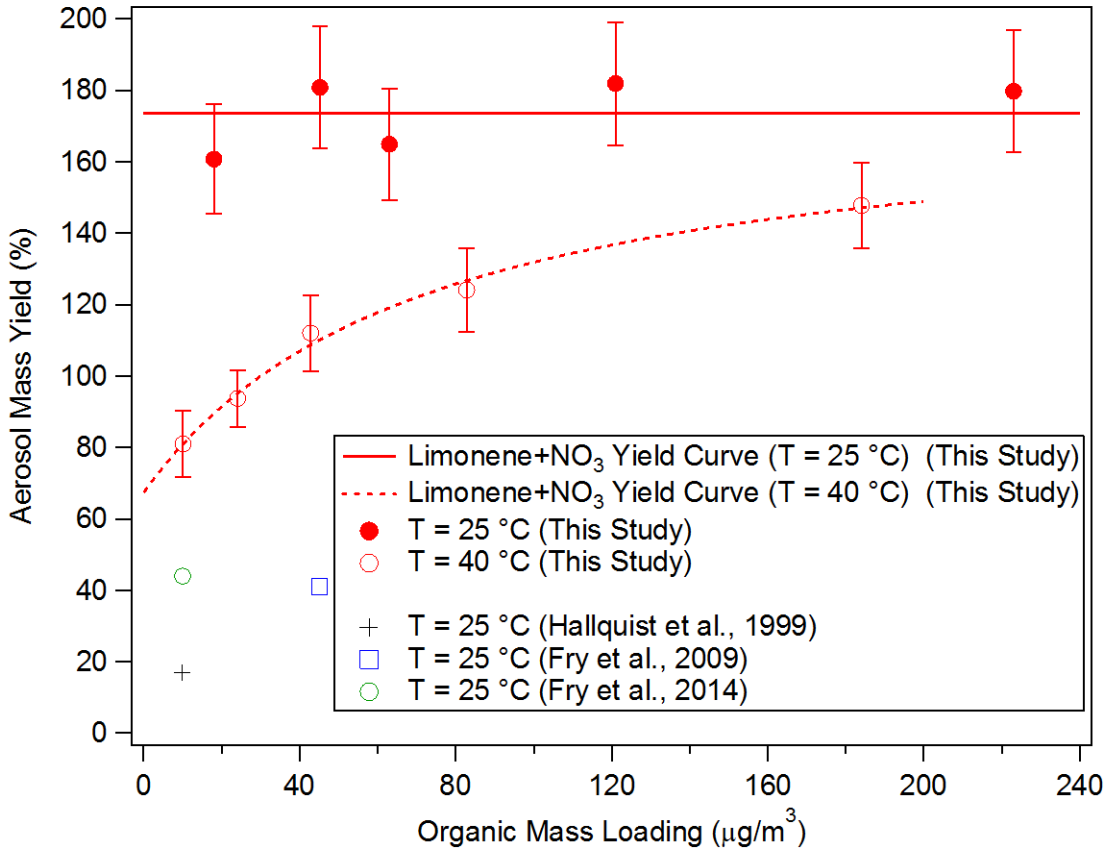

Figure 3.2: Aerosol mass yield as a function of organic loading for the limonene+NO_3 reaction at 25 °C and 40 °C. The density of aerosol used to calculate the aerosol mass yield is determined in the limonene+NO_3 experiments without inorganic seed aerosol (DeCarlo et al., 2004). The aerosol mass yield at 25 °C is approximately constant while the aerosol mass yield at 40 °C is fitted using Eq. 3.1, which is modified from the two-product model proposed by Odum et al. (1996) The aerosol mass yields obtained in this study are compared to those by Hallquist et al. (1999) and Fry et al. (2009) The x-axis error bars are calculated using one standard deviation of volume measured by SMPS at peak aerosol growth. The y-axis error bars are calculated with an 8% uncertainty in hydrocarbon injection and one standard deviation of the aerosol volume measured by SMPS at peak aerosol growth.

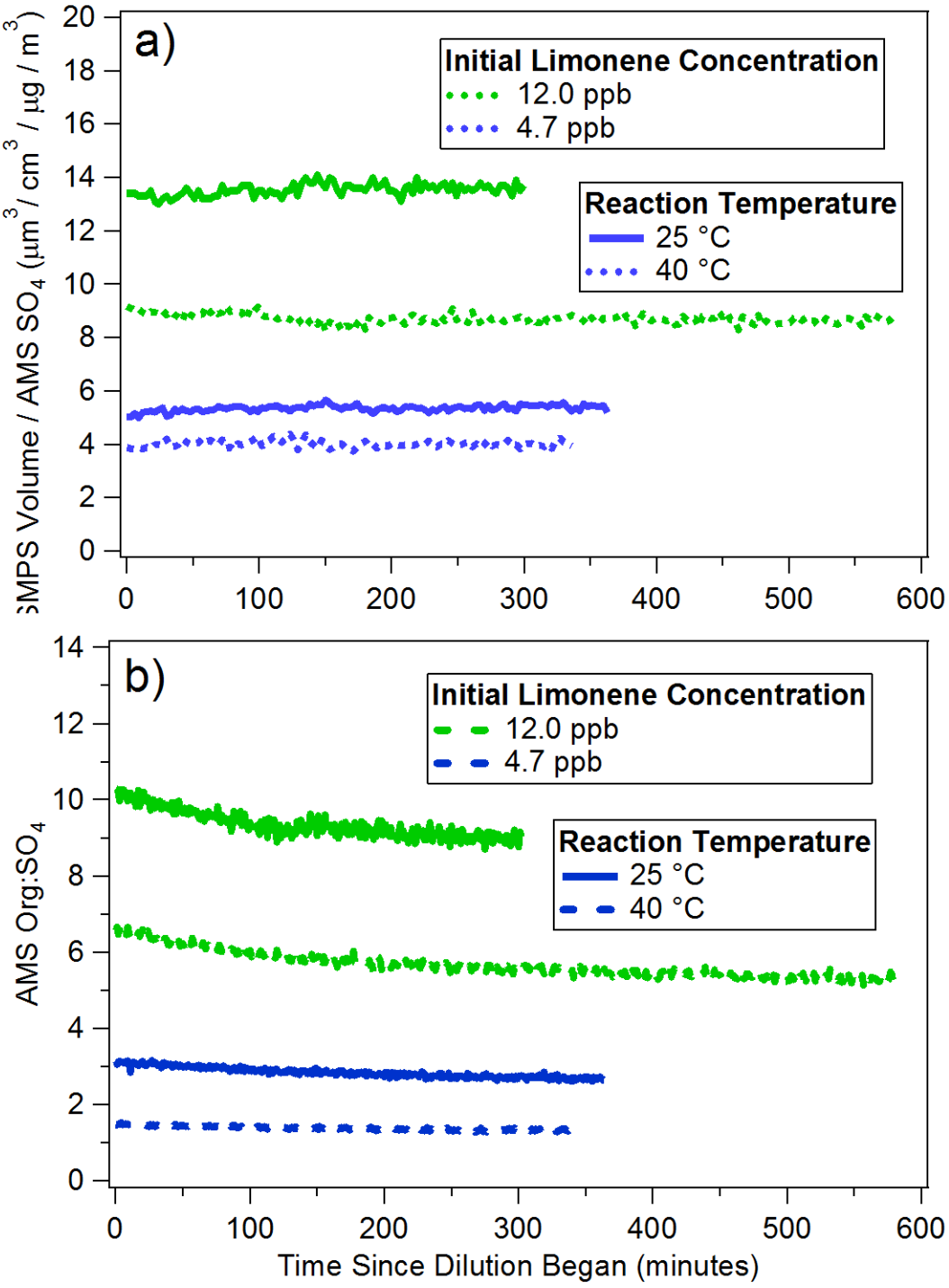

Figure 3.3: Aerosol volume (a) or AMS Org (b) normalized by AMS SO_4 for all experiments that undergo isothermal dilution. Normalizing the data by AMS SO_4 accounts for any decrease in aerosol mass that may be caused by particle wall loss in addition to dilution. Under all conditions, aerosol evaporation caused by isothermal dilution is negligible.

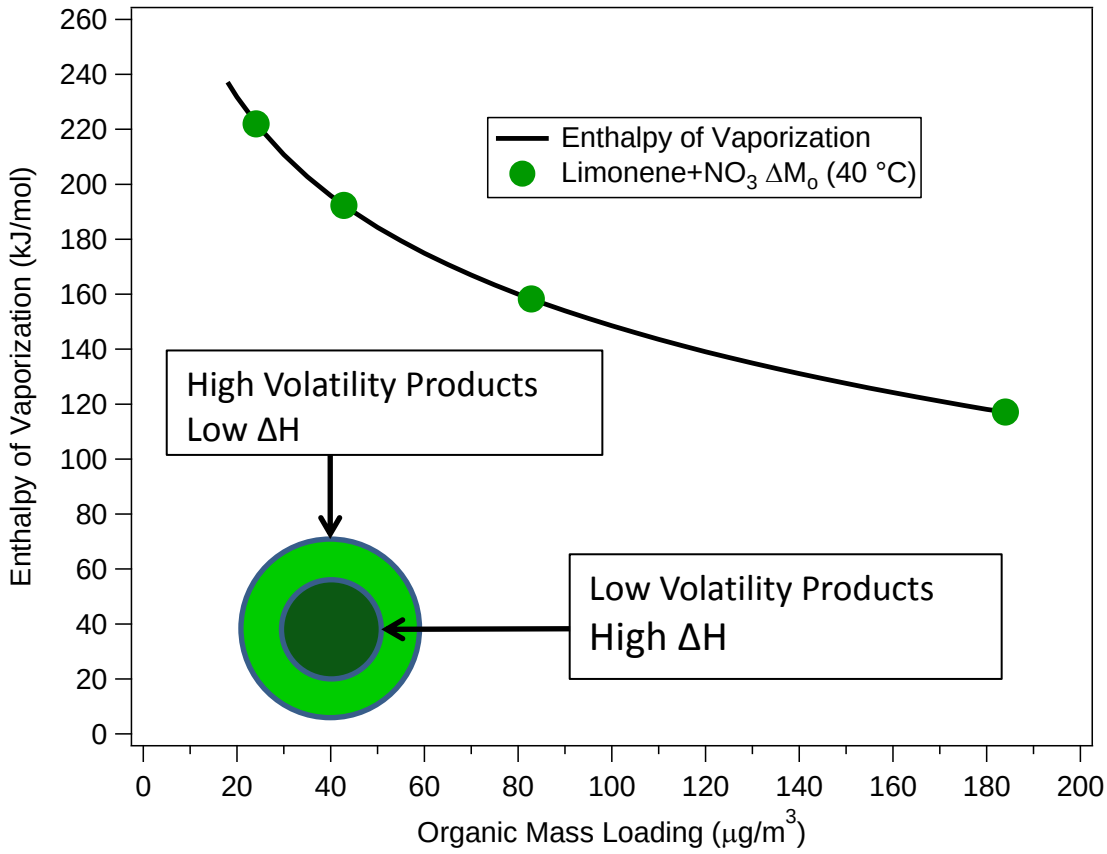

Figure 3.4: The enthalpy of vaporization for the limonene+NO_3 reaction as a function of mass loading. At low mass loadings, the least volatile reaction products dominate the particle phase. These products are more likely to have a higher enthalpy of vaporization than the high volatility products. As the mass loading of aerosol increases, volatile products with high enthalpy of vaporization will contribute more to the aerosol phase and lower the overall effective enthalpy of vaporization.

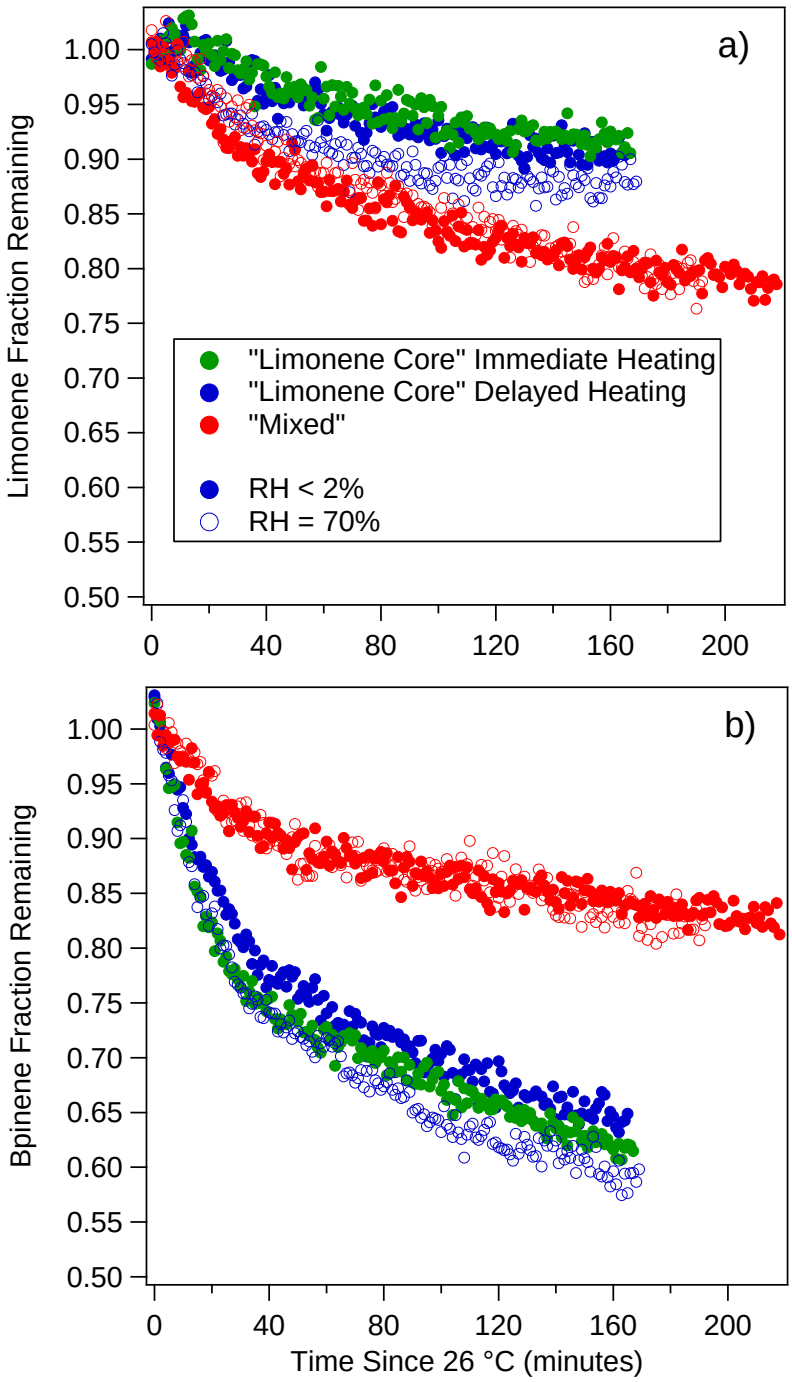

Figure 3.5: The fraction of aerosol remaining for a) limonene SOA and b) β-pinene SOA. Only the time after the chamber has reached a temperature of 26 °C is considered for this analysis. The limonene SOA evaporates less in the 'Limonene Core' experiments than in the 'Mixed' experiments. The β-pinene SOA evaporates more in the 'Limonene Core' experiments than in the 'Mixed' experiments.

Table 3.1: Experimental conditions for all experiments

Experiment	Reaction Temperature (°C)	Relative Humidity (%)	Seed	VOC	Initial VOC Concentration (ppb)	Perturbation
1	24.3	< 3%	AS[a]	Limonene	2.01	Heating
2	24.4	< 2%	AS	Limonene	4.48	Dilution
3	24.4	<2%	AS	Limonene	4.77	Heating
4[b]	25.0	< 2%	AS	Limonene	6.86	Heating
5[b]	24.4	< 2%	AS	Limonene	11.98	Dilution
6	24.2	< 2%	AS	Limonene	22.29	Heating
7	38.5	< 2%	AS	Limonene	2.23	None
8	39.4	< 2%	AS	Limonene	4.85	Dilution
9[b]	39.5	< 2%	AS	Limonene	6.86	None
10[b]	38.7	< 2%	AS	Limonene	11.98	Dilution
11	38.7	<2%	AS	Limonene	22.29	None
12	24.3	< 2%	None	Limonene	4.79	Heating
13	24.2	54%	None	Limonene	3.70	Heating
14	24.9	44%	AS	Limonene	3.99	Heating
15	24.8	<2%	AS	Limonene/ β-pinene[c]	4.00/7.11	Heating (Immediate)
16	24.8	<2%	AS	Limonene/ β-pinene[c]	4.00/7.11	Heating
17	24.9	70%	AS	Limonene/ β-pinene[c]	4.00/7.11	Heating
18	24.8	<2%	AS	Limonene + β-pinene[d]	4.00/7.11	Heating
19	24.9	70%	AS	Limonene + β-pinene[d]	4.00/7.11	Heating
20	24.4	< 2%	AS	β-pinene	7.11	Heating

[a]$(NH_4)_2SO_4$ Seed
[b]O_3 and NO_2 are introduced to the chamber to form NO_3 before limonene is injected
[c]Limonene reacted prior to β-pinene injection
[d]Limonene and β-pinene are reacted simultaneously

CHAPTER 4

IMPACTS AND FUTURE WORK

4.1 Impacts

The results from this dissertation aid our interpretation of ambient measurements, which in turn can help improve global and regional aerosol modeling efforts. For example, using the results presented in Chapter 2 (i.e. aerosol mass yields of the β-pinene+NO_3 reaction), it was shown that the oxidation of monoterpenes via the NO_3 radical is an important contributor to organic aerosol in the Southeastern United States, with as much as 50% of nighttime aerosol being produced by the monoterpene+NO_3 reaction (Xu et al., 2015c). Additionally, as a result of this work, updates to the aerosol mass yield of BVOC+NO_3 chemistry have been implemented into the Community Multi-Scale Air Quality (CMAQ) model, an atmospheric model which includes chemistry. Consequently, a modeling study by Pye et al. (2015) shows that reducing NO_x emissions by 25% can result in a 9% decrease in organic aerosol concentrations (Pye et al., 2015). These efforts will continue to inform atmospheric policy and are essential to determining control strategies to limit atmospheric aerosol and their effects on climate, human health and visibility.

4.2 Suggestions for Future Work

Although this body of work has made substantial gains in the understanding of the role BVOC+NO_3 reactions on the formation of SOA and organic nitrates and their subsequent fates, there are still a number of outstanding questions that must be answered.

Nah et al. (2016) has shown that organic nitrates formed by the BVOC+NO_3 reaction can act as either a permanent NO_x sink or NO_x reservoir for different precursors. Since different precursors have different overall effects on the NO_x cycle, it is important to examine each major BVOC+NO_3 reaction to determine impacts of NO_3 chemistry on the NO_x cycle. There still exists large uncertainty in the role of organic nitrates on the NO_x cycle. However, recent modeling efforts have found that the relative importance of organic nitrate formation on the NO_x cycle will continue to increase as NO_x emissions in the United States continue to decrease (Fisher et al., 2016).

1. What is the effect of peroxy radical fate, humidity, and temperature on the aerosol properties of other BVOC+NO_3 chemistry?
2. What are the aerosol mass and organic nitrate yields for the NO_3 radical addition to first generation products of the BVOC+OH or BVOC+O_3 reactions?
3. What are the gas-particle partitioning coefficients of the organic nitrates produced by the BVOC+NO_3 reactions?
4. What is the difference in vapor pressure between organic nitrates and their hydrolysis products?
5. Aside from particulate water and aerosol acidity, does inorganic aerosol composition affect the hydrolysis rate of organic nitrates?
6. What are the photolysis and photooxidation rates for organic nitrates in both the gas and particle phase? Do these photolysis rates differ from organic nitrates

produced through other pathways, such as through photooxidation of BVOCs under high NO_x conditions?

7. What is the effect of the presence of differing functional groups on the reaction rates and NO_x yield from the photooxidation of organic nitrates?

APPENDIX A

SUPPLEMENTARY INFORMATION FOR CHAPTER 2

A.1 Formaldehyde needed for dry "RO_2+HO_2 dominant" Experiments

Formaldehyde is added to the chamber in order to enhance the RO_2+HO_2 chemistry. Without formaldehyde injection, simulation results based on the Master Chemical Mechanism (Equations are given at the end of Supplement) show that RO_2+RO_2 would be the dominant fate. However, once sufficient formaldehyde is added to the chamber experiments, we determine that the RO_2+HO_2 pathway is substantially greater than the RO_2+RO_2 pathway.

To determine the concentration of formaldehyde needed to favor the RO_2+HO_2 channel significantly over the RO_2+RO_2 channel, a comparison of relative reaction rates is required. Specifically, in order to favor a branching ratio of RO_2+HO_2 to RO_2+RO_2 by 95% (19:1), it is necessary that

$$k_{RO_2+HO_2}[HO_2][RO_2] = 19k_{RO_2+RO_2}[RO_2][RO_2] \quad \text{(A.1)}$$

$$k_{RO_2+HO_2}[HO_2] = 19k_{RO_2+RO_2}[RO_2] \quad \text{(A.2)}$$

$$k_{RO_2+HO_2}\frac{d[HO_2]}{dt} = 19k_{RO_2+RO_2}\frac{d[RO_2]}{dt} \quad \text{(A.3)}$$

Rates of production for each radical can then be used as a surrogate for the approximate concentrations as the radicals are expected to be consumed immediately upon production. The rates of production are:

$$\frac{d[HO_2]}{dt} = k_{HCHO+NO_3}[HCHO][NO_3] \quad \text{(A.4)}$$

$$\frac{d[RO_2]}{dt} = k_{\beta pin+NO_3}[\beta pin][NO_3] \quad \text{(A.5)}$$

Thus Eq. (A.3) becomes:

$$k_{RO_2+HO_2}k_{HCHO+NO_3}[HCHO][NO_3] = 19k_{RO_2+RO_2}k_{\beta pin+NO_3}[\beta pin][NO_3] \quad \text{(A.6)}$$

$$k_{RO_2+HO_2}k_{HCHO+NO_3}[HCHO] = 19k_{RO_2+RO_2}k_{\beta pin+NO_3}[\beta pin] \quad \text{(A.7)}$$

Therefore, the ratio of formaldehyde to β-pinene should be ($k_{RO2+RO2}$ = 9.2E-14 cm^3 $molecules^{-1}$ s^{-1}; $k_{\beta pin+NO3}$ = 2.5E-12 cm^3 $molecules^{-1}$ s^{-1}; $k_{RO2+HO2}$ = 9.2E-14 cm^3 $molecules^{-1}$ s^{-1}; $k_{HCHO+NO3}$ = 5.5E-16 cm^3 $molecules^{-1}$ s^{-1}, all rate constants are from MCM v3.2 (Saunders et al., 2003a)):

$$\frac{[HCHO]}{[\beta pin]} = \frac{19k_{RO_2+RO_2}k_{\beta pin+NO_3}}{k_{RO_2+HO_2}k_{HCHO+NO_3}} = 350 \quad \text{(A.8)}$$

A.2 Results from Filter Sample Analysis

The UHPLC-MS total ion chromatogram for a typical "RO_2+NO_3 dominant" experiment under dry conditions is displayed in Figure A.5, which also represents the features observed in all other experiments under dry and humid conditions. Excluding the solvent peak at ~0.2 min and discarding the presence of any relevant species in the controls, the chromatogram in Figure A.5 reveals peaks with retention times of 3.26, 3.28, 6.19, 6.27, 7.03, and 7.08 min. These peaks are displayed in the extracted ion chromatograms (EIC) for species with *m/z* 489, 244, 473, 489, 505 and 522.

The collisional induced dissociation (CID) of the peak at ~3.26 min is displayed in Figure A.6 for the interval 30-70 V. Clearly, two anions with *m/z* 244 and 489 are observed at 3.26 min under low fragmentation voltage (30 and 40 V). The prominent peak *m/z* 290 is mainly due the presence of an adduct of the parent peak with formic acid: [M-H] + HCOOH = 244 + 46 = 290. Support for the previous observation is also based on the appearance of the adduct [M-H] + CH_3COOH = 244 + 60 = 304 in the presence of acetic acid, instead of formic acid, in the mobile phase. The ion observed at *m/z* 197 becomes more intense at higher fragmentation voltage before starting to break apart above 60 V. The parent peak *m/z* 244 must undergo the concerted loss of nitrous acid, HNO_2, to produce *m/z* 197. The loss of HNO_2 explains the change from an even to an odd mass, which may be facilitated by intramolecular hydrogen transfer from the hydroxyl group to the leaving -NO_2 moiety, leaving a carboxylate group as a rearranged fragment. The confirmation of the presence of a –COOH group in the neutral molecule with molecular

mass 245 amu arises from the decarboxylative loss of 44 amu from the fragment ion *m/z* 197 that generates a new fragment at *m/z* 153.

The MS peak at *m/z* 489 in Figure A.6 does not show the formation of either a formic acid or an acetic acid adduct. In addition, the lack of a constant ratio for the ion count of species at *m/z* 244 and 489 in all experiments suggests that different formation pathways result in both products. The careful analysis of the data presented showing the formation of formate or acetate adducts for the species at *m/z* 244, and its excellent ionization at very low fragmentation voltage suggest that the co-eluting species at *m/z* 489 should be a carboxylic acid molecule in the mechanistic scheme (Figure A.7) to be presented below.

The chromatographic peak eluting at 6.19 min in Figure A.5 displayed as an EIC for *m/z* 505 with broad features corresponds to a species with molecular weight (MW) of 506 amu. Given the nitrogen rule, this species with even MW must contain an even number of nitrogen atoms. The combination of two β-pinene molecules, which have incorporated nitrate radicals, provides a starting mass of 396 amu for this species. The mass difference (506 – 396) amu = 110 amu eliminates the possibility of including a third β-pinene molecule or two more nitrate radicals in this product. Therefore, a general formula of $C_{20}H_{30}N_2O_{13}$ is assigned to this species. The ring and double bond equivalency (RDB) defines the number of unsaturated bonds in the compound:

$$RDB = 1 + \frac{\sum_i^{imax} N_i(V_i - 2)}{2} \qquad \text{(AR9)}$$

where i_{max} is the total number of different elements in the molecular formula, N_i is the number of atoms of element i, and V_i is the valence of atom I (Pavia et al., 2008). For $C_{20}H_{30}N_2O_{13}$, RDB = 7 from limiting the calculated formulas that make sense chemically, a -C=O group should be included in the structures of the mechanism forming species with this MW. Similarly, the EIC for *m/z* 522 shows a broad peak that could correspond to a less polar isomer species eluting at 6.27 min. A molecular structure with two β-pinene units and an odd number of nitrogen atoms is assigned to be $C_{20}H_{33}N_3O_{13}$ (MW = 523 amu) with RDB = 6 in the mechanism presented below.

Remarkably, a second species with *m/z* 489 elutes at 7.09 min in the EIC of Figure A.5, which possesses a carbonyl group absorbing with λ_{max} = 275 nm in the UV-visible spectrum. This molecule elutes later in the chromatogram, in the region of species with lower polarity –without a -COOH group– because it corresponds to a less polar structural isomer than that eluting at 3.26 min. The most likely general formula for this species is $C_{20}H_{30}N_2O_{12}$ (MW = 490) with RDB = 7, shown as the non-carboxylic acid structure in the mechanism introduced in the next section. A slightly lighter species with *m/z* 473 (MW = 474 amu) and retention time of 7.03 min also contains a carbonyl group in the UV-visible spectrum. The even molecular weight of this molecule indicates a species with an even number of nitrogen atoms. The similar retention times between both species (*m/z* 474 and 490) and the mass difference of only 16 amu suggests a common molecular structure that differs by one oxygen atom. The molecular formula $C_{20}H_{33}N_2O_{11}$ (MW = 474 amu) is represented by the proposed structures displayed in Figure A.7.

Figure A.7 shows the further oxidation of some of the products shown in Figure 2.7 of the main text. Panel A of Figure A.7 shows the hydroxycarbonyl nitrate product with MW = 229 amu can be further oxidized to the peroxy radical **V** by hydrogen abstraction from C_4 (R27) and subsequent reaction with oxygen (R28). Hydrogen abstraction from the dihydroxycarbonyl nitrate generated from **V** by R29 occurs preferentially on a $–CH_3$ group (C_9 or C_{10}) by R30, proceeding through an alkyl radical with true trigonal pyramidal geometry, an unfavorable intermediate for C_5, C_7, and C_8 due to the geometric constrains imposed by the cyclobutane ring (Vereecken and Peeters, 2012). Less likely is the abstraction occurring at C_4, due to both the hindrance created by the alcohol substituent and the slight strain from the adjacent butane ring. Addition of O_2 is also included in R30 (Atkinson and Arey, 2003b), resulting in a peroxy radical **W**. Reaction R31 for **W** + **L**$^{\bullet}$ produces an alcohol ($R^{31}OH$) which can undergo a second H-abstraction by step 1 of R32 at the same carbon, C_{10}. C_{10} is slightly more electropositive than C_9 due to the hydroxyl substituent, and abstraction of the only H remaining at the more hindered C_4 of W is less likely to occur than at C_{10}. Step 2 of R32 shows the formation of a peroxy radical **Y** through combination with molecular oxygen (Atkinson and Arey, 2003b). Panel B shows the oxidation of the hydroxynitrate acid product, $R^{20}COOH$, through hydrogen abstraction and reaction with molecular oxygen in R33 to peroxy radical **X**. Panel C shows in reaction R34 how a second nitrate radical can add to the newly generated double bond of the hydroxynitrate product of R7 (Figure 2.7, Chapter 2). The nitrate radical adds to the less substituted C_7, leaving a relatively stable tertiary alkyl radical on C_2, which combines with O_2 via reaction R35 to form a peroxy radical **Z**.

Figure A.8 shows how intermediates presented in Figure 2.7 of the main text, **S**, **T**, and **U** combine with radicals **V**, **W**, **X**, **Y**, **Z** presented in Figure A.7 to produce the heavier MW products observed in aerosol filter extracts by UHPLC-MS via RO_2+RO_2 reactions. It is noted that each product in Figure A.8 may be formed from the combination of other intermediates not explicitly drawn in Figure 2.7 in Chapter 2 and Figure A.7. These findings are in agreement with previous work showing the formation of organic peroxides during the oxidation of terpenes (Docherty et al., 2005; Ng et al., 2008a; Venkatachari and Hopke, 2008). Figure A.8 shows that the major heavy MW species in the UHPLC chromatogram of Figure A.5 can be generated from the same early oxidation intermediates **S**, **T**, and **U**, implying the possible existence of more than one isomer for each mass. The later observation is consistent with the EIC in Figure A.5 showing broad peaks in the UHPLC-MS for *m/z* 505, 522, and the later 489, and a clear shoulder for *m/z* 473.

A.3 Model Calculations for "RO_2+NO_3 dominant" Experiments

To ensure that the reaction conditions are favorable for the RO_2+NO_3 reaction, a simple chemical model is developed using the Master Chemical Mechanism (MCM v3.2) as a basis (Saunders et al., 2003a). Reactions and their rate constants are shown in Table A.1. The RO_2 fate in a typical "RO_2+NO_3 dominant" experiment (Experiment 5 in Table 2.1 of Chapter 2) is shown in Figure A.10.

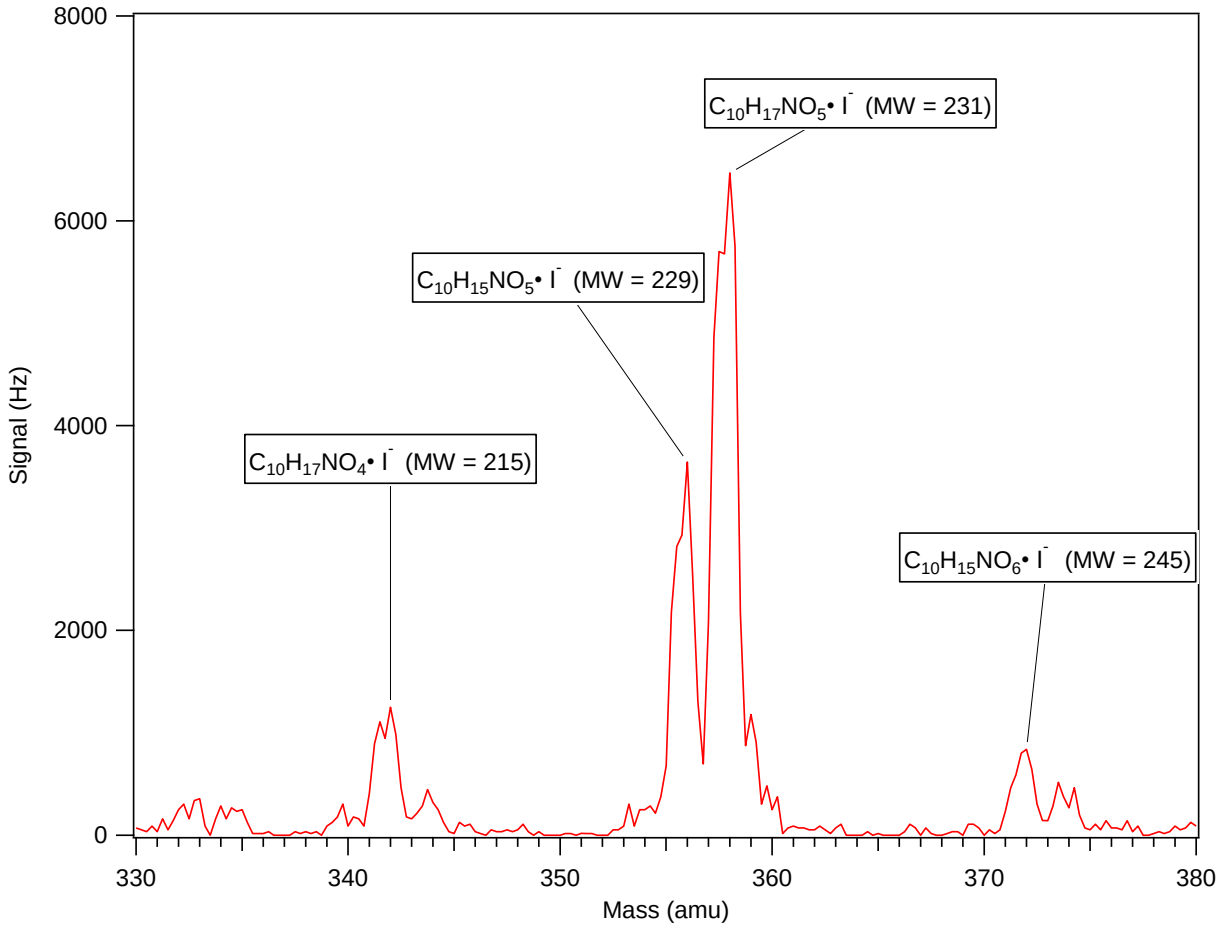

Figure A.1: Chemical Ionization Mass Spectrometry (CIMS) spectra for a typical "RO_2+HO_2 dominant" experiment under dry conditions showing the major gas-phase compounds from the β-pinene+NO_3 reaction. The measured species are proposed to be organic nitrates due to their odd molecular weights. The specific molecular formulas for the ions shown are inferred from the chemical mechanism (Figure 2.7, Chapter 2).

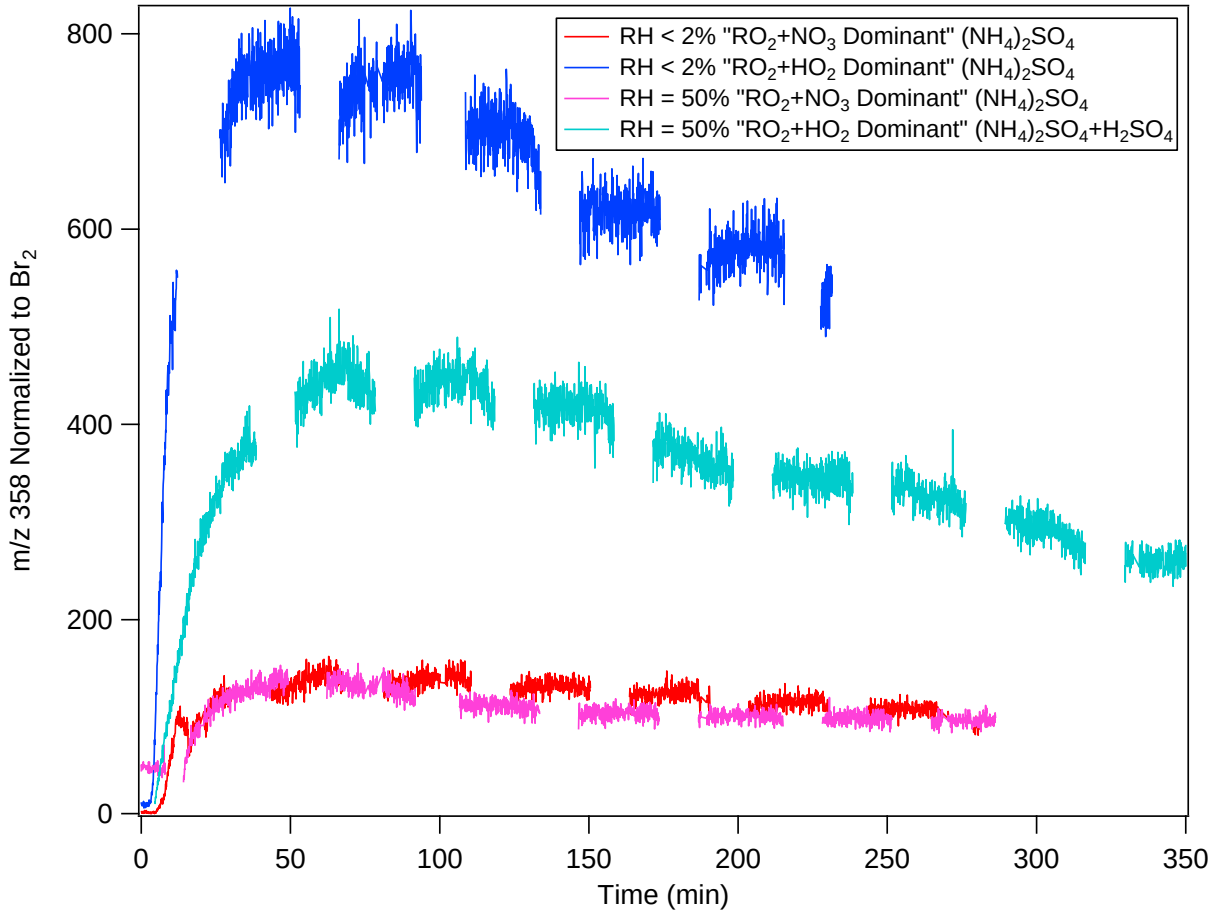

Figure A.2: CIMS time series for *m/z* 358 for the β-pinene+NO_3 reaction at all conditions. *m/z* 358 corresponds to a molecule-iodide adduct where the molecule has a molecular weight of 231 amu. The signal is normalized to the instrument sensitivity to Br_2 to account for any sensitivity changes in the CIMS (Neuman et al., 2010). The species at *m/z* 358 is proposed to be either from a hydroperoxide (ROOH) or a dihydroxynitrate. It is significantly higher in experiments where RO_2+HO_2 is the dominant reaction pathway. Gaps in the data are from periodic measurements of the CIMS background. It is noted that the data shown above have not been corrected for CIMS background.

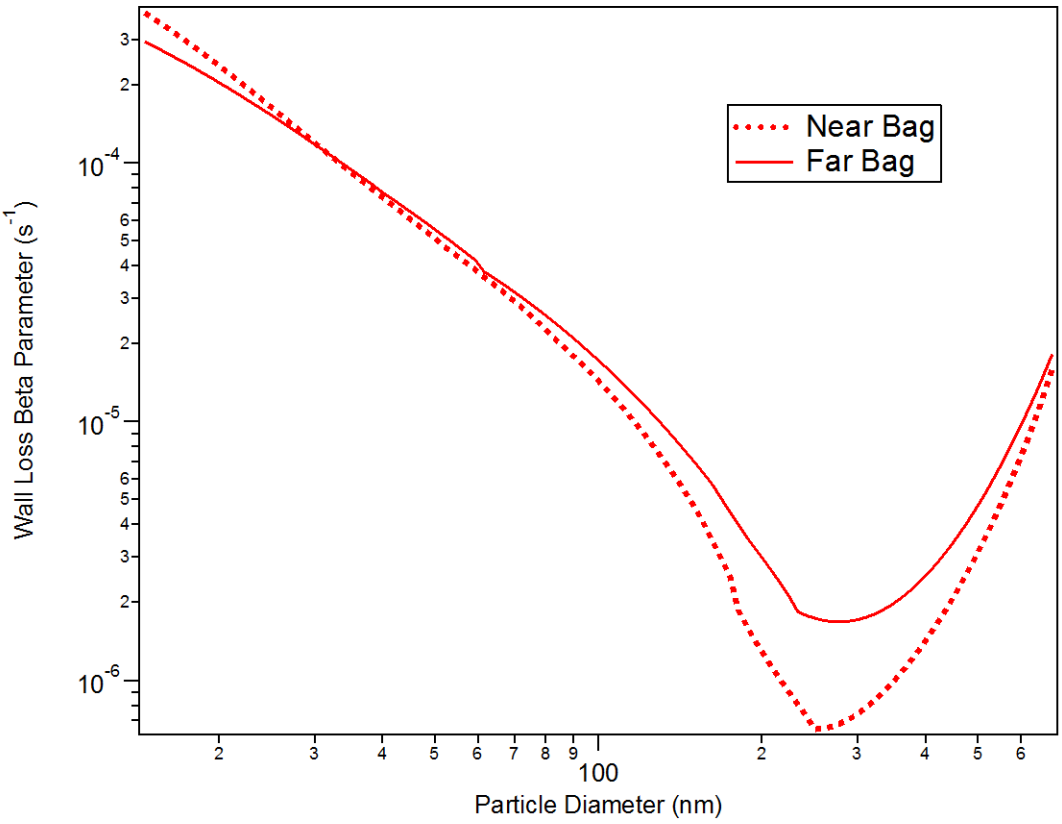

Figure A.3: Size-dependent particle wall loss rates, β, calculated for both chambers at GTEC. Wall loss rates are determined by wall loss experiments performed using ammonium sulfate seed particles atomized from an 8 mM solution and measuring their decay over time. The first-order decay coefficients were measured for each particle bin over the course of each wall-loss experiment

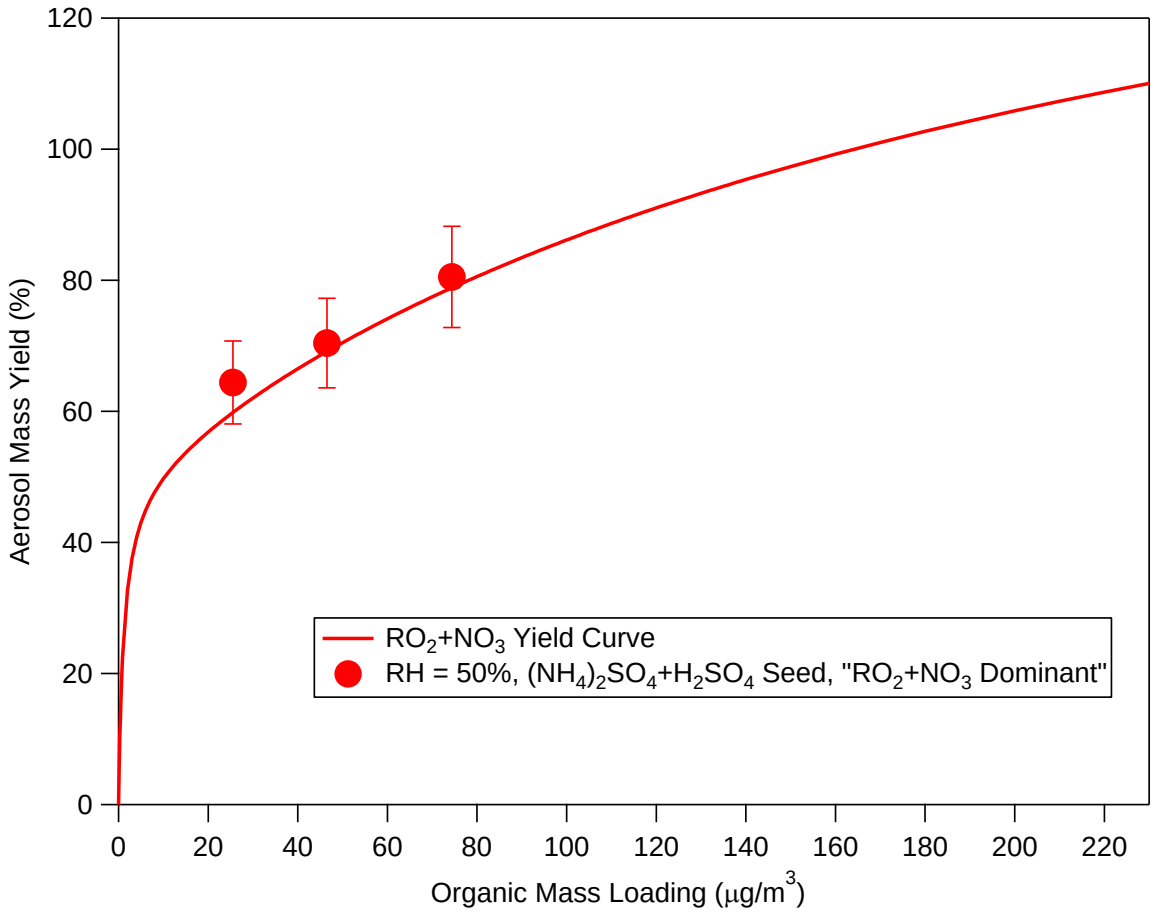

Figure A.4: The yields for the experiments using $(NH_4)_2SO_4$+H_2SO_4 seed (circles) reported alongside the yields for the experiments using $(NH_4)_2SO_4$ seed (red curve) in "RO_2+NO_3 dominant" experiments. As seen in this figure, results from the experiments with $(NH_4)_2SO_4$+H_2SO_4 seed are in agreement with the yield curve generated by the two-product model (Odum et al., 1996) for experiments conducted in the presence of $(NH_4)_2SO_4$ seed.

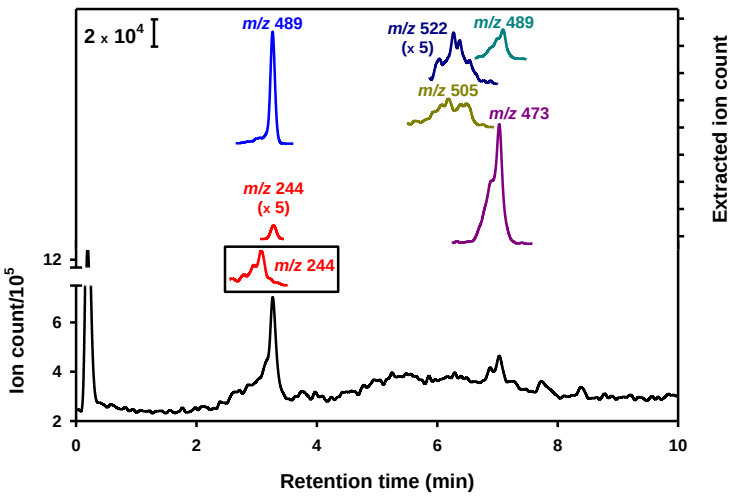

Figure A.5: Total (bottom panel and left axis) and extracted (top panel and right axis) ion chromatogram (EIC) for eluting peaks at *m/z* 244, 489, 505, 522, and 473, and 489 in the UHPLC-MS chromatogram of a "RO_2+NO_3 dominant" experiment under dry conditions, in the presence of 0.1 mM HCOOH (fragmentor voltage = 50 v). The box shows the EIC for *m/z* 244 using 0.4 mM CH_3COOH instead of HCOOH (fragmentor voltage = 30 v).

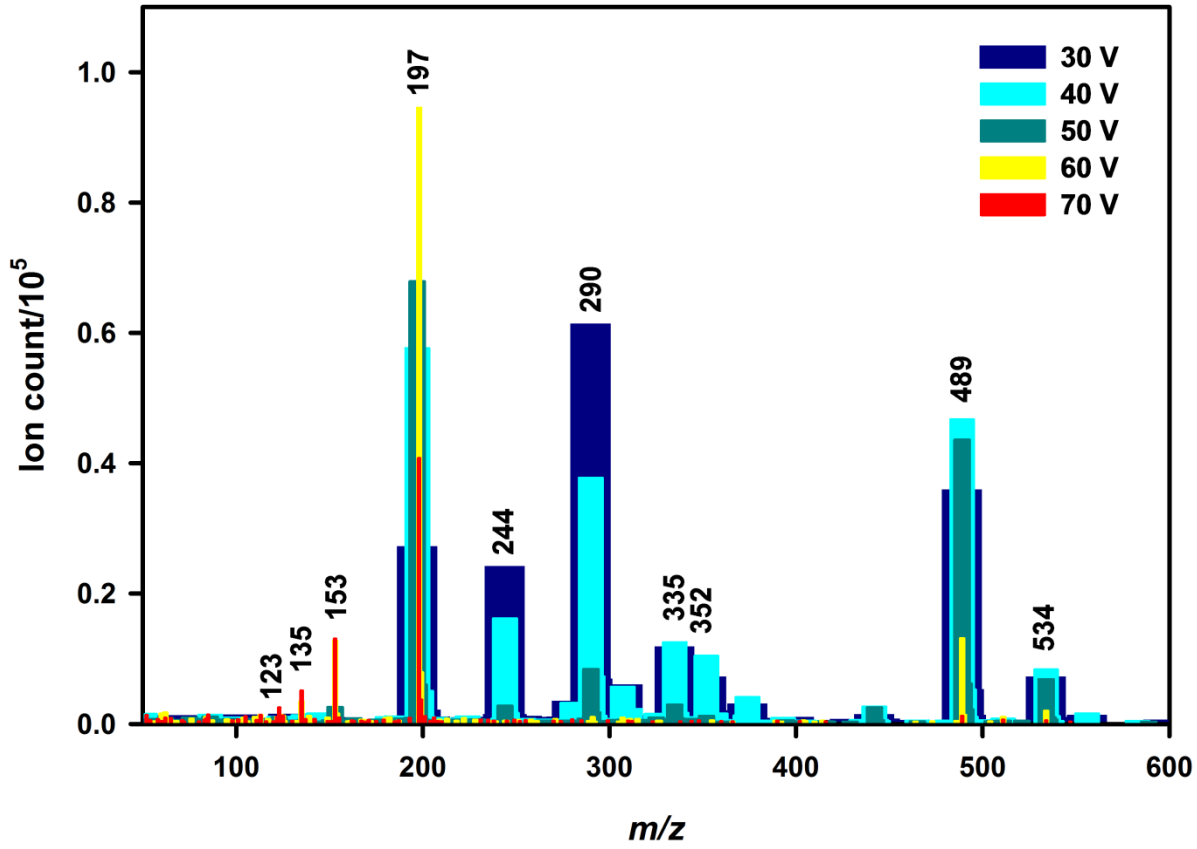

Figure A.6: Collisional induced dissociation mass spectra of chromatographic peak in Figure A.5 at 3.27 ± 0.03 min between 30 and 70 V.

.

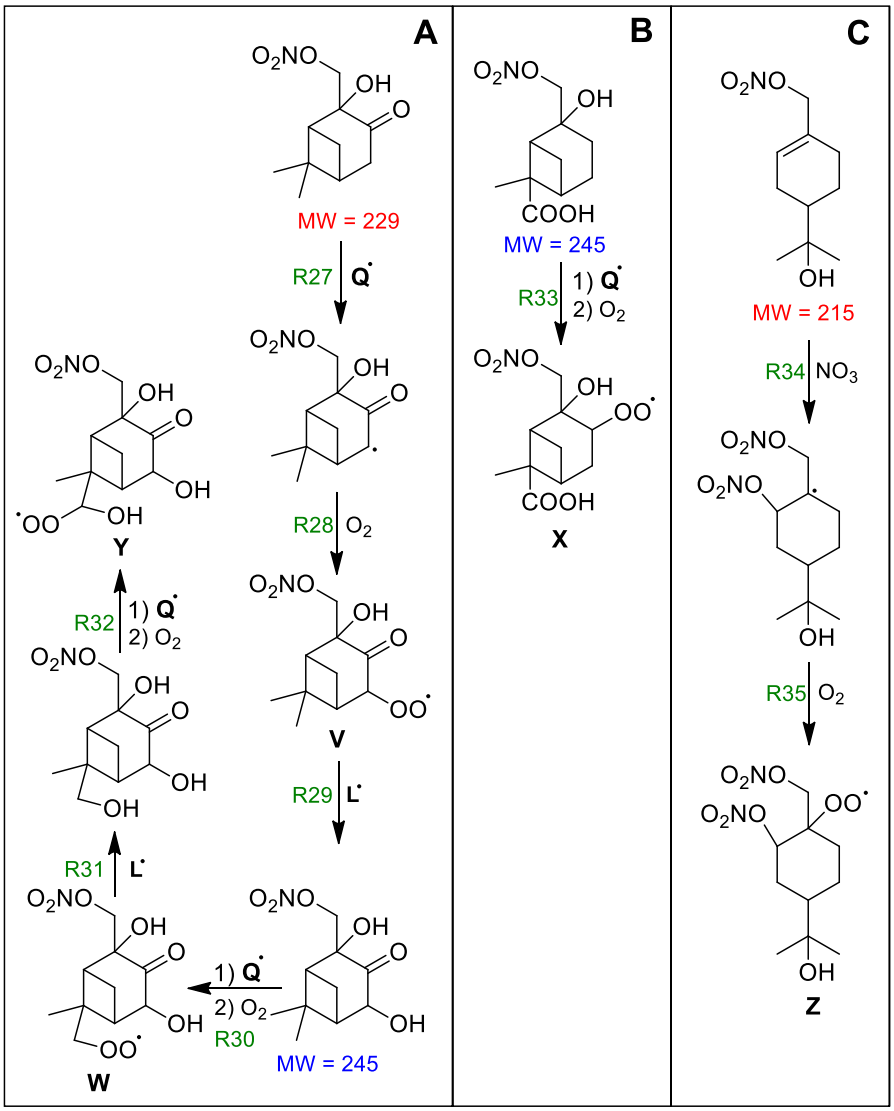

Figure A.7: Proposed pathways for the further oxidation of products proposed in Figure 2.7 of Chapter 2. Named radicals are proposed to react to form the higher molecular weight species in Figure A.8.

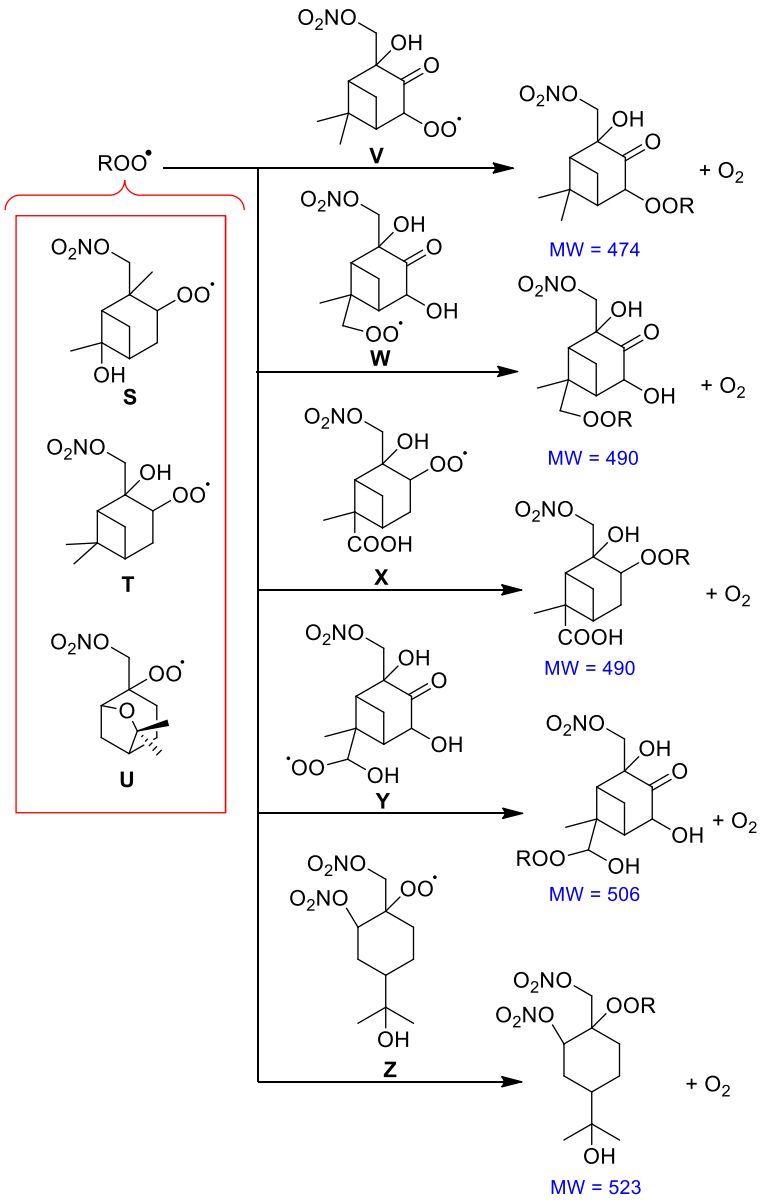

Figure A.8: Proposed pathways for the production of organic peroxides from radicals **S**, **T**, and **U** (Figure 2.7, Chapter 2) by reaction with radicals **V, W, X, Y, and Z** (Figure A.7).

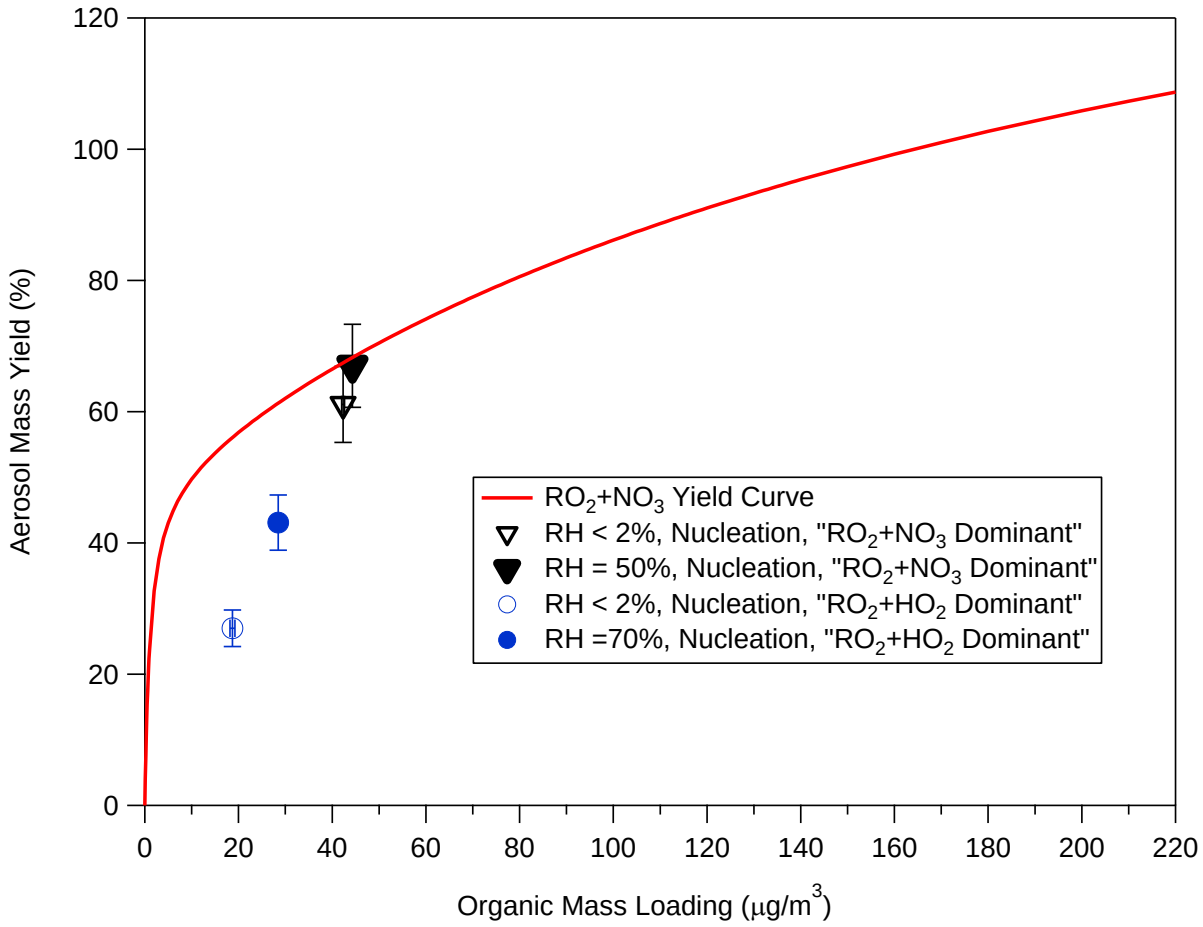

Figure A.9: The yields for nucleation experiments for all conditions are reported alongside the yields for experiments with $(NH_4)_2SO_4$ seed. The yields from the nucleation and seeded experiments in the "RO_2+NO_3 dominant" experiments are in agreement with each other while the "RO_2+HO_2 dominant" experiments are significantly lower than under seeded conditions. The y-axis error bars represent uncertainty in yield calculated by an 8% uncertainty in chamber volume, 5% uncertainty in hydrocarbon injection, and one standard deviation of the aerosol volume measured by SMPS at peak growth.

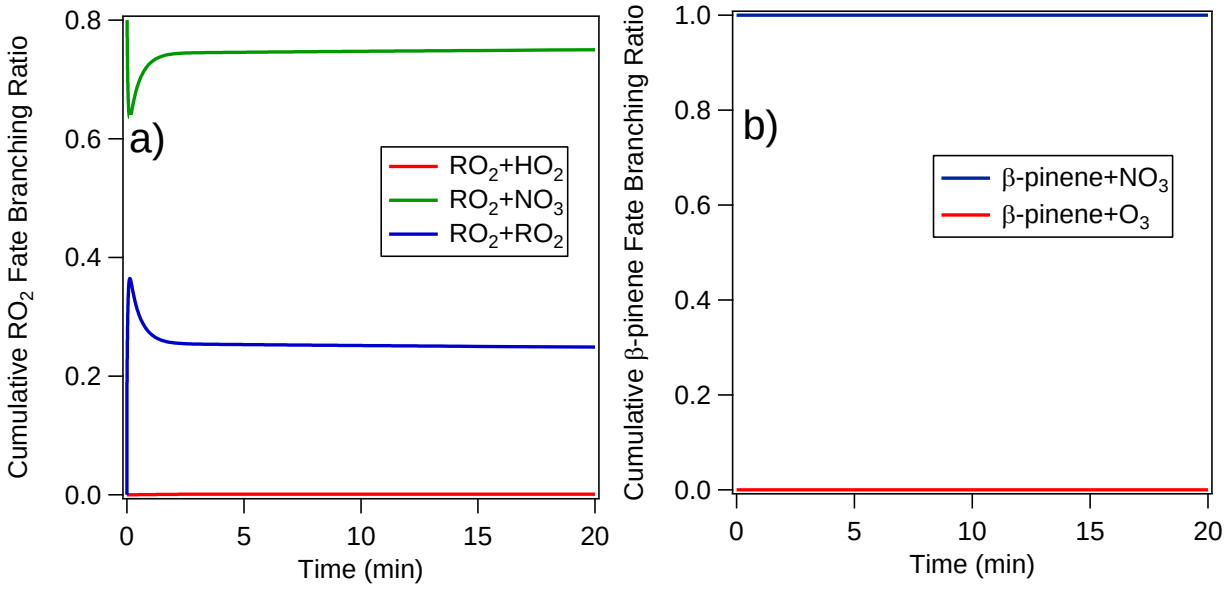

Figure A.10: a) The RO_2 branching ratio and b) β-pinene fate for a typical "RO_2+NO_3 dominant" experiment (Experiment 5 in Table 2.1 of Chapter 2). The branching ratios are determined from the reactions in the Master Chemical Mechanism (MCM v 3.2). The plots show the cumulative amount of products formed from each possible reaction.

Table A.1: List of reactions and their rate constants for the β-pinene+NO_3 system. Reactions are adapted from MCMv3.2 (Saunders et al., 2003a)[a].

Reaction:	**Rate Constant:**
$NO_2 + O_3 \rightarrow NO_3 + O_2$	$3.2 \cdot 10^{-17}$ cc molecules^{-1} s^{-1} [b]
$NO_2 + NO_3 \rightarrow N_2O_5$	$6.7 \cdot 10^{-12}$ cc molecules^{-1} s^{-1} [b]
$N_2O_5 \rightarrow NO_2 + NO_3$	$2.2 \cdot 10^{-1}$ s^{-1} [b]
$OH + O_3 \rightarrow HO_2 + O_2$	$7.3 \cdot 10^{-14}$ cc molecules^{-1} s^{-1} [b]
$OH + HO_2 \rightarrow H_2O_2 + O_2$	$1.1 \cdot 10^{-10}$ cc molecules^{-1} s^{-1} [b]
$HO_2 + O_3 \rightarrow OH + 2O_2$	$1.9 \cdot 10^{-15}$ cc molecules^{-1} s^{-1} [b]
$HO_2 + HO_2 \rightarrow H_2O_2 + O_2$	$1.4 \cdot 10^{-12}$ cc molecules^{-1} s^{-1} [b]
$NO + HO_2 \rightarrow NO_2 + OH$	$8.1 \cdot 10^{-12}$ cc molecules^{-1} s^{-1} [b]
$NO + O_3 \rightarrow O_2 + NO_2$	$1.9 \cdot 10^{-14}$ cc molecules^{-1} s^{-1} [b]
$NO + NO_3 \rightarrow 2\ NO_2$	$2.6 \cdot 10^{-11}$ cc molecules^{-1} s^{-1} [b]
$HCHO + NO_3 \rightarrow HNO3 + CO + HO_2$	$5.5 \cdot 10^{-16}$ cc molecules^{-1} s^{-1}
β-pinene + $NO_3 + O_2 \rightarrow$ NBPINAO2	$0.8 \cdot 2.51 \cdot 10^{-12}$ cc molecules^{-1} s^{-1}
β-pinene + $NO_3 + O_2 \rightarrow$ NBPINBO2	$0.2 \cdot 2.51 \cdot 10^{-12}$ cc molecules^{-1} s^{-1}
β-pinene + $O_3 + O_2 \rightarrow$ NOPINONE + CH200F	$0.4 \cdot 1.5 \cdot 10^{-17}$ cc molecules^{-1} s^{-1}
β-pinene + $O_3 + O_2 \rightarrow$ NOPINOOA + HCHO	$0.6 \cdot 1.5 \cdot 10^{-17}$ cc molecules^{-1} s^{-1}
NBPINAO2 + $HO_2 \rightarrow$ NBPINAOOH	$2.09 \cdot 10^{-11}$ cc molecules^{-1} s^{-1}
NBPINAO2 + NO → NBPINAO	$9.04 \cdot 10^{-12}$ cc molecules^{-1} s^{-1}
NBPINAO2 + $NO_3 \rightarrow$ NBPINAO	$2.3 \cdot 10^{-12}$ cc molecules^{-1} s^{-1}
NBPINAO2 + $RO_2 \rightarrow$ NBPINAO	$0.7 \cdot 9.2 \cdot 10^{-14}$ cc molecules^{-1} s^{-1}
NBPINAO → NOPINONE + HCHO + NO_2	10^6 s^{-1}
NBPINAO2 + $RO_2 \rightarrow$ BPINBNO3	$0.3 \cdot 9.2 \cdot 10^{-14}$ cc molecules^{-1} s^{-1}
NBPINBO2 + $HO_2 \rightarrow$ NBPINBOOH	$2.09 \cdot 10^{-11}$ cc molecules^{-1} s^{-1}
NBPINBO2 + NO → NBPINBO	$9.04 \cdot 10^{-12}$ cc molecules^{-1} s^{-1}
NBPINBO2 + $NO_3 \rightarrow$ NBPINBO	$2.3 \cdot 10^{-12}$ cc molecules^{-1} s^{-1}
NBPINBO2 + $RO_2 \rightarrow$ NBPINBO	$0.6 \cdot 2 \cdot 10^{-12}$ cc molecules^{-1} s^{-1}

Table A.1 Continued

NBPINAO → NOPINONE + HCHO + NO_2	$7 \cdot 10^{3}$ s^{-1}
NBPINAO2 + RO_2 → BPINANO3	$0.2 \cdot 2 \cdot 10^{-12}$ cc molecules^{-1} s^{-1}
NBPINAO2 + RO_2 → NC91CHO	$0.6 \cdot 2 \cdot 10^{-12}$ cc molecules^{-1} s^{-1}
NC91CHO + NO_3 → NC91CO3	$2.32 \cdot 10^{-14}$ cc molecules^{-1} s^{-1}
NC91CO3 + HO_2 → NC91CO3H	$0.56 \cdot 1.39 \cdot 10^{-11}$ cc molecules^{-1} s^{-1}
NC91CO3 + HO_2 → NOPINONE + NO3 + OH + HCHO	$0.44 \cdot 1.39 \cdot 10^{-11}$ cc molecules^{-1} s^{-1}
NC91CO3 + NO → NOPINONE + HCHO + $2NO_2$	$1.98 \cdot 10^{-11}$ cc molecules^{-1} s^{-1}
NC91CO3 + NO_2 → NC91PAN	$9.4 \cdot 10^{-12}$ cc molecules^{-1} s^{-1}
NC91PAN →NC91CO3 + NO_2	$3.0 \cdot 10^{-4}$ s^{-1}
NC91CO3 + NO_3 → NOPINONE + HCHO + $2NO_2$	$4.0 \cdot 10^{-12}$ cc molecules^{-1} s^{-1}
NC91CO3 + RO_2 → NOPINONE+ HCHO + NO_2	10^{-11} cc molecules^{-1} s^{-1}
CH2OOFA → CH2OO	$0.37 \cdot 10^{6}$ s^{-1}
CH2OOFA → CO	$0.5 \cdot 10^{6}$ s^{-1}
CH2OOFA → HO_2 + CO + OH	$0.13 \cdot 10^{6}$ s^{-1}
CH2OO + CO → HCHO	$1.2 \cdot 10^{-15}$ cc molecules^{-1} s^{-1}
CH2OO + NO → HCHO	$1.0 \cdot 10^{-14}$ cc molecules^{-1} s^{-1}
CH2OO + NO_2→ HCHO	$1.0 \cdot 10^{-15}$ cc molecules^{-1} s^{-1}
CH2OO + H_2O→ HCHO	$6.0 \cdot 10^{-18}$ cc molecules^{-1} s^{-1}
CH2OO + H_2O→HCOOH	$1.0 \cdot 10^{-17}$ cc molecules^{-1} s^{-1}

[a]Unless otherwise noted, all reaction rates are from MCM v. 3.2

[b]Reaction rates are from Sander et al. (2011) and the references therein

APPENDIX B

Supplemental Information to Chapter 3

B.1 Experimental Procedure

Prior to each experiment, the chambers are flushed with zero air for at least 24 hours. All experiments are performed by first injecting formalin solution (Sigma-Aldrich, 37% HCHO) into a glass bulb and flowed over with clean air until the solution evaporates. The concentration of HCHO ranges from 1.2-13.0 ppm. Ammonium sulfate seed aerosol is injected into the chamber via atomization of an 8 mM $(NH_4)_2SO_4$ seed solution. The initial seed number and mass concentrations are approximately 20000 cm^{-3} and 21 $\mu g\ m^{-3}$, respectively. After the concentration of seed aerosol has stabilized, either limonene (Sigma-Aldrich, 97%) or β-pinene (Sigma-Aldrich, $\geq$ 99%) is injected by passing air over a known volume of liquid inside a glass bulb. NO_2 (Matheson Tri Gas, 500 ppm) and O_3 (generated by passing purified air through a UV photochemical cell) are then introduced into a flow tube (1.3 L min^{-1} flow rate, 71 s residence time) to produce NO_3 and N_2O_5 (Boyd et al., 2015), which are injected into the chamber and typically marks the beginning of the reaction.

B.2 Calculation of the Aerosol Mass Yield

The aerosol mass is calculated at peak aerosol growth, by multiplying the volume concentration (over a 30 minute average) with the density of the aerosol. The maximum volume concentration is determined after accounting for particle wall loss using the method described by Keywood et al. (2004) The density is calculated by comparing the

mass distribution vacuum aerodynamic diameter from the HR-ToF-AMS with the volume distribution mobility diameter from the SMPS (DeCarlo et al., 2004). From nucleation experiments (Experiments 12 and 13 in Table 3.1), the density of the aerosol produced by the limonene+NO_3 system under dry and humid (RH = 50%) conditions is determined to be 1.64 g cm^{-3} and 1.77 g cm^{-3}, respectively.

B.3 Hydrolysis of Particulate Organic Nitrates

Due to the high yields of particulate organic nitrates from the limonene+NO_3 reaction, the fate of these organic nitrates can have an impact on the concentrations and cycling of ambient atmospheric nitrogen species. The BVOC+NO_3 reaction directly converts atmospheric NO_x into particulate organic nitrate species, which can act as either a sink or reservoir of NO_x with respect to photochemical processing (Nah et al., 2016). These particulate nitrate species can also undergo hydrolysis to form nitric acid (Sato, 2008; Szmigielski et al., 2010; Darer et al., 2011; Hu et al., 2011; Liu et al., 2012; Bean and Hildebrandt Ruiz, 2015; Boyd et al., 2015; Rindelaub et al., 2015) and enhance partitioning of gas-phase organic nitrates to the particle phase (Pye et al., 2015). Although organic nitrate species produced by photooxidation of BVOC under high NO_x conditions appear to undergo rapid hydrolysis (Liu et al., 2012; Bean and Hildebrandt Ruiz, 2015; Rindelaub et al., 2015), organic nitrates formed by the β-pinene+NO_3 system do not undergo hydrolysis significantly owing to a likely abundance of primary/secondary organic nitrates species (Boyd et al., 2015). Using the approach described in Boyd et al. (2015), the rate of organic nitrate hydrolysis can be inferred from the change in the NO_3:Org ratio as measured by the HR-ToF-AMS (Figure B.2). Similar

to the β-pinene+NO_3 system, organic nitrates produced by the limonene+NO_3 system undergo slow conversion to nitric acid via hydrolysis, thus are likely primary/secondary organic nitrates (Darer et al., 2011; Hu et al., 2011).

B.4 Determining the Enthalpy of Vaporization from Two Yield Curves Obtained at Different Temperatures

The enthalpy of vaporization (ΔH_v) can be used to obtain a yield curve, Y, at one temperature (40 °C) from the yields at another temperature (25 °C):

$$Y\ (25\ °C) = Y\ (\Delta H_v, 40\ °C) \tag{B.1}$$

Based on Figure 3.2, Y (25 °C) is constant, Y_{25}, while Y (40 °C) can be fitted to Eq. (3.1). Substitution of the Clausius-Clapyeron(Chung and Seinfeld, 2002) equation for K_2 in Eq. (3.1) yields:

$$Y_{25} = \alpha_1 + \frac{M_o \alpha_2 K_2 \frac{T(298K)}{T(313K)} \exp\left(\frac{\Delta H_v}{R}\left(\frac{1}{T(298K)} - \frac{1}{T(313K)}\right)\right)}{1 + M_o K_2 \frac{T(298K)}{T(313K)} \exp\left(\frac{\Delta H_v}{R}\left(\frac{1}{T(298K)} - \frac{1}{T(313K)}\right)\right)} \tag{B.2}$$

Solving Eq. (B.2) for ΔH_v gives the following dependence of ΔH_v on M_o:

$$\Delta H_v = \alpha_1 + \frac{ln\left(\frac{Y_{25} - \alpha_1}{(\alpha_1 + \alpha_2 - Y_{25}) * M_o K_2 \frac{T(298K)}{T(313K)}}\right)}{\left(\frac{1}{R}\left(\frac{1}{T(298K)} - \frac{1}{T(313K)}\right)\right)} \tag{B.3}$$

B.5 Chemical Differences of SOA from the Limonene+NO_3 Reaction at 25 °C and 40 °C

Although it is possible that the differences in 'Heating Ratio' and 'Formation Ratio' are due to chemical differences in SOA between reactions at 25 °C and 40 °C, this appears to be unlikely. Among these possible chemical differences that may affect volatility are the formation of higher generation oxidation products or the formation of oligomers (Saleh et al., 2013). It is possible that more first-generation products (i.e., only one double bond reacted) would remain in the gas phase at higher temperatures than at lower temperatures, due to their higher volatility. These gas-phase first-generation products could be oxidized at higher temperatures by a second NO_3 radical to form higher-generation products. Since nitrate radicals tend to oxidize BVOC through addition to a double bond, these higher-generation products would have an increase in nitrate mass (and thus an increase in N:C ratio) Therefore, if there were more higher-generation products in the particle phase at higher temperatures, the N:C ratio should increase with temperature (Figure B.6). Since N:C is within experimental uncertainty (22%) (Aiken et al., 2008) between 25 °C and 40 °C, there is no evidence to support that more higher-generation products are formed at higher temperatures. This suggests that it is likely that kinetic limitations, not differences in aerosol composition, are responsible for the slowed evaporation of SOA particles.

B.6 Enthalpy of Vaporization Determined for Each Bin of the Volatility Basis Set

To further illustrate the differences between the aerosol mass remaining from heat-induced evaporation and aerosol mass formed at higher temperatures, the data presented in Figure 3.2 is presented in the context of a volatility basis set with C^* ($\mu g\ m^{-3}$) =

[0.1,1,10,100] (Donahue et al., 2006). The coefficients for each bin are calculated from the aerosol mass yields at 25 °C and 40 °C with each bin coefficient and enthalpy of vaporization set as adjustable parameters. The parameters are chosen to give a least squares fit to the data presented in Figure 3.2. The volatility basis set is presented in Figure B.10 with the effective enthalpy of vaporization (ΔH_v^{form} ; green numbers in Figure B.10) of each volatility bin. Calculated enthalpies for aerosol formed at two different temperatures increase with C^*, qualitatively in agreement with those from Epstein et al. (2009). A value for ΔH_v^{form} could not be determined from our experimental data for $C^* = 0.1$ μg m^{-3}, due largely to the mass loadings of aerosol formed in this study. At mass loadings greater than 10 μg m^{-3}, > 99% of the products at $C^* = 0.1$ μg m^{-3} are in the particle phase and can therefore be treated as effectively non-volatile.

Furthermore, given the fits of α for each bin, the 'Heating Ratio' calculated in Figure B.5 is multiplied by the mass yields at 25 °C to determine the "effective" aerosol mass yields by heating. Since the 'Heating Ratios' are consistent across all mass loadings, the enthalpy of vaporization is set to be a constant value for all volatility bins. The value that corresponds to the least squares fit between the VBS and the "effective" aerosol mass yields determined experimentally is 110 kJ mol^{-1}. Each bin is assigned this enthalpy of vaporization (ΔH_v^{evap}; yellow numbers in Figure B.10). With the volatility bins that are fitted, ΔH_v^{evap} is consistent with the ΔH_v^{form} for the aerosol-producing bin with the highest C^*. The highest C^* products are most likely to form after the lower volatility products condense and therefore likely form the outermost layer of the SOA produced by

the limonene+NO_3 reaction. This supports our hypothesis that the outermost layers of SOA particles may control the degree of aerosol evaporation upon heating.

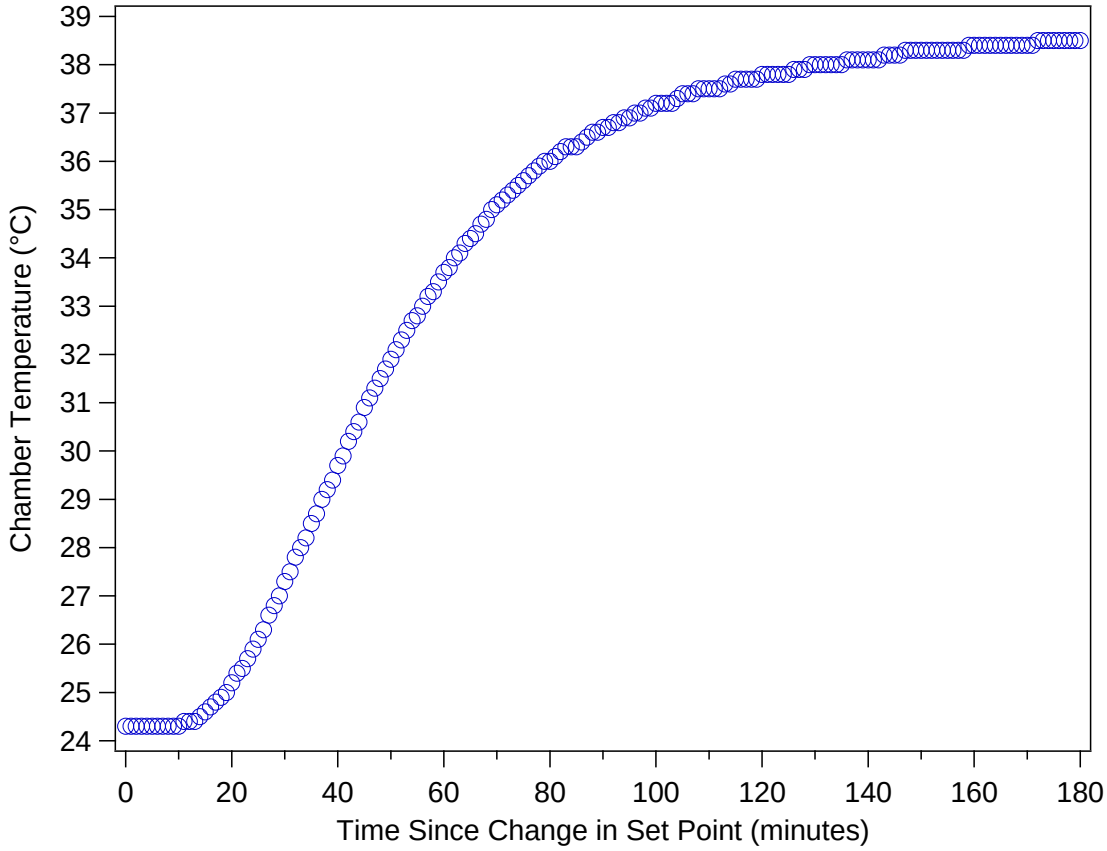

Figure B.1: A typical temperature profile for a limonene+NO_3 experiment (Experiment 3 in Table 3.1) that is heated to 40 °C after SOA is formed at an initial reaction temperature of 25 °C. There is an approximately 10 minute delay between the time the temperature increases and the time of setting the chamber temperature to the 40 °C set point. The temperature increase is rapid and becomes stable within approximately 2 hours.

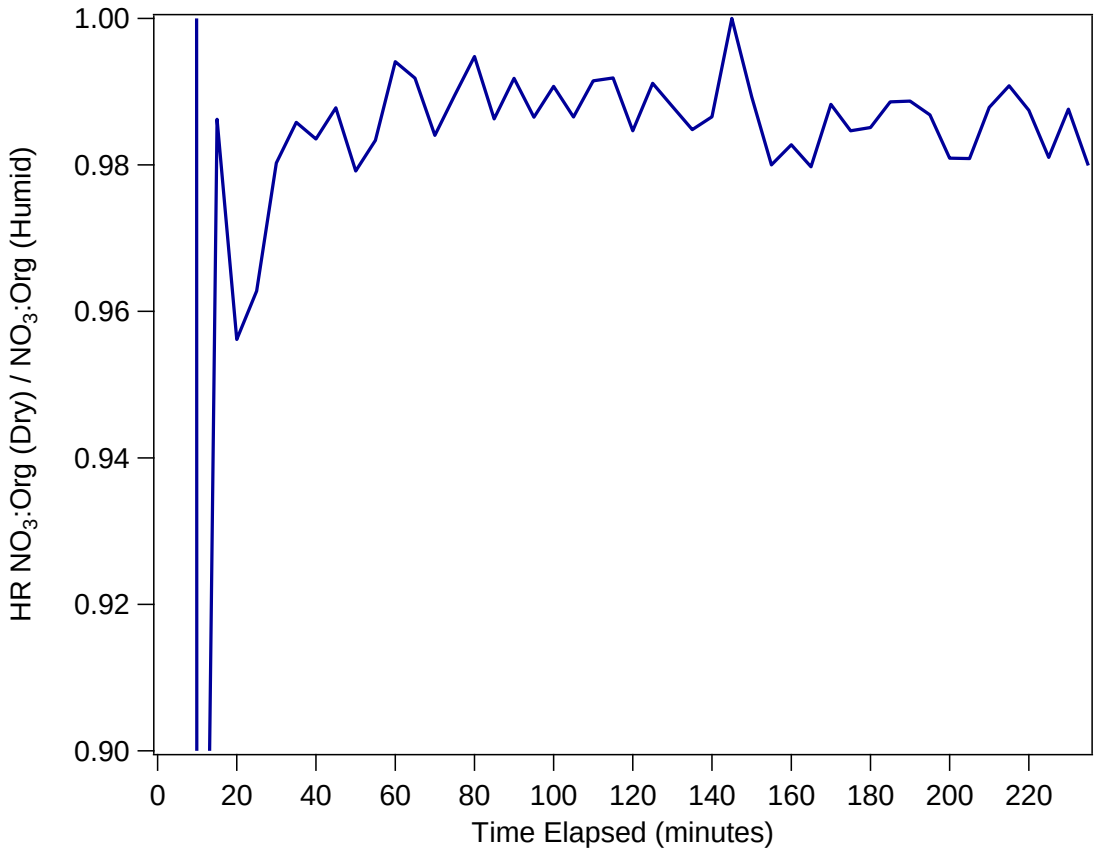

Figure B.2: The AMS Nitrate:Org ratio of a humid (RH = 70%) 'Limonene Core' experiment normalized by the AMS Nitrate:Org for the corresponding dry 'Limonene Core' experiment, 5-minute averaged. Only the time period prior to β-pinene injection is considered for this analysis. The near-unity of the normalized Nitrate:Org ratio indicates that the particulate organic nitrates produced by the limonene+NO_3 reaction do not hydrolyze appreciably.

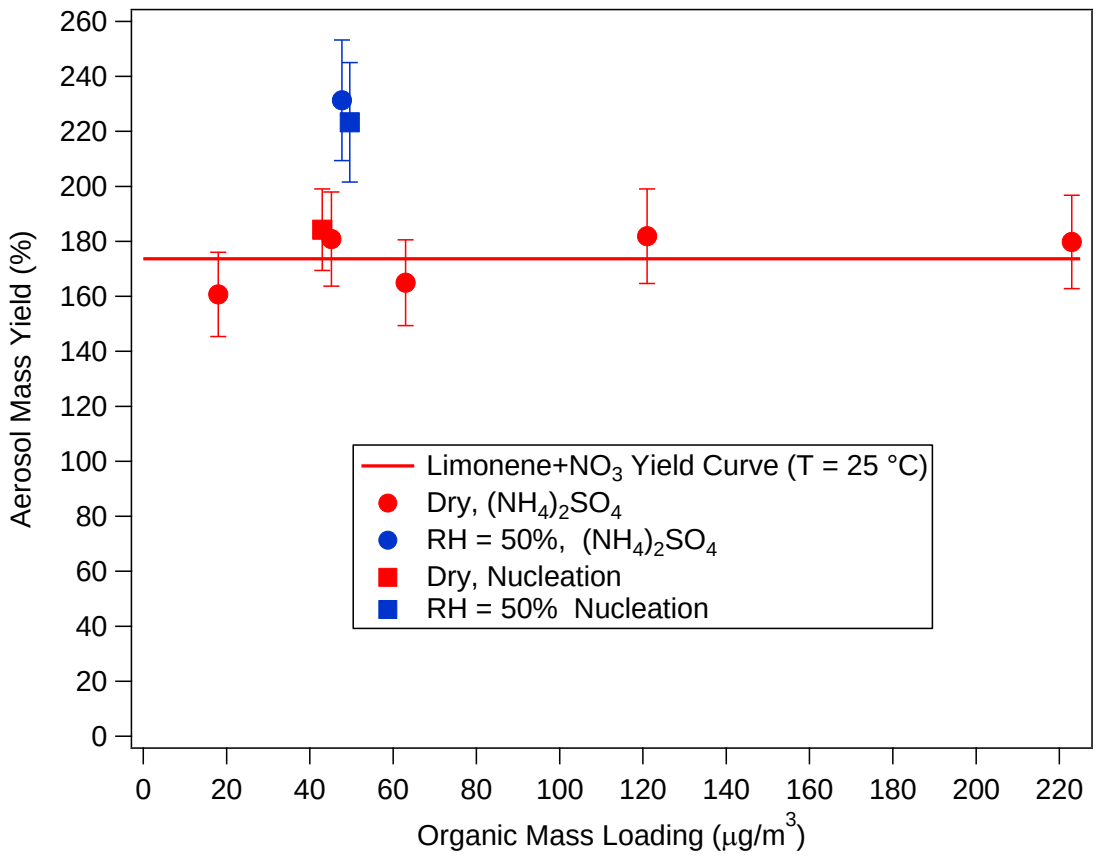

Figure B.3: Aerosol mass yield for the limonene+NO_3 reaction at 25 °C. Under humid (RH = 50%) conditions, the aerosol mass yield is slightly higher compared to dry conditions. The nucleation experiments have similar yields to experiments in which ammonium sulfate is used as seed aerosol. The nucleation experiments are also useful in determining the density of the organic aerosol formed from the limonene+NO_3 reaction (DeCarlo et al., 2004). The x-axis error bars are calculated using one standard deviation of volume measured by SMPS at peak aerosol growth. The y-axis error bars are calculated with an 8% uncertainty in hydrocarbon injection and one standard deviation of the aerosol volume measured by SMPS at peak growth.

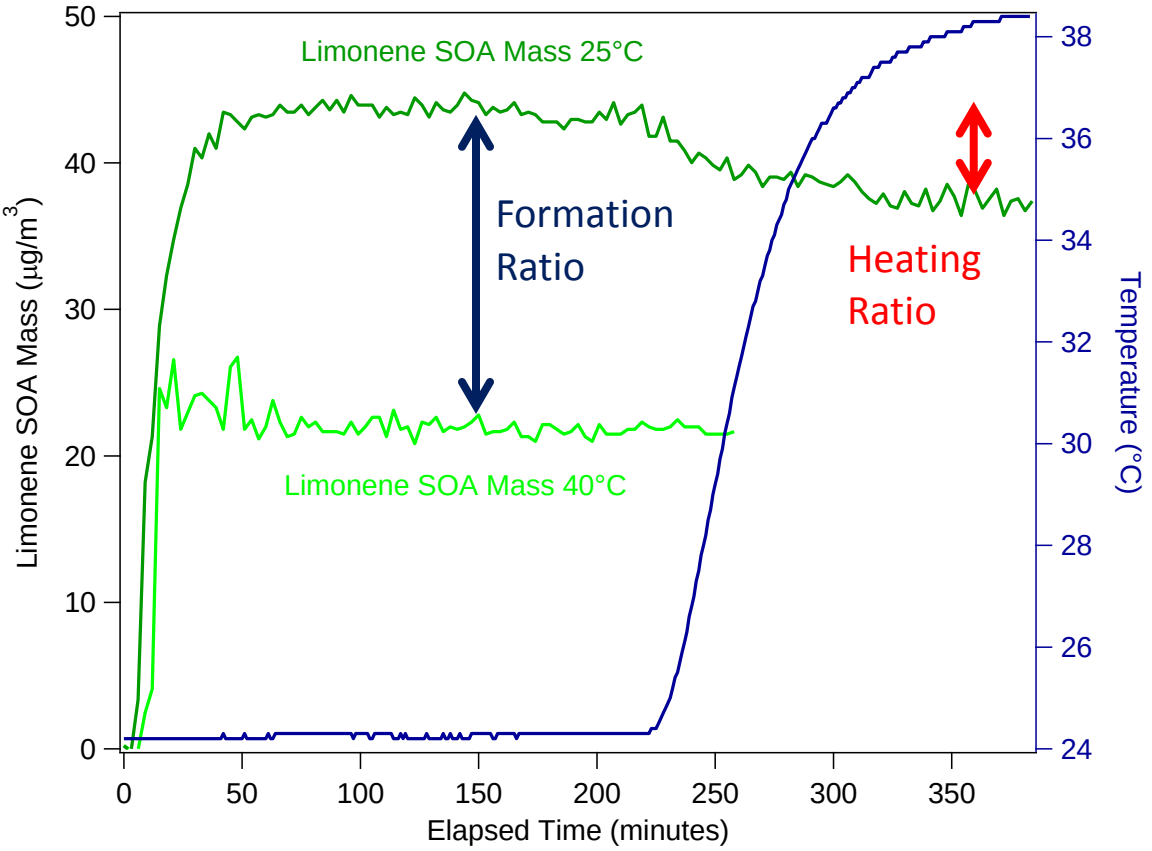

Figure B.4: The particle wall-loss corrected limonene SOA mass concentration for two limonene+NO_3 experiments. When heating from 25 °C to 40 °C (dark green trace), there is evaporation of organics as indicated by a decrease in limonene SOA mass. The organic mass at 40 °C after heating divided by the organic mass at 25 °C is defined as the "Heating Ratio". The mass formed at 40 °C divided by the mass formed at 25 °C is defined as the "Formation Ratio". Since the "Heating Ratio" is much smaller than the "Formation Ratio" at low loadings, there appears to be a resistance to aerosol evaporation induced by heating.

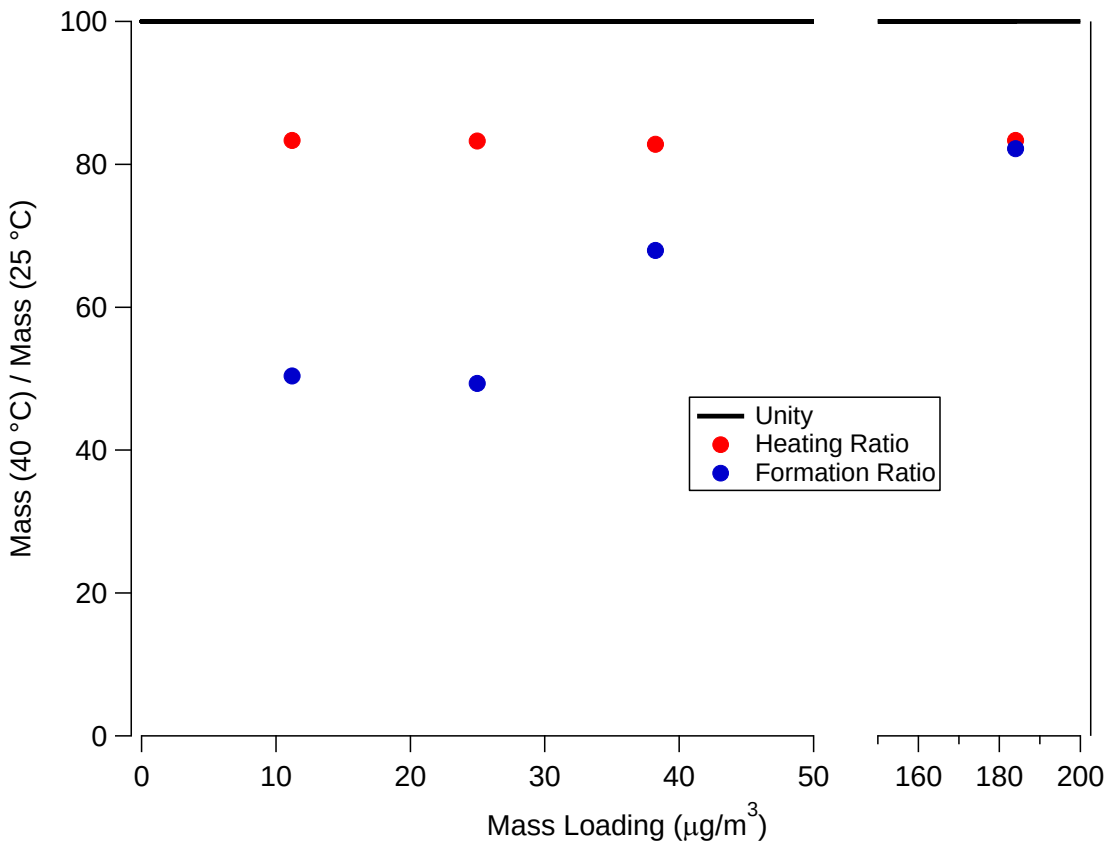

Figure B.5: The relative amount of aerosol mass at 40 °C compared to the aerosol mass at 25 °C as a function of mass loading as determined by both the "Formation Ratio" and "Heating Ratio". Mass loadings reported (x-axis) are for the mass of aerosol produced at 40 °C. The "Formation Ratio" is often lower than the "Heating Ratio". As discussed in the main text, the "Heating Ratio" is typically calculated once the aerosol is heated to 38 °C. It is noted that the "Heating Ratio" for the lowest mass loading experiment was calculated once the chamber reached 35 °C. The difference between the "Formation Ratio" and "Heating Ratio" appears to be less pronounced with increasing mass loading and are approximately equal at high mass loadings (~180 μg m^{-3}). Nevertheless, a substantial resistance to evaporation appears to exist in most cases.

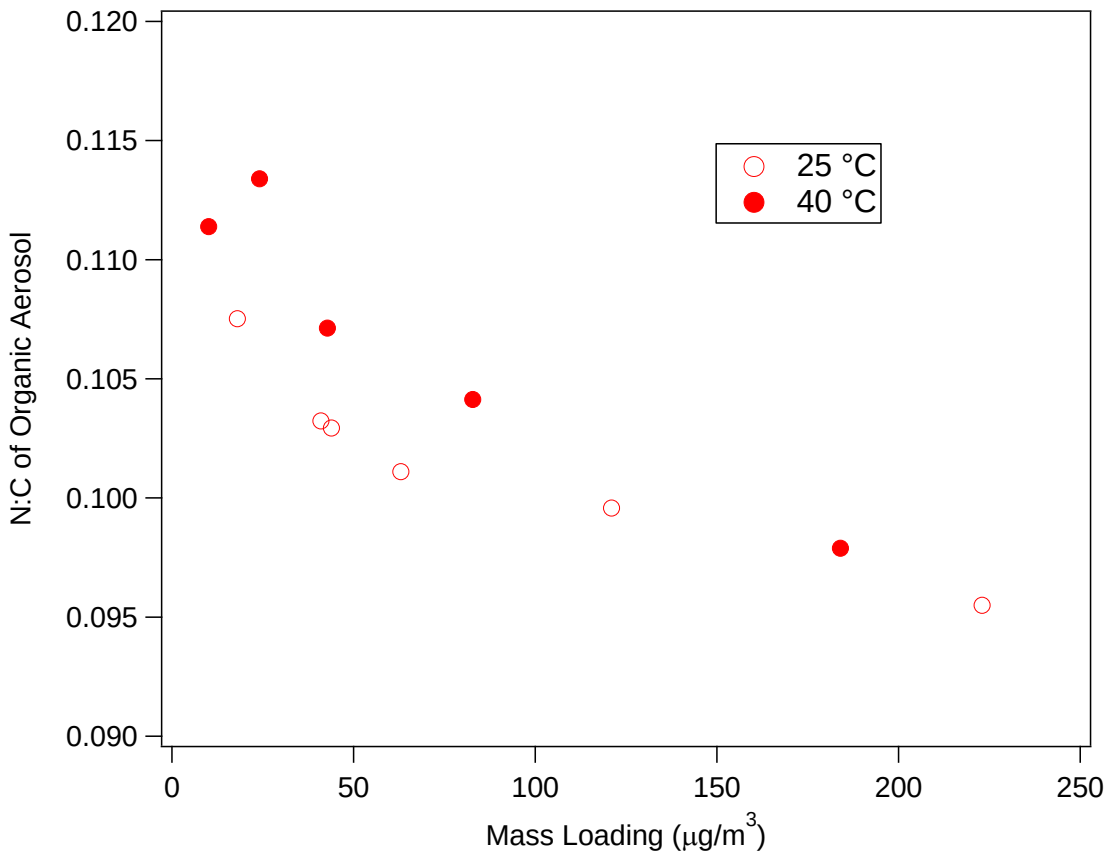

Figure B.6: The AMS N:C ratio of SOA formed from the limonene+NO_3 reaction as a function of mass loading. There appears to be a very slight dependence of N:C on organic mass loading. However, the N:C is similar between 25 °C and 40°C, within experimental error, for experiments with similar organic mass loadings.

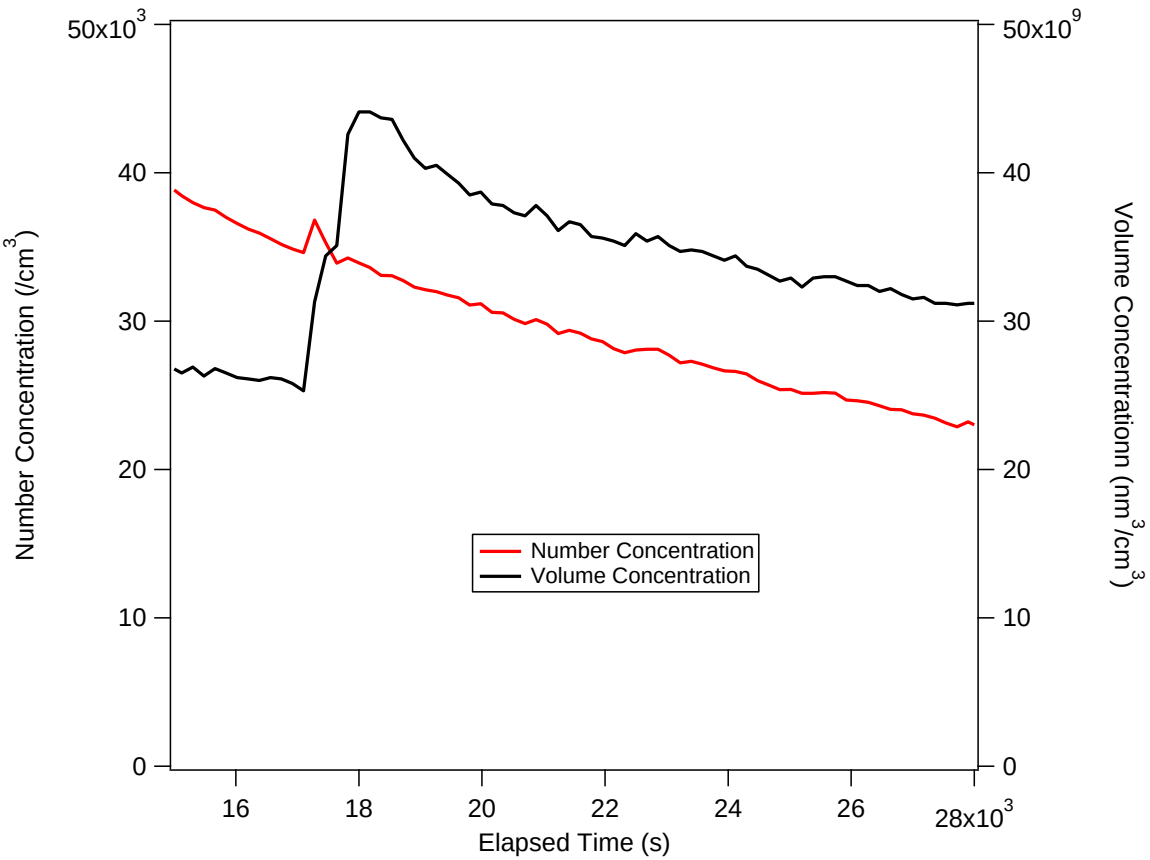

Figure B.7: The number and volume concentration from a 'Limonene Core' experiment (Experiment 15 in Table 3.1). The introduction of β-pinene SOA is marked by an increase in the total volume concentration. This corresponds to a negligible increase in the number concentration. This suggests that the β-pinene SOA condenses onto the existing limonene SOA.

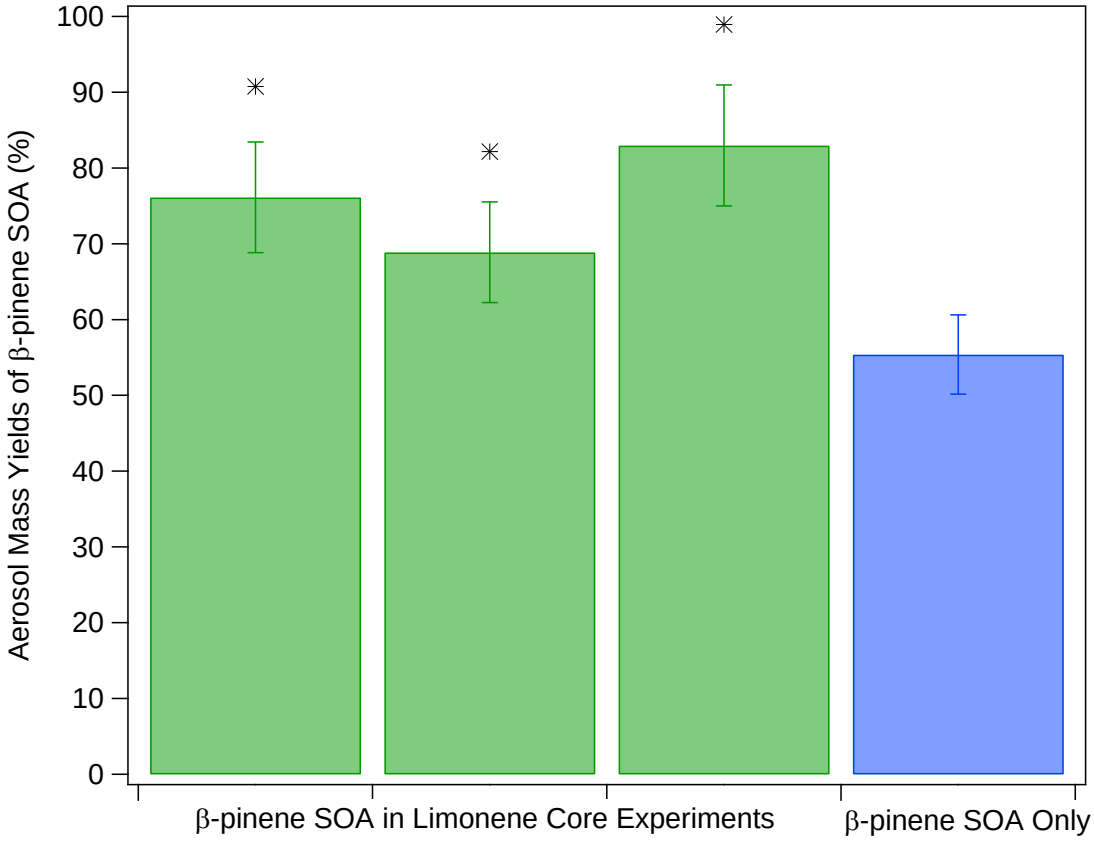

Figure B.8: Aerosol mass yield for the β-pinene+NO_3 reaction. Yields from the 'Limonene' Core' Experiments (Experiments 15-17 in Table 3.1) are compared to the yield from the experiment with only β-pinene SOA with inorganic seeds (Experiment 20 in Table 3.1). The presence of SOA formed from the limonene+NO_3 reactions increases the yield of β-pinene SOA for the same amount of β-pinene reacted. Asterisks indicate a one standard deviation difference in yield. The standard deviation in yield is calculated by an 8% uncertainty in chamber volume, 5% uncertainty in hydrocarbon injection, and one standard deviation of the aerosol volume measured by SMPS at peak growth.

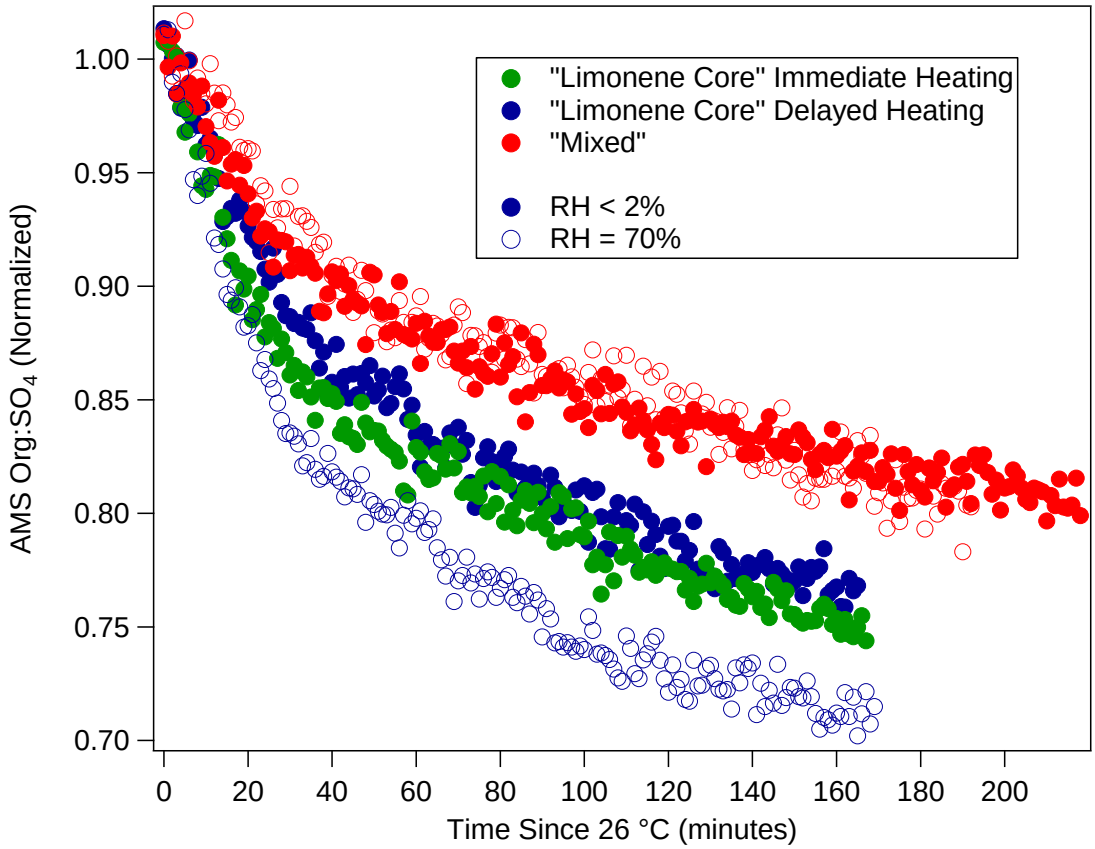

Figure B.9: The AMS HR Org:SO_4 for the 'Mixed' and 'Limonene Core' experiments. The Org:SO_4 ratio is normalized to the Org:SO_4 ratio averaged over 5 minutes after the chamber achieves a temperature of 26 °C. Decrease in Org:SO_4 is due organic aerosol evaporation. The 'Mixed' experiments have less overall organic evaporation than the 'Limonene Core' experiments. While increasing humidity does not increase the organic evaporation in the 'Mixed' experiment, humidity appears to increase the overall evaporation in the 'Delayed Heating' experiments slightly.

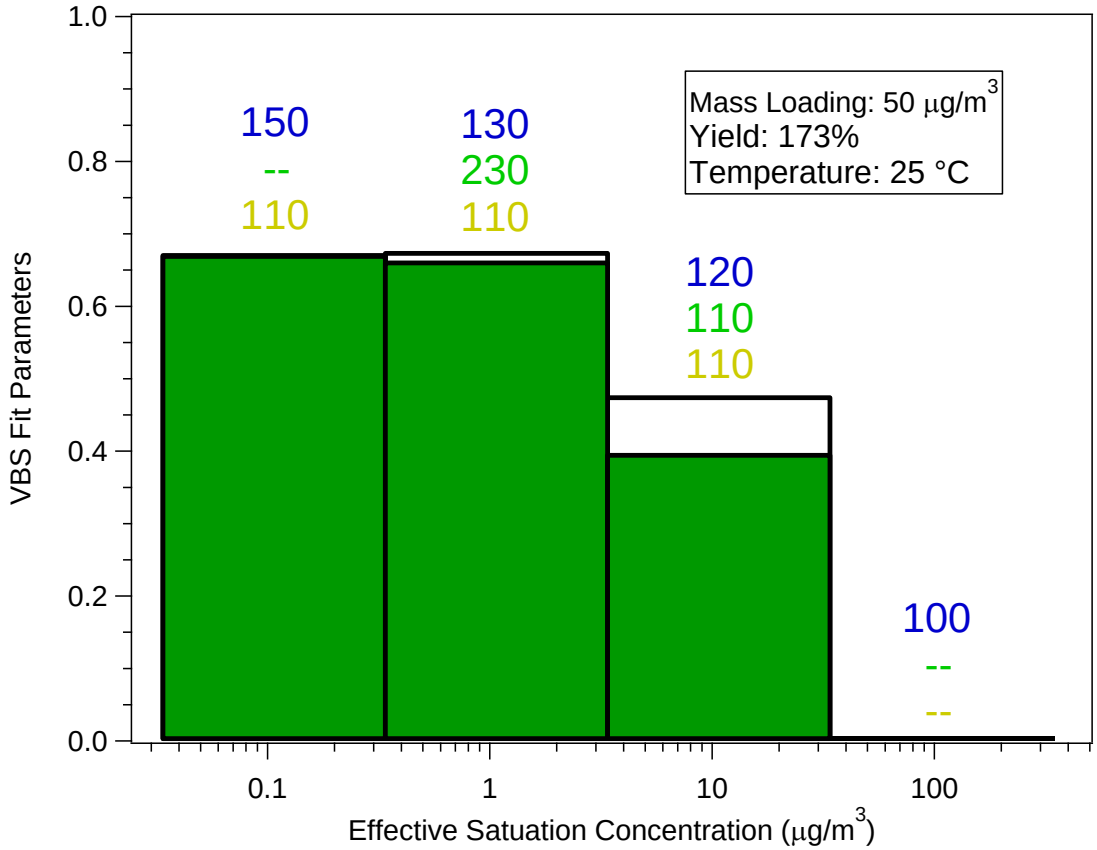

Figure B.10: Volatility basis set for the limonene+NO_3 system at a given mass loading of 50 μg m^{-3} at 25 °C with C* = [0.1,1,10,100]. The enthalpy of vaporization (kJ mol^{-1}) is determined for each bin according to the parameterization by Epstein et al. (2009) (blue), enthalpy of vaporization based on the formation at two different temperatures (green), and enthalpy of vaporization from heating aerosol (yellow). The enthalpy of vaporizations for formation and heating are in best agreement for the most volatile bin that still contains products in the particle phase. This is possibly because the most volatile bin may be most concentrated on the outer layers of the aerosol, which may be the layers that evaporate the most while hindering the evaporation of the inner layers.

APPENDIX C

Photochemical Aging of α-pinene and β-pinene Secondary Organic Aerosol formed from Nitrate Radical Oxidation

C.1 Introduction

Atmospheric organic aerosol (OA) has important impacts on climate and human health (Hallquist et al., 2009). A substantial fraction of OA is composed of secondary organic aerosol (SOA), which is formed from the oxidation of volatile organic compounds (VOCs). Biogenic volatile organic compounds (BVOCs) are key precursors for SOA formation due to their high emissions and reactivity with atmospheric gas-phase oxidants (Kanakidou et al., 2005). The nitrate radical (NO_3), which is derived almost exclusively from the reaction of NO_2 with O_3 (Brown and Stutz, 2012), is the dominant nighttime oxidant in most urban and rural environments (Winer et al., 1984; Brown et al., 2013). NO_3 reacts rapidly with BVOCs to produce SOA and organic nitrates (ON) (Boyd et al., 2015; Griffin et al., 1999; Fry et al., 2014). A substantial fraction of ambient nighttime SOA and gas- and particle-phase ON is attributed to NO_3+BVOC reactions (Xu et al., 2015c). Gas- and particle-phase ON play important roles in the atmosphere as their fates could influence the nitrogen cycle and O_3 production (Brown and Stutz, 2012; Perring et al., 2013). They either return NO_x to the atmosphere via further oxidation and photolysis (NO_x recycling), or act as terminal NO_x sinks through deposition and hydrolysis. Currently, there is a large uncertainty in our understanding of ON formation and fate, which affects our ability to accurately model regional and global NO_x and O_3 budgets (Browne and Cohen, 2012).

The text in this chapter is reproduced, in part, by: Nah, T., Sanchez, J., Boyd, C. M., and Ng, N. L.: Photochemical Aging of α-pinene and β-pinene Secondary Organic Aerosol formed from Nitrate Radical Oxidation, Environ. Sci. Technol., 50, 222-231, doi:10.1021/acs.est.5b04594, 2016.

Despite their importance in the nocturnal atmosphere, NO_3+BVOC reaction mechanisms and products remain poorly characterized. There is also a lack of knowledge on how SOA and ON from nighttime NO_3+BVOC reactions evolve in the atmosphere. Ambient SOA is highly oxygenated due to atmospheric aging, which is defined as the multigenerational oxidation of aerosol (Rudich et al., 2007; Ng et al., 2010). Aerosol lifetimes in the atmosphere typically range between 1 and 2 weeks (Kanakidou et al., 2005); half of its lifetime is at night where NO_3 and O_3 are the primary oxidants and half of it is in the day where OH photooxidation is dominant. Therefore, in order to accurately assess how nighttime chemistry influences daytime O_3 production and the nitrogen cycle, it is important to understand the multigenerational chemistry and characterize the composition of nighttime SOA and ON formed from NO_3 chemistry over their diurnal lifecycle.

Here, we study how the transition from night to day oxidation environments affects the fates of nighttime monoterpene SOA and ON formed from NO_3 chemistry. Laboratory experiments are conducted to investigate how the chemical compositions of α-pinene and β-pinene SOA and ON from NO_3 oxidation change during dark and photochemical aging. The SOA and ON are characterized using real-time gas- and particle-phase measurements, which are used to propose mechanisms for SOA and ON formation and aging. α-pinene and β-pinene are chosen because together they constitute ~50 % of the global monoterpene emissions.(Guenther et al., 2012) These results provide fundamental

data that can be used to interpret ambient monoterpene SOA and ON diurnal behavior, and to evaluate the extent to which ON serve as permanent vs. temporary NO_x sinks.

C.2 Experimental

Experiments were conducted in the Georgia Tech Environmental Chamber (GTEC) facility (Boyd et al., 2015) at room temperature (24 °C) under humid conditions (50 to 54 % RH). The parent hydrocarbons used in this study were α-pinene (Sigma-Aldrich, ≥ 99 %) and β-pinene (Sigma-Aldrich, ≥ 99 %). Inorganic seed particles were introduced into the chamber via atomization of a $MgSO_4/H_2SO_4$ ($[MgSO_4]:[H_2SO_4]$ = 1:2, molar ratio) solution. The initial seed number and volume concentrations were ~16 000 particles cm^{-3} and ~36 μm^3 cm^{-3}, respectively. The pH of the $MgSO_4/H_2SO_4$ seed at 50 % RH is -0.4 based on calculations using ISORROPIA.(Fountoukis and Nenes, 2007) An acidic seed was used to mimic aerosol conditions (pH 0 to 2) found in the Southeastern United States (Guo et al., 2015; Xu et al., 2015c). The experimental conditions are summarized in Table D.1 (Appendix D).

A variety of products can be formed by peroxy (RO_2) radical chemistry (RO_2+HO_2 vs. RO_2+NO_3 vs. RO_2+RO_2 pathways) in the NO_3+α-pinene and NO_3+β-pinene reactions. Formaldehyde (HCHO) was first added into the chamber to enhance the RO_2+HO_2 pathway (Nguyen et al., 2014; Boyd et al., 2015). 16 and 10 ppm HCHO were introduced into the chamber for the α-pinene and β-pinene experiments, respectively, to ensure that the branching ratios for the RO_2+HO_2, RO_2+NO_3, RO_2+RO_2 pathways were ~5:4:1, which was chosen to allow us to characterize products formed primarily from the RO_2+HO_2 and RO_2+NO_3 pathways. Formalin solution (Sigma-Aldrich, 37 % HCHO)

was injected into a gently heated glass bulb, and the vapor was carried into the chamber using 5 L min^{-1} of purified air until all the formalin solution evaporated. The HCHO concentration in the chamber was estimated from the injected HCHO volume and chamber volume. A previous study by Kroll et al. (2005) on the reactive uptake of HCHO on aqueous seed aerosol suggests that HCHO will not partition to the particle phase under humid conditions (50 to 55 % RH), similar to the experimental conditions in this study. Seed particles were then introduced into the chamber, followed by the injection of a known volume of the parent hydrocarbon (α-pinene or β-pinene). The parent hydrocarbon concentration was monitored using a Gas Chromatograph-Flame Ionization Detector (GC-FID, Agilent 7890A). NO_2 (Matheson Tri Gas, 500 ppm) and O_3 (generated by passing purified air through a UV photochemical cell, 138 ppm) were then introduced into a flow tube (1.3 L min^{-1} flow rate, 71 s residence time) for 7 min to produce NO_3 and N_2O_5 (Boyd et al., 2015), which were injected into the chamber.

For all experiments, the start of NO_2 and O_3 injection into the flow tube marked the beginning of the reaction (i.e., reaction time = 0 min). All the α-pinene and β-pinene reacted within ~10 min of the start of the reaction. To ensure that > 99 % of the parent hydrocarbon reacted with NO_3 instead of O_3 in the chamber, the concentration ratio of NO_2 and O_3 injected into the flow tube was kept at ~5:2. The reactions and rate constants used to model the branching ratios are shown in Table D.2 (Appendix D). Aerosol peak growth occurred within 15 to 20 min of the start of the reaction in all experiments. H_2O_2 was introduced into the chamber by passing purified air over 25 μL of H_2O_2 solution (Sigma-Aldrich, 50 % wt. in H_2O) in a gently heated glass bulb ~1.5 to 2 h after aerosol

peak growth has been achieved in the NO_3 reaction. The H_2O_2 concentration in the chamber was estimated to be ~1 ppm from the injected H_2O_2 volume and chamber volume. After all the H_2O_2 evaporated, all the blacklights lights (Sylvania, 24922) surrounding the Teflon chambers were turned on to initiate the photooxidation reaction. The NO_2 photolysis rate (j_{NO2}) of the chamber facility is 0.28 min^{-1} when all of the blacklights are turned on (Boyd et al., 2015). To determine the OH concentration during these photochemical aging experiments, a separate experiment on the photochemical aging of SOA from the NO_3+β-pinene reaction was performed during which ~8 ppb of cyclohexane was injected into the chamber prior to the introduction of H_2O_2. After ~1 ppm H_2O_2 was introduced into the chamber, all the chamber blacklights were switched on and the cyclohexane decay (due to reaction with OH) was measured as a function of photochemical aging time. Based on the measured cyclohexane decay and the rate constant of the OH+cyclohexane reaction (7.21×10^{-12} cm^3 $molec.^{-1}$ s^{-1}) (Atkinson, 1997b), the OH concentration in the chamber was ~5×10^6 molec. cm^{-3}. The OH concentration in the chamber during the photochemical aging of SOA from the NO_3+α-pinene reaction is expected to be similar.

O_3, NO_x and NO_2 concentrations were measured by an O_3 Analyzer (Teledyne T400), an ultrasensitive chemiluminescence NO_x monitor (Teledyne 200EU) and a Cavity Attenuated Phase Shift (CAPS) NO_2 monitor (Aerodyne Research Inc.), respectively. Aerosol size distributions, number and volume concentrations were measured by a Scanning Mobility Particle Sizer (SMPS, TSI), which consists of a Differential Mobility Analyzer (DMA, TSI 3081) and a Condensation Particle Counter (CPC, TSI 3775). A

High Resolution Time-of-Flight Aerosol Mass Spectrometer (HR-ToF-AMS, Aerodyne Research Inc.) measured the bulk aerosol elemental composition (DeCarlo et al., 2006; Canagaratna et al., 2015). A Filter Inlet for Gases and AEROsols (FIGAERO, Aerodyne Research Inc.) coupled to a High-Resolution Time-of-Flight Chemical Ionization Mass Spectrometer (HR-ToF-CIMS, Aerodyne Research Inc.) measured the molecular composition of the gas- and particle-phase ON products. Operation of the FIGAERO-HR-ToF-CIMS are detailed in Section D.1 (Appendix D).

C.3 Results and Discussion

C.3.1 SOA formation from NO_3 oxidation of β-pinene and α-pinene

The particle wall loss-corrected β-pinene SOA mass yield and loading (52.7±5.1 % at 34.8±0.9 μg m^{-3}) are significantly higher than that of α-pinene (3.6±0.4 % at 2.5±0.1 μg m^{-3}) even though the concentrations of reacted β-pinene and α-pinene are similar (i.e., 12 ppb) (Appendix D, Table D.1 and Section D.2). This striking difference in the β-pinene and α-pinene SOA mass yields could be explained by the products formed during the NO_3 reaction.(Fry et al., 2014) For the NO_3+β-pinene reaction, several gas-phase ON compounds with carboxylic acid, alcohol and peroxide functional groups have been previously identified as first-generation oxidation products.(Boyd et al., 2015) These ON species generally have low volatilities and will condense efficiently onto seed particles, resulting in high SOA yields. In contrast, pinonaldehyde is the major first-generation product in the NO_3+α-pinene reaction since the nitrate functional group is typically lost in the form of NO_2 during the reaction.(Spittler et al., 2006; Perraud et al., 2010) The later generation products formed from NO_3+pinonaldehyde have high vapor pressures(Perraud

et al., 2010) and do not condense efficiently onto seed particles, thus leading to low SOA yields.

The HR-ToF-AMS mass spectra of SOA from the NO_3+β-pinene and NO_3+α-pinene reactions are shown in Figures D.1a and D.2a (*Appendix D*). In the β-pinene SOA mass spectra, *m/z* 67 ($C_5H_7^+$) and *m/z* 91 ($C_7H_7^+$) have relatively large signals, similar to those observed previously by Boyd et al. (2015). In contrast, *m/z* 67 ($C_5H_7^+$) has a low ion signal and *m/z* 91 ($C_7H_7^+$) has a relatively large signal in the α-pinene SOA mass spectrum. Nitrogen-containing ions ($C_xH_yO_zN$) comprise ~10 % of the combined organic and nitrate signal, and are detected mainly as NO^+ and NO_2^+ ions. The high NO^+/NO_2^+ ratio in the HR-ToF-AMS mass spectrum indicates the presence of particle-phase ON in aerosol.(Farmer et al., 2010; Xu et al., 2015a) The NO^+/NO_2^+ ratios are 8.7 and 8.8 for the β-pinene and α-pinene SOA, respectively, which fall within the range (i.e., 5 - 15) reported by previous studies.(Fry et al., 2009; Boyd et al., 2015; Bruns et al., 2010) The molar fractions of particle-phase ON in β-pinene and α-pinene SOA are estimated to be 70 % and 80 %, respectively (upper limit) based on their bulk aerosol N/C ratios (~0.07 and ~0.08, respectively). Based on the nitrate-to-organics mass ratios (NO_3/Org) of β-pinene and α-pinene SOA (~0.16 for both monoterpenes) and the molecular weights of their ON products (200 - 300 amu) (Appendix D, Tables D.3 and D.4), the particle-phase ON mass fraction of β-pinene and α-pinene SOA are estimated to both be ~60 %. Thus, these results demonstrate that not only do particle-phase ON constitute a significant fraction of β-pinene and α-pinene SOA, the particle-phase ON molar and mass fractions

in β-pinene and α-pinene SOA are similar despite their SOA mass loadings being drastically different.

Although field studies have shown that aging can lead to the formation of highly oxygenated ambient SOA (Ng et al., 2010). most laboratory studies have focused on OH aging (Kroll et al., 2009; Donahue et al., 2012; Henry and Donahue, 2012). Figure C.1 shows the HR-ToF-AMS measurements of the organics and nitrate components of β-pinene and α-pinene SOA. The organics and nitrate mass concentrations are normalized to that of sulfate (Org/SO_4 and NO_3/SO_4 ratios, respectively) to account for changes in the HR-ToF-AMS aerosol collection efficiency during the reaction.(Henry and Donahue, 2012) For both β-pinene and α-pinene, the Org/SO_4 and NO_3/SO_4 ratios increase instantaneously at the onset of the reaction, peak at ~30 min, then decrease as the reaction progresses further (Figures C.1a and C.1b). The decrease in the Org/SO_4 and NO_3/SO_4 ratios may be attributed to particle wall loss due to diffusion-limited aerosol growth(Loza et al., 2012) and/or aerosol evaporation resulting from aerosol aging.(Donahue et al., 2012; Henry and Donahue, 2012) The organic fraction of the aerosol are separated primarily into three components based on their chemical formulas, the non-oxidized, slightly oxidized and highly oxidized fragments (CH, CHO1 and CHOgt1 organic families, respectively), and plotted as a function of reaction time. The CH family consists of C_xH_y fragments, the CHO1 family consists of C_xH_yO fragments, and the CHOgt1 family consists of $C_xH_yO_z$ fragments where z is greater than 1. Although these organic families exhibit similar trends (i.e., increase before decreasing), the non-oxidized CH organic family decreases more rapidly than the more oxidized CHO1 and CHOgt1

organic families in both the NO_3+β-pinene and NO_3+α-pinene reactions (Figures C.1c and C.1d). While this suggests that highly oxygenated particle-phase organic species are formed during the NO_3 reaction, the mass concentrations of the CHO1 and CHOgt1 organic families are significantly smaller than that of the CH organic family. This observation is consistent with the fairly constant bulk elemental compositions (H/C, O/C and N/C ratios) of β-pinene and α-pinene SOA during the NO_3 reaction (Figures C.1e and C.1f). These results demonstrate that the extent to which dark NO_3 aging influences the chemical composition of β-pinene and α-pinene SOA and ON is small in the timescale of our experiments.

One important particle-phase ON loss process is hydrolysis. Tertiary ON hydrolyze within minutes, while secondary and primary ON hydrolyze on the order of hours to days.(Darer et al., 2011; Hu et al., 2011; Boyd et al., 2015) Based on the chemical structures of β-pinene and α-pinene, the NO_3+β-pinene reaction will lead to the formation of tertiary and primary ON, while the NO_3+α-pinene reaction will form tertiary and secondary ON. Under the dark conditions in the chamber, the loss of particle-phase ON via hydrolysis alone will result in a decrease in the NO_3/Org ratio due to the formation (and subsequent evaporation) of nitric acid.(Boyd et al., 2015) The NO_3/Org ratio of β-pinene SOA decreases by ~10 % during the NO_3 reaction, suggesting that ~10 % of the particle-phase ON are lost via hydrolysis (Figure C.1g). It is likely that the particle-phase ON lost are tertiary ON, and the remaining particle-phase ON are primary particle-phase ON which do not hydrolyze at appreciable rates.(Boyd et al., 2015) Surprisingly, the NO_3/Org ratio of α-pinene SOA stays fairly constant during the NO_3 reaction (Figure

C.1h), which suggests that tertiary ON are not formed in the NO_3+α-pinene reaction. Taken together, these results show that hydrolysis is a minor loss channel for particle-phase ON formed from the NO_3+β-pinene and NO_3+α-pinene reactions. This is consistent with particle-phase ON comprising a significant fraction of the β-pinene and α-pinene SOA as discussed above. We note that the α-pinene SOA yield doubled in the presence of acidic seed aerosol. It is possible that there are the acid-catalyzed particle-phase reactions (e.g., particle-phase reactions of nitroxyl alcohols and carbonyls with sulfuric acid to form sulfated ON)(Surratt et al., 2008) occurring during the NO_3+α-pinene and NO_3+β-pinene reactions, and this warrants further study.

A total of 41 species with molecular compositions consistent with ON is measured in both the gas and particle phase during the NO_3+β-pinene reaction (Appendix D, Table D.3). Figure C.2 shows the HR-ToF-CIMS mass spectra of particle- and gas-phase ON formed from the NO_3+β-pinene reaction. The observed ON have 7 to 10 carbon atoms (referred to as C_7, C_8, C_9 and C_{10} ON) and are highly oxygenated with 4 to 9 oxygen atoms. Although previous laboratory studies have reported the formation of gas- and particle-phase C_{10} ON with 4 to 6 oxygen atoms from NO_3 reactions,(Boyd et al., 2015) this is the first direct observation of ON with more than 6 oxygen atoms from NO_3+BVOC chemistry. The highly oxygenated ON with high particle-phase signals typically have low gas-phase signals. This is consistent with volatility trends, where compounds with similar numbers of carbon and hydrogen atoms but more oxygen atoms are expected to have lower volatilities and thus partition more strongly into the particle phase.(Pankow and Asher, 2008) These results clearly demonstrate that highly

oxygenated gas- and particle-phase ON can be formed from nighttime NO_3 chemistry alone, and does not require multiday photochemical aging processes. Dinitrates are not detected during the NO_3 reaction, which is likely due to β-pinene only having one double bond. Also, while sulfated ON may be formed during the NO_3 reaction (via particle-phase reactions of nitroxyl alcohols and carbonyls with sulfuric acid),(Surratt et al., 2008) they are not detected here possibly due to thermal decomposition caused by the FIGAERO thermal desorption process.(Lopez-Hilfiker et al., 2015)

One striking feature of these highly oxygenated gas- and particle-phase ON species is their rapid formation. (Appendix D, Figure D.3). While Boyd et al. (2015) has proposed a detailed reaction mechanism to explain the formation of gas- and particle-phase C_{10} ON with 4 to 6 oxygen atoms in the NO_3+β-pinene reaction, the formation mechanisms for gas- and particle-phase ON with more than 6 oxygen atoms detected in this study are unclear. While some of these highly oxygenated gas- and particle-phase ON may be later generation products formed from dark aerosol aging (Boyd et al., 2015), these highly oxygenated gas- and particle-phase ON molecules are likely also formed by autoxidation, which occurs via successive inter- and intramolecular H atom abstractions by peroxy radicals followed by O_2 addition (Crounse et al., 2013; Ehn et al., 2014; Jokinen et al., 2015) (Appendix D, Figure D.4). Computational studies have shown that autoxidation is a very fast process, resulting in the rapid formation of highly oxygenated low volatility products (Crounse et al., 2013; Ehn et al., 2014). The rapid formation of highly oxygenated gas- and particle-phase ON in this study is consistent with the autoxidation mechanism. Moreover, these results imply that autoxidation is highly competitive with

other peroxy radical reaction pathways (e.g., alkoxy radical formation) in the NO_3+β-pinene reaction.

Figure C.3 shows the contributions of particle- and gas-phase C_8, C_9 and C_{10} ON signals relative to the total ON signal (sum of these three groups) as a function of reaction time. Gas- and particle-phase C_7 ON are not included since their signals are very low relative to those of C_8, C_9 and C_{10} ON. The C_{10} ON account for the highest fraction of the total ON signal in both the particle and gas phase during the NO_3 reaction. Specifically, the number of C_8, C_9 and C_{10} ON species detected during the reaction are 19 C_{10} ON vs. 9 C_9 ON vs. 7 C_8 ON (Appendix D, Table D.3). These results suggest that the alkoxy radical formation pathway (and consequently C-C bond scission) is minor, resulting in small fractions of gas- and particle-phase C_8 and C_9 ON. This is consistent with autoxidation being highly competitive with other peroxy radical reaction pathways (e.g., alkoxy radical formation).

Unlike the large number of speciated ON species detected in the NO_3+β-pinene reaction, only 5 molecular compositions consistent with ON are measured in both the gas and particle phase during the NO_3+α-pinene reaction (Appendix D, Table D.4). One possible explanation for the suppressed formation of ON in the NO_3+α-pinene reaction relative to the NO_3+β-pinene reaction may be the different peroxy and alkoxy radical fates in the two systems.(Fry et al., 2014) In the NO_3+β-pinene reaction, the tertiary alkoxy radical preferentially undergoes a rapid H atom shift to form a new peroxy radical,(Boyd et al., 2015) which can then undergo autoxidation to form highly oxygenated ON (Appendix D,

Figure D.4). Moreover, the autoxidation rate likely increases as the reaction progresses (Crounse et al., 2013), resulting in the formation of a large number of highly oxygenated gas- and particle-phase ON. In contrast, the tertiary alkoxy radical formed in the NO_3+α-pinene reaction mainly dissociates to form pinonaldehyde while losing the nitrate functional group in the form of NO_2 (Appendix D, Figure D.5) (Spittler et al., 2006; Perraud et al., 2010; Yeh et al., 2015), resulting in the formation of a small number of gas- and particle-phase ON.

Figure C.4 shows the HR-ToF-CIMS mass spectra of particle- and gas-phase ON formed from the NO_3+α-pinene reaction. The $C_{10}H_{15}NO_6I^-$ ion has the highest signal in both gas- and particle-phase measurements of the NO_3+α-pinene system. The $C_{10}H_{15}NO_6I^-$ ion is likely the iodide-adduct of pinonaldehyde-PAN (molecular formula $C_{10}H_{15}NO_6$), a second-generation product of the NO_3+α-pinene reaction (Perraud et al., 2010) (Appendix D, Figure D.5). Although pinonaldehyde may also be formed from α-pinene ozonolysis (Yu et al., 1999), O_3 concentrations in these experiments are very low (< 2 ppb) and the rate constant for the NO_3 reaction is ~10^4 times faster than the O_3 reaction. Therefore, pinonaldehyde and pinonaldehyde-PAN are likely products of the NO_3 reaction. Another PAN-like product observed is norpinonaldehyde-PAN,(Perraud et al., 2010) which is detected as $C_9H_{13}NO_6I^-$ (Figure C.4). Norpinonaldehyde-PAN, which is a third-generation product formed from the NO_3 reaction of norpinonaldehyde (Appendix D, Figure D.5), has low gas- and particle-phase signals and is likely a minor product of the NO_3+α-pinene reaction. Pinonaldehyde and norpinonaldehyde are not polar enough to be detected by our measurement technique. While it is not known whether

pinonaldehyde-PAN and norpinonaldehyde-PAN are present in significant concentrations in the atmosphere, PAN-like species serve as reservoirs and a means of transport for NO_x in the nocturnal atmosphere.(Perraud et al., 2010)

C.3.2 Photochemical aging of β-pinene and α-pinene SOA

These results show that particle-phase ON comprises a significant fraction of SOA from NO_3+β-pinene and NO_3+α-pinene reactions. This gives rise to the question: what are the photochemical fates of these monoterpene SOA and ON during the transition from night to day oxidation environments? To answer this question, the SOA and ON from the NO_3+β-pinene and NO_3+α-pinene reactions were photochemically aged ~2 to 2.5 h after aerosol peak growth has been achieved. For both the β-pinene and α-pinene systems, the SOA become increasingly oxidized during photochemical aging (Appendix D, Figures D.1b and D.2b), likely through a combination of functionalization and fragmentation reactions.(Kroll et al., 2009; Henry and Donahue, 2012) The non-oxidized CH and slightly oxidized CHO1 organic families decrease at significantly faster rates, while the highly oxidized CHOgt1 organic families increase (Figures C.1c and C.1d). These observations are consistent with the increase in bulk aerosol O/C ratio and decrease in H/C ratio, presumably due to OH oxidation via H atom abstraction (Figures C.1e and C.1f).(Kroll et al., 2009)

One striking difference between the β-pinene and α-pinene systems is that their particle-phase ON exhibit different photochemical fates during photochemical aging. The slight decrease in the β-pinene SOA NO_3/Org ratio indicates that the particle-phase ON formed

from the NO_3+β-pinene reaction are generally resilient to photochemical aging (Figure C.1g). Thus, a large fraction of reactive nitrogen is retained in the β-pinene SOA (likely in the form of the nitrate functional group) during photochemical aging in the timescale of our experiments. In contrast, the drastic decrease in the α-pinene SOA NO_3/Org ratio indicates that almost all of particle-phase ON evaporates from the α-pinene SOA during photochemical aging (Figure C.1h). The decrease in the α-pinene SOA NO_3/Org ratio is not due to particle-phase ON volatilization resulting from an increase in chamber temperature (from 24 to 27 °C) caused by heating from the chamber lights. As shown in Figure D.6 (Appendix D), there is negligible change in the α-pinene SOA NO_3/Org ratio when the chamber temperature is increased from 24 to 27 °C under dark conditions (i.e., no photochemical aging). Instead, the decreasing trends are due to fragmentation of particle- and/or gas-phase ON (as a result of photolysis and/or OH reactions) becoming increasingly important during photochemical aging of α-pinene SOA. For instance, fragmentation of particle-phase ON via cleavage of the nitrate functional group from the carbon chain can result in the release of reactive nitrogen back to the gas phase. Moreover, if photolysis and/or OH reactions cause fragmentation of gas-phase ON to form other products, the corresponding particle-phase ON will repartition back to the gas phase to maintain gas-particle equilibrium, leading to an overall decrease in particle-phase ON. Currently, we are not able to separate the effect of OH oxidation from photolysis in this study. More studies are needed to determine the relative contribution of OH oxidation relative to photolysis.

The distinctive trends observed during photochemical aging are likely a result of different ON products formed from the NO_3+β-pinene and NO_3+α-pinene reactions. Firstly, the gas- and particle-phase ON from the NO_3+α-pinene reaction may be photolabile while those from the NO_3+β-pinene reaction are not. Previous studies have shown that photolysis is likely insignificant compared to OH oxidation for ON molecules with more than 4 carbon atoms.(Perring et al., 2013; Roberts and Fajer, 1989) However, these studies were conducted using monofunctional ON while the ON formed in our systems are highly oxygenated multifunctional compounds and contains 10 carbon atoms. The NO_3+α-pinene reaction forms various ON products with a carbonyl group adjacent to the nitrate functional group.(Perraud et al., 2010; Spittler et al., 2006) The close proximity of these two functional groups may enhance light absorption by the carbonyl group during photochemical aging, resulting in ON photolysis to release NO_2.(Perring et al., 2013; Müller et al., 2014) In contrast, the nitrate functional group of ON products from the NO_3+β-pinene reaction is further away from the carbonyl group.(Boyd et al., 2015) The lack of interaction between these two functional groups likely results in negligible light absorption and photolysis of these ON species during photochemical aging. In addition, while ON products from the NO_3+β-pinene reaction may have a hydroxyl group adjacent to the nitrate functional group (Appendix D, Figure D.4), recent work by Romonosky et al. (2015) suggests that the close proximity of these two functional groups does not promote light absorption and photolysis. Nevertheless, further study is needed to determine the role of oxygenated functional groups in the photolysis of multifunctional monoterpene ON. Secondly, the ON products from the NO_3+β-pinene and NO_3+α-pinene reactions may also react with OH at different rates. For example, the highly oxygenated

ON from the NO_3+β-pinene reaction may have fewer H atoms in C-H bonds available for abstraction by OH during photochemical aging, making them more resistant to OH oxidation compared to the less oxygenated ON from the NO_3+α-pinene reaction. Previous studies have investigated the reactivities of small (< C_7) monofunctional ON with OH,(Aschmann et al., 2011; Aschmann et al., 2012) but no systematic study on the reactivities of larger (e.g., C_{10}) multifunctional ON is currently available, and this warrants further study to better understand the photochemical fates of monoterpene ON.

The time series of speciated gas- and particle-phase ON compounds measured by the HR-ToF-CIMS provides more insights into the changes in gas- and particle-phase ON composition during photochemical aging. The decrease in the fraction of particle- and gas-phase C_{10} β-pinene ON is accompanied by increases in the fractions of particle- and gas-phase C_8 and C_9 ON (Figure C.3). This feature highlights the increasing importance of C-C bond cleavage (fragmentation) of gas- and particle-phase ON during photochemical aging of β-pinene SOA. As the NO_3/Org ratio of β-pinene SOA decreases very slightly during photochemical aging (Figure C.1g), this suggests that the nitrate functional group is generally not cleaved off from the carbon chain of particle-phase ON molecules and not released back into the gas phase during these fragmentation reactions.

For the α-pinene SOA, while the HR-ToF-AMS measurements show that the NO_3/Org ratio decreases during photochemical aging (Figure C.1h), only particle-phase ON species with low signals exhibit a decreasing trend (Appendix D, Figure D.7). This suggests that only a subset of gas- and particle-phase ON molecules from the NO_3+α-

pinene reaction are detected by our measurement technique. Alternatively, the instrument's sensitivity to gas- and particle-phase ON molecules from the NO_3+α-pinene reaction may not be uniform as assumed in this study. Nevertheless, the time series of particle- and gas-phase pinonaldehyde-PAN ($C_{10}H_{15}NO_6I^-$ ion) and norpinonaldehyde-PAN ($C_9H_{13}NO_6I^-$ ion) provide insights on how PAN-like species evolve during photochemical aging (Appendix D, Figure D.8). The increase in particle- and gas-phase pinonaldehyde-PAN and norpinonaldehyde-PAN is due to reaction of pinonaldehyde and norpinonaldehyde with OH in the presence of NO_2 (Chan et al., 2010) (Appendix D, Figure D.5). Even though pinonaldehyde-PAN and norpinonaldehyde-PAN are likely photolabile compounds, their formation rates (via OH reaction) may be faster than their photodissociation rates, resulting in the observed increase during photochemical aging. The decrease of particle- and gas-phase pinonaldehyde-PAN during the later stages of photochemical aging is likely due to reaction to form higher generation products.

C.4 Implications

This work provides direct evidence for the formation of highly oxygenated gas- and particle-phase ON from NO_3+BVOC chemistry. The rapid formation of these highly oxygenated ON is consistent with the fast autoxidation mechanism, which could play a significant role in influencing nighttime SOA and ON composition. Previous studies on the OH and O_3 reaction of BVOCs have also reported the formation of highly oxygenated organic species via autoxidation.(Ehn et al., 2014; Jokinen et al., 2015) Therefore, the role of autoxidation in the oxidation of different BVOCs under different reaction conditions warrants further study.

One of the largest uncertainties regarding the impact of gas- and particle-phase ON on NO_x and O_3 budgets is the extent to which these ON species serve as permanent vs. temporary NO_x sinks.(Browne and Cohen, 2012) Studies have shown that the modeling of O_3 production is sensitive to the assumptions made regarding the recycling of NO_x from ON species, and may result in an over- or under-prediction of surface O_3.(Perring et al., 2013) The photochemical fates of particle-phase ON from NO_3+β-pinene and NO_3+α-pinene reactions during the transition from night to day oxidation environments are investigated in this study to provide insights into the extent to which these ON species act as permanent or temporary NO_x sinks in monoterpene-rich areas. A large fraction of reactive nitrogen is released in the form of NO_2 from the α-pinene SOA back into the gas phase during photochemical aging. Therefore, this study suggests that particle-phase ON from NO_3+α-pinene chemistry serve as temporary NO_x sinks since NO_2 is released back into the atmosphere by photolysis and/or oxidation during the night-to-day transition. In contrast to the α-pinene system, reactive nitrogen is generally retained in the β-pinene SOA during photochemical aging in the timescale of these experiments. Therefore, these results suggest that particle-phase ON from NO_3+β-pinene chemistry serve as permanent NO_x sinks in the atmosphere. These results have significant implications for NO_x and O_3 budgets in areas with high monoterpene emissions, such as the Southeastern United States.(Xu et al., 2015c) Based on ambient measurements obtained in summer 2013 and 2014 as part of the Southern Oxidant and Aerosol Study (SOAS) and Southeastern Center of Air Pollution and Epidemiology study (SCAPE),(Xu et al., 2015c; Xu et al., 2015a) the fractional loss of NO_x to gas- and particle-phase ON formation from NO_3+BVOC is estimated to be substantial in the Southeastern United States, ~99 % and ~80 % at a rural

and urban site, respectively (Appendix D, Sections D.3 and D.4). Particle-phase ON from NO_3+β-pinene chemistry comprise ~16 % and ~13 % of the total summer nighttime NO_x loss in rural and urban sites in the Southeastern United States, respectively. The omission of terpene ON in current models could contribute to the overestimation of surface O_3 in the Southeastern United States.(Fiore et al., 2009; Mao et al., 2013) Since these results show that particle-phase β-pinene ON from NO_3 chemistry can serve as permanent NO_x sinks at rural and urban sites in the Southeastern United States, implementing these findings into current modeling frameworks will lead to improved O_3 simulations in this region. More generally, these results underscore the importance of accurate treatment of nighttime NO_3+BVOC chemistry and the fates of ON species in models for improving regional and global simulations of NO_x budget, ozone and SOA formation.

This study lays the foundation for understanding how the transition from night to day oxidation environments impacts the fates of nighttime monoterpene SOA and ON from NO_3 chemistry. The observations of α-pinene and β-pinene particle-phase ON having drastically different photochemical fates demonstrate that results obtained for specific BVOC systems cannot be generalized to all BVOCs present in the atmosphere. The transition from day to night oxidation environments likely changes the composition of biogenic SOA and ON as well. Therefore, this study highlights the need to conduct systematic studies on other BVOC systems to not only understand nighttime and daytime SOA and ON formation alone, but also how their compositions change over their entire diurnal lifecycle in order to better model SOA and ON chemistry for more accurate predictions of NO_x and O_3 budgets.

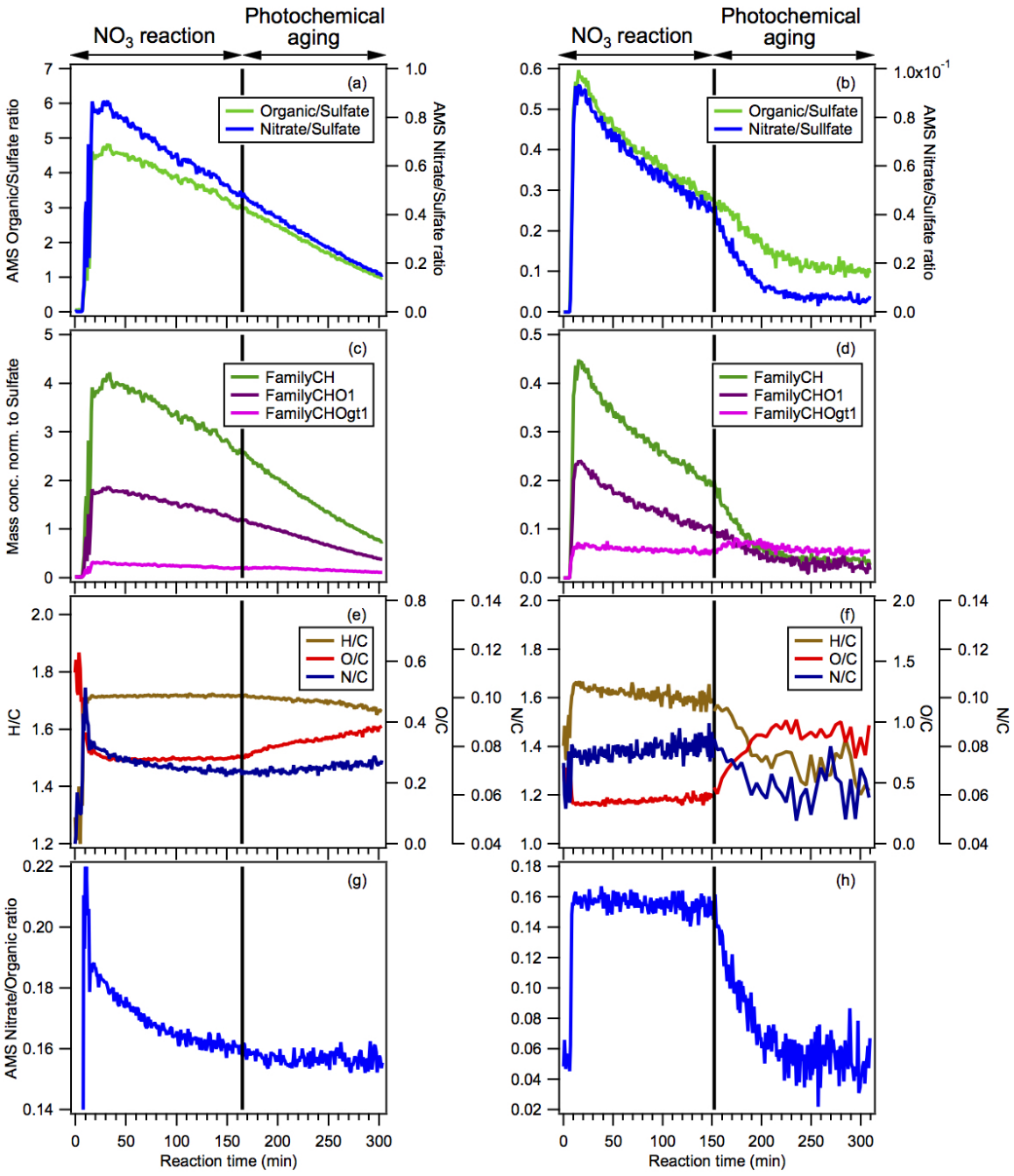

Figure C.1: HR-ToF-AMS measurements of the β-pinene (panels a, c, e and g) and α-pinene (panels b, d, f and h) reactions. Panels (a) and (b): Time series of AMS organic and nitrate mass concentrations normalized to the sulfate mass concentration of the SOA. Panels (c) and (d): Time series of major AMS organic families (CH, CHO1 and CHOgt1) normalized to the sulfate mass concentration of the SOA. Panels (e) and (f): Time series of H/C, O/C and N/C ratios of the SOA. Panels (g) and (h): Time series of AMS nitrate mass concentration normalized to the organic mass concentration of the SOA. The β-pinene and α-pinene SOA are photochemically aged at reaction time = 165 min (indicated by the black lines in panels a, c, e and g) and 152 min (indicated by the black lines in

panels b, d, f and h), respectively. In panel (f), the H/C, O/C and N/C ratios shown after reaction time = 152 min are 5 min-averaged values, since the data is noisy due to low α-pinene SOA mass loadings during photochemical aging.

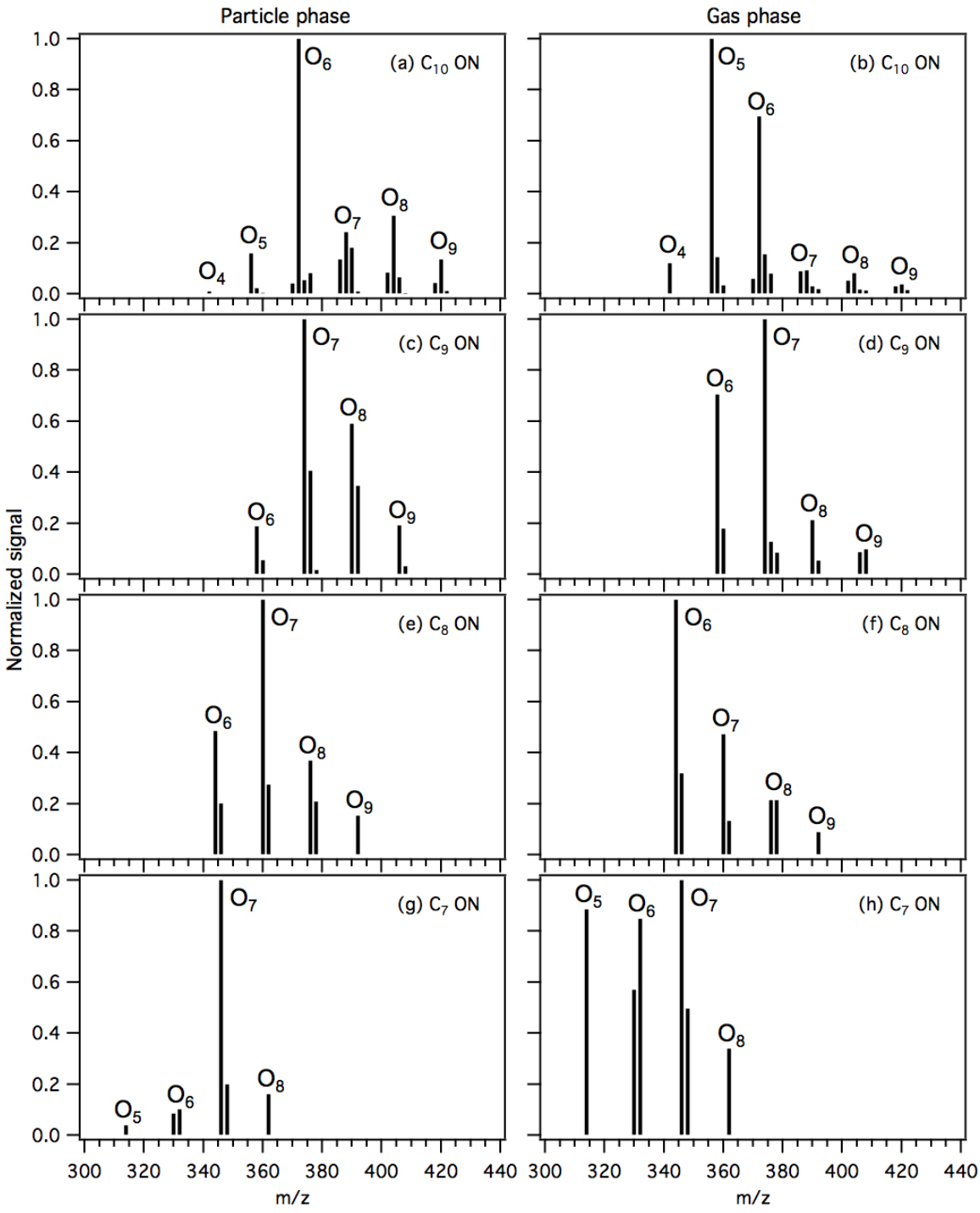

Figure C.2: HR-ToF-CIMS mass spectra of particle- and gas-phase ON formed during NO_3+β-pinene reaction. Panels (a), (c), (e) and (g) show the mass spectra of particle-phase C_{10}, C_9, C_8 and C_7 ON, respectively. Panels (b), (d), (f) and (h) show the mass spectra of gas-phase C_{10}, C_9, C_8 and C_7 ON, respectively. The m/z of the ON species include the mass of the I^- ion, i.e., *m/z* = 126.905. Also shown is the number of oxygen

atoms that these ON species have. All the signals in each panel are normalized to the ON species with the highest signal within the panel.

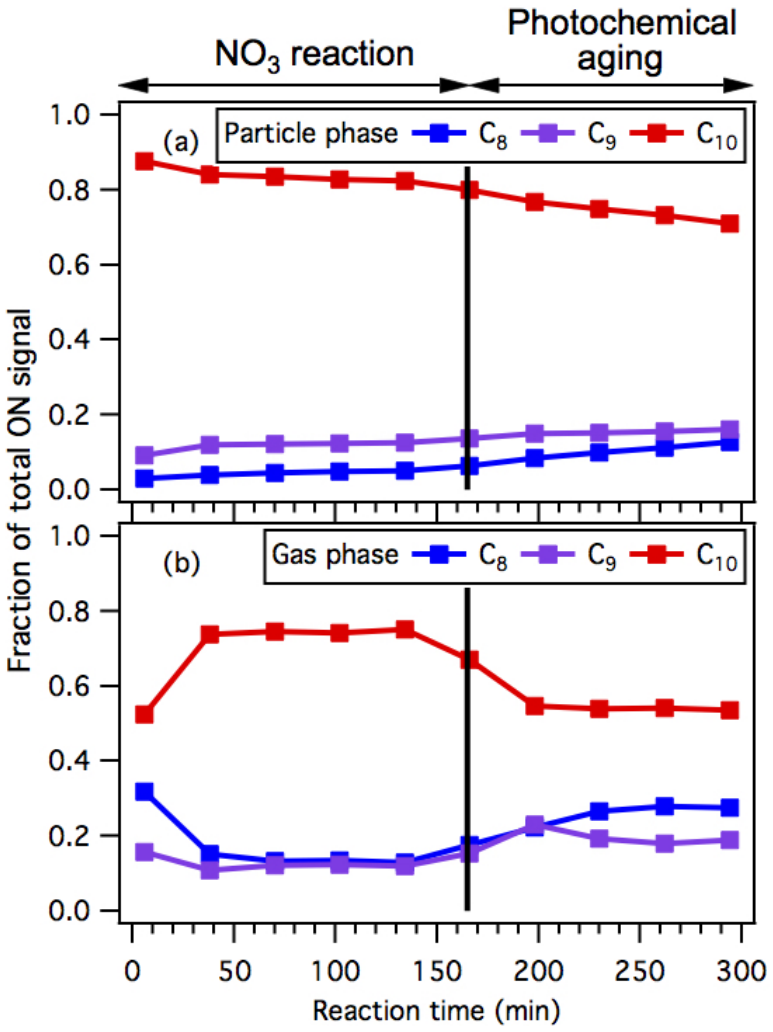

Figure C.3: ON molecules, formed from the NO_3+β-pinene reaction, grouped by their number of carbon atoms. Time series of the fraction of (a) particle-phase, and (b) gas-phase C_8, C_9 and C_{10} ON to total ON. The SOA is photochemically aged at reaction time = 165 min (indicated by the black lines in the four panels).

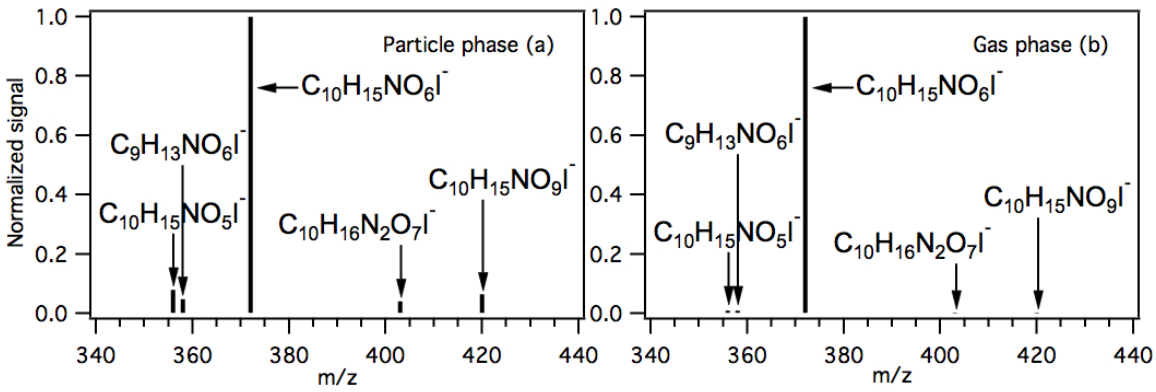

Figure C.4: HR-ToF-CIMS mass spectra of (a) particle-phase, and (b) gas-phase ON formed during NO_3+α-pinene reaction. The *m/z* of the ON species include the mass of the I^- ion, i.e., *m/z* = 126.905. The signals in panels (a) and (b) are all normalized by the signal of $C_{10}H_{15}NO_6I^-$, which is the species with the highest signal.

APPENDIX D

SUPPLEMENTARY INFORMATION TO APPENDIX C

D.1 Operation of the FIGAERO-HR-ToF-CIMS

A Filter Inlet for Gases and AEROsols (FIGAERO, Aerodyne Research Inc.) coupled to a High-Resolution Time-of-Flight Chemical Ionization Mass Spectrometer (HR-ToF-CIMS, Aerodyne Research Inc.) is used to characterize the molecular composition of the gas- and particle-phase ON products. Detailed descriptions of the FIGAERO and HR-ToF-CIMS can be found elsewhere.(Bertram et al., 2011; Lopez-Hilfiker et al., 2014) The reagent ion employed in our HR-ToF-CIMS system is the Iodide (I^-) ion. Previous studies have shown that I^- is sensitive to various polar oxygenated compounds and ON.(Huey, 2007; Aljawhary et al., 2013; Lee et al., 2014; Boyd et al., 2015) The ionization depends on the ability of I^- to hydrogen bond stably with the oxygenated and nitrate functional groups of these compounds to form molecule-iodide adducts. I^- ions are generated by flowing 5 L min^{-1} of dry ultrahigh purity (UHP) N_2 through a permeation tube containing methyl iodide, then through a ^{210}Po radioactive source (NRD, P-2021) into the ion-molecule reaction (IMR) region of the HR-ToF-CIMS. Gas-phase species are drawn from the chamber at ~ 2 L min^{-1} through perfluorotetrafluoroethylene (PTFE) tubing into the FIGAERO unit for gas-phase measurements. To avoid depletion of the I^- reagent ion during the ionization process, the gas-phase sample flow is diluted to a ~ 1:8 ratio using UHP N_2. Particles are drawn from the chamber at ~14 L min^{-1} through a stainless steel tube onto a PTFE filter (Pall Corp, Zefluor 25 mm, 1 μm pore-size) in the FIGAERO unit for particle-phase measurements. Particles are collected on the PTFE

filter for 12 and 8 min during gas-phase measurements in the α-pinene and β-pinene experiments, respectively. The collected particles are then thermally desorbed in UHP N_2, which is delivered at 3 L min^{-1} across the PTFE filter. During the thermal desorption process, the UHP N_2 is gradually heated at 30 °C min^{-1} from 25 to 200 °C, and then held at 200 °C for ~10 min to allow signals to return to their preheating levels. Background particle-phase measurements are also conducted by placing a particle filter (PALL Life Sciences, 12144 Capsule) immediately upstream of the FIGAERO unit to account for gas adsorption and absorption onto the Teflon filter and within the HR-ToF-CIMS IMR region. Results presented here have been normalized to the reagent ion signal and background subtracted.

Only FIGAERO-HR-ToF-CIMS measurements of ON products formed during the α-pinene and β-pinene reactions are presented in this study. Since standards for the ON products are not available, the HR-ToF-CIMS is not calibrated for these compounds and their concentrations are not quantified. Here we assume that the I^- ionization sensitivity is similar for all the ON products detected. While this assumption is likely over-simplified (Lee et al., 2014; Lopez-Hilfiker et al., 2014; Lopez-Hilfiker et al., 2015), it allows us to gain qualitative insights into the reaction mechanisms based on the identification of these products (via their molecular formulas) and how their signals change during the reaction. Previous work by Lee et al. (2014) suggested that monoalcohols and monocarbonyls may not be detected by I^- ionization due to their weak polarity and hydrogen bonding. Particle-phase organic species with very low vapor pressures (e.g., oligomer-like

compounds and sulfated organic nitrates) also may not be detected due to thermal decomposition upon heating (Lopez-Hilfiker et al., 2015). Therefore, we cannot rule out the possibility that the detected ON products in this study are only a subset of products formed during the reaction. It is also important to note that while the HR-ToF-CIMS allows for the determination of the products' molecular formula, it does not provide information on their molecular structures.

D.2 SOA Mass Yield Calculations

In both the NO_3+β-pinene and NO_3+α-pinene experiments, aerosol peak growth occurs within 15 to 20 min of the start of the reaction. All aerosol growth data are corrected for particle wall loss by applying size-dependent first order loss coefficients, which are determined from separate seed-only experiments. After correcting for particle wall loss, the peak aerosol mass concentration is obtained by multiplying the corrected aerosol volume concentration by the aerosol density. The aerosol density is calculated from the ratio of the vacuum aerodynamic diameter (measured by the HR-ToF-AMS) and the mobility diameter (measured by the SMPS) of aerosol generated during nucleation experiments.(DeCarlo et al., 2004; Bahreini et al., 2005) The densities of the β-pinene and α-pinene SOA are 1.43 and 1.46 g cm^{-3}, respectively. The density of β-pinene SOA measured in this study is within the range of densities measured previously by Boyd et al. (2015) (1.41-1.61 g cm^{-3}). The aerosol mass yield (Y) is obtained by dividing the peak aerosol mass concentration (ΔM_0) by the reacted hydrocarbon mass concentration (ΔHC), $Y= \Delta M_0/\Delta HC$ (Odum et al., 1996; Bowman et al., 1997; Odum et al., 1997b; Odum et al., 1997a).

D.3 NO_x Loss Estimation

To estimate the fraction of summer nighttime NO_x loss attributable to particle-phase ON from nighttime NO_3+β-pinene chemistry in rural Southeastern U.S., we used ambient nighttime NO_x, O_3 and BVOCs measurements obtained during the Southern Oxidant and Aerosol Study (SOAS) field campaign conducted from June to July 2013 at the Centreville ground site in rural Alabama. (Xu et al., 2015c) previously showed that the average nighttime O_3, NO_2 and NO_3 concentrations at SOAS are 21 ppb, 0.54 ppb and 7.6×10^{-2} ppt, respectively. The authors also estimated that the lifetime of NO_3 with respect to reaction with BVOCs was 8 s, indicating the high reactivity of NO_3 at SOAS. In contrast, the lifetimes of N_2O_5 with respect to heterogeneous uptake onto aqueous particles and homogeneous reaction with H_2O are 1900 s and 1.2×10^{10} s, respectively.

Due to the high reactivity of NO_3 at SOAS (i.e., 8 s), we assume (as Xu et al. (2015c) previously had) that NO_3 is at steady state at SOAS. This allows us to calculate the nighttime NO_x lifetime with respect to (gas- and particle-phase) ON and nitric acid (HNO_3) formation at SOAS using Eq. (D.1) and (D.2), respectively. The use of these equations in a steady-state model to describe the effects of biogenic ON chemistry on the NO_x lifetime is previously discussed in detail by Browne and Cohen (2012) Since nighttime OH concentrations at SOAS are currently not known, for simplicity, we assume that it is zero here. We test how our calculated values change at different OH concentrations in the Sensitivity Test section (Appendix D).

$$t_{NO_x \rightarrow ON} = \frac{[NO_2]+[NO_3]+2\cdot[N_2O_5]}{b_{isoprene}k_{NO_3+isoprene}[NO_3][\text{isoprene}]+b_{a\text{-}pinene}k_{NO_3+a\text{-pinene}}[NO_3][a\text{-pinene}]+b_{b\text{-}pinene}k_{NO_3+b\text{-pinene}}[NO_3][b\text{-pinene}]} \quad \text{(D.1)}$$

$$t_{NO_x \rightarrow HNO_3} = \frac{[NO_2]+[NO_3]+2\cdot[N_2O_5]}{2k_{N_2O_5\ \text{het. ydrolysis}}[N_2O_5]+2k_{N_2O_5\ \text{hom. hydrolysis}}[N_2O_5]+k_{NO_3+propanal}[NO_3][\text{propanal}]+_{NO_3+propanal}[NO_3][\text{n-butanal}]} \quad \text{(D.2)}$$

We estimate that the average N_2O_5 concentration at SOAS is 2.98×10^{-2} ppt using the concentrations of NO_2 and NO_3 and $k_{eq} = 2.9\times10^{-11}$ cm^3 $molec.^{-1}$ s^{-1} (from JPL kinetics (Sander, 2011) at 25 °C). Since isoprene (1.92 ppb), α-pinene (0.35 ppb) and β-pinene (0.32 ppb) are the most dominant BVOCs at SOAS,(Xu et al., 2015c) only these three BVOCs are included in the calculation of NO_x lifetime at night with respect to ON formation in Eq. (D.1). Similar to Browne et al.,(Browne and Cohen, 2012) we use the parameter β to denote the fraction of ON that retains the nitrate functionality during NO_3 reaction in Eq. (D.1). Here, we assign β values of 70 %, 20 % and 45 % for isoprene, α-pinene and β-pinene, respectively, based on previous measurements by Rollins et al. (2009), Hallquist et al. (1999), Fry et al. (2009), respectively. The only aldehydes we considered in Eq. (D.2) are n-butanal (0.024 ppb) and propanal (0.08 ppb) since these are the only available aldehyde concentrations measured at SOAS in the current literature (Xu et al., 2015c). The heterogeneous and homogeneous N_2O_5 rate constants used in Eq. (D.2) are 5.3×10^{-4} s^{-1} and 8.3×10^{-11} s^{-1}, respectively, which are derived from their SOAS lifetime calculations by Xu et al. (2015c).

From Eq. (D.1) and (D.2), we estimate the NO_x lifetimes at night with respect to the formation of ON and HNO_3 at SOAS to be ~46 h and ~4547 h, respectively. As a result, the fractional loss of NO_x to ON (from NO_3+isoprene, NO_3+α-pinene and NO_3+β-pinene chemistry) is estimated to be ~99 % at SOAS. In addition, we estimate that the fractional loss of NO_x to gas- and particle-phase ON from NO_3+β-pinene chemistry at SOAS is ~21

%. Fry et al. (2014) previously measured that 76 % of the total gas- and particle-phase ON from NO_3+β-pinene chemistry is in the particle phase. Therefore, the loss of NO_x to particle-phase ON from NO_3+β-pinene chemistry at SOAS is ~16 %.

To compare the fraction of summertime nighttime NO_x loss attributable to particle-phase ON from nighttime NO_3+β-pinene chemistry in rural Southeastern U.S. to that in urban Southeastern U.S., we used the average ambient nighttime NO_2 (14.4 ppb) and O_3 (21 ppb) concentrations reported in Xu et al. (2015a) in Aug 2014 during the Southeastern Center of Air Pollution and Epidemiology study (SCAPE, EPA Clean Air Center) at the Jefferson Street (JST) site in downtown Atlanta. Since BVOC concentrations are not measured at the JST site, we assume that all the BVOC concentrations at JST are similar to those at SOAS (Xu et al., 2015c) (i.e., the concentrations of isoprene, α-pinene, β-pinene, propanal and n-butanal at JST are 1.92, 0.35, 0.32 ppb, 0.08 ppb and 0.024 ppb, respectively). We also assume that the NO_3 lifetime to reaction with BVOCs at JST is similar to that at SOAS (i.e., 8 s) and that NO_3 is at steady state at JST. For simplicity, we assume that the ambient water concentration at JST is the same as SOAS, and that therefore, the lifetime of N_2O_5 with respect to homogeneous reaction with H_2O at JST is the same as that at SOAS (i.e., 1.2×10^{10} s) (Xu et al., 2015c). For the lifetime of N_2O_5 with respect to heterogeneous uptake onto aqueous particles, we assume that the aerosol surface area concentration at JST is 200 $\mu m^2\ cm^{-3}$, similar to that measured by Xu et al. (2015c) in rural Alabama during the SOAS field campaign. Since we assume that the aerosol surface area concentration at JST is similar to that at SOAS (i.e., 200 $\mu m^2\ cm^{-3}$), the lifetime of N_2O_5 with respect to heterogeneous uptake onto aqueous particles at JST is similar to that at SOAS (i.e., 1900 s). Using the concentrations of O_3 and NO_2 at JST and

k_{NO2+O3} = 3.52×10^{-17} cm^3 $molec.^{-1}$ s^{-1} (Saunders et al., 2003b), we estimate the NO_3 concentration at JST to be 2.03×10^{-3} ppb. We estimate the average N_2O_5 concentration at JST to be 2.12×10^{-2} ppb using the concentrations of NO_2 and NO_3 and $k_{eq} = 2.9\times10^{-11}$ cm^3 $molec.^{-1}$ s^{-1} (from JPL kinetics (Sander, 2011) at 25 °C).

Using Eq. (D.1) and (D.2), we estimate the NO_x lifetimes at night with respect to the formation of ON and HNO_3 at JST to be ~46 h and ~178 h, respectively. As a result, the fractional loss of NO_x to ON (from NO_3+isoprene, NO_3+α-pinene and NO_3+β-pinene chemistry) is estimated to be ~80 % at JST. In addition, we estimate that the fractional loss of NO_x to gas- and particle-phase ON from NO_3+β-pinene chemistry at JST is ~17 %. Therefore, the loss of NO_x to particle-phase ON from NO_3+β-pinene chemistry at JST is ~13 %.

D.4 Sensitivity Test

We calculate how the nighttime NO_x lifetime with respect to nitric acid (HNO_3) formation at SOAS and JST changes when different assumptions of the OH concentrations are used (1×10^3, 1×10^4, 1×10^5 molec. cm^{-3}). Instead of using Eq. (D.2), we use Eq. (D.3), which accounts for the reaction of OH with NO_2 to form nitric acid, to calculate the nighttime NO_x lifetime with respect to nitric acid (HNO_3) formation at SOAS and JST. As shown below, a substantial fraction of NO_x is lost to ON formation regardless of the assumed OH concentrations.

$$t_{NO_x \rightarrow HNO_3} = \frac{[NO_2]+[NO_3]+2\cdot[N_2O_5]}{2k_{N_2O_5\ \text{het. ydrolysis}}[N_2O_5]+2k_{N_2O_5\ \text{hom. hydrolysis}}[N_2O_5]+k_{NO_3+propanal}[NO_3][\text{propanal}]+_{NO_3+propanal}[NO_3][\text{n-butanal}]+k_{NO_2+OH}[NO_2][OH]} \quad \text{(D. 3)}$$

When the OH concentration at SOAS is assumed to be 1×10^{3}, 1×10^{4}, and 1×10^{5} molec. cm^{-3}, the fractional loss of NO_x to ON (from NO_3+isoprene, NO_3+α-pinene and NO_3+β-pinene chemistry) are ~99 %, ~97 % and 79 %, respectively. Correspondingly, the fractional loss of NO_x to gas- and particle-phase ON from NO_3+β-pinene chemistry are ~21 %, ~20 % and ~16 %, respectively. The fractional loss of NO_x to particle-phase ON from NO_3+β-pinene chemistry are then ~16 %, ~15 % and ~12 %, respectively.

When the OH concentration at JST is assumed to be 1×10^{3}, 1×10^{4}, and 1×10^{5} molec. cm^{-3}, the fractional loss of NO_x to ON (from NO_3+isoprene, NO_3+α-pinene and NO_3+β-pinene chemistry) are ~80 %, ~78 % and ~66 %, respectively. Correspondingly, the fractional loss of NO_x to gas- and particle-phase ON from NO_3+β-pinene chemistry are ~17 %, ~16 % and ~14 %, respectively. The fractional loss of NO_x to particle-phase ON from NO_3+β-pinene chemistry are then ~13 %, ~12 % and ~10 %, respectively.

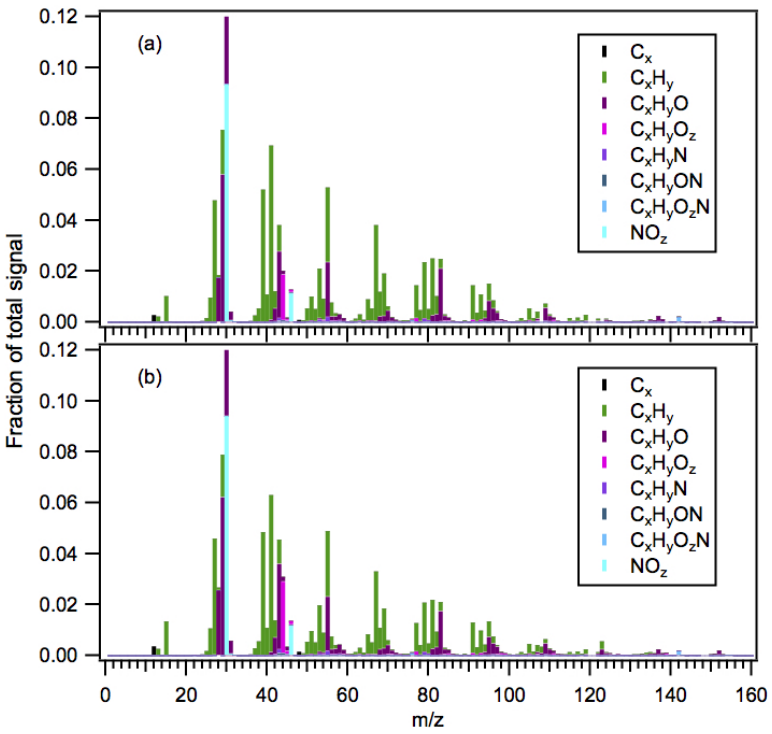

Figure D.1: HR-ToF-AMS mass spectra of SOA formed during (a) NO_3+β-pinene reaction, and (b) subsequent photochemical aging. Both mass spectra are colored by the ion type to indicate the contribution of each ion type to the mass spectra. Only ions up to *m/z* 160 are shown as signals beyond *m/z* 160 are minimal. In the NO_3+β-pinene SOA mass spectrum (panel a), *m/z* 67 ($C_5H_7^+$) and *m/z* 91 ($C_7H_7^+$) have relatively large signals. As suggested previously by Boyd et al.,(Boyd et al., 2015) these two ions can potentially be used as indicators for SOA formed from monoterpene oxidation. Panel b shows that the CO_2^+ ion signal (*m/z* 44) in the β-pinene SOA mass spectrum increases during photochemical aging, consistent with previous aerosol aging studies.(Kroll et al., 2009) The CO_2^+ fragment ion arises from the thermal decomposition of carboxylic acid in the HR-ToF-AMS,(Duplissy et al., 2011) and is typically used to infer aerosol aging.(Ng et al., 2011)

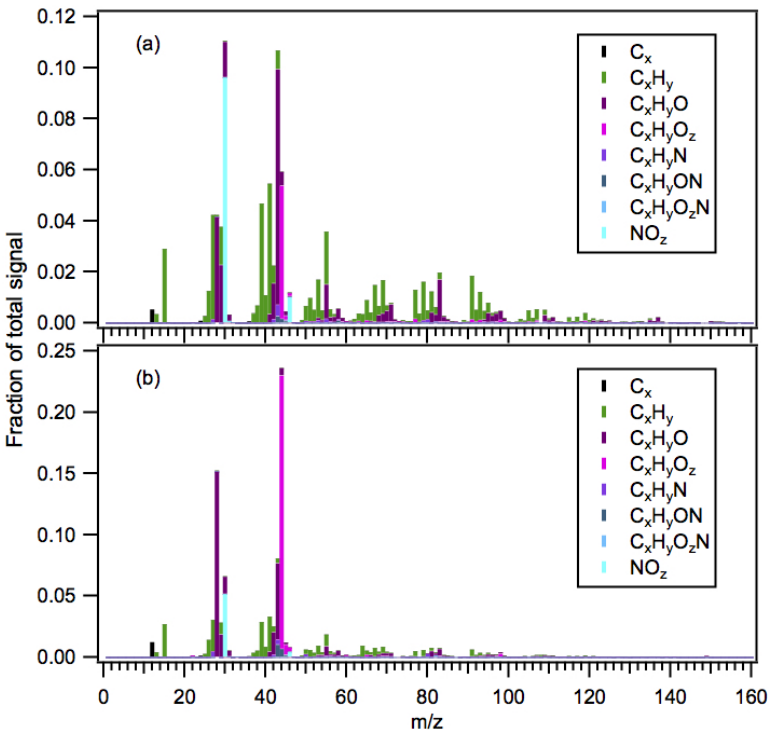

Figure D.2: HR-ToF-AMS mass spectra of SOA formed during (a) NO_3+α-pinene reaction, and (b) subsequent photochemical aging. Both mass spectra are colored by the ion type to indicate the contribution of each ion type to the mass spectra. Only ions up to *m/z* 160 are shown as signals beyond *m/z* 160 are minimal. In the NO_3+α-pinene SOA mass spectrum (panel a), *m/z* 67 ($C_5H_7^+$) has a small ion signal while *m/z* 91 ($C_7H_7^+$) has a relatively large signal. Panel b shows that the CO_2^+ ion signal (*m/z* 44) in the α-pinene SOA mass spectrum increases during photochemical aging.

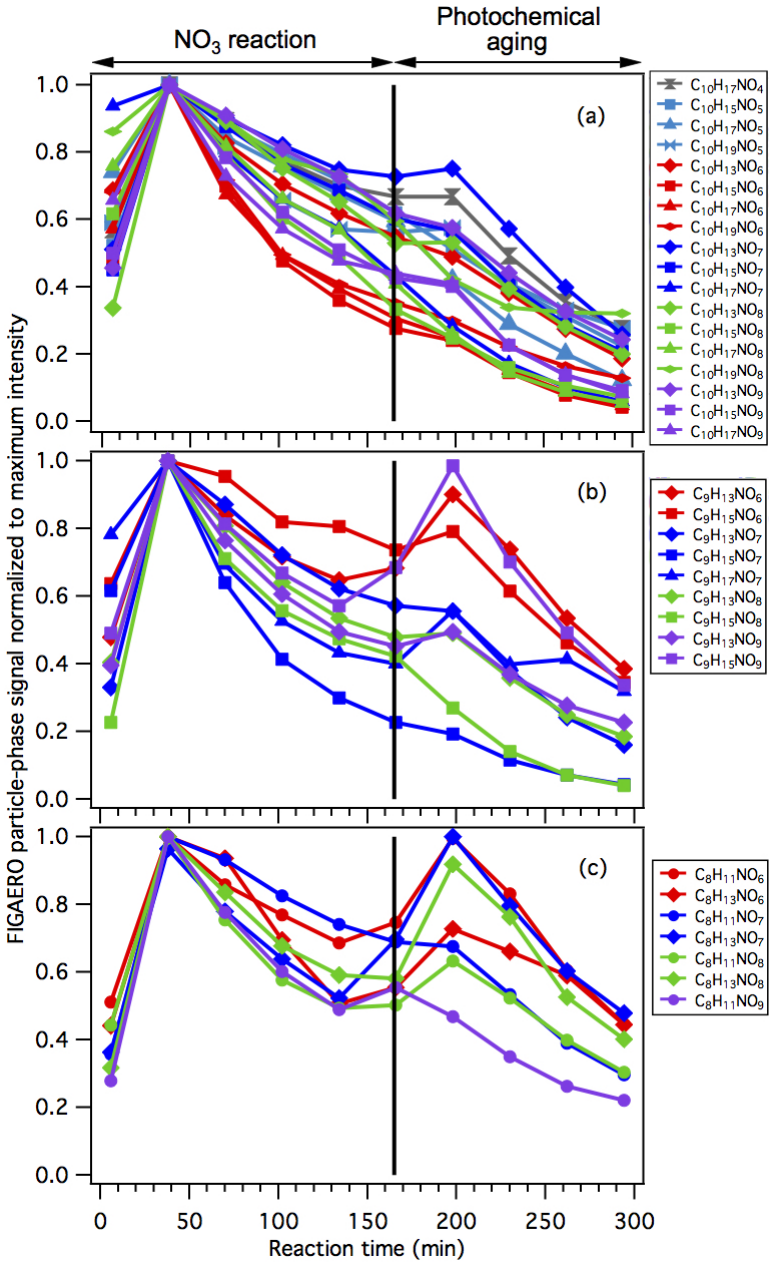

Figure D.3: Time series of particle-phase (a) C_{10}, (b) C_9 and (c) C_8 ON during the β-pinene reaction. These highly oxygenated ON species are detected within 6 min of the start of the NO_3 reaction. The SOA is photochemically aged at reaction time = 165 min (indicated by the black lines in the three panels).

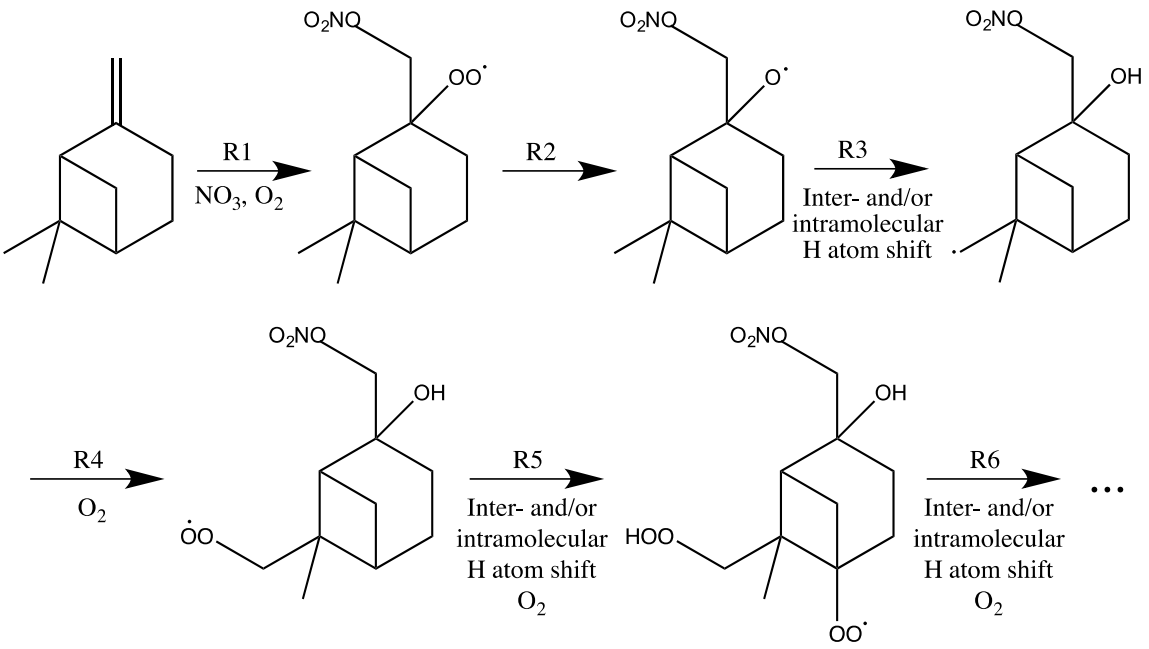

Figure D.4: A simplified reaction mechanism showing some of the possible reaction pathways that form highly oxygenated gas- and particle-phase C_{10} ON in the NO_3+β-pinene reaction. The NO_3+β-pinene reaction is initiated predominantly by NO_3 addition to the less substituted carbon of the C=C double bond to form tertiary peroxy radicals in the presence of O_2 (R1).(Boyd et al., 2015; Wayne et al., 1991) Reaction of the tertiary peroxy radical produces a tertiary alkoxy radical (R2),(Atkinson and Arey, 2003a) which can undergo a hydrogen atom shift to form an alkyl radical (R3).(Carter et al., 1976; Eberhard et al., 1995; Atkinson, 1997a; Dibble, 2001; Vereecken and Peeters, 2010; Vereecken and Francisco, 2012) Subsequent O_2 addition to the alkyl radical site forms a new peroxy radical (R4), which can undergo further reaction via inter- and/or intramolecular H atom abstraction followed by O_2 addition (i.e., autoxidation) to form highly oxygenated gas- and particle-phase C_{10} ON (R5, 6 and so forth).(Ehn et al., 2014; Jokinen et al., 2014; Rissanen et al., 2015; Mentel et al., 2015; Crounse et al., 2013) It should be noted that the peroxy radicals formed in step R1 can also undergo autoxidation in addition to forming alkoxy radicals. Alkoxy radicals formed via peroxy radical reaction can also dissociate via C-C bond scission(Atkinson, 1997a) before undergoing autoxidation to form highly oxygenated gas- and particle-phase C_7, C_8 and C_9 ON. A detailed reaction mechanism showing the formation of C_{10} ON with 4 to 6 oxygen atoms has been shown previously by Boyd et al. (2015).

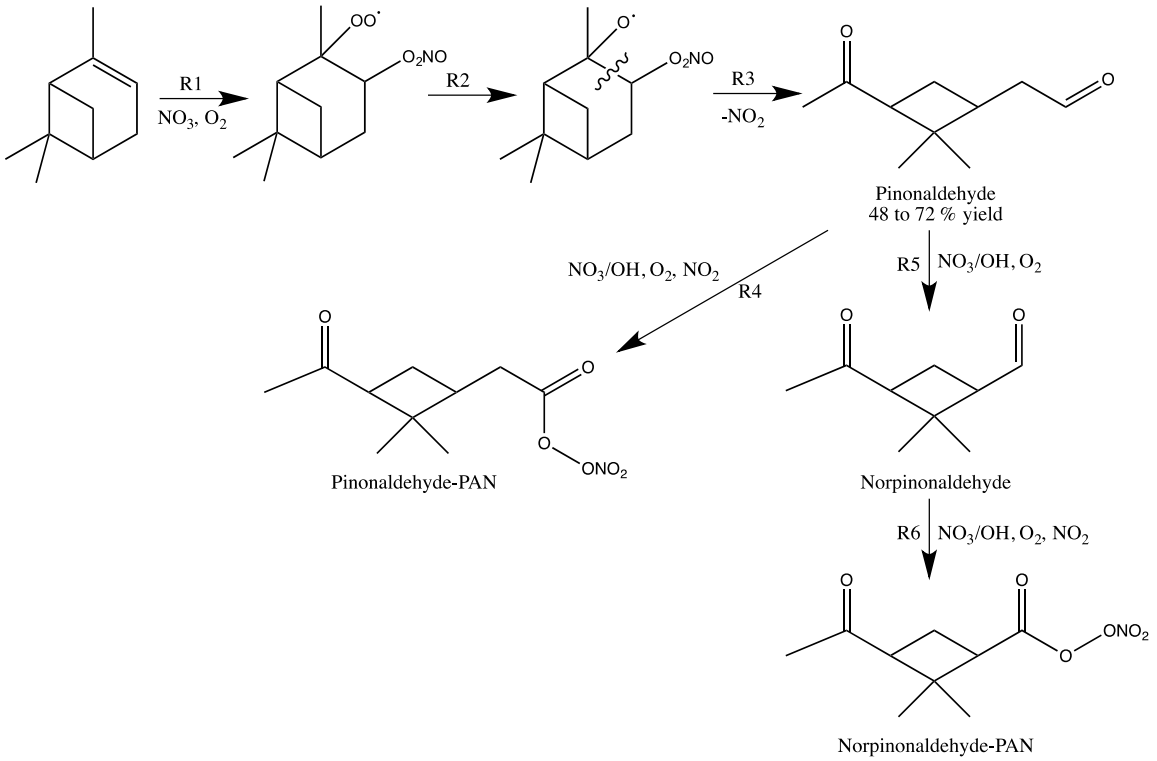

Figure D.5: Partial reaction mechanism for the NO_3+α-pinene reaction to form pinonaldehyde (major first generation product), norpinonaldehyde, pinonaldehyde-PAN and norpinonaldehyde-PAN. Detailed reaction mechanisms can be found in Perraud et al. (2010) and Spittler et al. (2006). Note that pinonaldehyde-PAN, norpinonaldehyde and norpinonaldehyde-PAN can also be formed during photochemical aging via H abstraction of the aldehydic H radicals (Chan et al., 2010).

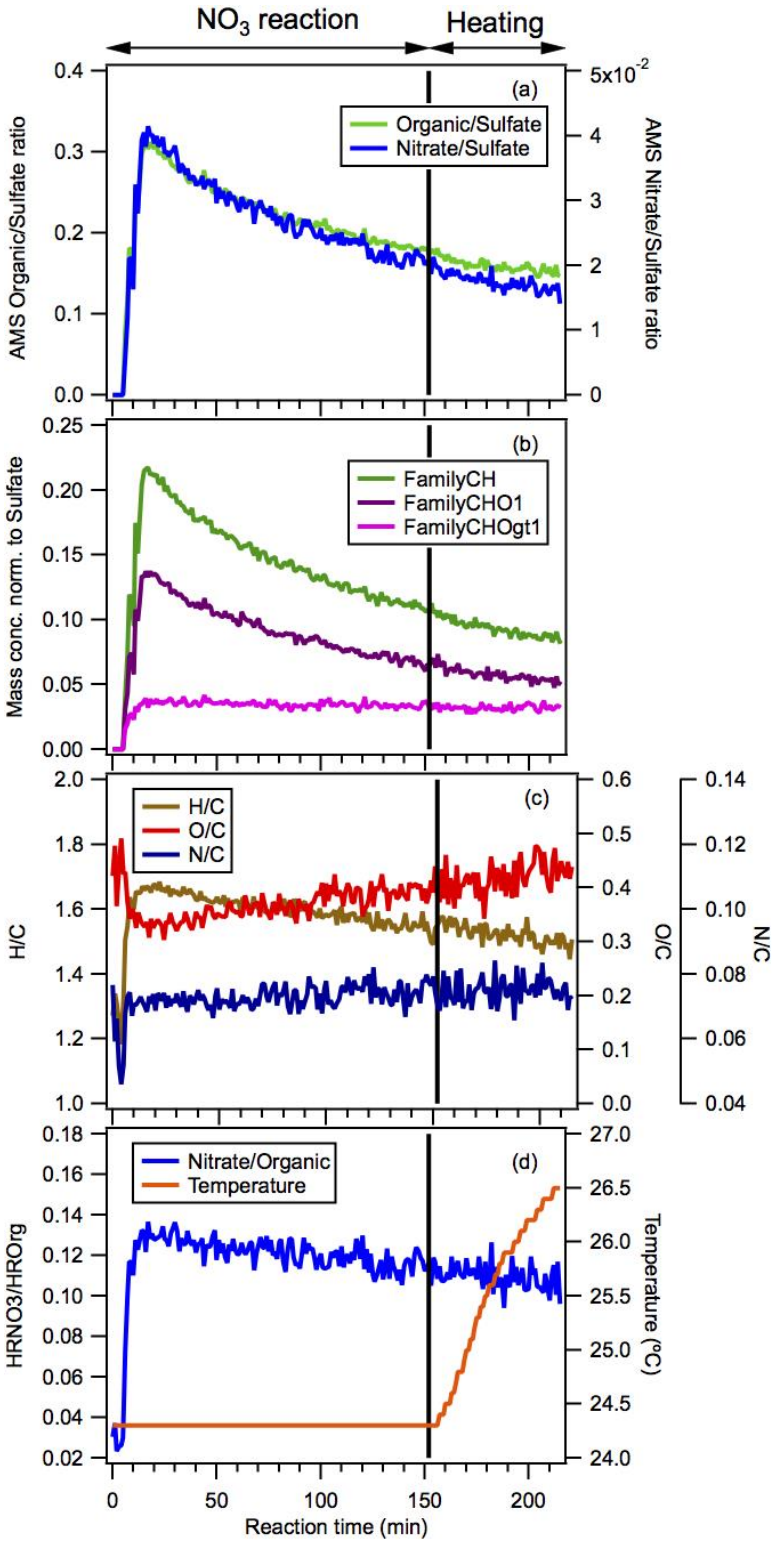

Figure D.6: HR-ToF-AMS measurements of the α-pinene reaction. Panel (a): Time series of AMS organic and nitrate mass concentrations normalized to the sulfate mass concentration of the SOA. Panel (b): Time series of major AMS organic families (CH,

CHO1 and CHOgt1) normalized to the sulfate mass concentration of the SOA. Panel (c): Time series of H/C, O/C and N/C ratios of the SOA. The nitrate functional group is included in the calculation of N/C ratios. Panel (d): Time series of AMS nitrate mass concentration normalized to the organic mass concentration of the SOA. Also shown in panel (d) is the temperature profile of the chamber reactor. The α-pinene SOA is heated at reaction time = 152 min (indicated by the black lines in panels a-d) under dark conditions.

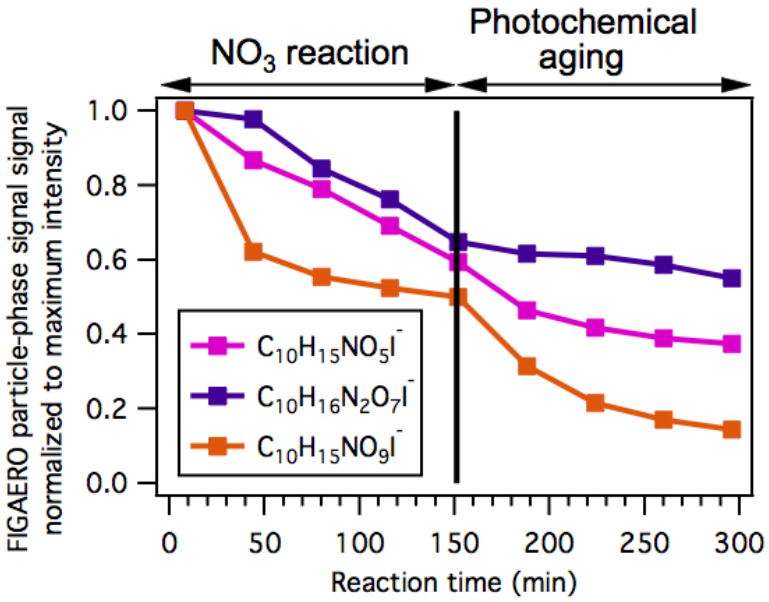

Figure D.7: Time series of particle-phase $C_{10}H_{15}NO_5I^-$, $C_{10}H_{16}N_2O_7I^-$, $C_{10}H_{15}NO_9I^-$ ions during the α-pinene reaction. The SOA is photochemically aged at reaction time = 152 min (indicated by the black lines in the panel).

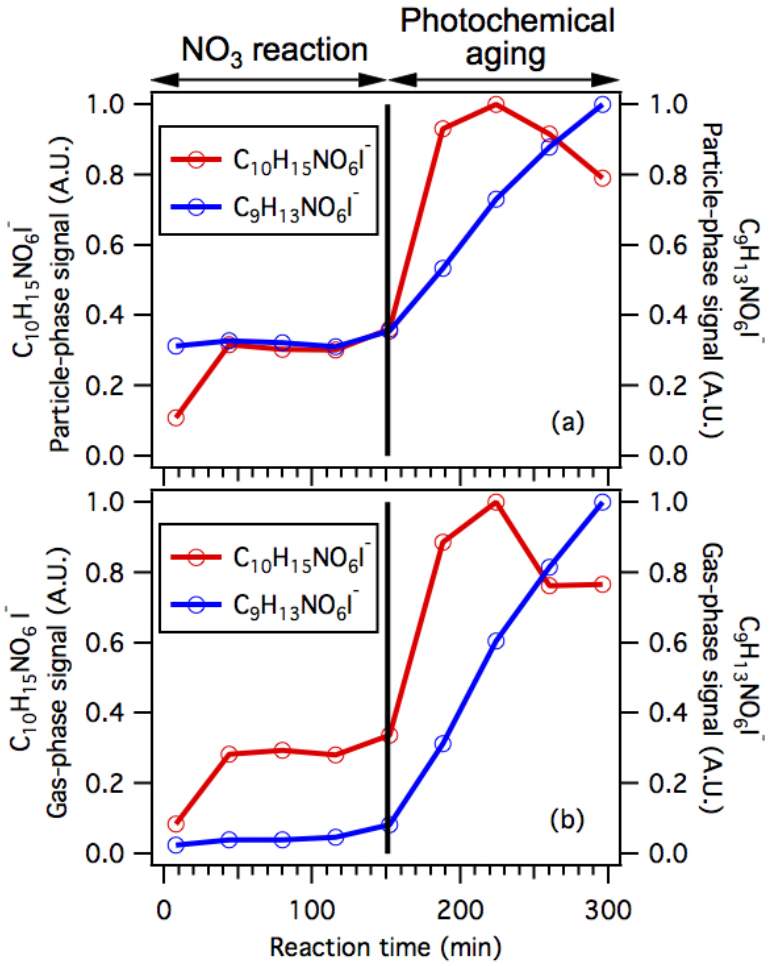

Figure D.8: Time series of (a) particle-phase and (b) gas-phase $C_9H_{13}NO_6I^-$ and $C_{10}H_{15}NO_6I^-$ ions during the α-pinene reaction. The SOA is photochemically aged at reaction time = 152 min (indicated by the black lines in the two panels).

Table D.1: Experimental conditions and aerosol mass yields for all experiments[a]

Experiment	RH (%)	Parent Hydrocarbon	Seed	ΔHC[c] ($\mu g\ m^{-3}$)	ΔM_o[d] ($\mu g\ m^{-3}$)	Y (%)
1	54	β-pinene	MS+SA[b]	66.1±6.2	34.8±0.9[e]	52.7±5.1
2	54	α-pinene	MS+SA[b]	68.1±6.4	2.5±0.1[f]	3.6±0.4
3	53	β-pinene	None	69.2±6.5	35.1±0.6[e]	50.7±4.8
4	50	α-pinene	None	68.1±6.4	1.2±0.1[f]	1.7±0.2

[a]SOA mass yield calculations are shown above (Appdendix D, SOA Mass Yield Calculations).

[b]Magnesium sulfate/sulfuric acid seed

[c]Uncertainties in the hydrocarbon concentrations are calculated from a 8 % uncertainty in chamber volume and 5 % uncertainty in injected hydrocarbon mass.

[d]Uncertainties in the aerosol mass loading are calculated from one standard deviation of the aerosol volume as measured by the scanning mobility particle sizer.

[e]The aerosol mass loading is calculated using the density = 1.43 g cm^{-3} obtained from the NO_3+β-pinene nucleation experiment (Experiment 3).

[f]The aerosol mass loading is calculated using the density = 1.46 g cm^{-3} obtained from the NO_3+α-pinene nucleation experiment (Experiment 4).

Table D.2: List of reactions and their rate constants for the NO_3+β-pinene and NO_3+α-pinene systems.

Reaction	**Rate Constant[a]**
$NO_2 + O_3 \rightarrow NO_3 + O_2$	$3.52 \cdot 10^{-17}$ cm^3 $molecules^{-1}$ s^{-1} [a]
$NO_2 + NO_3 \rightarrow N_2O_5$	$6.7 \cdot 10^{-12}$ cm^3 $molecules^{-1}$ s^{-1} [a]
$N_2O_5 \rightarrow NO_2 + NO_3$	$2.2 \cdot 10^{-1}$ s^{-1} [a]
$OH + O_3 \rightarrow HO_2 + O_2$	$7.3 \cdot 10^{-14}$ cm^3 $molecules^{-1}$ s^{-1} [a]
$OH + HO_2 \rightarrow H_2O_2 + O_2$	$1.1 \cdot 10^{-10}$ cm^3 $molecules^{-1}$ s^{-1} [a]
$HO_2 + O_3 \rightarrow OH + 2O_2$	$1.9 \cdot 10^{-15}$ $cm^3 molecules^{-1}$ s^{-1} [a]
$HO_2 + HO_2 \rightarrow H_2O_2 + O_2$	$1.4 \cdot 10^{-12}$ cm^3 $molecules^{-1}$ s^{-1} [a]
$NO + HO_2 \rightarrow NO_2 + OH$	$8.1 \cdot 10^{-12}$ cm^3 $molecules^{-1}$ s^{-1} [a]
$NO + O_3 \rightarrow O_2 + NO_2$	$1.9 \cdot 10^{-14}$ cm^3 $molecules^{-1}$ s^{-1} [a]
$NO + NO_3 \rightarrow 2\ NO_2$	$2.6 \cdot 10^{-11}$ cm^3 $molecules^{-1}$ s^{-1} [a]
$HCHO + NO_3 \rightarrow HNO3 + CO + HO_2$	$5.5 \cdot 10^{-16}$ cm^3 $molecules^{-1}$ s^{-1}
β-pinene + $NO_3 + O_2 \rightarrow$ NBPINAO2	$0.8 \cdot 2.51 \cdot 10^{-12}$ cm^3 $molecules^{-1}$ s^{-1}
β-pinene + $NO_3 + O_2 \rightarrow$ NBPINBO2	$0.2 \cdot 2.51 \cdot 10^{-12}$ cm^3 $molecules^{-1}$ s^{-1}
β-pinene + $O_3 + O_2 \rightarrow$ NOPINONE + CH200F	$0.4 \cdot 1.5 \cdot 10^{-17}$ cm^3 $molecules^{-1}$ s^{-1}
β-pinene + $O_3 + O_2 \rightarrow$ NOPINOOA + HCHO	$0.6 \cdot 1.5 \cdot 10^{-17}$ cm^3 $molecules^{-1}$ s^{-1}
NBPINAO2 + $HO_2 \rightarrow$ NBPINAOOH	$2.09 \cdot 10^{-11}$ cm^3 $molecules^{-1}$ s^{-1}
NBPINAO2 + NO → NBPINAO	$9.04 \cdot 10^{-12}$ cm^3 $molecules^{-1}$ s^{-1}
NBPINAO2 + $NO_3 \rightarrow$ NBPINAO	$2.3 \cdot 10^{-12}$ cm^3 $molecules^{-1}$ s^{-1}
NBPINAO2 + $RO_2 \rightarrow$ NBPINAO	$0.7 \cdot 9.2 \cdot 10^{-14}$ cm^3 $molecules^{-1}$ s^{-1}
NBPINAO → NOPINONE + HCHO + NO_2	10^6 s^{-1}
NBPINAO2 + $RO_2 \rightarrow$ BPINBNO3	$0.3 \cdot 9.2 \cdot 10^{-14}$ cm^3 $molecules^{-1}$ s^{-1}
NBPINBO2 + $HO_2 \rightarrow$ NBPINBOOH	$2.09 \cdot 10^{-11}$ cm^3 $molecules^{-1}$ s^{-1}
NBPINBO2 + NO → NBPINBO	$9.04 \cdot 10^{-12}$ cm^3 $molecules^{-1}$ s^{-1}
NBPINBO2 + $NO_3 \rightarrow$ NBPINBO	$2.3 \cdot 10^{-12}$ cm^3 $molecules^{-1}$ s^{-1}
NBPINBO2 + $RO_2 \rightarrow$ NBPINBO	$0.6 \cdot 2 \cdot 10^{-12}$ cm^3 $molecules^{-1}$ s^{-1}
NBPINAO → NOPINONE + HCHO + NO_2	$7 \cdot 10^3$ s^{-1}
NBPINAO2 + $RO_2 \rightarrow$ BPINANO3	$0.2 \cdot 2 \cdot 10^{-12}$ cm^3 $molecules^{-1}$ s^{-1}
NBPINAO2 + $RO_2 \rightarrow$ NC91CHO	$0.6 \cdot 2 \cdot 10^{-12}$ cm^3 $molecules^{-1}$ s^{-1}
NC91CHO + $NO_3 \rightarrow$ NC91CO3	$2.32 \cdot 10^{-14}$ cm^3 $molecules^{-1}$ s^{-1}
NC91CO3 + $HO_2 \rightarrow$ NC91CO3H	$0.56 \cdot 1.39 \cdot 10^{-11}$ cm^3 $molecules^{-1}$ s^{-1}
NC91CO3 + $HO_2 \rightarrow$ NOPINONE + NO3 + OH + HCHO	$0.44 \cdot 1.39 \cdot 10^{-11}$ cc $molecules^{-1}$ s^{-1}
NC91CO3 + NO → NOPINONE + HCHO + $2NO_2$	$1.98 \cdot 10^{-11}$ cm^3 $molecules^{-1}$ s^{-1}
NC91CO3 + $NO_2 \rightarrow$ NC91PAN	$9.4 \cdot 10^{-12}$ cm^3 $molecules^{-1}$ s^{-1}
NC91PAN →NC91CO3 + NO_2	$3.0 \cdot 10^{-4}$ s^{-1}
NC91CO3 + $NO_3 \rightarrow$ NOPINONE + HCHO + $2NO_2$	$4.0 \cdot 10^{-12}$ cm^3 $molecules^{-1}$ s^{-1}
NC91CO3 + $RO_2 \rightarrow$ NOPINONE+ HCHO + NO_2	10^{-11} cm^3 $molecules^{-1}$ s^{-1}
CH2OOFA → CH2OO	$0.37 \cdot 10^6$ s^{-1}

Table D.2 Continued

CH2OOFA → CO	$0.5 \cdot 10^{6}$ s^{-1}
CH2OOFA → HO_2 + CO + OH	$0.13 \cdot 10^{6}$ s^{-1}
CH2OO + CO → HCHO	$1.2 \cdot 10^{-15}$ cm^3 $molecules^{-1}$ s^{-1}
CH2OO + NO → HCHO	$1.0 \cdot 10^{-14}$ cm^3 $molecules^{-1}$ s^{-1}
CH2OO + NO_2→ HCHO	$1.0 \cdot 10^{-15}$ cm^3 $molecules^{-1}$ s^{-1}
CH2OO + H_2O→ HCHO	$6.0 \cdot 10^{-18}$ cm^3 $molecules^{-1}$ s^{-1}
CH2OO + H_2O→HCOOH	$1.0 \cdot 10^{-17}$ cm^3 $molecules^{-1}$ s^{-1}
α-pinene + NO_3 + O_2 → NAPINAO2	$0.65 \cdot 6.21 \cdot 10^{-12}$ cm^3 $molecules^{-1}$ s^{-1}
α-pinene + NO_3 + O_2 → NAPINBO2	$0.35 \cdot 6.21 \cdot 10^{-12}$ cm^3 $molecules^{-1}$ s^{-1}
α-pinene + O_3 + O_2 → APINOOA	$0.6 \cdot 9 \cdot 10^{-17}$ cm^3 $molecules^{-17}$ s^{-1}
α-pinene + O_3 + O_2 → APINOOB	$0.4 \cdot 9 \cdot 10^{-17}$ cm^3 $molecules^{-17}$ s^{-1}
NAPINAO2 + HO_2 → Products	$2.09 \cdot 10^{-11}$ cm^3 $molecules^{-1}$ s^{-1}
NAPINBO2 + HO_2 → Products	$2.09 \cdot 10^{-11}$ cm^3 $molecules^{-1}$ s^{-1}
NAPINAO2 + NO → Products	$9.04 \cdot 10^{-12}$ cm^3 $molecules^{-1}$ s^{-1}
NAPINBO2 + NO → Products	$9.04 \cdot 10^{-12}$ cm^3 $molecules^{-1}$ s^{-1}
NAPINAO2 + NO_3 → Products	$2.3 \cdot 10^{-12}$ cm^3 $molecules^{-1}$ s^{-1}
NAPINBO2 + NO_3 → Products	$2.3 \cdot 10^{-12}$ cm^3 $molecules^{-1}$ s^{-1}
NAPINAO2 + RO_2 → Products	$6.7 \cdot 10^{-15}$ cm^3 $molecules^{-1}$ s^{-1}
NAPINBO2 + RO_2 → Products	$2.5 \cdot 10^{-13}$ cm^3 $molecules^{-1}$ s^{-1}

[a]Unless noted, reactions are adapted from MCMv3.2.(Saunders et al., 2003b)

[a]Reaction rates are from JPL kinetics(Sander, 2011) and the references therein.

Table D.3: List of ON formed from the NO_3+β-pinene reaction (includes mass of the I^- ion, *m/z* = 126.905). Due to the resolving power of the HR-ToF-CIMS used in this study (~ 4000), these formula assignments are tentative and need to be confirmed by higher resolution measurements.

Molecule-iodide adduct formula	**Exact *m/z***	**Molecule-iodide adduct formula**	**Exact *m/z***
$C_{10}H_{17}NO_4I^-$	342.020782	$C_9H_{15}NO_6I^-$	359.994965
$C_{10}H_{15}NO_5I^-$	356.000031	$C_9H_{13}NO_7I^-$	373.974182
$C_{10}H_{17}NO_5I^-$	358.015686	$C_9H_{15}NO_7I^-$	375.989868
$C_{10}H_{19}NO_5I^-$	360.031311	$C_9H_{17}NO_7I^-$	378.005524
$C_{10}H_{13}NO_6I^-$	369.97934	$C_9H_{13}NO_8I^-$	389.969147
$C_{10}H_{15}NO_6I^-$	371.994965	$C_9H_{15}NO_8I^-$	391.984833
$C_{10}H_{17}NO_6I^-$	374.01062	$C_9H_{13}NO_9I^-$	405.96405
$C_{10}H_{19}NO_6I^-$	376.026306	$C_9H_{15}NO_9I^-$	407.979706
$C_{10}H_{13}NO_7I^-$	385.974213	$C_8H_{11}NO_6I^-$	343.963654
$C_{10}H_{15}NO_7I^-$	387.989868	$C_8H_{13}INO_6I^-$	345.979309
$C_{10}H_{17}NO_7I^-$	390.005524	$C_8H_{11}NO_7I^-$	359.958588
$C_{10}H_{19}NO_7I^-$	392.02121	$C_8H_{13}NO_7I^-$	361.974213
$C_{10}H_{13}NO_8I^-$	401.969147	$C_8H_{11}NO_8I^-$	375.953491
$C_{10}H_{15}NO_8I^-$	403.984772	$C_8H_{13}NO_8I^-$	377.969147
$C_{10}H_{17}NO_8I^-$	406.000427	$C_8H_{11}NO_9I^-$	391.948395
$C_{10}H_{19}NO_8I^-$	408.016052	$C_7H_9NO_5I^-$	313.953094
$C_{10}H_{13}NO_9I^-$	417.96405	$C_7H_9NO_6I^-$	329.947998
$C_{10}H_{15}NO_9I^-$	419.979675	$C_7H_{1l}NO_6I^-$	331.963654
$C_{10}H_{17}NO_9I^-$	421.995361	$C_7H_9NO_7I^-$	345.942932
$C_9H_{13}NO_6I^-$	357.979309	$C_7H_{11}NO_7I^-$	347.958588
		$C_7H_9NO_8I^-$	361.937836

Table D.4: List of ON formed from the NO3+α-pinene reaction (includes mass of the I- ion, m/z = 126.905). Due to the resolving power of the HR-ToF-CIMS used in this study (~ 4000), these formula assignments are tentative and need to be confirmed by higher resolution measurements.

Molecule-iodide adduct formula	**Exact *m/z***
$C_{10}H_{15}NO_5I^-$	356.000031
$C_{10}H_{15}NO_6I^-$	371.994965
$C_{10}H_{16}N_2O_7I^-$	403.000763
$C_{10}H_{15}NO_9I^-$	419.979706
$C_9H_{13}NO_6I^-$	357.979309

REFERENCES

Abramson, E., Imre, D., Beranek, J., Wilson, J., and Zelenyuk, A.: Experimental determination of chemical diffusion within secondary organic aerosol particles, Physical Chemistry Chemical Physics, 15, 2983-2991, doi:10.1039/c2cp44013j, 2013.

Aiken, A. C., Decarlo, P. F., Kroll, J. H., Worsnop, D. R., Huffman, J. A., Docherty, K. S., Ulbrich, I. M., Mohr, C., Kimmel, J. R., Sueper, D., Sun, Y., Zhang, Q., Trimborn, A., Northway, M., Ziemann, P. J., Canagaratna, M. R., Onasch, T. B., Alfarra, M. R., Prevot, A. S. H., Dommen, J., Duplissy, J., Metzger, A., Baltensperger, U., and Jimenez, J. L.: O/C and OM/OC ratios of primary, secondary, and ambient organic aerosols with high-resolution time-of-flight aerosol mass spectrometry, Environ. Sci. Technol., 42, 4478-4485, doi:10.1021/es703009q, 2008.

Akagi, S. K., Yokelson, R. J., Burling, I. R., Meinardi, S., Simpson, I., Blake, D. R., McMeeking, G. R., Sullivan, A., Lee, T., Kreidenweis, S., Urbanski, S., Reardon, J., Griffith, D. W. T., Johnson, T. J., and Weise, D. R.: Measurements of reactive trace gases and variable O3 formation rates in some South Carolina biomass burning plumes, Atmos. Chem. Phys., 13, 1141-1165, doi:10.5194/acp-13-1141-2013, 2013.

Aljawhary, D., Lee, A. K. Y., and Abbatt, J. P. D.: High-resolution chemical ionization mass spectrometry (ToF-CIMS): application to study SOA composition and processing, Atmos. Meas. Tech., 6, 3211-3224, doi:10.5194/amt-6-3211-2013, 2013.

Arey, J., Aschmann, S. M., Kwok, E. S. C., and Atkinson, R.: Alkyl Nitrate, Hydroxyalkyl Nitrate, and Hydroxycarbonyl Formation from the NOx−Air

Photooxidations of C5−C8 n-Alkanes, The Journal of Physical Chemistry A, 105, 1020-1027, doi:10.1021/jp003292z, 2001.

Aschmann, S. M., Tuazon, E. C., Arey, J., and Atkinson, R.: Products of the OH radical-initiated reactions of 2-propyl nitrate, 3-methyl-2-butyl nitrate and 3-methyl-2-pentyl nitrate, Atmospheric Environment, 45, 1695-1701, doi:10.1016/j.atmosenv.2010.12.061, 2011.

Aschmann, S. M., Arey, J., and Atkinson, R.: Products of the OH radical-initiated reactions of 2- and 3-hexyl nitrate, Atmospheric Environment, 46, 264-270, doi:10.1016/j.atmosenv.2011.09.073, 2012.

Atkinson, R.: KINETICS AND MECHANISMS OF THE GAS-PHASE REACTIONS OF THE NO3 RADICAL WITH ORGANIC-COMPOUNDS, Journal of Physical and Chemical Reference Data, 20, 459-507, 1991.

Atkinson, R.: Atmospheric Reactions of Alkoxy and β-Hydroxyalkoxy Radicals, Int. J. Chem. Kinet., 29, 99-111, doi:10.1002/(SICI)1097-4601(1997)29:2<99::AID-KIN3>3.0.CO;2-F, 1997a.

Atkinson, R.: Gas-phase tropospheric chemistry of volatile organic compounds .1. Alkanes and alkenes, Journal of Physical and Chemical Reference Data, 26, 215-290, 1997b.

Atkinson, R., and Arey, J.: Atmospheric degradation of volatile organic compounds, Chemical Reviews, 103, 4605-4638, 2003a.

Atkinson, R., and Arey, J.: Gas-phase Tropospheric Chemistry of Biogenic Volatile Organic Compounds: A Review, Atmos. Environ., 37, 197-219, 2003b.

Ayres, B. R., Allen, H. M., Draper, D. C., Brown, S. S., Wild, R. J., Jimenez, J. L., Day, D. A., Campuzano-Jost, P., Hu, W., de Gouw, J., Koss, A., Cohen, R. C., Duffey, K. C., Romer, P., Baumann, K., Edgerton, E., Takahama, S., Thornton, J. A., Lee, B. H., Lopez-Hilfiker, F. D., Mohr, C., Wennberg, P. O., Nguyen, T. B., Teng, A., Goldstein, A. H., Olson, K., and Fry, J. L.: Organic nitrate aerosol formation via NO3 + biogenic volatile organic compounds in the southeastern United States, Atmos. Chem. Phys., 15, 13377-13392, doi:10.5194/acp-15-13377-2015, 2015.

Bahreini, R., Keywood, M. D., Ng, N. L., Varutbangkul, V., Gao, S., Flagan, R. C., Seinfeld, J. H., Worsnop, D. R., and Jimenez, J. L.: Measurements of Secondary Organic Aerosol from Oxidation of Cycloalkenes, Terpenes, and m-Xylene Using an Aerodyne Aerosol Mass Spectrometer, Environ. Sci. Technol., 39, 5674-5688, doi:10.1021/es048061a, 2005.

Barsanti, K. C., Carlton, A. G., and Chung, S. H.: Analyzing experimental data and model parameters: implications for predictions of SOA using chemical transport models, Atmos. Chem. Phys., 13, 12073-12088, doi:10.5194/acp-13-12073-2013, 2013.

Bean, J. K., and Hildebrandt Ruiz, L.: Hydrolysis and gas-particle partitioning of organic nitrates formed from the oxidation of α-pinene in environmental chamber experiments, Atmos. Chem. Phys. Discuss., 15, 20629-20653, doi:10.5194/acpd-15-20629-2015, 2015.

Beaver, M. R., St Clair, J. M., Paulot, F., Spencer, K. M., Crounse, J. D., LaFranchi, B. W., Min, K. E., Pusede, S. E., Wooldridge, P. J., Schade, G. W., Park, C., Cohen, R. C., and Wennberg, P. O.: Importance of biogenic precursors to the budget of organic nitrates: observations of multifunctional organic nitrates by CIMS and TD-LIF during BEARPEX 2009, Atmos. Chem. Phys., 12, 5773-5785, doi:10.5194/acp-12-5773-2012, 2012.

Berndt, T., and Boge, O.: Gas-phase reaction of NO3 radicals with isoprene: A kinetic and mechanistic study, International Journal of Chemical Kinetics, 29, 755-765, doi:10.1002/(sici)1097-4601(1997)29:10<755::aid-kin4>3.0.co;2-l, 1997a.

Berndt, T., and Boge, O.: Products and mechanism of the gas-phase reaction of NO3 radicals with alpha-pinene, Journal of the Chemical Society-Faraday Transactions, 93, 3021-3027, doi:10.1039/a702364b, 1997b.

Bertram, T. H., Kimmel, J. R., Crisp, T. A., Ryder, O. S., Yatavelli, R. L. N., Thornton, J. A., Cubison, M. J., Gonin, M., and Worsnop, D. R.: A field-deployable, chemical ionization time-of-flight mass spectrometer, Atmos. Meas. Tech., 4, 1471-1479, doi:10.5194/amt-4-1471-2011, 2011.

Bonn, B., and Moorgat, G. K.: New particle formation during a- and b-pinene oxidation by O3, OH and NO3, and the influence of water vapour: particle size distribution studies, Atmos. Chem. Phys., 2, 183-196, doi:10.5194/acp-2-183-2002, 2002.

Bowman, F. M., Odum, J. R., Seinfeld, J. H., and Pandis, S. N.: Mathematical model for gas-particle partitioning of secondary organic aerosols, Atmospheric Environment, 31, 3921-3931, doi:10.1016/s1352-2310(97)00245-8, 1997.

Boyd, C. M., Sanchez, J., Xu, L., Eugene, A. J., Nah, T., Tuet, W. Y., Guzman, M. I., and Ng, N. L.: Secondary organic aerosol formation from the β-pinene+NO3 system: effect of humidity and peroxy radical fate, Atmos. Chem. Phys., 15, 7497-7522, doi:10.5194/acp-15-7497-2015, 2015.

Brown, S. S., deGouw, J. A., Warneke, C., Ryerson, T. B., Dube, W. P., Atlas, E., Weber, R. J., Peltier, R. E., Neuman, J. A., Roberts, J. M., Swanson, A., Flocke, F., McKeen, S. A., Brioude, J., Sommariva, R., Trainer, M., Fehsenfeld, F. C., and Ravishankara, A. R.: Nocturnal isoprene oxidation over the Northeast United States in summer and its impact on reactive nitrogen partitioning and secondary organic aerosol, Atmos. Chem. Phys., 9, 3027-3042, 2009.

Brown, S. S., and Stutz, J.: Nighttime radical observations and chemistry, Chem. Soc. Rev., 41, 6405-6447, doi:10.1039/c2cs35181a, 2012.

Brown, S. S., Dube, W. P., Bahreini, R., Middlebrook, A. M., Brock, C. A., Warneke, C., de Gouw, J. A., Washenfelder, R. A., Atlas, E., Peischl, J., Ryerson, T. B., Holloway, J. S., Schwarz, J. P., Spackman, R., Trainer, M., Parrish, D. D., Fehshenfeld, F. C., and Ravishankara, A. R.: Biogenic VOC oxidation and organic aerosol formation in an urban nocturnal boundary layer: aircraft vertical profiles in Houston, TX, Atmos. Chem. Phys., 13, 11317-11337, doi:10.5194/acp-13-11317-2013, 2013.

Browne, E. C., and Cohen, R. C.: Effects of biogenic nitrate chemistry on the NOx lifetime in remote continental regions, Atmos. Chem. Phys., 12, 11917-11932, doi:10.5194/acp-12-11917-2012, 2012.

Browne, E. C., Min, K. E., Wooldridge, P. J., Apel, E., Blake, D. R., Brune, W. H., Cantrell, C. A., Cubison, M. J., Diskin, G. S., Jimenez, J. L., Weinheimer, A. J., Wennberg, P. O., Wisthaler, A., and Cohen, R. C.: Observations of total RONO2 over the boreal forest: NOx sinks and HNO3 sources, Atmos. Chem. Phys., 13, 4543-4562, doi:10.5194/acp-13-4543-2013, 2013.

Browne, E. C., Wooldridge, P. J., Min, K. E., and Cohen, R. C.: On the role of monoterpene chemistry in the remote continental boundary layer, Atmos. Chem. Phys., 14, 1225-1238, doi:10.5194/acp-14-1225-2014, 2014.

Bruns, E. A., Perraud, V., Zelenyuk, A., Ezell, M. J., Johnson, S. N., Yu, Y., Imre, D., Finlayson-Pitts, B. J., and Alexander, M. L.: Comparison of FTIR and Particle Mass Spectrometry for the Measurement of Particulate Organic Nitrates, Environ. Sci. Technol., 44, 1056-1061, doi:10.1021/es9029864, 2010.

Canagaratna, M. R., Jimenez, J. L., Kroll, J. H., Chen, Q., Kessler, S. H., Massoli, P., Hildebrandt Ruiz, L., Fortner, E., Williams, L. R., Wilson, K. R., Surratt, J. D., Donahue, N. M., Jayne, J. T., and Worsnop, D. R.: Elemental ratio measurements of organic compounds using aerosol mass spectrometry: characterization, improved calibration, and implications, Atmos. Chem. Phys., 15, 253-272, doi:10.5194/acp-15-253-2015, 2015.

Cappa, C. D., and Wilson, K. R.: Evolution of organic aerosol mass spectra upon heating: implications for OA phase and partitioning behavior, Atmos. Chem. Phys., 11, 1895-1911, doi:10.5194/acp-11-1895-2011, 2011.

Carter, W. P. L., Darnall, K. R., Lloyd, A. C., Winer, A. M., and Pitts Jr, J. N.: Evidence for Alkoxy Radical Isomerization in Photooxidations of C_4-C_6 Alkanes under Simulated Atmospheric Conditions, Chem. Phys. Lett., 42, 22-27, doi:http://dx.doi.org/10.1016/0009-2614(76)80543-X, 1976.

Cerully, K. M., Bougiatioti, A., Hite, J. R., Guo, H., Xu, L., Ng, N. L., Weber, R. J., and Nenes, A.: On the Link Between Hygroscopicity, Volatility, and Oxidation State of Ambient and Water-Soluble Aerosol in the Southeastern United Sates., Atmos. Chem. Phys. Discuss., 14, 30835-30877, doi:doi:10.5194/acpd-14-30835-2014, 2014.

Cerully, K. M., Bougiatioti, A., Hite Jr, J. R., Guo, H., Xu, L., Ng, N. L., Weber, R., and Nenes, A.: On the link between hygroscopicity, volatility, and oxidation state of ambient and water-soluble aerosols in the southeastern United States, Atmos. Chem. Phys., 15, 8679-8694, doi:10.5194/acp-15-8679-2015, 2015.

Chan, A. W. H., Chan, M. N., Surratt, J. D., Chhabra, P. S., Loza, C. L., Crounse, J. D., Yee, L. D., Flagan, R. C., Wennberg, P. O., and Seinfeld, J. H.: Role of aldehyde chemistry and NOx concentrations in secondary organic aerosol formation, Atmos. Chem. Phys., 10, 7169-7188, doi:10.5194/acp-10-7169-2010, 2010.

Chen, Q., Farmer, D. K., Rizzo, L. V., Pauliquevis, T., Kuwata, M., Karl, T. G., Guenther, A., Allan, J. D., Coe, H., Andreae, M. O., Pöschl, U., Jimenez, J. L., Artaxo, P., and Martin, S. T.: Submicron particle mass concentrations and sources in the Amazonian wet season (AMAZE-08), Atmos. Chem. Phys., 15, 3687-3701, doi:10.5194/acp-15-3687-2015, 2015.

Chen, X., Hulbert, D., and Shepson, P. B.: Measurement of the organic nitrate yield from OH reaction with isoprene, Journal of Geophysical Research: Atmospheres, 103, 25563-25568, doi:10.1029/98JD01483, 1998.

Chhabra, P. S., Flagan, R. C., and Seinfeld, J. H.: Elemental analysis of chamber organic aerosol using an aerodyne high-resolution aerosol mass spectrometer, Atmos. Chem. Phys., 10, 4111-4131, doi:10.5194/acp-10-4111-2010, 2010.

Chung, S. H., and Seinfeld, J. H.: Global distribution and climate forcing of carbonaceous aerosols, Journal of Geophysical Research: Atmospheres, 107, 4407, doi:10.1029/2001JD001397, 2002.

Crounse, J. D., Nielsen, L. B., Jorgensen, S., Kjaergaard, H. G., and Wennberg, P. O.: Autoxidation of Organic Compounds in the Atmosphere, J. Phys. Chem. Lett., 4, 3513-3520, doi:10.1021/jz4019207, 2013.

Darer, A. I., Cole-Filipiak, N. C., O'Connor, A. E., and Elrod, M. J.: Formation and Stability of Atmospherically Relevant Isoprene-Derived Organosulfates and Organonitrates, Environ. Sci. Technol., 45, 1895-1902, doi:10.1021/es103797z, 2011.

Day, D. A., Liu, S., Russell, L. M., and Ziemann, P. J.: Organonitrate group concentrations in submicron particles with high nitrate and organic fractions in coastal southern California, Atmospheric Environment, 44, 1970-1979, doi:10.1016/j.atmosenv.2010.02.045, 2010.

de Gouw, J. A., Middlebrook, A. M., Warneke, C., Goldan, P. D., Kuster, W. C., Roberts, J. M., Fehsenfeld, F. C., Worsnop, D. R., Canagaratna, M. R., Pszenny, A. A. P., Keene,

W. C., Marchewka, M., Bertman, S. B., and Bates, T. S.: Budget of organic carbon in a polluted atmosphere: Results from the New England Air Quality Study in 2002, Journal of Geophysical Research-Atmospheres, 110, D16305, doi:16310.11029/12004JD005623, 2005.

DeCarlo, P. F., Slowik, J. G., Worsnop, D. R., Davidovits, P., and Jimenez, J. L.: Particle morphology and density characterization by combined mobility and aerodynamic diameter measurements. Part 1: Theory, Aerosol Sci. Technol., 38, 1185-1205, doi:10.1080/027868290903907, 2004.

DeCarlo, P. F., Kimmel, J. R., Trimborn, A., Northway, M. J., Jayne, J. T., Aiken, A. C., Gonin, M., Fuhrer, K., Horvath, T., Docherty, K. S., Worsnop, D. R., and Jimenez, J. L.: Field-deployable, high-resolution, time-of-flight aerosol mass spectrometer, Analytical Chemistry, 78, 8281-8289, doi:10.1021/ac061249n, 2006.

Dibble, T. S.: Reactions of the alkoxy radicals formed following OH-addition to alpha-pinene and beta-pinene. C-C bond scission reactions, Journal of the American Chemical Society, 123, 4228-4234, doi:10.1021/ja003553i, 2001.

Dillon, T. J., and Crowley, J. N.: Direct detection of OH formation in the reactions of HO(2) with CH(3)C(O)O(2) and other substituted peroxy radicals, Atmos. Chem. Phys., 8, 4877-4889, 2008.

Docherty, K. S., Wu, W., Lim, Y. B., and Ziemann, P. J.: Contributions of Organic Peroxides to Secondary Aerosol Formed from Reactions of Monoterpenes with O_3, Environ. Sci. Technol., 39, 4049-4059, 2005.

Donahue, N. M., Robinson, A. L., Stanier, C. O., and Pandis, S. N.: Coupled partitioning, dilution, and chemical aging of semivolatile organics, Environ. Sci. Technol., 40, 2635-2643, doi:10.1021/es052297c, 2006.

Donahue, N. M., Henry, K. M., Mentel, T. F., Kiendler-Scharr, A., Spindler, C., Bohn, B., Brauers, T., Dorn, H. P., Fuchs, H., Tillmann, R., Wahner, A., Saathoff, H., Naumann, K.-H., Moehler, O., Leisner, T., Mueller, L., Reinnig, M.-C., Hoffmann, T., Salo, K., Hallquist, M., Frosch, M., Bilde, M., Tritscher, T., Barmet, P., Praplan, A. P., DeCarlo, P. F., Dommen, J., Prevot, A. S. H., and Baltensperger, U.: Aging of biogenic secondary organic aerosol via gas-phase OH radical reactions, Proceedings of the National Academy of Sciences of the United States of America, 109, 13503-13508, doi:10.1073/pnas.1115186109, 2012.

Duplissy, J., DeCarlo, P. F., Dommen, J., Alfarra, M. R., Metzger, A., Barmpadimos, I., Prevot, A. S. H., Weingartner, E., Tritscher, T., Gysel, M., Aiken, A. C., Jimenez, J. L., Canagaratna, M. R., Worsnop, D. R., Collins, D. R., Tomlinson, J., and Baltensperger, U.: Relating hygroscopicity and composition of organic aerosol particulate matter, Atmos. Chem. Phys., 11, 1155-1165, doi:10.5194/acp-11-1155-2011, 2011.

Eberhard, J., Muller, C., Stocker, D. W., and Kerr, J. A.: Isomerization of Alkoxy Radicals under Atmospheric Conditions, Environ. Sci. Technol., 29, 232-241, doi:10.1021/es00001a600, 1995.

Eddingsaas, N. C., Loza, C. L., Yee, L. D., Seinfeld, J. H., and Wennberg, P. O.: alpha-pinene photooxidation under controlled chemical conditions - Part 1: Gas-phase

composition in low- and high-NOx environments, Atmos. Chem. Phys., 12, 6489-6504, doi:10.5194/acp-12-6489-2012, 2012.

Ehn, M., Thornton, J. A., Kleist, E., Sipila, M., Junninen, H., Pullinen, I., Springer, M., Rubach, F., Tillmann, R., Lee, B., Lopez-Hilfiker, F., Andres, S., Acir, I. H., Rissanen, M., Jokinen, T., Schobesberger, S., Kangasluoma, J., Kontkanen, J., Nieminen, T., Kurten, T., Nielsen, L. B., Jorgensen, S., Kjaergaard, H. G., Canagaratna, M., Dal Maso, M., Berndt, T., Petaja, T., Wahner, A., Kerminen, V. M., Kulmala, M., Worsnop, D. R., Wildt, J., and Mentel, T. F.: A large source of low-volatility secondary organic aerosol, Nature, 506, 476-+, doi:10.1038/nature13032, 2014.

Epstein, S. A., Riipinen, I., and Donahue, N. M.: A Semiempirical Correlation between Enthalpy of Vaporization and Saturation Concentration for Organic Aerosol, Environ. Sci. Technol., 44, 743-748, doi:10.1021/es902497z, 2009.

Ervens, B., Turpin, B. J., and Weber, R. J.: Secondary organic aerosol formation in cloud droplets and aqueous particles (aqSOA): a review of laboratory, field and model studies, Atmos. Chem. Phys., 11, 11069-11102, doi:10.5194/acp-11-11069-2011, 2011.

Farmer, D. K., Matsunaga, A., Docherty, K. S., Surratt, J. D., Seinfeld, J. H., Ziemann, P. J., and Jimenez, J. L.: Response of an aerosol mass spectrometer to organonitrates and organosulfates and implications for atmospheric chemistry, Proceedings of the National Academy of Sciences of the United States of America, 107, 6670-6675, doi:10.1073/pnas.0912340107, 2010.

Farmer, E. H., Koch, H. P., and Sutton, D. A.: The Course of Autoxidation Reactions in Polyisoprenes and Allied Compounds. Part VII. Rearrangement of Double Bonds During Autoxidation, J. Chem. Soc., 541-547, doi:10.1039/JR9430000541, 1943.

Fiore, A. M., Dentener, F. J., Wild, O., Cuvelier, C., Schultz, M. G., Hess, P., Textor, C., Schulz, M., Doherty, R. M., Horowitz, L. W., MacKenzie, I. A., Sanderson, M. G., Shindell, D. T., Stevenson, D. S., Szopa, S., Van Dingenen, R., Zeng, G., Atherton, C., Bergmann, D., Bey, I., Carmichael, G., Collins, W. J., Duncan, B. N., Faluvegi, G., Folberth, G., Gauss, M., Gong, S., Hauglustaine, D., Holloway, T., Isaksen, I. S. A., Jacob, D. J., Jonson, J. E., Kaminski, J. W., Keating, T. J., Lupu, A., Marmer, E., Montanaro, V., Park, R. J., Pitari, G., Pringle, K. J., Pyle, J. A., Schroeder, S., Vivanco, M. G., Wind, P., Wojcik, G., Wu, S., and Zuber, A.: Multimodel estimates of intercontinental source-receptor relationships for ozone pollution, J. Geophys. Res.-Atmos., 114, D04301, doi:10.1029/2008jd010816, 2009.

Fisher, J. A., Jacob, D. J., Travis, K. R., Kim, P. S., Marais, E. A., Chan Miller, C., Yu, K., Zhu, L., Yantosca, R. M., Sulprizio, M. P., Mao, J., Wennberg, P. O., Crounse, J. D., Teng, A. P., Nguyen, T. B., St. Clair, J. M., Cohen, R. C., Romer, P., Nault, B. A., Wooldridge, P. J., Jimenez, J. L., Campuzano-Jost, P., Day, D. A., Shepson, P. B., Xiong, F., Blake, D. R., Goldstein, A. H., Misztal, P. K., Hanisco, T. F., Wolfe, G. M., Ryerson, T. B., Wisthaler, A., and Mikoviny, T.: Organic nitrate chemistry and its implications for nitrogen budgets in an isoprene- and monoterpene-rich atmosphere: constraints from aircraft (SEAC4RS) and ground-based (SOAS) observations in the Southeast US, Atmos. Chem. Phys. Discuss., 2016, 1-38, doi:10.5194/acp-2016-52, 2016.

Fountoukis, C., and Nenes, A.: ISORROPIA II: a computationally efficient thermodynamic equilibrium model for K+-Ca2+-Mg2+-Nh(4)(+)-Na+-SO42--NO3--Cl--H2O aerosols, Atmos. Chem. Phys., 7, 4639-4659, 2007.

Fry, J. L., Kiendler-Scharr, A., Rollins, A. W., Wooldridge, P. J., Brown, S. S., Fuchs, H., Dubé, W., Mensah, A., dal Maso, M., Tillmann, R., Dorn, H. P., Brauers, T., and Cohen, R. C.: Organic nitrate and secondary organic aerosol yield from NO3 oxidation of β-pinene evaluated using a gas-phase kinetics/aerosol partitioning model, Atmos. Chem. Phys., 9, 1431-1449, doi:10.5194/acp-9-1431-2009, 2009.

Fry, J. L., Kiendler-Scharr, A., Rollins, A. W., Brauers, T., Brown, S. S., Dorn, H. P., Dubé, W. P., Fuchs, H., Mensah, A., Rohrer, F., Tillmann, R., Wahner, A., Wooldridge, P. J., and Cohen, R. C.: SOA from limonene: role of NO3 in its generation and degradation, Atmos. Chem. Phys., 11, 3879-3894, doi:10.5194/acp-11-3879-2011, 2011.

Fry, J. L., Draper, D. C., Zarzana, K. J., Campuzano-Jost, P., Day, D. A., Jimenez, J. L., Brown, S. S., Cohen, R. C., Kaser, L., Hansel, A., Cappellin, L., Karl, T., Roux, A. H., Turnipseed, A., Cantrell, C., Lefer, B. L., and Grossberg, N.: Observations of gas- and aerosol-phase organic nitrates at BEACHON-RoMBAS 2011, Atmos. Chem. Phys., 13, 8585-8605, doi:10.5194/acp-13-8585-2013, 2013.

Fry, J. L., Draper, D. C., Barsanti, K. C., Smith, J. N., Ortega, J., Winkler, P. M., Lawler, M. J., Brown, S. S., Edwards, P. M., Cohen, R. C., and Lee, L.: Secondary Organic Aerosol Formation and Organic Nitrate Yield from NO3 Oxidation of Biogenic Hydrocarbons, Environ. Sci. Technol., 48, 11944-11953, doi:10.1021/es502204x, 2014.

Fuentes, J., Wang, D., Bowling, D., Potosnak, M., Monson, R., Goliff, W., and Stockwell, W.: Biogenic Hydrocarbon Chemistry within and Above a Mixed Deciduous Forest, Journal of Atmospheric Chemistry, 56, 165-185, doi:10.1007/s10874-006-9048-4, 2007.

Fuentes, J. D., Lerdau, M., Atkinson, R., Baldocchi, D., Bottenheim, J. W., Ciccioli, P., Lamb, B., Geron, C., Gu, L., Guenther, A., Sharkey, T. D., and Stockwell, W.: Biogenic hydrocarbons in the atmospheric boundary layer: A review, Bull. Amer. Meteorol. Soc., 81, 1537-1575, doi:10.1175/1520-0477(2000)081<1537:bhitab>2.3.co;2, 2000.

Gao, S., Ng, N. L., Keywood, M., Varutbangkul, V., Bahreini, R., Nenes, A., He, J., Yoo, K. Y., Beauchamp, J. L., Hodyss, R. P., Flagan, R. C., and Seinfeld, J. H.: Particle Phase Acidity and Oligomer Formation in Secondary Organic Aerosol, Environ. Sci. Technol., 38, 6582-6589, doi:10.1021/es049125k, 2004.

Gaston, C. J., Thornton, J. A., and Ng, N. L.: Reactive uptake of N2O5 to internally mixed inorganic and organic particles: the role of organic carbon oxidation state and inferred organic phase separations, Atmos. Chem. Phys., 14, 5693-5707, doi:10.5194/acp-14-5693-2014, 2014.

Grieshop, A. P., Donahue, N. M., and Robinson, A. L.: Is the gas-particle partitioning in alpha-pinene secondary organic aerosol reversible?, Geophysical Research Letters, 34, doi:10.1029/2007gl029987, 2007.

Grieshop, A. P., Miracolo, M. A., Donahue, N. M., and Robinson, A. L.: Constraining the Volatility Distribution and Gas-Particle Partitioning of Combustion Aerosols Using

Isothermal Dilution and Thermodenuder Measurements, Environ. Sci. Technol., 43, 4750-4756, doi:10.1021/es8032378, 2009.

Griffin, R. J., Cocker, D. R., Flagan, R. C., and Seinfeld, J. H.: Organic aerosol formation from the oxidation of biogenic hydrocarbons, Journal of Geophysical Research-Atmospheres, 104, 3555-3567, doi:10.1029/1998jd100049, 1999.

Guenther, A. B., Jiang, X., Heald, C. L., Sakulyanontvittaya, T., Duhl, T., Emmons, L. K., and Wang, X.: The Model of Emissions of Gases and Aerosols from Nature version 2.1 (MEGAN2.1): an extended and updated framework for modeling biogenic emissions, Geoscientific Model Development, 5, 1471-1492, doi:10.5194/gmd-5-1471-2012, 2012.

Guo, H., Xu, L., Bougiatioti, A., Cerully, K. M., Capps, S. L., Hite, J. R., Carlton, A. G., Lee, S. H., Bergin, M. H., Ng, N. L., Nenes, A., and Weber, R. J.: Particle water and pH in the southeastern United States, Atmos. Chem. Phys. Discuss., 14, 27143-27193, doi:10.5194/acpd-14-27143-2014, 2014.

Guo, H., Xu, L., Bougiatioti, A., Cerully, K. M., Capps, S. L., Hite Jr, J. R., Carlton, A. G., Lee, S. H., Bergin, M. H., Ng, N. L., Nenes, A., and Weber, R. J.: Fine-particle water and pH in the southeastern United States, Atmos. Chem. Phys., 15, 5211-5228, doi:10.5194/acp-15-5211-2015, 2015.

Hallquist, M., Wangberg, I., Ljungstrom, E., Barnes, I., and Becker, K. H.: Aerosol and product yields from NO3 radical-initiated oxidation of selected monoterpenes, Environ. Sci. Technol., 33, 553-559, doi:10.1021/es980292s, 1999.

Hallquist, M., Wenger, J. C., Baltensperger, U., Rudich, Y., Simpson, D., Claeys, M., Dommen, J., Donahue, N. M., George, C., Goldstein, A. H., Hamilton, J. F., Herrmann, H., Hoffmann, T., Iinuma, Y., Jang, M., Jenkin, M. E., Jimenez, J. L., Kiendler-Scharr, A., Maenhaut, W., McFiggans, G., Mentel, T. F., Monod, A., Prevot, A. S. H., Seinfeld, J. H., Surratt, J. D., Szmigielski, R., and Wildt, J.: The formation, properties and impact of secondary organic aerosol: current and emerging issues, Atmos. Chem. Phys., 9, 5155-5236, 2009.

Hasson, A. S., Tyndall, G. S., Orlando, J. J., Singh, S., Hernandez, S. Q., Campbell, S., and Ibarra, Y.: Branching Ratios for the Reaction of Selected Carbonyl-Containing Peroxy Radicals with Hydroperoxy Radicals, The Journal of Physical Chemistry A, 116, 6264-6281, doi:10.1021/jp211799c, 2012.

Hatch, L. E., Luo, W., Pankow, J. F., Yokelson, R. J., Stockwell, C. E., and Barsanti, K. C.: Identification and quantification of gaseous organic compounds emitted from biomass burning using two-dimensional gas chromatography-time-of-flight mass spectrometry, Atmos. Chem. Phys., 15, 1865-1899, doi:10.5194/acp-15-1865-2015, 2015.

Henry, K. M., and Donahue, N. M.: Photochemical Aging of α-Pinene Secondary Organic Aerosol: Effects of OH Radical Sources and Photolysis, The Journal of Physical Chemistry A, 116, 5932-5940, doi:10.1021/jp210288s, 2012.

Hildebrandt, L., Henry, K. M., Kroll, J. H., Worsnop, D. R., Pandis, S. N., and Donahue, N. M.: Evaluating the Mixing of Organic Aerosol Components Using High-Resolution

Aerosol Mass Spectrometry, Environ. Sci. Technol., 45, 6329-6335, doi:10.1021/es200825g, 2011.

Hoyle, C. R., Berntsen, T., Myhre, G., and Isaksen, I. S. A.: Secondary organic aerosol in the global aerosol – chemical transport model Oslo CTM2, Atmos. Chem. Phys., 7, 5675-5694, doi:10.5194/acp-7-5675-2007, 2007.

Hu, K. S., Darer, A. I., and Elrod, M. J.: Thermodynamics and kinetics of the hydrolysis of atmospherically relevant organonitrates and organosulfates, Atmos. Chem. Phys., 11, 8307-8320, doi:10.5194/acp-11-8307-2011, 2011.

Huey, L. G.: Measurement of trace atmospheric species by chemical ionization mass spectrometry: Speciation of reactive nitrogen and future directions, Mass Spectrom. Rev., 26, 166-184, doi:10.1002/mas.20118, 2007.

Iinuma, Y., Muller, C., Berndt, T., Boge, O., Claeys, M., and Herrmann, H.: Evidence for the existence of organosulfates from beta-pinene ozonolysis in ambient secondary organic aerosol, Environ. Sci. Technol., 41, 6678-6683, doi:10.1021/es070938t, 2007.

Jacobs, M. I., Burke, W. J., and Elrod, M. J.: Kinetics of the reactions of isoprene-derived hydroxynitrates: gas phase epoxide formation and solution phase hydrolysis, Atmos. Chem. Phys., 14, 8933-8946, doi:10.5194/acp-14-8933-2014, 2014.

Jaoui, M., Kleindienst, T. E., Docherty, K. S., Lewandowski, M., and Offenberg, J. H.: Secondary organic aerosol formation from the oxidation of a series of sesquiterpenes: alpha-cedrene, beta-caryophyllene, alpha-humulene and alpha-farnesene with O-3, OH and NO3 radicals, Environmental Chemistry, 10, 178-193, doi:10.1071/en13025, 2013.

Jenkin, M. E., Hurley, M. D., and Wallington, T. J.: Investigation of the radical product channel of the CH3C(O)O2 + HO2 reaction in the gas phase, Physical Chemistry Chemical Physics, 9, 3149-3162, doi:10.1039/B702757E, 2007.

Jokinen, T., Sipila, M., Richters, S., Kerminen, V. M., Paasonen, P., Stratmann, F., Worsnop, D., Kulmala, M., Ehn, M., Herrmann, H., and Berndt, T.: Rapid Autoxidation Forms Highly Oxidized RO2 Radicals in the Atmosphere, Angew. Chem.-Int. Edit., 53, 14596-14600, doi:10.1002/anie.201408566, 2014.

Jokinen, T., Berndt, T., Makkonen, R., Kerminen, V. M., Junninen, H., Paasonen, P., Stratmann, F., Herrmann, H., Guenther, A. B., Worsnop, D. R., Kulmala, M., Ehn, M., and Sipila, M.: Production of extremely low volatile organic compounds from biogenic emissions: Measured yields and atmospheric implications, Proc. Natl. Acad. Sci. U. S. A., 112, 7123-7128, 2015.

Kanakidou, M., Seinfeld, J. H., Pandis, S. N., Barnes, I., Dentener, F. J., Facchini, M. C., Van Dingenen, R., Ervens, B., Nenes, A., Nielsen, C. J., Swietlicki, E., Putaud, J. P., Balkanski, Y., Fuzzi, S., Horth, J., Moortgat, G. K., Winterhalter, R., Myhre, C. E. L., Tsigaridis, K., Vignati, E., Stephanou, E. G., and Wilson, J.: Organic aerosol and global climate modelling: a review, Atmos. Chem. Phys., 5, 1053-1123, 2005.

Kerdouci, J., Picquet-Varrault, B., and Doussin, J. F.: Prediction of Rate Constants for Gas-Phase Reactions of Nitrate Radical with Organic Compounds: A New Structure-Activity Relationship, ChemPhysChem, 11, 3909-3920, doi:10.1002/cphc.201000673, 2010.

Kerdouci, J., Picquet-Varrault, B., and Doussin, J. F.: Structure-activity relationship for the gas-phase reactions of NO3 radical with organic compounds: Update and extension to aldehydes, Atmospheric Environment, 84, 363-372, doi:10.1016/j.atmosenv.2013.11.024, 2014.

Keywood, M. D., Varutbangkul, V., Bahreini, R., Flagan, R. C., and Seinfeld, J. H.: Secondary organic aerosol formation from the ozonolysis of cycloalkenes and related compounds, Environ. Sci. Technol., 38, 4157-4164, doi:10.1021/es035363o, 2004.

Kirchner, F., and Stockwell, W. R.: Effect of peroxy radical reactions on the predicted concentrations of ozone, nitrogenous compounds, and radicals, Journal of Geophysical Research: Atmospheres, 101, 21007-21022, doi:10.1029/96JD01519, 1996.

Kolesar, K. R., Chen, C., Johnson, D., and Cappa, C. D.: The influences of mass loading and rapid dilution of secondary organic aerosol on particle volatility, Atmospheric Chemistry and Physics, 15, 9327-9343, doi:10.5194/acp-15-9327-2015, 2015.

Kroll, J. H., Ng, N. L., Murphy, S. M., Varutbangkul, V., Flagan, R. C., and Seinfeld, J. H.: Chamber studies of secondary organic aerosol growth by reactive uptake of simple carbonyl compounds, J. Geophys. Res.-Atmos., 110, 10, doi:10.1029/2005jd006004, 2005.

Kroll, J. H., Ng, N. L., Murphy, S. M., Flagan, R. C., and Seinfeld, J. H.: Secondary Organic Aerosol Formation from Isoprene Photooxidation, Environ. Sci. Technol., 40, 1869-1877, doi:10.1021/es0524301, 2006.

Kroll, J. H., and Seinfeld, J. H.: Chemistry of secondary organic aerosol: Formation and evolution of low-volatility organics in the atmosphere, Atmospheric Environment, 42, 3593-3624, doi:http://dx.doi.org/10.1016/j.atmosenv.2008.01.003, 2008.

Kroll, J. H., Smith, J. D., Che, D. L., Kessler, S. H., Worsnop, D. R., and Wilson, K. R.: Measurement of fragmentation and functionalization pathways in the heterogeneous oxidation of oxidized organic aerosol, Physical Chemistry Chemical Physics, 11, 8005-8014, doi:10.1039/b905289e, 2009.

Kwan, A. J., Chan, A. W. H., Ng, N. L., Kjaergaard, H. G., Seinfeld, J. H., and Wennberg, P. O.: Peroxy radical chemistry and OH radical production during the NO3-initiated oxidation of isoprene, Atmos. Chem. Phys., 12, 7499-7515, doi:10.5194/acp-12-7499-2012, 2012.

Lee, B. H., Lopez-Hilfiker, F. D., Mohr, C., Kurten, T., Worsnop, D. R., and Thornton, J. A.: An Iodide-Adduct High-Resolution Time-of-Flight Chemical-Ionization Mass Spectrometer: Application to Atmospheric Inorganic and Organic Compounds, Environ. Sci. Technol., 48, 6309-6317, doi:10.1021/es500362a, 2014.

Lee, B. H., Mohr, C., Lopez-Hilfiker, F. D., Lutz, A., Hallquist, M., Lee, L., Romer, P., Cohen, R. C., Iyer, S., Kurtén, T., Hu, W., Day, D. A., Campuzano-Jost, P., Jimenez, J. L., Xu, L., Ng, N. L., Guo, H., Weber, R. J., Wild, R. J., Brown, S. S., Koss, A., de Gouw, J., Olson, K., Goldstein, A. H., Seco, R., Kim, S., McAvey, K., Shepson, P. B., Starn, T., Baumann, K., Edgerton, E. S., Liu, J., Shilling, J. E., Miller, D. O., Brune, W., Schobesberger, S., D'Ambro, E. L., and Thornton, J. A.: Highly functionalized organic

nitrates in the southeast United States: Contribution to secondary organic aerosol and reactive nitrogen budgets, Proceedings of the National Academy of Sciences, 113, 1516-1521, doi:10.1073/pnas.1508108113, 2016.

Lewis, C. W., Klouda, G. A., and Ellenson, W. D.: Radiocarbon measurement of the biogenic contribution to summertime PM-2.5 ambient aerosol in Nashville, TN, Atmospheric Environment, 38, 6053-6061, doi:http://dx.doi.org/10.1016/j.atmosenv.2004.06.011, 2004.

Li, Y., Chen, Q., Guzman, M., Chan, C., and Martin, S.: Second-generation products contribute substantially to the particle-phase organic material produced by β-caryophyllene ozonolysis, Atmos. Chem. Phys., 11, 121-132, 2011.

Liu, S., Shilling, J. E., Song, C., Hiranuma, N., Zaveri, R. A., and Russell, L. M.: Hydrolysis of Organonitrate Functional Groups in Aerosol Particles, Aerosol Sci. Technol., 46, 1359-1369, doi:10.1080/02786826.2012.716175, 2012.

Lopez-Hilfiker, F. D., Mohr, C., Ehn, M., Rubach, F., Kleist, E., Wildt, J., Mentel, T. F., Lutz, A., Hallquist, M., Worsnop, D., and Thornton, J. A.: A novel method for online analysis of gas and particle composition: description and evaluation of a Filter Inlet for Gases and AEROsols (FIGAERO), Atmos. Meas. Tech., 7, 983-1001, doi:10.5194/amt-7-983-2014, 2014.

Lopez-Hilfiker, F. D., Mohr, C., Ehn, M., Rubach, F., Kleist, E., Wildt, J., Mentel, T. F., Carrasquillo, A. J., Daumit, K. E., Hunter, J. F., Kroll, J. H., Worsnop, D. R., and Thornton, J. A.: Phase partitioning and volatility of secondary organic aerosol

components formed from alpha-pinene ozonolysis and OH oxidation: the importance of accretion products and other low volatility compounds, Atmos. Chem. Phys., 15, 7765-7776, doi:10.5194/acp-15-7765-2015, 2015.

Loza, C. L., Chan, A. W. H., Galloway, M. M., Keutsch, F. N., Flagan, R. C., and Seinfeld, J. H.: Characterization of Vapor Wall Loss in Laboratory Chambers, Environ. Sci. Technol., 44, 5074-5078, doi:10.1021/es100727v, 2010.

Loza, C. L., Chhabra, P. S., Yee, L. D., Craven, J. S., Flagan, R. C., and Seinfeld, J. H.: Chemical aging of m-xylene secondary organic aerosol: laboratory chamber study, Atmos. Chem. Phys., 12, 151-167, doi:10.5194/acp-12-151-2012, 2012.

Loza, C. L., Coggon, M. M., Nguyen, T. B., Zuend, A., Flagan, R. C., and Seinfeld, J. H.: On the Mixing and Evaporation of Secondary Organic Aerosol Components, Environ. Sci. Technol., 47, 6173-6180, doi:10.1021/es400979k, 2013.

Mao, J., Ren, X., Zhang, L., Van Duin, D. M., Cohen, R. C., Park, J. H., Goldstein, A. H., Paulot, F., Beaver, M. R., Crounse, J. D., Wennberg, P. O., DiGangi, J. P., Henry, S. B., Keutsch, F. N., Park, C., Schade, G. W., Wolfe, G. M., Thornton, J. A., and Brune, W. H.: Insights into hydroxyl measurements and atmospheric oxidation in a California forest, Atmos. Chem. Phys., 12, 8009-8020, doi:10.5194/acp-12-8009-2012, 2012.

Mao, J. Q., Paulot, F., Jacob, D. J., Cohen, R. C., Crounse, J. D., Wennberg, P. O., Keller, C. A., Hudman, R. C., Barkley, M. P., and Horowitz, L. W.: Ozone and organic nitrates over the eastern United States: Sensitivity to isoprene chemistry, J. Geophys. Res.-Atmos., 118, 11256-11268, doi:10.1002/jgrd.50817, 2013.

Marley, N. A., Gaffney, J. S., Tackett, M., Sturchio, N. C., Heraty, L., Martinez, N., Hardy, K. D., Marchany-Rivera, A., Guilderson, T., MacMillan, A., and Steelman, K.: The impact of biogenic carbon sources on aerosol absorption in Mexico City, Atmos. Chem. Phys., 9, 1537-1549, 2009.

Matsunaga, A., and Ziemann, P. J.: Yields of beta-hydroxynitrates, dihydroxynitrates, and trihydroxynitrates formed from OH radical-initiated reactions of 2-methyl-1-alkenes, Proceedings of the National Academy of Sciences of the United States of America, 107, 6664-6669, doi:10.1073/pnas.0910585107, 2010.

McLaren, R., Salmon, R. A., Liggio, J., Hayden, K. L., Anlauf, K. G., and Leaitch, W. R.: Nighttime chemistry at a rural site in the Lower Fraser Valley, Atmospheric Environment, 38, 5837-5848, doi:10.1016/j.atmosenv.2004.03.074, 2004.

McNeill, V. F., Wolfe, G. M., and Thornton, J. A.: The Oxidation of Oleate in Submicron Aqueous Salt Aerosols: Evidence of a Surface Process, The Journal of Physical Chemistry A, 111, 1073-1083, doi:10.1021/jp066233f, 2007.

Mentel, T. F., Springer, M., Ehn, M., Kleist, E., Pullinen, I., Kurten, T., Rissanen, M., Wahner, A., and Wildt, J.: Formation of highly oxidized multifunctional compounds: autoxidation of peroxy radicals formed in the ozonolysis of alkenes - deduced from structure-product relationships, Atmos. Chem. Phys., 15, 6745-6765, doi:10.5194/acp-15-6745-2015, 2015.

Miller, B.: Advanced Organic Chemistry: Reactions and Mechanisms, Journal of Chemical Education, 76, 320, 1999.

Miller, B.: Advanced Organic Chemistry: Reactions and Mechanisms, 2nd ed., Pearson/Prentice Hall, Lebanon, IN, 2003.

Müller, J. F., Peeters, J., and Stavrakou, T.: Fast photolysis of carbonyl nitrates from isoprene, Atmos. Chem. Phys., 14, 2497-2508, doi:10.5194/acp-14-2497-2014, 2014.

Nah, T., Sanchez, J., Boyd, C. M., and Ng, N. L.: Photochemical Aging of α-pinene and β-pinene Secondary Organic Aerosol formed from Nitrate Radical Oxidation, Environ. Sci. Technol., 50, 222-231, doi:10.1021/acs.est.5b04594, 2016.

Neuman, J. A., Nowak, J. B., Huey, L. G., Burkholder, J. B., Dibb, J. E., Holloway, J. S., Liao, J., Peischl, J., Roberts, J. M., Ryerson, T. B., Scheuer, E., Stark, H., Stickel, R. E., Tanner, D. J., and Weinheimer, A.: Bromine measurements in ozone depleted air over the Arctic Ocean, Atmos. Chem. Phys., 10, 6503-6514, doi:10.5194/acp-10-6503-2010, 2010.

Ng, N. L., Kroll, J. H., Chan, A. W. H., Chhabra, P. S., Flagan, R. C., and Seinfeld, J. H.: Secondary organic aerosol formation from m-xylene, toluene, and benzene, Atmos. Chem. Phys., 7, 3909-3922, doi:10.5194/acp-7-3909-2007, 2007a.

Ng, N. L., Chhabra, P. S., Chan, A. W. H., Surratt, J. D., Kroll, J. H., Kwan, A. J., McCabe, D. C., Wennberg, P. O., Sorooshian, A., Murphy, S. M., Dalleska, N. F., Flagan, R. C., and Seinfeld, J. H.: Effect of NOx level on secondary organic aerosol (SOA) formation from the photooxidation of terpenes, Atmos. Chem. Phys., 7, 5159-5174, 2007b.

Ng, N. L., Kwan, A. J., Surratt, J. D., Chan, A. W. H., Chhabra, P. S., Sorooshian, A., Pye, H. O. T., Crounse, J. D., Wennberg, P. O., and Flagan, R. C.: Secondary Organic Aerosol (SOA) Formation from Reaction of Isoprene with Nitrate Radicals (NO_3), Atmos. Chem. Phys., 8, 4117-4140, 2008a.

Ng, N. L., Kwan, A. J., Surratt, J. D., Chan, A. W. H., Chhabra, P. S., Sorooshian, A., Pye, H. O. T., Crounse, J. D., Wennberg, P. O., Flagan, R. C., and Seinfeld, J. H.: Secondary organic aerosol (SOA) formation from reaction of isoprene with nitrate radicals (NO3), Atmos. Chem. Phys., 8, 4117-4140, 2008b.

Ng, N. L., Canagaratna, M. R., Zhang, Q., Jimenez, J. L., Tian, J., Ulbrich, I. M., Kroll, J. H., Docherty, K. S., Chhabra, P. S., Bahreini, R., Murphy, S. M., Seinfeld, J. H., Hildebrandt, L., Donahue, N. M., DeCarlo, P. F., Lanz, V. A., Prevot, A. S. H., Dinar, E., Rudich, Y., and Worsnop, D. R.: Organic aerosol components observed in Northern Hemispheric datasets from Aerosol Mass Spectrometry, Atmos. Chem. Phys., 10, 4625-4641, doi:10.5194/acp-10-4625-2010, 2010.

Ng, N. L., Canagaratna, M. R., Jimenez, J. L., Chhabra, P. S., Seinfeld, J. H., and Worsnop, D. R.: Changes in organic aerosol composition with aging inferred from aerosol mass spectra, Atmos. Chem. Phys., 11, 6465-6474, doi:10.5194/acp-11-6465-2011, 2011.

Nguyen, T. B., Roach, P. J., Laskin, J., Laskin, A., and Nizkorodov, S. A.: Effect of humidity on the composition of isoprene photooxidation secondary organic aerosol, Atmos. Chem. Phys., 11, 6931-6944, doi:DOI 10.5194/acp-11-6931-2011, 2011.

Nguyen, T. B., Crounse, J. D., Schwantes, R. H., Teng, A. P., Bates, K. H., Zhang, X., St. Clair, J. M., Brune, W. H., Tyndall, G. S., Keutsch, F. N., Seinfeld, J. H., and Wennberg, P. O.: Overview of the Focused Isoprene eXperiment at the California Institute of Technology (FIXCIT): mechanistic chamber studies on the oxidation of biogenic compounds, Atmos. Chem. Phys., 14, 13531-13549, doi:10.5194/acp-14-13531-2014, 2014.

Odum, J. R., Hoffmann, T., Bowman, F., Collins, D., Flagan, R. C., and Seinfeld, J. H.: Gas/Particle Partitioning and Secondary Organic Aerosol Yields, Environ. Sci. Technol., 30, 2580-2585, doi:10.1021/es950943+, 1996.

Odum, J. R., Jungkamp, T. P. W., Griffin, R. J., Forstner, H. J. L., Flagan, R. C., and Seinfeld, J. H.: Aromatics, reformulated gasoline, and atmospheric organic aerosol formation, Environ. Sci. Technol., 31, 1890-1897, doi:10.1021/es960535l, 1997a.

Odum, J. R., Jungkamp, T. P. W., Griffin, R. J., Flagan, R. C., and Seinfeld, J. H.: The atmospheric aerosol-forming potential of whole gasoline vapor, Science, 276, 96-99, doi:10.1126/science.276.5309.96, 1997b.

Offenberg, J. H., Kleindienst, T. E., Jaoui, M., Lewandowski, M., and Edney, E. O.: Thermal properties of secondary organic aerosols, Geophysical Research Letters, 33, L03816, doi:10.1029/2005GL024623, 2006.

Orlando, J. J., and Tyndall, G. S.: Laboratory studies of organic peroxy radical chemistry: an overview with emphasis on recent issues of atmospheric significance, Chemical Society Reviews, 41, 6294-6317, doi:10.1039/C2CS35166H, 2012.

Ouchi, A., Liu, C., Kaneda, M., and Hyugano, T.: Photochemical C–C Bond Formation between Alcohols and Olefins by an Environmentally Benign Radical Reaction, Eur. J. Org. Chem., 2013, 3807-3816, doi:10.1002/ejoc.201300115, 2013.

Pankow, J. F.: AN ABSORPTION-MODEL OF GAS-PARTICLE PARTITIONING OF ORGANIC-COMPOUNDS IN THE ATMOSPHERE, Atmospheric Environment, 28, 185-188, doi:10.1016/1352-2310(94)90093-0, 1994.

Pankow, J. F., and Asher, W. E.: SIMPOL.1: a simple group contribution method for predicting vapor pressures and enthalpies of vaporization of multifunctional organic compounds, Atmos. Chem. Phys., 8, 2773-2796, 2008.

Pavia, D., Lampman, G., Kriz, G., and Vyvyan, J.: Introduction to spectroscopy, Cengage Learning, 2008.

Perraud, V., Bruns, E. A., Ezell, M. J., Johnson, S. N., Greaves, J., and Finlayson-Pitts, B. J.: Identification of Organic Nitrates in the NO3 Radical Initiated Oxidation of α-Pinene by Atmospheric Pressure Chemical Ionization Mass Spectrometry, Environ. Sci. Technol., 44, 5887-5893, doi:10.1021/es1005658, 2010.

Perring, A. E., Wisthaler, A., Graus, M., Wooldridge, P. J., Lockwood, A. L., Mielke, L. H., Shepson, P. B., Hansel, A., and Cohen, R. C.: A product study of the isoprene+NO3 reaction, Atmos. Chem. Phys., 9, 4945-4956, doi:10.5194/acp-9-4945-2009, 2009.

Perring, A. E., Pusede, S. E., and Cohen, R. C.: An Observational Perspective on the Atmospheric Impacts of Alkyl and Multifunctional Nitrates on Ozone and Secondary Organic Aerosol, Chemical Reviews, 113, 5848-5870, doi:10.1021/cr300520x, 2013.

Presto, A. A., Huff Hartz, K. E., and Donahue, N. M.: Secondary Organic Aerosol Production from Terpene Ozonolysis. 2. Effect of NOx Concentration, Environ. Sci. Technol., 39, 7046-7054, doi:10.1021/es050400s, 2005.

Presto, A. A., and Donahue, N. M.: Investigation of alpha-pinene plus ozone secondary organic aerosol formation at low total aerosol mass, Environ. Sci. Technol., 40, 3536-3543, doi:10.1021/es052203z, 2006.

Pye, H. O. T., Chan, A. W. H., Barkley, M. P., and Seinfeld, J. H.: Global modeling of organic aerosol: the importance of reactive nitrogen (NOx and NO3), Atmos. Chem. Phys., 10, 11261-11276, doi:10.5194/acp-10-11261-2010, 2010.

Pye, H. O. T., Luecken, D. J., Xu, L., Boyd, C. M., Ng, N. L., Baker, K. R., Ayres, B. R., Bash, J. O., Baumann, K., Carter, W. P. L., Edgerton, E., Fry, J. L., Hutzell, W. T., Schwede, D. B., and Shepson, P. B.: Modeling the Current and Future Roles of Particulate Organic Nitrates in the Southeastern United States, Environ. Sci. Technol., 49, 14195-14203, doi:10.1021/acs.est.5b03738, 2015.

Qi, L., Nakao, S., Tang, P., and Cocker, D. R., III: Temperature effect on physical and chemical properties of secondary organic aerosol from m-xylene photooxidation, Atmos. Chem. Phys., 10, 3847-3854, 2010.

Qi, L., Nakao, S., and Cocker, D. R., III: Aging of secondary organic aerosol from alpha-pinene ozonolysis: Roles of hydroxyl and nitrate radicals, Journal of the Air & Waste Management Association, 62, 1359-1369, doi:10.1080/10962247.2012.712082, 2012.

Rastogi, N., Zhang, X. L., Edgerton, E. S., Ingall, E., and Weber, R. J.: Filterable water-soluble organic nitrogen in fine particles over the southeastern USA during summer, Atmospheric Environment, 45, 6040-6047, doi:10.1016/j.atmosenv.2011.07.045, 2011.

Rayez, M.-T., Rayez, J.-C., Kerdouci, J., and Picquet-Varrault, B.: Theoretical Study of the Gas-Phase Reactions of NO3 Radical with a Series of trans-2-Unsaturated Aldehydes: From Acrolein to trans-2-Octenal, The Journal of Physical Chemistry A, 118, 5149-5155, doi:10.1021/jp503619d, 2014.

Renbaum-Wolff, L., Grayson, J. W., Bateman, A. P., Kuwata, M., Sellier, M., Murray, B. J., Shilling, J. E., Martin, S. T., and Bertram, A. K.: Viscosity of alpha-pinene secondary organic material and implications for particle growth and reactivity, Proceedings of the National Academy of Sciences of the United States of America, 110, 8014-8019, doi:10.1073/pnas.1219548110, 2013.

Riipinen, I., Pierce, J. R., Donahue, N. M., and Pandis, S. N.: Equilibration time scales of organic aerosol inside thermodenuders: Evaporation kinetics versus thermodynamics, Atmospheric Environment, 44, 597-607, doi:10.1016/j.atmosenv.2009.11.022, 2010.

Rindelaub, J. D., McAvey, K. M., and Shepson, P. B.: The photochemical production of organic nitrates from α-pinene and loss via acid-dependent particle phase hydrolysis, Atmospheric Environment, 100, 193-201, doi:http://dx.doi.org/10.1016/j.atmosenv.2014.11.010, 2015.

Rissanen, M. P., Kurten, T., Sipila, M., Thornton, J. A., Kausiala, O., Garmash, O., Kjaergaard, H. G., Petaja, T., Worsnop, D. R., Ehn, M., and Kulmala, M.: Effects of

Chemical Complexity on the Autoxidation Mechanisms of Endocyclic Alkene Ozonolysis Products: From Methylcyclohexenes toward Understanding alpha-Pinene, The journal of physical chemistry. A, 119, 4633-4650, doi:10.1021/jp510966g, 2015.

Roberts, J. M., and Fajer, R. W.: UV Absorption Cross-Sections Of Organic Nitrates Of Potential Atmospheric Importance And Estimation Of Atmospheric Lifetimes, Environ. Sci. Technol., 23, 945-951, doi:10.1021/es00066a003, 1989.

Robinson, E. S., Saleh, R., and Donahue, N. M.: Organic Aerosol Mixing Observed by Single-Particle Mass Spectrometry, J. Phys. Chem. A, 117, 13935-13945, doi:10.1021/jp405789t, 2013.

Robinson, E. S., Saleh, R., and Donahue, N. M.: Probing the Evaporation Dynamics of Mixed SOA/Squalane Particles Using Size-Resolved Composition and Single-Particle Measurements, Environmental Science & Technology, 49, 9724-9732, doi:10.1021/acs.est.5b01692, 2015.

Rollins, A. W., Kiendler-Scharr, A., Fry, J. L., Brauers, T., Brown, S. S., Dorn, H. P., Dube, W. P., Fuchs, H., Mensah, A., Mentel, T. F., Rohrer, F., Tillmann, R., Wegener, R., Wooldridge, P. J., and Cohen, R. C.: Isoprene oxidation by nitrate radical: alkyl nitrate and secondary organic aerosol yields, Atmos. Chem. Phys., 9, 6685-6703, 2009.

Rollins, A. W., Browne, E. C., Min, K. E., Pusede, S. E., Wooldridge, P. J., Gentner, D. R., Goldstein, A. H., Liu, S., Day, D. A., Russell, L. M., and Cohen, R. C.: Evidence for NOx Control over Nighttime SOA Formation, Science, 337, 1210-1212, doi:10.1126/science.1221520, 2012.

Rollins, A. W., Pusede, S., Wooldridge, P., Min, K. E., Gentner, D. R., Goldstein, A. H., Liu, S., Day, D. A., Russell, L. M., Rubitschun, C. L., Surratt, J. D., and Cohen, R. C.: Gas/particle partitioning of total alkyl nitrates observed with TD-LIF in Bakersfield, Journal of Geophysical Research-Atmospheres, 118, 6651-6662, doi:10.1002/jgrd.50522, 2013.

Romonosky, D. E., Nguyen, L. Q., Shemesh, D., Nguyen, T. B., Epstein, S. A., Martin, D. B. C., Vanderwal, C. D., Gerber, R. B., and Nizkorodov, S. A.: Absorption spectra and aqueous photochemistry of beta-hydroxyalkyl nitrates of atmospheric interest, Molecular Physics, 113, 2179-2190, doi:10.1080/00268976.2015.1017020, 2015.

Rudich, Y., Donahue, N. M., and Mentel, T. F.: Aging of organic aerosol: Bridging the gap between laboratory and field studies, Annu. Rev. Phys. Chem., 58, 321-352, doi:10.1146/annurev.physchem.58.032806.104432, 2007.

Russell, G. A.: Deuterium-isotope Effects in the Autoxidation of Aralkyl Hydrocarbons. Mechanism of the Interaction of Peroxy Radicals, J. Am. Cgem. Soc., 79, 3871-3877, doi:10.1021/ja01571a068, 1957.

Russell, M., and Allen, D. T.: Predicting secondary organic aerosol formation rates in southeast Texas, Journal of Geophysical Research: Atmospheres, 110, D07S17, doi:10.1029/2004JD004722, 2005.

Saathoff, H., Naumann, K. H., Möhler, O., Jonsson, Å. M., Hallquist, M., Kiendler-Scharr, A., Mentel, T. F., Tillmann, R., and Schurath, U.: Temperature dependence of

yields of secondary organic aerosols from the ozonolysis of α-pinene and limonene, Atmos. Chem. Phys., 9, 1551-1577, doi:10.5194/acp-9-1551-2009, 2009.

Saha, P. K., and Grieshop, A. P.: Exploring Divergent Volatility Properties from Yield and Thermodenuder Measurements of Secondary Organic Aerosol from α-Pinene Ozonolysis, Environ. Sci. Technol., doi:10.1021/acs.est.6b00303, 2016.

Saleh, R., Donahue, N. M., and Robinson, A. L.: Time Scales for Gas-Particle Partitioning Equilibration of Secondary Organic Aerosol Formed from Alpha-Pinene Ozonolysis, Environ. Sci. Technol., 47, 5588-5594, doi:10.1021/es400078d, 2013.

Sander, S. P., Abbatt, J., Barker, J. R., Burkholder, J. B., Friedl, R. R., Golden, D. M., Huie, R. E., Kolb, C. E., Kurylo, M. J., Moortgat, G. K., Orkin, V. L., Wine, P. H.: Chemical kinetics and photochemical data for use in atmospheric studies: Evaluation Number 17, Jet Propulsion Laboratory, 2011.

Sato, K.: Detection of nitrooxypolyols in secondary organic aerosol formed from the photooxidation of conjugated dienes under high-NOx conditions, Atmospheric Environment, 42, 6851-6861, doi:10.1016/j.atmosenv.2008.05.010, 2008.

Saukko, E., Lambe, A. T., Massoli, P., Koop, T., Wright, J. P., Croasdale, D. R., Pedernera, D. A., Onasch, T. B., Laaksonen, A., Davidovits, P., Worsnop, D. R., and Virtanen, A.: Humidity-dependent phase state of SOA particles from biogenic and anthropogenic precursors, Atmos. Chem. Phys., 12, 7517-7529, doi:10.5194/acp-12-7517-2012, 2012.

Saunders, S. M., Jenkin, M. E., Derwent, R. G., and Pilling, M. J.: Protocol for the development of the Master Chemical Mechanism, MCM v3 (Part A): tropospheric degradation of non-aromatic volatile organic compounds, Atmos. Chem. Phys., 3, 161-180, 2003a.

Saunders, S. M., Jenkin, M. E., Derwent, R. G., and Pilling, M. J.: Protocol for the development of the Master Chemical Mechanism, MCM v3 (Part A): tropospheric degradation of non-aromatic volatile organic compounds, Atmos. Chem. Phys., 3, 161-180, doi:10.5194/acp-3-161-2003, 2003b.

Schichtel, B. A., Malm, W. C., Bench, G., Fallon, S., McDade, C. E., Chow, J. C., and Watson, J. G.: Fossil and contemporary fine particulate carbon fractions at 12 rural and urban sites in the United States, Journal of Geophysical Research: Atmospheres, 113, D02311, doi:10.1029/2007JD008605, 2008.

Schröder, K., Junge, K., Spannenberg, A., and Beller, M.: Design of a bio-inspired imidazole-based iron catalyst for epoxidation of olefins: Mechanistic insights, Catalysis Today, 157, 364-370, doi:10.1016/j.cattod.2010.04.034, 2010.

Shiraiwa, M., Ammann, M., Koop, T., and Poeschl, U.: Gas uptake and chemical aging of semisolid organic aerosol particles, Proceedings of the National Academy of Sciences of the United States of America, 108, 11003-11008, doi:10.1073/pnas.1103045108, 2011.

Slusher, D. L., Huey, L. G., Tanner, D. J., Flocke, F. M., and Roberts, J. M.: A thermal dissociation–chemical ionization mass spectrometry (TD-CIMS) technique for the

simultaneous measurement of peroxyacyl nitrates and dinitrogen pentoxide, Journal of Geophysical Research: Atmospheres, 109, D19315, doi:10.1029/2004JD004670, 2004.

Song, C., Zaveri, R. A., Shilling, J. E., Alexander, M. L., and Newburn, M.: Effect of Hydrophilic Organic Seed Aerosols on Secondary Organic Aerosol Formation from Ozonolysis of α-Pinene, Environ. Sci. Technol., 45, 7323-7329, doi:10.1021/es201225c, 2011.

Song, M., Liu, P. F., Hanna, S. J., Li, Y. J., Martin, S. T., and Bertram, A. K.: Relative humidity-dependent viscosities of isoprene-derived secondary organic material and atmospheric implications for isoprene-dominant forests, Atmos. Chem. Phys., 15, 5145-5159, doi:10.5194/acp-15-5145-2015, 2015.

Spittler, M., Barnes, I., Bejan, I., Brockmann, K. J., Benter, T., and Wirtz, K.: Reactions of NO3 radicals with limonene and alpha-pinene: Product and SOA formation, Atmospheric Environment, 40, S116-S127, doi:10.1016/j.atmosenv.2005.09.093, 2006.

Stockwell, C. E., Veres, P. R., Williams, J., and Yokelson, R. J.: Characterization of biomass burning emissions from cooking fires, peat, crop residue, and other fuels with high-resolution proton-transfer-reaction time-of-flight mass spectrometry, Atmos. Chem. Phys., 15, 845-865, doi:10.5194/acp-15-845-2015, 2015.

Stolle, A., Ondruschka, B., and Hopf, H.: Thermal Rearrangements of Monoterpenes and Monoterpenoids, Helvetica Chimica Acta, 92, 1673-1719, doi:10.1002/hlca.200900041, 2009.

Suarez-Bertoa, R., Picquet-Varrault, B., Tamas, W., Pangui, E., and Doussin, J. F.: Atmospheric Fate of a Series of Carbonyl Nitrates: Photolysis Frequencies and OH-Oxidation Rate Constants, Environ. Sci. Technol., 46, 12502-12509, doi:10.1021/es302613x, 2012.

Surratt, J. D., Lewandowski, M., Offenberg, J. H., Jaoui, M., Kleindienst, T. E., Edney, E. O., and Seinfeld, J. H.: Effect of Acidity on Secondary Organic Aerosol Formation from Isoprene, Environ. Sci. Technol., 41, 5363-5369, doi:10.1021/es0704176, 2007.

Surratt, J. D., Gomez-Gonzalez, Y., Chan, A. W. H., Vermeylen, R., Shahgholi, M., Kleindienst, T. E., Edney, E. O., Offenberg, J. H., Lewandowski, M., Jaoui, M., Maenhaut, W., Claeys, M., Flagan, R. C., and Seinfeld, J. H.: Organosulfate formation in biogenic secondary organic aerosol, J. Phys. Chem. A, 112, 8345-8378, doi:10.1021/jp802310p, 2008.

Svendby, T. M., Lazaridis, M., and Torseth, K.: Temperature dependent secondary organic aerosol formation from terpenes and aromatics, Journal of Atmospheric Chemistry, 59, 25-46, doi:10.1007/s10874-007-9093-7, 2008.

Szmigielski, R., Vermeylen, R., Dommen, J., Metzger, A., Maenhaut, W., Baltensperger, U., and Claeys, M.: The acid effect in the formation of 2-methyltetrols from the photooxidation of isoprene in the presence of NOx, Atmospheric Research, 98, 183-189, doi:http://dx.doi.org/10.1016/j.atmosres.2010.02.012, 2010.

Talukdar, R. K., Herndon, S. C., Burkholder, J. B., Roberts, J. M., and Ravishankara, A. R.: Atmospheric fate of several alkyl nitrates .1. Rate coefficients of the reactions alkyl

nitrates with isotopically labelled hydroxyl radicals, Journal of the Chemical Society-Faraday Transactions, 93, 2787-2796, 1997.

Thornton, J. A., Braban, C. F., and Abbatt, J. P. D.: N2O5 hydrolysis on sub-micron organic aerosols: the effect of relative humidity, particle phase, and particle size, Physical Chemistry Chemical Physics, 5, 4593-4603, doi:10.1039/B307498F, 2003.

Tsigaridis, K., Daskalakis, N., Kanakidou, M., Adams, P. J., Artaxo, P., Bahadur, R., Balkanski, Y., Bauer, S. E., Bellouin, N., Benedetti, A., Bergman, T., Berntsen, T. K., Beukes, J. P., Bian, H., Carslaw, K. S., Chin, M., Curci, G., Diehl, T., Easter, R. C., Ghan, S. J., Gong, S. L., Hodzic, A., Hoyle, C. R., Iversen, T., Jathar, S., Jimenez, J. L., Kaiser, J. W., Kirkevag, A., Koch, D., Kokkola, H., Lee, Y. H., Lin, G., Liu, X., Luo, G., Ma, X., Mann, G. W., Mihalopoulos, N., Morcrette, J. J., Mueller, J. F., Myhre, G., Myriokefalitakis, S., Ng, N. L., O'Donnell, D., Penner, J. E., Pozzoli, L., Pringle, K. J., Russell, L. M., Schulz, M., Sciare, J., Seland, O., Shindell, D. T., Sillman, S., Skeie, R. B., Spracklen, D., Stavrakou, T., Steenrod, S. D., Takemura, T., Tiitta, P., Tilmes, S., Tost, H., van Noije, T., van Zyl, P. G., von Salzen, K., Yu, F., Wang, Z., Wang, Z., Zaveri, R. A., Zhang, H., Zhang, K., Zhang, Q., and Zhang, X.: The AeroCom evaluation and intercomparison of organic aerosol in global models, Atmos. Chem. Phys., 14, 10845-10895, doi:10.5194/acp-14-10845-2014, 2014.

Turrà, N., Neuenschwander, U., Baiker, A., Peeters, J., and Hermans, I.: Mechanism of the Catalytic Deperoxidation of tert-Butylhydroperoxide with Cobalt(II) Acetylacetonate, Chem.-Eur. J., 16, 13226-13235, doi:10.1002/chem.201000489, 2010.

Vaden, T. D., Imre, D., Beranek, J., Shrivastava, M., and Zelenyuk, A.: Evaporation kinetics and phase of laboratory and ambient secondary organic aerosol, Proceedings of the National Academy of Sciences of the United States of America, 108, 2190-2195, doi:10.1073/pnas.1013391108, 2011.

Venkatachari, P., and Hopke, P. K.: Characterization of Products formed in the Reaction of Ozone with α-pinene: Case for Organic Peroxides, J. Environ. Monitor., 10, 966-974, 2008.

Vereecken, L., and Peeters, J.: Nontraditional (Per)oxy Ring-Closure Paths in the Atmospheric Oxidation of Isoprene and Monoterpenes, J. Phys. Chem. A, 108, 5197-5204, doi:10.1021/jp049219g, 2004.

Vereecken, L., and Peeters, J.: A structure-activity relationship for the rate coefficient of H-migration in substituted alkoxy radicals, Phys. Chem. Chem. Phys., 12, 12608-12620, doi:10.1039/c0cp00387e, 2010.

Vereecken, L., and Peeters, J.: A Theoretical Study of the OH-initiated Gas-phase Oxidation Mechanism of β-pinene ($C_{10}H_{16}$): First Generation Products, Phys. Chem. Chem. Phys., 14, 3802-3815, doi:10.1039/C2CP23711C, 2012.

Vereecken, L., and Francisco, J. S.: Theoretical studies of atmospheric reaction mechanisms in the troposphere, Chem. Soc. Rev., 41, 6259-6293, doi:10.1039/c2cs35070j, 2012.

Verma, V., Fang, T., Guo, H., King, L., Bates, J. T., Peltier, R. E., Edgerton, E., Russell, A. G., and Weber, R. J.: Reactive oxygen species associated with water-soluble PM2.5 in the southeastern United States: spatiotemporal trends and source apportionment, Atmos. Chem. Phys., 14, 12915-12930, doi:10.5194/acp-14-12915-2014, 2014.

Wängberg, I., Barnes, I., and Becker, K. H.: Product and Mechanistic Study of the Reaction of NO3 Radicals with α-Pinene, Environ. Sci. Technol., 31, 2130-2135, doi:10.1021/es960958n, 1997.

Warren, B., Austin, R. L., and Cocker, D. R., III: Temperature dependence of secondary organic aerosol, Atmospheric Environment, 43, 3548-3555, doi:10.1016/j.atmosenv.2009.04.011, 2009.

Wayne, R. P., Barnes, I., Biggs, P., Burrows, J. P., Canosamas, C. E., Hjorth, J., Lebras, G., Moortgat, G. K., Perner, D., Poulet, G., Restelli, G., and Sidebottom, H.: THE NITRATE RADICAL - PHYSICS, CHEMISTRY, AND THE ATMOSPHERE, Atmospheric Environment Part a-General Topics, 25, 1-203, doi:10.1016/0960-1686(91)90192-a, 1991.

Weber, R. J., Sullivan, A. P., Peltier, R. E., Russell, A., Yan, B., Zheng, M., de Gouw, J., Warneke, C., Brock, C., Holloway, J. S., Atlas, E. L., and Edgerton, E.: A study of secondary organic aerosol formation in the anthropogenic-influenced southeastern United States, Journal of Geophysical Research: Atmospheres, 112, D13302, doi:10.1029/2007JD008408, 2007a.

Weber, R. J., Sullivan, A. P., Peltier, R. E., Russell, A., Yan, B., Zheng, M., de Gouw, J., Warneke, C., Brock, C., Holloway, J. S., Atlas, E. L., and Edgerton, E.: A study of secondary organic aerosol formation in the anthropogenic-influenced southeastern United States, J. Geophys. Res.-Atmos., 112, D13302, doi:13310.11029/12007JD008408, 2007b.

Wilson, J., Imre, D., Beránek, J., Shrivastava, M., and Zelenyuk, A.: Evaporation Kinetics of Laboratory-Generated Secondary Organic Aerosols at Elevated Relative Humidity, Environ. Sci. Technol., 49, 243-249, doi:10.1021/es505331d, 2015.

Winer, A. M., Atkinson, R., and Pitts, J. N.: Gaseous Nitrate Radical - Possible Nighttime Atmospheric Sink For Biogenic Organic Compounds, Science, 224, 156-159, doi:10.1126/science.224.4645.156, 1984.

Xu, H., Wentworth, P. J., Howell, N. W., and Joens, J. A.: Temperature Dependent Near-UV Molar Absorptivities of Aliphatic Aldehydes and Ketones in Aqueous Solution, Spectrochim. Acta A, 49, 1171-1178, doi:http://dx.doi.org/10.1016/0584-8539(93)80076-M, 1993.

Xu, L., Kollman, M. S., Song, C., Shilling, J. E., and Ng, N. L.: Effects of NOx on the Volatility of Secondary Organic Aerosol from Isoprene Photooxidation, Environ. Sci. Technol., 48, 2253-2262, doi:10.1021/es404842g, 2014.

Xu, L., Suresh, S., Guo, H., Weber, R. J., and Ng, N. L.: Aerosol characterization over the southeastern United States using high-resolution aerosol mass spectrometry: spatial and seasonal variation of aerosol composition and sources with a focus on organic nitrates, Atmos. Chem. Phys., 15, 7307-7336, doi:10.5194/acp-15-7307-2015, 2015a.

Xu, L., Suresh, S., Guo, H., Weber, R. J., and Ng, N. L.: Aerosol characterization over the southeastern United States using high resolution aerosol mass spectrometry: spatial and seasonal variation of aerosol composition, sources, and organic nitrates, Atmos. Chem. Phys. Discuss., 15, 10479-10552, doi:10.5194/acpd-15-10479-2015, 2015b.

Xu, L., Guo, H., Boyd, C. M., Klein, M., Bougiatioti, A., Cerully, K. M., Hite, J. R., Isaacman-VanWertz, G., Kreisberg, N. M., Knote, C., Olson, K., Koss, A., Goldstein, A. H., Hering, S. V., de Gouw, J., Baumann, K., Lee, S.-H., Nenes, A., Weber, R. J., and Ng, N. L.: Effects of anthropogenic emissions on aerosol formation from isoprene and monoterpenes in the southeastern United States, Proceedings of the National Academy of Sciences of the United States of America, 112, 37-42, doi:10.1073/pnas.1417609112, 2015c.

Xu, L., Williams, L. R., Young, D. E., Allan, J. D., Coe, H., Massoli, P., Fortner, E., Chhabra, P., Herndon, S., Brooks, W. A., Jayne, J. T., Worsnop, D. R., Aiken, A. C., Liu, S., Gorkowski, K., Dubey, M. K., Fleming, Z. L., Visser, S., Prévôt, A. S. H., and Ng, N. L.: Wintertime aerosol chemical composition, volatility, and spatial variability in the greater London area, Atmos. Chem. Phys., 16, 1139-1160, doi:10.5194/acp-16-1139-2016, 2016.

Ye, J., Gordon, C. A., and Chan, A. W. H.: Enhancement in Secondary Organic Aerosol Formation in the Presence of Preexisting Organic Particle, Environ. Sci. Technol., 50, 3572-3579, doi:10.1021/acs.est.5b05512, 2016.

Yeh, G. K., and Ziemann, P. J.: Alkyl Nitrate Formation from the Reactions of C8–C14 n-Alkanes with OH Radicals in the Presence of NOx: Measured Yields with Essential Corrections for Gas–Wall Partitioning, The Journal of Physical Chemistry A, 118, 8147-8157, doi:10.1021/jp500631v, 2014.

Yeh, G. K., Claflin, M. S., and Ziemann, P. J.: Products and Mechanism of the Reaction of 1-Pentadecene with NO3 Radicals and the Effect of a -ONO2 Group on Alkoxy Radical Decomposition, The journal of physical chemistry. A, 119, 10684-10696, doi:10.1021/acs.jpca.5b07468, 2015.

Yu, J. Z., Cocker, D. R., Griffin, R. J., Flagan, R. C., and Seinfeld, J. H.: Gas-phase ozone oxidation of monoterpenes: Gaseous and particulate products, J. Atmos. Chem., 34, 207-258, doi:10.1023/a:1006254930583, 1999.

Yu, Y., Ezell, M. J., Zelenyuk, A., Imre, D., Alexander, L., Ortega, J., D'Anna, B., Harmon, C. W., Johnson, S. N., and Finlayson-Pitts, B. J.: Photooxidation of alpha-pinene at high relative humidity in the presence of increasing concentrations of NOx, Atmospheric Environment, 42, 5044-5060, doi:10.1016/j.atmosenv.2008.02.026, 2008.

Zaveri, R. A., Berkowitz, C. M., Brechtel, F. J., Gilles, M. K., Hubbe, J. M., Jayne, J. T., Kleinman, L. I., Laskin, A., Madronich, S., Onasch, T. B., Pekour, M. S., Springston, S. R., Thornton, J. A., Tivanski, A. V., and Worsnop, D. R.: Nighttime chemical evolution of aerosol and trace gases in a power plant plume: Implications for secondary organic nitrate and organosulfate aerosol formation, NO3 radical chemistry, and N2O5

heterogeneous hydrolysis, Journal of Geophysical Research-Atmospheres, 115, D12304, doi:10.1029/2009jd013250, 2010.

Zhang, H., Worton, D. R., Shen, S., Nah, T., Isaacman-VanWertz, G., Wilson, K. R., and Goldstein, A. H.: Fundamental Time Scales Governing Organic Aerosol Multiphase Partitioning and Oxidative Aging, Environ. Sci. Technol., doi:10.1021/acs.est.5b02115, 2015a.

Zhang, X., Cappa, C. D., Jathar, S. H., McVay, R. C., Ensberg, J. J., Kleeman, M. J., and Seinfeld, J. H.: Influence of vapor wall loss in laboratory chambers on yields of secondary organic aerosol, Proceedings of the National Academy of Sciences of the United States of America, 111, 5802-5807, doi:10.1073/pnas.1404727111, 2014.

Zhang, X., Schwantes, R. H., McVay, R. C., Lignell, H., Coggon, M. M., Flagan, R. C., and Seinfeld, J. H.: Vapor wall deposition in Teflon chambers, Atmos. Chem. Phys., 15, 4197-4214, doi:10.5194/acp-15-4197-2015, 2015b.

Zhao, R., Lee, A. K. Y., and Abbatt, J. P. D.: Investigation of Aqueous-Phase Photooxidation of Glyoxal and Methylglyoxal by Aerosol Chemical Ionization Mass Spectrometry: Observation of Hydroxyhydroperoxide Formation, J. Phys. Chem. A, 116, 6253-6263, doi:10.1021/jp211528d, 2012.

Zheng, W., Flocke, F. M., Tyndall, G. S., Swanson, A., Orlando, J. J., Roberts, J. M., Huey, L. G., and Tanner, D. J.: Characterization of a thermal decomposition chemical ionization mass spectrometer for the measurement of peroxy acyl nitrates (PANs) in the atmosphere, Atmos. Chem. Phys., 11, 6529-6547, doi:10.5194/acp-11-6529-2011, 2011.

Zhou, S. M., Shiraiwa, M., McWhinney, R. D., Poschl, U., and Abbatt, J. P. D.: Kinetic limitations in gas-particle reactions arising from slow diffusion in secondary organic aerosol, Faraday Discussions, 165, 391-406, doi:10.1039/c3fd00030c, 2013.

Ziemann, P. J., and Atkinson, R.: Kinetics, products, and mechanisms of secondary organic aerosol formation, Chemical Society Reviews, 41, 6582-6605, doi:10.1039/c2cs35122f, 2012.